UNIVERSITÉ DE SHERBROOKE
Faculté de génie
Département de génie civil

APPLICATION DE LA MÉTHODE D'ÉMISSION ACOUSTIQUE POUR LA SURVEILLANCE DU COMPORTEMENT AU CISAILLEMENT DES JOINTS ACTIFS

Thèse de doctorat
Spécialité: génie civil

Zabihallah MORADIAN

Jury: Gérard BALLIVY (directeur)
Patrice RIVARD
Giovanni GRASSELLI
Kaveh SALEH
Clermont GRAVEL
Mathieu NUTH

Sherbrooke (Québec) Canada May 2011

Your file Votre référence
ISBN: 978-0-494-83299-8

Our file Notre référence
ISBN: 978-0-494-83299-8

Acknowledgement

Among many people who helped me to complete this thesis, first I want to express my sincere gratitude to my supervisor, Professor Gérard Ballivy at Université de Sherbrooke, for his guidance throughout the duration of the study. I am greatly indebted for his support, advice, and suggestions to my research work. I would like to thank my co-supervisor, Professor Patrice Rivard, for his great assistance and his guidance during various parts of the work. Dr. Clermont Gravel has assisted me with many interesting discussions and comments. He is greatly acknowledged. I thank Dr. Serge Kodjo for his support and many inspirations and also for his useful comments.

I would like to express my thanks to Prof. Giovanni Grasselli, Dr. Kaveh Saleh and Prof. Mathieu Nuth for evaluating my thesis and giving their useful comments and suggestions.

Gratitude is also expressed to those working at Laboratory of Rock Mechanics and Applied Geology, Civil Engineering Department, Université de Sherbrooke especially, Georges Lalonde, Baptiste Rousseau and Danick Charbonneau who have helped me to carry out laboratory tests.

There are many colleagues and friends who deserve my sincere gratitude and acknowledgements. I thank all of them for their encouragement in various ways. I am so grateful that I have come to know and make friends with these wonderful People during my graduate study.

I want to thank my family and especially my parents, because their support has been invaluable. Finally, special thanks to my beloved wife who made this work possible with her patience and support.

Zabihallah Moradian, Sherbrooke, May 2011

Abstract:
A key requirement in evaluation of sliding stability of concrete dams is monitoring shear behavior of 1) concrete joints in dam body, 2) concrete-rock interfaces and 3) rock discontinuities in dam foundation. The methodology consisted of creating a database of observed shear behaviors of the mentioned joints using acoustic emission (AE) technique. Joint samples were fabricated by tension splitting of the cores and pouring concrete on rock joint replica for simulating concrete-rock interfaces. Variations of key parameters including joint geometry, normal stress, displacement rate and bonding percentage were incorporated in the analysis. An analysis was also carried out on natural joints from Daniel Johnson (Manic 5) Dam, Quebec, founded on gneiss to granitic rock. Parametric-based and signal-basedd analysis methods were used to evaluate the potential of AE for monitoring shear behavior of various kinds of joint with different characteristics. Using AE parameters such as amplitude, count, energy, duration and rise time, this study was done as a feasibility study for AE monitoring of sliding surfaces within dam, dam-rock interface or inside rock foundation. It was found that AE has a good capability for showing the initial shear movement of the non-bonded joints. For bonded joints this technique can show that AE activities are occurring before breaking of adhesive bond. This is important because recording AE signals after an initial breakage of the joint would be too late to install stabilization work to be done beforehand. Of course in the eventuality that a rupture includes a sequence of events even recording AE signals of the first break is still useful. It is recommended to use this method combined with other instrumentation methods (e.g. load measuring instruments) to detect the initial shear movement of the bonded joints. Following experimental work and analysis of crack propagation and asperity degradation along shearing process, four different periods were observed in shear stress-displacement behavior of joints. These periods are: 1) Pre-peak linear period in which AE activities are initiated and show the beginning of shear displacement, 2) Pre-peak non-linear period in which AE signals are generated from crack initiation and degradation of the secondary asperities, 3) Post-peak period where first order asperities are sheared off and joints pass their maximum shear strength and 4) Residual period in which AE activities decrease and reach their minimum values.
The applicability of AE localization technique was evaluated using image analysis and scanned surfaces of the joints by laser. The results indicated that this method can locate regions with rupture governing characteristics. This provides the possibility to reinforce support systems and be aware about possible structure failures before any unexpected mechanical disturbance.
Keywords: Acoustic emission; shear behavior; rock–rock joint; rock–concrete joint; concrete–concrete joint; normal load; joint roughness; bonding percentage; displacement rate; AE parameters; AE source locations

Résumé:
Une exigence clé dans l'évaluation de la stabilité des barrages en béton est la surveillance du comportement au cisaillement des joints de béton dans le corps du barrage, des interfaces béton-roche et des discontinuités rocheuses dans les fondations du barrage. La méthodologie proposé dans cette étude consiste une base de données des comportements observés au cisaillement des joints du roc à l'aide de la technique d'émission acoustique (EA). Ces carottes de forage ont ensuite été rupturés par flexion pour obtenir des répliques de joints rocheux. Un joint de béton a ensuite été coulé sur les surfaces des joints rocheux pour simuler les interfaces béton-roche. L'analyse a compris des variations des paramètres clés, notamment la géométrie du joint, la contrainte normale, la vitesse de déplacement et le pourcentage de liaison. Une analyse a également été effectuée sur des échantillons de joints naturels du barrage Daniel Johnson (Manic 5), Québec, fondée sur le roc granitique. L'étude paramétrique et celle sur les signaux ont été utilisées pour évaluer le potentiel de l'EA pour surveiller le comportement en cisaillement de différents types de joints possédant des caractéristiques différentes. Les paramètres d'EA utilisés ont été l'amplitude, les comptes (counts), l'énergie, la duration et le temps de montée. Cette étude a été réalisée comme une étude de faisabilité pour la surveillance de surfaces de glissement au sein d'un barrage : l'interface barrage-roche ou à l'intérieur de la fondation rocheuse. Il a été constaté que l'EA a une bonne capacité à montrer le mouvement de cisaillement initial des joints non liés. Pour les joints liés, cette technique a démontré une activité d'EA un certain temps avant la rupture du lien adhésif. Ceci est important, puisqu'une fois le joint rompu, il serait trop tard pour installer des travaux correctifs. Bien sûr, si une rupture se produit par une séquence d'évènements, dans ce cas, le signal d'émission acoustique de la première rupture est utile. Il est recommandé d'utiliser une combinaison de cette méthode avec les méthodes classiques d'instrumention et de mesure (par exemple, les instruments de mesure de la charge) pour détecter le mouvement de cisaillement initial des joints liés. À partir de l'estimation de la propagation des fissures et de la dégradation des aspérités pendant le processus de cisaillement, quatre périodes différentes ont été observées dans le comportement contrainte-déplacement en cisaillement des joints. Ces périodes sont les suivantes: 1) période prépic linéaire dans lequel les activités d'EA sont initiées et où le point de départ du déplacement en cisaillement est montré, 2) période prépic non linéaire dans lequel les signaux d'EA sont générés à partir du début de la fissuration et de la dégradation des aspérités secondaire, 3) période post-pic alors que les aspérités de premier ordre sont arrachées et la résistance au cisaillement maximal est mobilisée par le joint et 4) période résiduelle dans lequel les activités d'EA sont diminuées et atteignent leur valeur minimale.
L'applicabilité de la technique de localisation d'EA a été évaluée par analyse d'images et numérisation par profilométrie laser des surfaces des joints. Les résultats indiquent que cette méthode peut reconnaître les régions présentant des caractéristiques de rupture. Ceci offre la possibilité de renforcer des systèmes de soutien de stuctures et de prévenir une rupture probable d'une structure suivant une perturbation mécanique inattendue.
Mots-clés: émission acoustique; comportement en cisaillement; joints roche-roche; joints roche-béton; joints béton-béton; charge normale; rugosité du joint, pourcentage de liaison; vitesse de déplacement; paramètres d'EA; localisation de sources d'EA

Table of Content

List of Figures

List of Tables

1. INTRODUCTION

1.1. Problem and rational

Since the early part of 20th century, and especially since the 1950s, the number of hydroelectric dams has increased across the Canadian landscape. The province of Québec has based a large part of its economic growth and activities in the energy sector on the development of the extensive water resources found throughout its territory. Québec is Canada's leading producer of hydroelectricity. It also has one of the world's largest hydroelectric facilities with more than 568 dams. Hydroelectricity, with 34 GW potential, accounts for almost 96% of all the electricity used in Québec (Hydro-Québec, 2010).

Over the past few years, the monitoring of dams in Canada and especially in Québec has acquired great importance not only for dam managers but also for scientific communities. Dam monitoring helps to understand the mechanisms of disruptive processes and define adequate prevention measures for the mitigation of their effects and reduce the loss of human lives and assets.

Concrete dams deform due to internal loads such as dead load, pore pressure, cooling, alkali-aggregate reaction in concrete, etc, external loads caused by weather and reservoir temperature, solar radiation, reservoir levels, uplift pressure, wind, earthquakes, ice, overflowing water, foundation settlement, etc. Figure 1-1 shows a typical concrete dam with various kinds of loads.

Movements caused by such loads must be within the tolerable ranges and do not cause structural distress. Sudden or unexpected direction or trend of surface movement could indicate developing problems.

The causes of dam failures and incidents have been catalogued (USCOLD 1975, 1988 and 1996 and ICOLD 1973, 1976, 1979 and 1995). The common causes of concrete dam failures and incidents are (ICOLD 1973):

- Overtopping from inadequate spillway capacity or spillway blockage resulting in erosion of the foundation at the toe of the dam or washout of an abutment or adjacent embankment structure.

- Foundation leakage and piping in pervious strata, soluble lenses, and rock discontinuities which accelerate the rupture/collapse of the structure.
- Sliding along weak discontinuities in foundations.

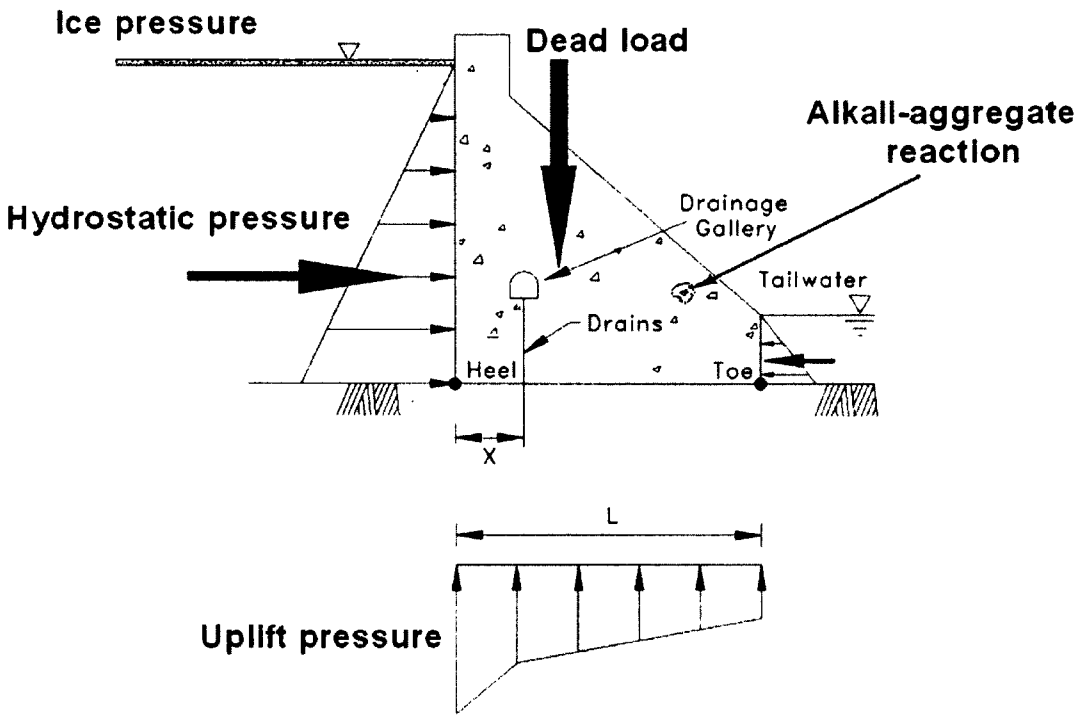

Figure 1-1: a concrete dam with various kinds of loads (after U.S. Army Corps of Engineers, 1995)

One example of dam failure due to sliding is St. Francis dam in USA. On March 12, 1928, the St. Francis dam catastrophically failed. Approximately 450 people lost their lives in the downstream zones. Among those that died, were many of the workers and their families that worked at the dam. The St. Francis Dam Failure is considered the greatest American civil engineering failure of the twentieth century (Doyce and Nunis, 2002). Figure 1-2 and 1-3 show the ST. Francis dam before and after failure.

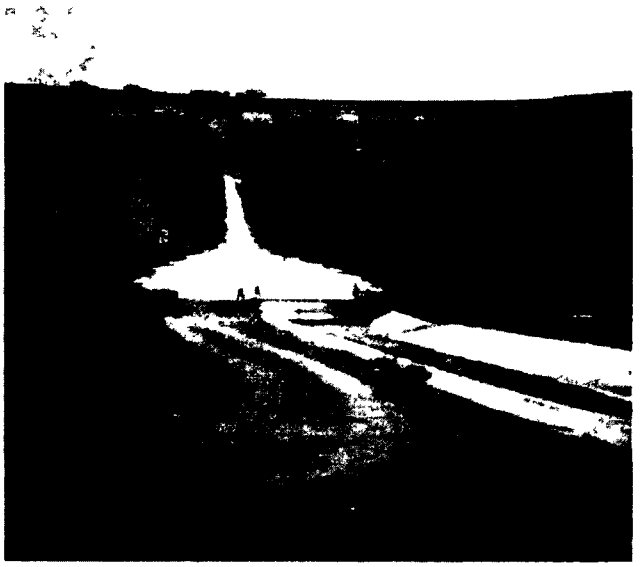

Figure 1-2: St. Francis dam before failure

Figure 1-3: St. Francis dam after failure

Another famous concrete dam failure was Malpasset Dam in France. The dam was a double curvature arch dam of 66.5 m maximum height, with a crest length of 223 m. The dam failed explosively on 2nd December 1959. A total of 433 casualties were reported (Goutal, 1999). Investigations after the accident showed that the key factors in the failure of the dam were the pore water pressure in the rock, and the nature of the rock. Under the increasing pressure of rising water, the arch separated from its foundation and rotated as a whole about its upper right end. The whole left side of the dam collapsed, followed by the middle part, and then the right

supports (Goutal, 1999). Figure 1-4 shows the Malpasset dam before failure. Figure 1-5 to 1-7 show the Malpasset dam after failure.

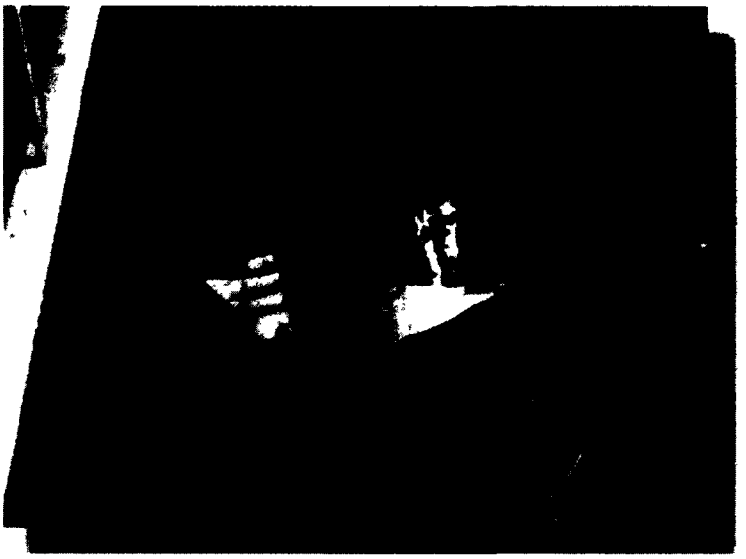

Figure 1-4: Malpasset Dam before failure

Figure 1-5: Maipasset Dam after failure

Figure 1-6: Looking from upstream, part of the wing wall remained on the left abutment

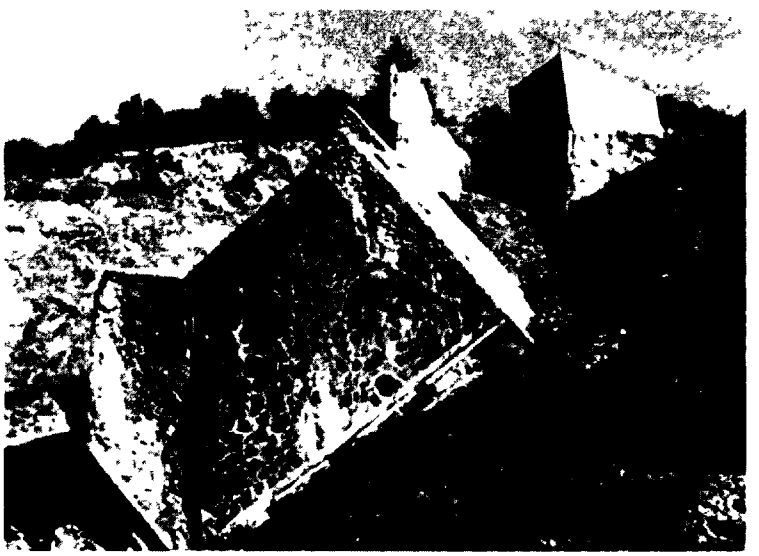

Figure 1-7: Almost nothing remained on the right abutment

But could failure have been avoided if the cracking had been investigated? This is one of the most important lessons learnt from the Malpasset dam failure that is taken very seriously today.

It can be noted that the use of adequate monitoring systems is a powerful tool for understanding kinematic aspects of mass movements and permits their correct analysis and interpretation; in addition, it is an essential aid in identifying and checking alarm situations.

Dams with complex foundations, known geologic anomalies, marginal design criteria, or unconservative assumptions usually require more instrumentation to demonstrate satisfactory performance than dams without those features. Collapses of dam structures such as Malpasset dam have demonstrated once again the need for a reliable tool for an early monitoring of damage progression.

1.2. Discontinuities in dam structure

Discontinuities play an important role in the behavior of dam under normal and shear loading conditions. They cause reduction of strength and increase of deformability in dam structures. Thus the safe management of dam operation requires a precise evaluation of the dam stability in terms of the shear strength of the concrete-rock contact, a concrete lift joint or a discontinuity in the rock mass. Figures 1-8 to 1-10 show the three kinds of failure in dam caused by discontinuities.

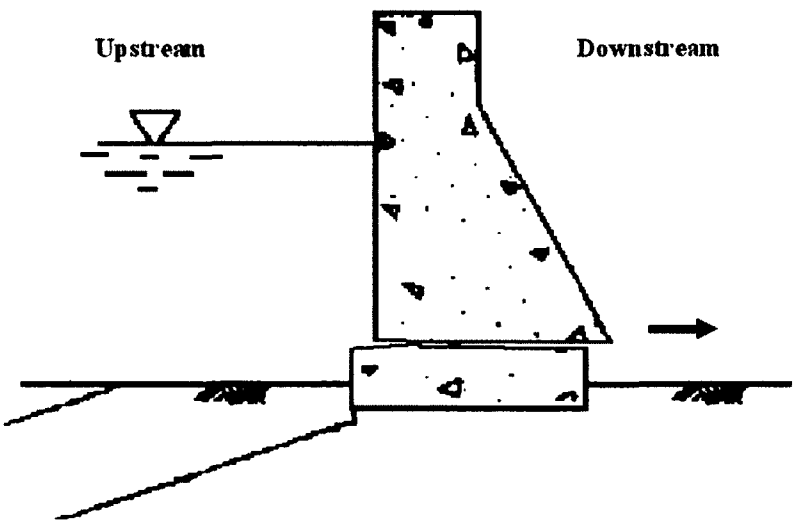

Figure 1-8: Failure along concrete discontinuity (after U.S. Army Corps of Engineers, 1994)

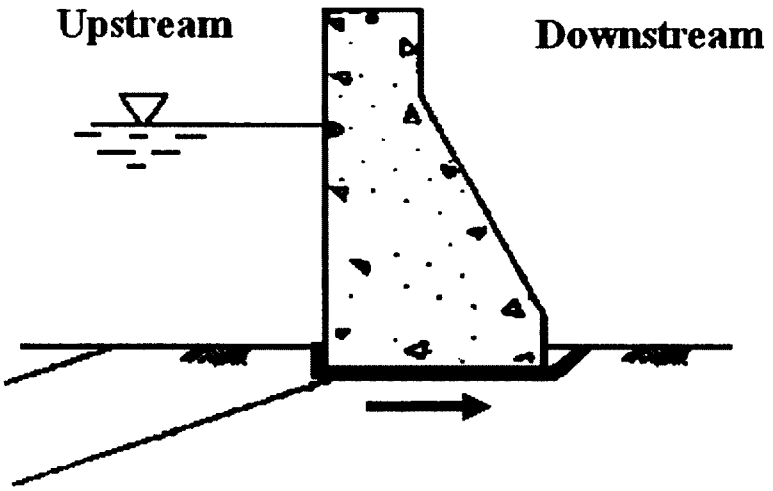

Figure 1-9: Failure along interface discontinuity (after U.S. Army Corps of Engineers, 1994)

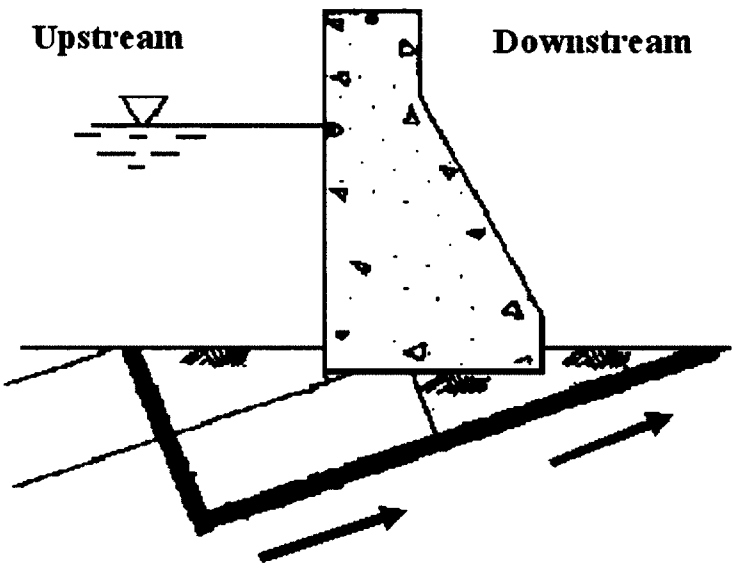

Figure 1-10: Failure along rock discontinuity (after U.S. Army Corps of Engineers, 1994)

The appropriate definition of failure generally depends on the shape (envelope) of the shear stress versus shear deformation/strain as well as the mode of potential failure. Regardless of the mode of potential failure, the selection of shear strength parameters for use in the design process invariably involves the testing of appropriate specimens. Selection of the type of test best suited for intact or discontinuous structure, as well as selection of design shear strength parameters, requires an appreciation of joint failure characteristics (U.S. Army Corps of

Engineers, 1994). Figure 1-11 illustrates three general shear stress-deformation curves commonly associated with joint failure.

The typical failure envelope for a clean discontinuity is curvilinear. At stress levels associated with low head gravity dams, retaining walls and slopes, almost all joints behave in a strain softening manner at failure. Strain softening failure is specified by a rapid increase in applied stress, with small strains, until a peak stress is obtained. Further increases in strain causes a rapid drop off in stress and then the residual stress value is reached.

Curve Type	Typical Joint Failure Mode
A	Intact or clean rough discontinuties
B	Clean smooth discontinuties
C	Discontinuties with thick soft fillings

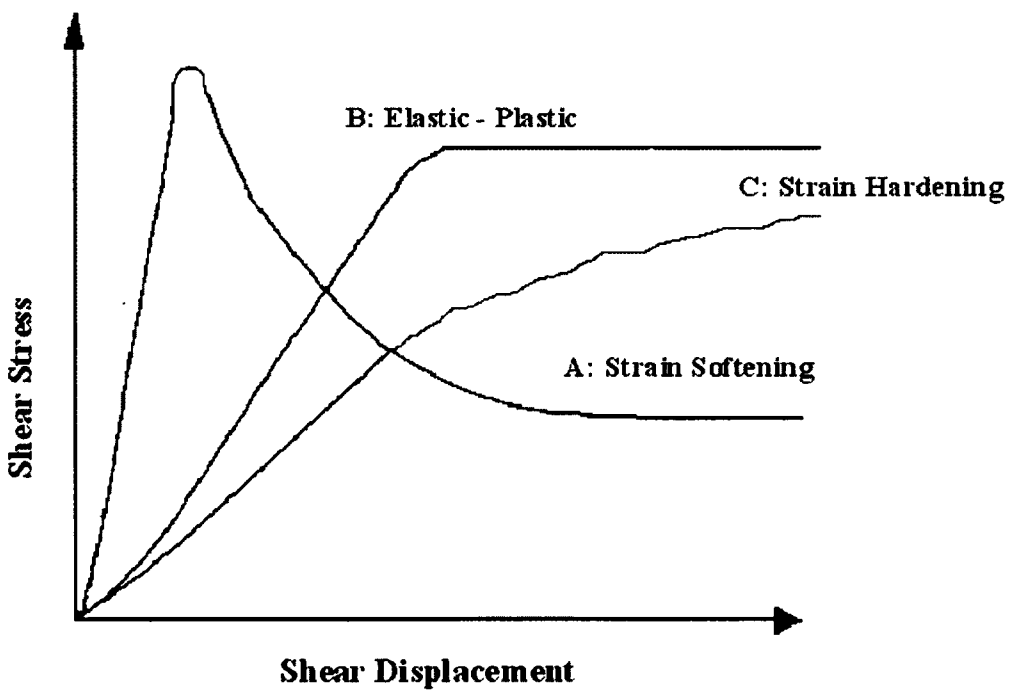

Figure 1-11: general shear stress versus shear displacement curves (modified after Nicholson 1983)

Mohr-Coulomb equation is one of the first equations representing the relationship between the peak shear strength τ_p and the normal stress σ_n:

$$\tau_p = c + \sigma_n \tan\phi \qquad (1\text{-}1)$$

Where c is the cohesive strength of the cemented surface and ϕ is the angle of friction.

In the case of the residual strength, the cohesion c has dropped to zero and Mohr-Coulomb equation is represented by:

$$\tau_p = \sigma_n \tan\phi_r \qquad (1\text{-}2)$$

Where ϕ_r is the residual angle of friction.

A natural discontinuity surface in hard rock is never as smooth as a sawn or ground surface. The undulations and asperities on a natural joint surface have a significant influence on its shear behaviour. Generally, this surface roughness increases the shear strength of the surface, and this strength increase is extremely important in terms of the stability of excavations in rock.

Patton (1966) demonstrated this influence by means of an experiment in which he carried out shear tests on saw-tooth specimens.

Shear displacement in these specimens occurs as a result of the surfaces moving up the inclined faces, causing dilation (an increase in volume) of the specimen. The shear strength of Patton's saw-tooth specimens can be represented by:

$$\tau_p = \sigma_n \tan(\phi_b + i) \qquad (1\text{-}3)$$

Where ϕ_b is the basic friction angle of the surface and i is the angle of the saw-tooth face.

Equation (1-3) is valid at low normal stresses where shear displacement is due to sliding along the inclined surfaces. At higher normal stresses, the strength of the intact material will be exceeded and the teeth will tend to break off, resulting in a shear strength behaviour that is more closely related to the intact material strength than to the frictional characteristics of the surfaces.

While Patton's approach has the merit of being very simple, it does not reflect the reality that changes in shear strength with increasing normal stress are gradual rather than abrupt.

Ladanyi and Archambault (1970) suggested the shear strength of the material adjacent to the discontinuity surfaces:

$$\tau = \frac{\sigma_n(1-a_s)(V+Tan\phi)+a_s.\tau_r}{1-(1-a_s)VTan\phi_B} \qquad (1\text{-}4)$$

where τ is joint shear strength, ϕ_B is basic friction angle, a_s is the proportion of the discontinuity surface which is sheared through projections of intact material, V is the dilation rate (dv/du) at peak shear strength, and τ_r is the shear strength of the intact material.

They defined a_s to be the area where shearing through the asperities takes place. Over the rest of the surface, 1 - a_s, the asperities are assumed to slide over each other without damage.

Barton (1973) studied the behaviour of natural rock joints and has proposed this equation:

$$\tau_p = \sigma_n \tan(\phi_b + JRC\log_{10}(\frac{JCS}{\sigma_n}) \qquad (1\text{-}5)$$

Where JRC is the Joint Roughness Coefficient and JCS is the Joint Wall Compressive Strength.

Surfaces of discontinuous rock are composed of irregularities or asperities ranging in roughness from almost smooth to sharply inclined peaks. Conceptually there are three modes of failure: asperity override at low normal stresses (sliding process), failure through asperities at high normal stresses (shearing process), and a combination of asperity override and failure through asperities at intermediate normal stresses.

Patton (1966) recognized that the asperity of a rough joint occurs on many scales. He first categorized asperity into first-order (waviness) and second-order (unevenness) categories. The behavior of rock joints is controlled primarily by the second-order asperity during small displacements and the first-order asperity governs the shearing behavior for large displacements. Barton (1973) and Hoek and Bray (1981) also stated that at low normal stress levels the second-order asperity (with higher-angle and narrow base length) controls the shearing process. As the normal stress increases, the second-order asperity is sheared off and the first-order asperity (with longer base length and lower-angle) takes over as the controlling factor.

As indicated in Figure 1-12, first-order irregularities generally have smaller angles of inclination than second-order irregularities.

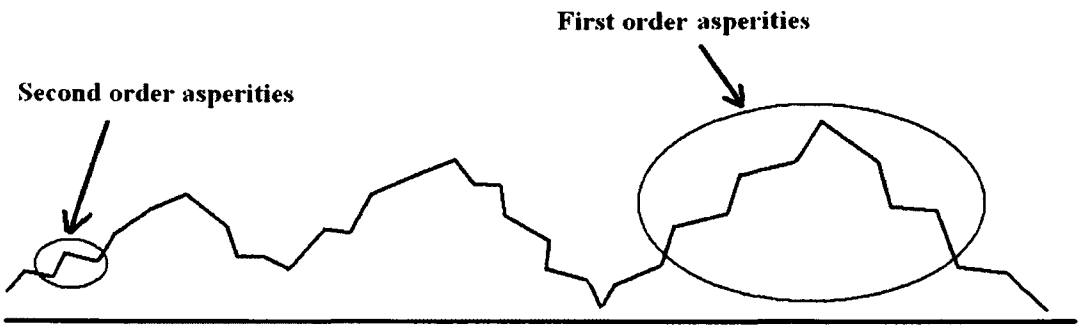

Figure 1-12: First order and second order asperities, the main undulations are considered as first order asperities and the small teeth on these undulations are considered as second order asperities

It is recognized that a precise measurement of the rough surface topography is necessary to study the shearing mechanism and predict the peak and residual strength of rock joints, as well as the amount of dilatation a discontinuity undergoes during shearing.

The joint roughness coefficient (JRC) proposed by Barton (1973), has been widely used in engineering practice. The JRC value scales the joint roughness in the range from 20 (rough) to 0 (smooth) and can be determined by various methods.

The JRC can be estimated by comparing the appearance of a discontinuity surface with standard profiles published by Barton and others. One of the most useful of these profile sets was published by Barton and Choubey (1977).

The appearance of the discontinuity surface is compared visually with the profiles shown and the JRC value corresponding to the profile which most closely matches that of the discontinuity surface is chosen. In the case of small scale laboratory specimens, the scale of the surface roughness will be approximately the same as that of the profiles illustrated. However, in the field the length of the surface of interest may be several meters or even tens of meters and the JRC value must be estimated for the full scale surface.

On the basis of extensive testing of joints, joint replicas, and a review of literature, Barton and Bandis (1982) proposed the scale corrections for JRC defined by the following relationship:

$$JRC_n = JRC_0\left(\frac{L_n}{L_0}\right)^{-0.02JRC_0} \qquad (1\text{-}6)$$

Where JRC_o, and L_o refer to 100 mm laboratory scale samples and JRC_n, and L_n refer to in situ sizes.

Many researchers have also investigated the applicability of various conventional statistical parameters for calculating the JRC. Tse and Cruden (1979) found that among eight different statistical parameters, two parameters, Z_2 (the slope of asperity) and SF (structure function) are strongly correlated with the values of JRC.

$$JRC_0 = 32.2 + 32.47\log(Z_2) \quad (1\text{-}7)$$

$$\text{JRC}=7.1496\ln(\text{SF}) + 37.014 \quad (1\text{-}8)$$

Detailed laboratory investigations, however, indicated that JRC varies not only from fracture to fracture but also with scale. The limitation of JRC and the conventional statistical parameters in quantifying joint roughness have also been reported by Kulatilake et al (1995). Therefore, surface roughness of rock joints need to be characterized using a scale-invariant parameter.

In recent years, because of the pioneering work of Mandelbrot (1983) on fractal geometry, there have been a number of studies to investigate the applicability of fractal models to characterize roughness of fracture surface. The attraction of a fractal model lies in its ability to predict scaling behavior, i.e., the relationship between surface geometry observed at different scales.

Assuming the rock surface profiles are self-similar fractals, researchers such as Carr and Warriner (1989), Lee et al. (1990), and Wakabayashi and Fukushige (1992) have developed relations between the fractal dimension D and the JRC_0. The relations are as follows:

Carr and Warriner (1989):

$$JRC_0 = -1022.55 + 1223.92D \quad (1\text{-}9)$$

Lee et al., (1990):

$$JRC_0 = -0.8780 + 37.7844\left(\frac{D-1}{0.015}\right) - 16.9304\left(\frac{D-1}{0.015}\right)^2 \quad (1\text{-}10)$$

Wakabayashi and Fukushige (1992):

$$JRC_0 = \sqrt{\frac{D-1}{0.00004413}} \quad (1\text{-}11)$$

Although all these approaches are useful for describing profiles, they are not sufficient to

capture the features necessary for characterising three dimensional (3D) roughness strength (Grasselli et al, 2002). Recently researchers have focused their attention on identifying 3D parameters to quantify the relationship between the surface roughness and shear strength (Gentier and Hopkins, 1997, Lanaro et al, 1998, Grasselli et al. 2002).

Generally, shearing of joints occurs in situ under a variety of boundary conditions. However, it is possible to identify two different characteristic behaviors: the first condition, where a rock block slides down a rock slope, the normal load acting on the joint surface remains constant during the shearing process. In this case, shearing occurs under a constant normal load (CNL, free dilation) condition. Figure 1-13 shows this boundary condition.

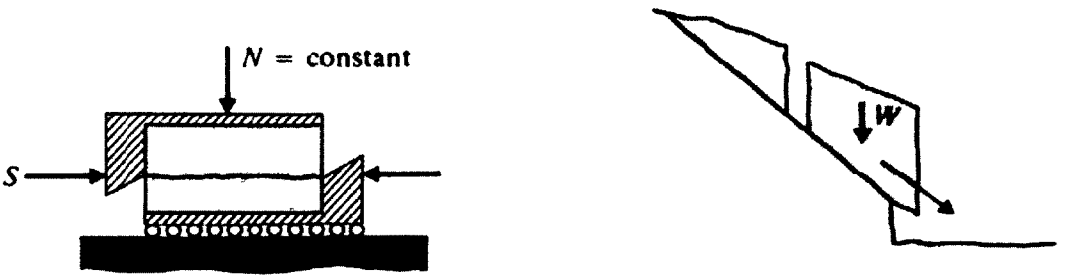

Figure 1-13: Constant normal load condition (after Brady and Brown, 2005)

The second condition, where a block on the roof or the sidewalls of an underground excavation is extruded into the opening, the normal load on the joint surface is no longer constant, but continuously evolved due to the restriction on the normal dilation (figure 1-14).

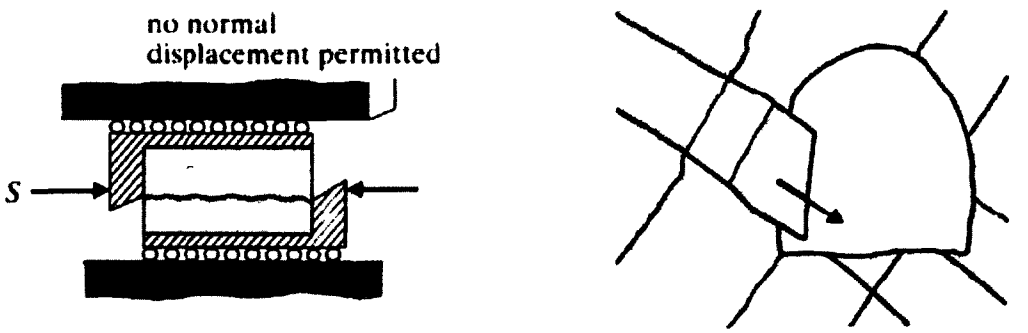

Figure 1-14: Simulation of constant normal stiffness condition (after Brady and Brown, 2005)

Nevertheless, the mechanical behavior of shear tests made under constant normal load (CNL) or constant normal stiffness (CNS) conditions differs only after the peak, when dilation plays an important role, inducing an increment in the normal stress. This increment is proportional to the stiffness of the rock. Before reaching the peak, since very little or no dilation has occurred, both types of shear tests follow the same path (Ohnishi and Dharmaratne 1990, Skinas et al 1990 and Olsson and Barton 2001).

For studying the joint behavior in dam body and under the foundations of dams, it can be assumed that the high water pressure against the face of the dam produces shearing along fractures. Depending on the orientations of the joint sets and their depth, each joint can dilate freely under a normal load in the range of 0.2– 5.0MPa. Therefore for these situations, the most appropriate laboratory experimental shear test set-up is the CNL condition (Grasselli, 2001).

1.3. Acoustic emission monitoring

Acoustic Emissions are stress waves produced by sudden movement in stressed materials. The classic sources of acoustic emissions are defect-related deformation processes such as crack initiation and crack propagation. The process of generation and detection is illustrated in Figure 1-15.

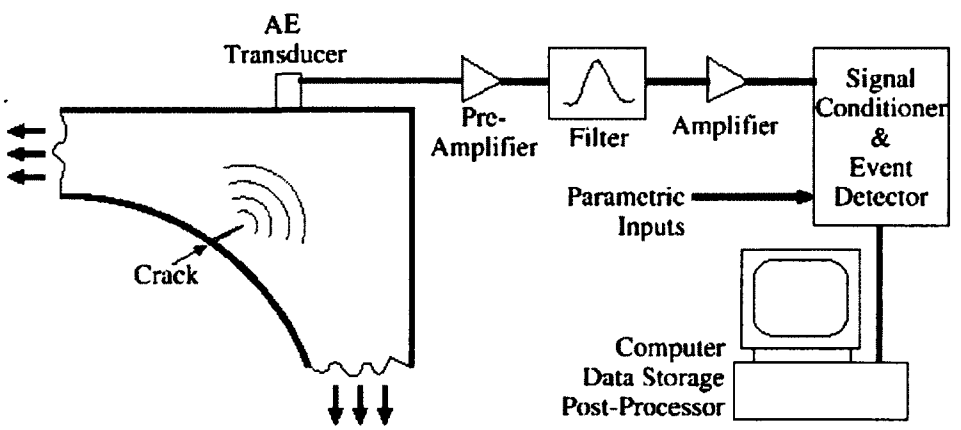

Figure 1-15: Basic principle of Acoustic Emission (after Huang et al., 1998)

Sudden movement at the source produces a stress wave, which radiates out into the structure and excites a sensitive piezoelectric transducer. As the stress in the material is raised, many of these emissions are generated. The signals from one or more sensors are amplified and measured to produce data for display and interpretation.

Without stress, there is no emission. Therefore, an acoustic emission (AE) inspection is usually carried out during a controlled loading of the structure. This can be a proof load before service, a controlled variation of load while the structure is in service, a fatigue test, a creep test, or a complex loading program. Often, a structure is going to be loaded anyway, and AE inspection is used because it gives valuable additional information about the performance of the structure under load. Other times, AE inspection is selected for reasons of economy or safety, and a special loading procedure is arranged to meet the needs of the AE test (Pollock, 2005).

In geologic material, the origin of AE activity appears to be related to processes of deformation and failure which are accompanied by a sudden release of energy. In such materials, which are basically polycrystalline in nature, AE activity may originate at the micro level as a result of dislocations, at the macro level by twining, grain boundary movement, or initiation and propagation of fractures through and between mineral grains and at the mega level by fracturing and failure of large areas of material or relative motion between structural units (Hardy, 2003).

Acoustic emission differs from most other nondestructive testing (NDT) methods in two key respects. First, the signal has its origin in the material itself, not in an external source. Second, acoustic emission detects movement or crack propagation, while most other methods detect existing geometrical discontinuities. The consequences of these fundamental differences are summarized in Table 1-1.

Table 1-1: Characteristics of acoustic emission method compared with other NDT methods (after Pollock, 2005)

Acoustic Emission	Other NDT Methods
Detects movement of defects	Detect geometric form of defects
Requires stress	Do not require stress
Each loading is unique	Inspection is directly repeatable
More material-sensitive	Less material-sensitive
Less geometry-sensitive	More geometry-sensitive
Less intrusive on plant/process	More intrusive on plant/process
Requires access only at sensors	Requires access to whole area of inspection
Tests whole structure at once	Scan local regions in sequence
Main problems: noise related	Main problems: geometry related

Precautions must be taken into account against interfering noise as an important part of AE technology. The first point is selection of an appropriate frequency range for AE monitoring. The acoustic noise background is highest at low frequencies. On the other hand because higher frequencies bring reduced detection range, there is an inherent trade-off between detection range and noise elimination (Pollock, 2005). The frequencies of interest for field and laboratory studies in the general geotechnical area (i.e., rock and soil mechanics) extend over a wide central region of the overall frequency rage (10^0<f<5 * 10^5 Hz). It is clear, therefore, that AE studies in the geotechnical filed overlap at low frequencies with seismology, and at high frequencies with material science related AE studies (Hardy, 2003).

Noises can be stopped at the source. Applying impedance mismatch barriers or damping materials at strategic points on the structure is another way to eliminate an acoustic noise. Differential sensors or sensors with built-in preamplifiers are useful for eliminating electrical noise problems which are often the result of poor grounding and shielding practices. If noises can not be omitted through hardware setup, the problem must be dealt with by software setting in the AE instrument. One of the effective ways is sensitivity adjustments including fixed and floating threshold techniques. Signal filtering for selective acceptance and recording of data based on time, load, or spatial origin are very useful for collecting agreeable signals. Moreover,

because noise sources often give characteristically different waveforms, advanced waveform analysis package can help us to differentiate noises from AE signals (Pollock, 2005).

Interesting aspects for acoustic emission are the monitoring of damage development in critical parts of a structure. Compared to other active ultrasonic methods that assess mainly the structure itself or existing failures, the power of AE analysis is the possibility to directly observe the process of deterioration. With AE analysis spatial and temporal correlations are examined. One aspect of monitoring a stressed structure is to localize AE sources and, in this way, to observe the region where damage takes place. On the other hand, investigation of the AE activity in terms of signal rate or event magnitude distribution could indicate the stage of damage progress. The aim is to obtain reliable relations that can be applied during the AE monitoring for condition assessment of the structural component. This way of data analysis could contribute to an early warning (alarm) system that is able to detect precursors of a soon failure.

When joints (construction joints in concrete, concrete-rock interfaces and rock joints in foundation) are under loading, once a critical state of shear stress is reached, a certain part of the joint is deformed. The identification of this predisposed stage before total failure is important to reduce the danger of sudden release of deformation energy. This prevention process can be done by AE monitoring.

Over the past few decades parameter-based and signal-based acoustic emission (AE) techniques were developed into a sophisticated tool for non-destructive testing of several materials.

Parameter-based AE techniques identify AE wave packets searching for particular parameters. The essential parameters for interpretation such as hits, amplitude and wave energy can be used with their occurrence rate or their accumulated trend in the time domain (Grosse 2007). Wave amplitudes exceeding a defined threshold value are referred to as AE events. Signals below the threshold value are considered as noise. Signal-based AE techniques consider the complete waveform. Typically, a waveform consists of a compression or primary wave (P-wave), a shear or secondary wave (S-wave) and surface waves. The arrival time (onset time) of the P-wave of each event can be determined (picked) and used to localize the respective source (Kurz et al. 2005).

1.4. Objectives of the thesis

The main objective of this research is to evaluate the application of acoustic emission for monitoring shear behavior of joint in laboratory as a feasibility study for monitoring shear behavior of active joints in dam body, interface joint between dam body and rock mass and rock joints in dam foundation. In fact simulating various kinds of joints with different characteristics and correlating AE and shear test results in laboratory helps us to have a better interpretation of shear process of the in situ discontinuities.

- A methodology for detecting and interpreting the AE signals during direct shear test of joints is developed. In this methodology, sample preparation, testing procedure, AE set up, recommendations for solving the problems during the test, data analysis, drawing the various graphs and finally interpretation of the results are discussed. By interpretation of test results one can obtain a better understanding of correlation between AE and joint behavior during pre-peak, peak and post-peak sections occurring within loading a joint in laboratory.
- By evaluation AE source locations over the joint surface at first one can determine the contribution percentage of joint surface in shearing process and then determine what happens with asperities during several stage of shear loading (initial point of shear displacement, yield point, maximum shear strength and residual shear strength).
- Surface roughness, bonding percentage, normal load and displacement rate are the most important parameters that affect the shear behavior of the joints. Any change in these parameters makes a significant change in shear behavior and consequently in generated AE signals. In this study the effect of these parameters on generated AE signals during direct shear test of different kinds of joints is investigated.

1.5. Originality of the thesis

During last years several studies have been done at Laboratory of Rock Mechanics in Université de Sherbrooke either on acoustic emission or on shear strength of rock and concrete joints. Nadia Feknous (1991) used acoustic emission for monitoring different stress levels and mechanisms of deterioration of rock-grout contacts in a rock hole which has been injected by cement grout. Aziz bouja (1994) used acoustic emission for controlling the quality of injection

in a fractured rock by injecting grout in a cored rock hole. Tarik El Malki (2006) tested bonded concrete-rock joints to investigate the effect of different shearing directions on shear strength parameters of the rock joints. Baptiste Rousseau (2010) tested bonded and non-bonded concrete-concrete; concrete-rock and rock-rock joints to investigate the effect of joint morphology (roughness) on shear strength parameters of the rock joints. Felix-Antoine Martin (2011) used identical non-bonded concrete-concrete joints in order to clearly identify the influence of temperature on the shear strength of joints.

There are a few researches related to application of AE for monitoring shear behavior of joints (Li & Nordlund 1990, Sasao et al. 2003, Hong & Jeon 2004, Rim & Choi 2005, Shiotani 2006, Ishida et al. 2010). The previous researchers applied shear test and detected AE signals. They showed that AE can be used to represent shear behavior of rock joints. For example they showed that AE signals are increased when joint is going to failure and AE signals attain their maximum values after peak shear stress. Some other researchers used AE method to localize AE events (Hong & Jeon 2004). They showed that with AE localization it is possible to find the zones which contribute in shearing process. The originality of this thesis can be categorized into the following sections:

- None of these researchers have described precisely the methodology for detecting AE signals during direct shear test, for example: sensor selection criteria, attaching the sensors, frequency range, noise, etc. In this study a methodology is developed with all of the required details for detecting and interpreting the AE signals during direct shear test for various kinds of joints.
- The previous researches have been done on limited number of joints, so their conclusions constrain to these limited samples. In this study it was tried to apply direct shear test and detect AE signals on various kinds of joints (rock-rock, rock-concrete and concrete-concrete joints) in two main categories: homogenous (using blocks of the Barre granite from Vermont, USA) and heterogeneous samples (samples from Manic 5 project which are almost heterogonous in mineralogy, porosity, etc).
- The shear behavior of joints is related to the joint characteristics (roughness, bonding etc.) and loading conditions (normal load, displacement rate etc.) while the previous researchers just studied the correlation between AE signals and shear stress-shear displacement graphs of the joints. None of them have verified the effect of these parameters on AE signals and

shear behavior of the joints. In this thesis it will be shown how AE signals, AE localization and finally the shear behavior of the joints are changed with applying different values of these parameters.

- Many researchers have studied the damaged zones of shear surfaces during direct shear test using scanned surfaces and image analysis. In fact by using scanned surfaces or image processing of joint surfaces it's cumbersome to identify which kind of asperity starts shearing and which kind of asperity damages after yield point, maximum shear strength or during residual section. In this thesis it will be tried to correlate the AE localization (which it is possible to localize the damaged zone in any loading stage) with the results of image processing and 2d and 3d graphs of the scanned surfaces.

1.6. Outline

The thesis is divided into 6 chapters. The first chapter includes context, research objectives and originality of the thesis. Chapter II, III, IV and V are presented by published or submitted papers extracted from the results of this study. Chapter II presents a study on characteristic features of acoustic emission parameters during direct shear test of rock joints. In the chapter 3 asperity damage during shear tests of joints is evaluated using acoustic emission. Chapter IV contains the results of AE monitoring during direct shear tests of bonded joints. In Chapter V the results of the AE source localization are correlated with shear damaged zones shown by scanned surfaces and image analysis. Finally Chapter VI provides conclusions and recommendation for future studies. Table 1-2 to 1-6 contain characteristics of the artificial and natural joints samples used in this thesis.

Table 1-2: Non-bonded rock-rock joints used in chapter 2 and 5

Sample	Diameter-X(cm)	Diameter-Y(cm)	Normal stress (MPa)
33	140	160	0.5-1-1.5-2-1.5-1-0.5
22	143	151	0.5
44	143	143	0.5
25	143	147	1
34	143	148	2-1.5-0.5-1.5-2
12	143	155	1
15	143	143	2

Table 1-3: Bonded concrete-rock joints used in chapter 3 for study the effect of normal load

sample	Diameter-X(cm)	Diameter-Y(cm)	Normal stress
43-1	14.3	15.5	0.25
43-2	14.3	15.5	0.75
31-1	14.3	15.2	0.5
31-2	14.3	15.2	1.25
54-1	14.3	15.1	0.15
54-2	14.3	15.1	0.65

Table 1-4: Bonded concrete-rock joints used in chapter 3 for study the effect of displacement rate

sample	Diameter-X(cm)	Diameter-Y(cm)	Displacement rate
32-1	14.3	14.7	0.10
32-2	14.3	14.7	0.15
21-1	14.3	14.7	0.05
21-2	14.3	14.7	0.10
24-1	14.3	14.7	0.20
24-2	14.3	14.7	0.25

Table 1-5: Bonded concrete-rock joints used in chapter 3 for study the effect of bonding percentage

sample	Diameter-X(cm)	Diameter-Y(cm)	Bonding (%)
42-1	14.3	14.8	10
42-2	14.3	14.8	28
14-1	14.3	14.8	50
14-2	14.3	14.8	75
41-1	14.3	15.5	0
41-2	14.3	15.5	100

Table 1-6: List of natural samples cored from Manic 5 dam and used in chapter 3

Sample number	Deep (m)	Diameter (mm)	Type	Bonded or non- bonded
MC4-CC-3.10	3,10	83	Concrete-concrete	Non-bonded
MC4-CC-2.34	2,34	83	Concrete-concrete	Non-bonded
MC4-CC-10.30	10,30	83	Concrete-concrete	Non-bonded
MC6-CC-2.18	2,18	145	Concrete-concrete	Non-bonded
MC6-CC-3.97	3,97	145	Concrete-concrete	Non-bonded
MC6-CC-8.35	8,35	145	Concrete-concrete	Non-bonded
MC4-CC-7.22	7,22	83	Concrete-concrete	Bonded
MC4-CC-6.98	6,98	83	Concrete-concrete	Bonded
MC4-CC-9.15	9,15	83	Concrete-concrete	Bonded
MC6-CC-6.60	6,60	145	Concrete-concrete	Bonded
MC6-CC-3.45	3,45	145	Concrete-concrete	Bonded
MC4-RC-13.44	13,44	83	Concrete-rock	Non-bonded
MC6-RC-5.36	5,36	145	Concrete-rock	Non-bonded
MC6-RC-7.63	7,63	145	Concrete-rock	Non-bonded
MC4-RC-5.20	5,20	83	Concrete-rock	Bonded
MC6-RC-9.20	9,20	145	Concrete-rock	Bonded
MC4-RC-13.76	13,76	145	Concrete-rock	Bonded
MC4-RR-5.54	5,54	83	Rock-rock	Non-bonded
MC4-RR-16.65	16,65	83	Rock-rock	Non-bonded
MC6-RR-10.48	10,48	145	Rock-rock	Non-bonded
MC6-RR-6.19	6,19	145	Rock-rock	Non-bonded
MC6-RR-10.00	10,00	145	Rock-rock	Non-bonded
MCC8-F-1A	0,40	200	Concrete-concrete	Non-bonded
MCC8-F-1B	0,23	200	Concrete-concrete	Non-bonded
MCC8-F-1C	0,50	200	Concrete-concrete	Bonded

2. STUDY ON THE CHARACTERISTIC FEATURES OF ACOUSTIC EMISSION PARAMETERS DURING DIRECT SHEAR TEST OF ROCK JOINTS

Autors and affiliation:
Z. Moradian: PhD student, Université de Sherbrooke, Faculté de génie, Département de génie civil.
G. Ballivy: professeur, Université de Sherbrooke, Faculté de génie, Département de génie civil.
P. Rivard: professeur, Université de Sherbrooke, Faculté de génie, Département de génie civil.

Date of submission: 8 November 2010

Acceptation state: Submitted

Journal: International Journal of Rock Mechanics and Mining Sciences

Reference: [IJRMMS-D-10-00324]

Titre français: Etude des caractéristiques des paramètres d'émission acoustique pendant l'essai de cisaillement direct des joints rocheux

Contribution in paper:
The author of the thesis has contributed in this paper as first, principal and corresponding author.

Résumé français:
Afin d'évaluer l'applicabilité de l'émission acoustique (EA) comme un indicateur de l'instabilité des discontinuités actives dans les structures d'un barrage, une vaste étude de faisabilité a été effectuée sur 40 échantillons. À cette fin, des essais de cisaillement direct en charge normale constante (CNC) ont été réalisés dans des conditions différentes (avec diverses charges normales et diverses vitesses de déplacement) et différentes caractéristiques (rugosités et pourcentages de liaison). Les signaux d'EA ont été acquis au moyen de capteurs placés sur les échantillons. Une analyse a été effectuée afin de trouver les différences entre les

paramètres d'EA à partir du comportement en cisaillement des joints rocheux pendant les essais de cisaillement direct. L'amplitude, les comptes (counts), l'énergie, la duration et le temps de montée, soit les cinq paramètres d'EA les plus largement utilisés sont comparés dans cette étude. Deux méthodes ont été utilisées pour vérifier les caractéristiques de ces paramètres. Dans la première méthode, plusieurs échantillons ont été testés sous des contraintes normales de 0,5, 1 et 2 MPa, respectivement. Dans la seconde méthode, la contrainte normale a été modifiée de 0,5 à 2 MPa dans la section résiduelle d'un même échantillon. Les résultats expérimentaux montrent que la charge normale a un effet significatif sur les caractéristiques des paramètres d'EA au cours des essais de cisaillement des joints rocheux. Une analyse combinant des paramètres d'EA avec le comportement contrainte-déplacement des joints rocheux est utile pour détecter le mouvement de cisaillement et pour déterminer les circonstances de la rupture des joints actifs à un stade beaucoup plus précoce, avant une rupture soudaine.

Abstract

In order to evaluate the applicability of the acoustic emission (AE) as an indicator of instability of active joints in dam structures, an extensive feasibility study was done on 40 joint samples. To this end, constant normal load direct shear tests (CNL) were conducted under different conditions (in various normal loads and displacement rates) and different joint characteristics (with various roughness and bonding percentages) and AE signals were acquired using attached sensors to the samples. An analysis was performed in order to find out the differences between acoustic emission parameters in showing shear behavior of rock joints subjected to direct shear test. Amplitude, counts, energy, duration and rise time as the five most widely used AE parameters are compared in this study. Two methods were used to verify the characteristics of these parameters. In the first method several samples were tested under normal stresses of 0.5, 1 and 2 MPa respectively. In the second method normal stress was changed from 0.5 to 2 MPa in the residual section of the same sample. Experimental results showed that normal load has a significant effect on characteristics of AE parameters during shear testing of rock joints. A combining analysis of the AE parameters with stress-displacement behavior of rock joints is useful in detecting shear movement and determining

failure circumstances of active joints at a much earlier stage, before unexpected collapse takes place.

2.1. Introduction

Stability or instability of rock mass mostly depends on rock joints. In order to monitor cracking and damaging of rock mass, instrumentation systems are installed. One of the most precise and fastest methods for monitoring crack initiation and propagation in rock mass is AE. AE is defined as rapid release of elastic waves by cracking and damaging of materials under load. Instability and failure is associated with large number of AE events, so that the greater AE activity the greater is the degree of the instability.

Parameter-based and signal-based techniques are two methods for analyzing AE signals which are currently applied. However, where a large number of AE signals have to be analyzed the parameter-based technique is chosen.

The five principal parameters (Figure 2-1) which have been used by researchers and have been accepted through the market processes are 1) amplitude: the highest peak voltage of an AE signal 2) count: number of times that the pulse crosses the threshold 3) duration: time interval between the first and the last threshold crossing 4) energy: area under the envelope of the signal and 5) rise time: time interval between first threshold crossing and signal peak.

Amplitude is directly related to the magnitude of the source event (Pollock 2003, Shiotani 2008). The amplitude is also an important parameter to determine the system's detectability (Shiotani 2008). Count depends on the magnitude of the source event (Pollock 2003) and also it depends strongly on the employed threshold and the operating frequency (Shiotani 2008). Duration depends on source magnitude, structural acoustics, and reverberation in much the same way as counts (Pollock 2003). Rise time is governed by wave propagation processes between source and sensor (Pollock 2003). Energy is sensitive to amplitude as well as duration, and it is less dependent on threshold setting and operating frequency (Pollock 2003).

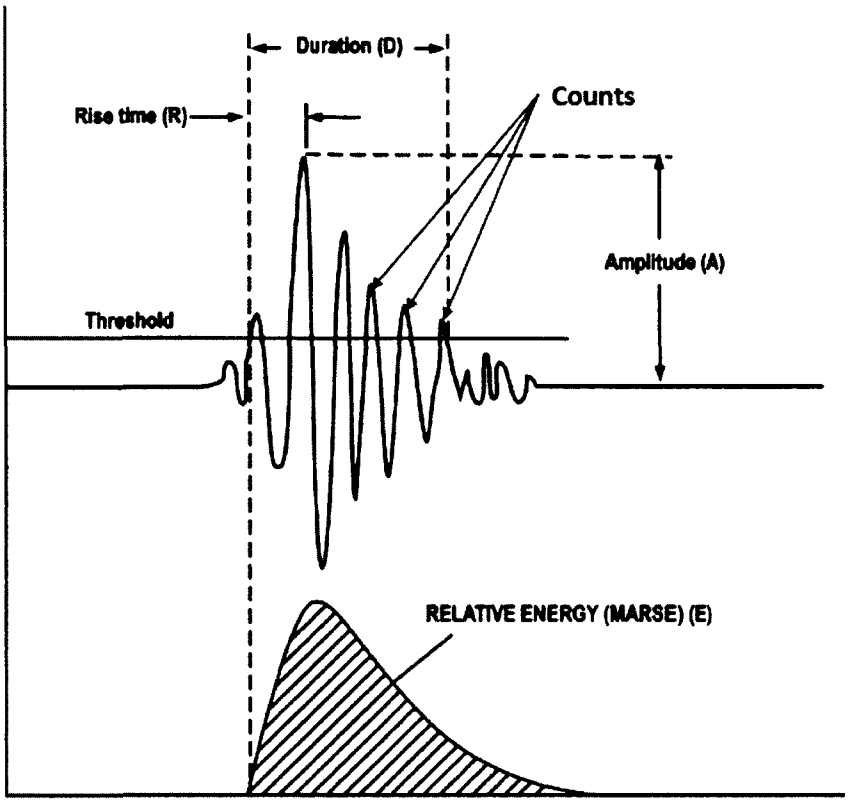

Figure 2-1: Common parameters of an AE waveform (Pollock 2003)

Previous researches have addressed application of AE parameters for monitoring rock joints both in laboratory (Li & Nordlund 1990, Hong & Jeon 2004, Rim & Choi 2005) and in site (Sasao et al. 2003 and Shiotani 2006, Ishida et al. 2010).

Li & Nordlund (1990) investigated the characteristics of AE count rate during shearing of rock joints with artificial and natural joints. Rim & Choi (2005) used AE count and energy during constant normal stiffness shear test of the artificial saw-tooth joints and replica of the natural rock joints. Sasao et al. (2003) used acoustic emission count and interpreted its results during excavation of a rock cliff with opening joints. Shiotani (2006) used AE energy and AE hit (number of detected signals on a channel) rate for evaluation of long-term stability for rock slope by means of acoustic emission technique. Ishida et al. (2010) used AE count rate during an in-situ direct shear test. From all of mentioned researches, it was found that a rapid rise of AE activity is produced as joint is approaching the failure point. Hong and Jeon (2004) showed that the maximum rates of the counts and energy are observed when the stress drops after peak shear stress.

Although several researchers have used AE parameters during their researches, however there is not a comprehensive study to show the capability of each parameter in showing shear behavior of rock joints. The principal objective of this study is to find how these parameters detect the initial movement of the joint surfaces, which one has a better indication in showing maximum shear strength, how these parameters change with normal load and finally whether interpretation of these parameters together will give a better insight about failure circumstances of the rock joints. To this end, the characteristics of the AE parameters are investigated by conducting direct shear tests on samples under various constant normal loads.

2.2. Methodology

2.2.1. Samples preparation and properties

Joint samples were prepared by tension splitting of rock cores, with 150 mm diameter, drilled on a large granite block (Barre granite from Vermont, USA). In order to allow the considered shear displacement (maximum 10 mm) without rotation of the upper surface, the shearing area of the rock joints was 17660 mm^2, greater than 2500 mm^2 in ISRM suggested method (Brown 1981). It was tried to prepare sample as close as possible to the natural joints. Table 2-1 shows physical and mechanical properties of the rock cores used for this study.

Table 2-1: Physical and mechanical properties of the granite rock cores

Parameter	Bulk specific gravity (-)	P-wave velocity (m/s)	Elastic modulus (GPa)	Poisson ratio (-)	Uniaxial compressive strength (MPa)
Number of the tests	3	3	3	3	3
Average value	2.63	4675	58.1	0.30	179

2.2.2. Scanning the joint surface and determining the roughness values

The joint surfaces (upper and lower surfaces) of samples are scanned using profilometer scanner before shear test. Figure 2-2 and 2-3 show a schematic view of the system and Zéphyr sensor. The characteristics of Zéphyr sensor are reported in Table 2-2.

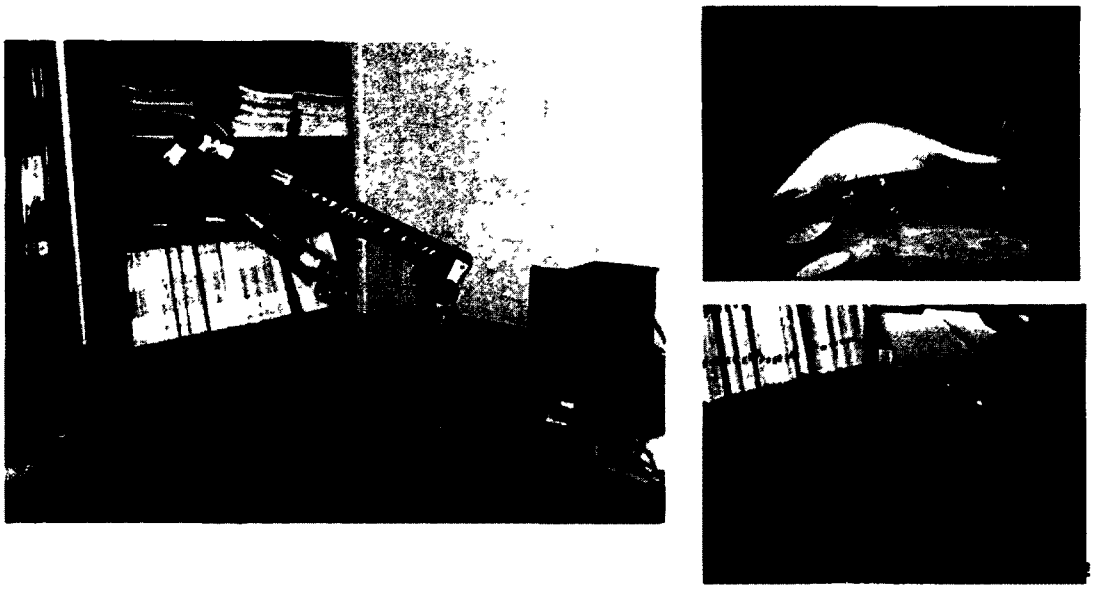

Figure 2-2: Kréon Surface Profilometer Scanner

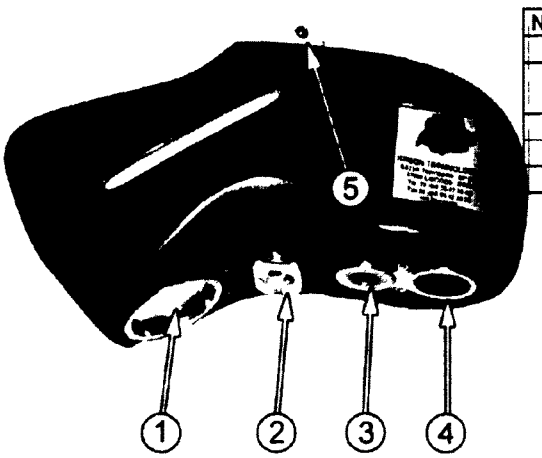

No.	Function
1	Camera
2	Green light. representing camera field area
3	Probe support
4	Laser source
5	Fitting

Figure 2-3: Zéphyr sensor overview

Table 2-2: Technical Characteristics of the Zéphyr Sensor Range: KZ25

Characteristics	**Values**
Sensor	KZ25
Laser diode	Class II
Wavelength	670 nm
Power (adjustable)	1 to 4 mW
Number of points/second	30 000
Depth of field	90 mm
Width of field	25 mm
Weight	0.360 kg
Operating temperature	0°C < t < 40°C

The profiles parallel to the direction of shear loading with a specific interval over the whole of scanned surfaces are drawn. The roughness values of the joints before test are calculated using the scanned results and are summarized in Table 2-3.

Table 2-3: Surface roughness parameters of the joint samples

Parameter	$Z_2 = \sqrt{\frac{1}{n}\sum_{i=1}^{n}\left(\frac{z_{i+1} - z_i}{\Delta y}\right)^2}$	JRC=32.2+32.47Log(Z2)
Sample 15	0.323	16
Sample 25	0.381	19
Sample 44	0.355	18
Sample 33	0.346	17
Sample 34	0.342	17

2.2.3. Attaching the AE sensors and encapsulating the sample

Sensor attachment to the samples required surface preparation with subbing sensor positions by a rotary sander. Putting lower replica in the lower half of the mould, the sample must be placed considering the shear direction. During grout pouring, the sensor positions were kept

by fixing a fiber piece between each sensor position and the wall of the mould. After pouring the fiber pieces were removed easily and sensors were put in considered holes and were attached to the sample. The Loctite Metal/Concrete Epoxy (01-81508) glue was used for attaching the sensors to the samples. This glue attaches the sensors properly to the sample and it can be removed easily after the test.

After being confident that the sensors have been attached properly to the sample, the positions of the sensors are measured for AE localization purpose. Smooth clay is used to separate the two halves of surfaces. Finally by putting the upper half of the mould and pouring the grout the mould is encapsulated. Photos A2-11 to A2-18 in appendix 2, show several steps for encapsulating the sample.

2.3. Shear testing and detecting AE signals

The shear test is carried out using a Material Testing System (MTS). The MTS press is servo-controlled and has a capacity of 2670 kN. A vertical section through the center of the apparatus has been showed on Figure 2-4. The apparatus consists of a rigid steel box (A) bolted to a thick disc (B) screwed in its center to the hydraulic piston of the press (C). Consequently, the shearing displacement is generated by the piston in the vertical direction. Two shear boxes (D and E) are designed to receive the two parts of the sample (F and G). The right-hand side shear box (D) stands against a load cell (I) fixed at the frame of the press (K) through a steel spacer (J). During shearing, the right part (F) of the sample remains stationary. The box (D) housing the right-hand side of the sample is fixed through steel sections (L) with steel bearings (M). The shear box on the left is fixed at the base of the apparatus (A).

The system blocks its movement and rotation in the direction normal to the plan of the section. It can move in the vertical direction (shearing displacement) and following a dilation of the sample, it can move in the normal direction to the plan of shearing (normal displacement). The left hand-side shear box (E) stands against a load cell (O) to measure the applied normal load. A metal beam on simple supports (Q) allows the shear apparatus to function in a constant normal stiffness condition.

A hydraulic jack can be used instead of the metal beam to work in a constant normal load condition. A ball joint (P) connects the steel beam or the jack to the rigid steel box. The normal and shear loads are measured directly by the respective load cells (O and I): the load cell (I) to a capacity of 90 kN whereas the load cell (O) to 50 kN.

Normal and shear displacements are measured by two extensometers of high precision having a run of 25±0.05 mm. Data acquisition is carried out by the control unit.

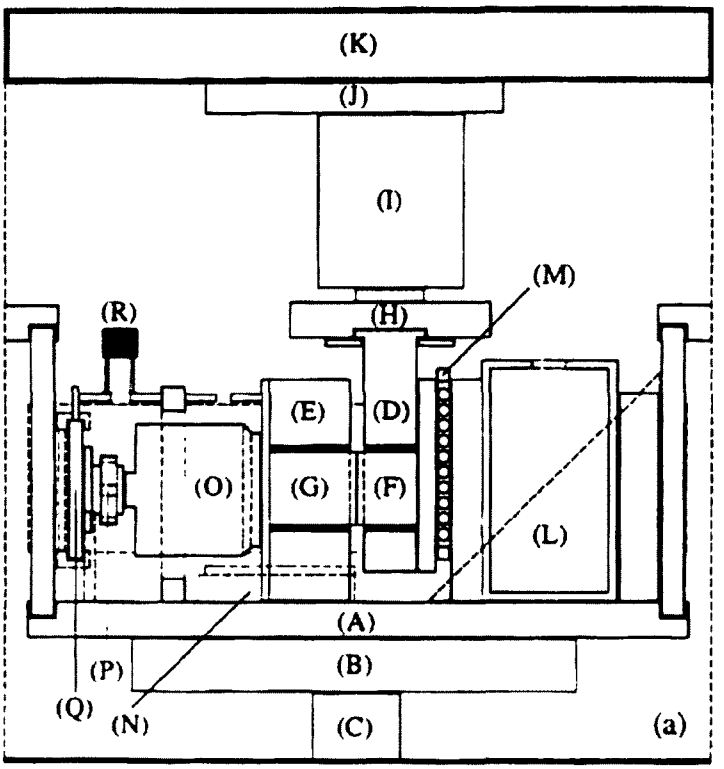

Figure 2-4: Diagram of vertical section through shear apparatus

The direct shear tests were performed on the specimens. The applied normal stresses were changed from 0.5 to 2 MPa. The rate of horizontal displacement in all tests was 0.15 mm/min and the test was finished when horizontal displacement attained 10 mm. The values of shear stress and shear and normal displacements due to applied shear loads have been recorded during each test.

During shearing the AE parameters were detected using PAC μ-SAMOS system. This system consists of two 8-channel AE data acquisition system (PCI-8). This system is very compact and can be operated from a notebook computer (Figure 2-5).

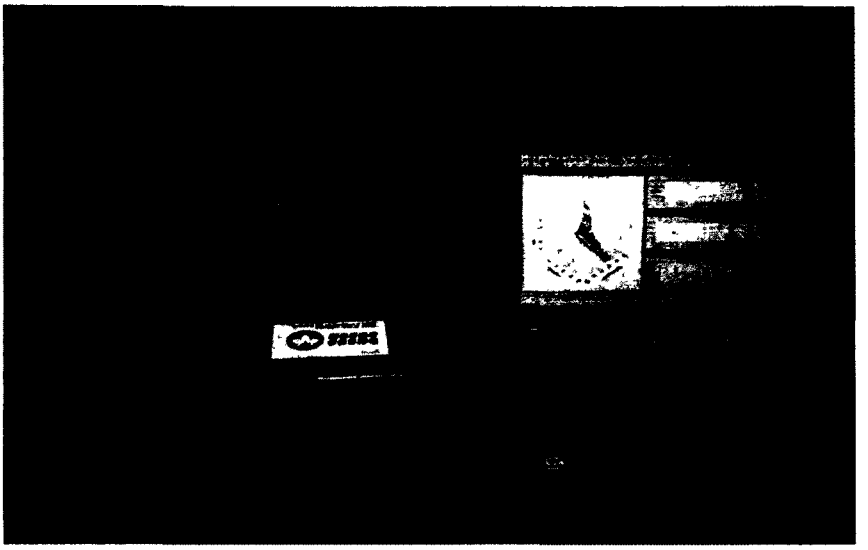

Figure 2-5: PAC AE system – μ-SAMOS

For detecting the AE signals six AE transducers (PAC, R3a transducer) were used for this research. Table 2-4 shows the characteristics of the transducers. According to Hardy H. R. (2003) the frequency range of laboratory tests conducted on rocks is 1 kHz <f<500 kHz. In this study, R3a sensors with frequency range of 25-530 KHz were chosen as propitiate sensors for geotechnical materials.

Table 2-4: characteristics of AE sensors used in this study

Model	R3α Sensor, General Purpose
Dimension (Dia×Ht) mm	19 x 22
Weight (gm)	41
Operating temperature (0C)	-65 to 175
Case material	Stainless steel
Face material	Ceramic
Connector type	SMA
Connection location	Side
Peak sensitivity (db)	80
Operating frequency range (kHz)	25 – 530
Resonant frequency (kHz)	29

In the next sections the results are presented and analyzed.

2.4. Study AE parameters by applying constant normal load during whole period of direct shear testing of the samples

Experimental results (Figures 2-6 and 2-7) show that shear stress and shear stiffness are increased however dilation is decreased by increasing normal load. On the other hand, shear stress graph has more significant peak strength and it drops markedly at higher values of normal load.

Figures 2-8, 2-9 and 2-10 show shear stress, rate and cumulative AE parameters vs. shear displacement under different values of constant normal load. As an overall view, it can be indicated that AE parameters increase by increasing of shear displacement of joint samples and they show a significant large increase prior to maximum shear strength.

AE signals show a more significant peak at maximum shear strength when normal load is increased. At low values of normal load, AEs decrease gradually after maximum shear stress whilst they decrease suddenly at higher values of normal load.

As normal load is increased the percentage of cumulative AE activity until maximum shear strength to the total cumulative AE activity is decreased. In fact by increasing the normal load, the AE activities are converged to nearby or even after shear strength peak. For example count show 34% and energy 28% of their total activity until maximum shear strength at normal load 0.5 MPa while they show 9% and 7% of their total activity until maximum shear strength at normal load 2 MPa. Joint surfaces under lower values of normal load slide at early stage of shear stress-shear displacement curve with lower shear stress; therefore, they generate more AE signals than surfaces under higher values of normal load which need more shear stress to slide. Table 2-5 summarizes characteristics of AE parameters under different values of normal load.

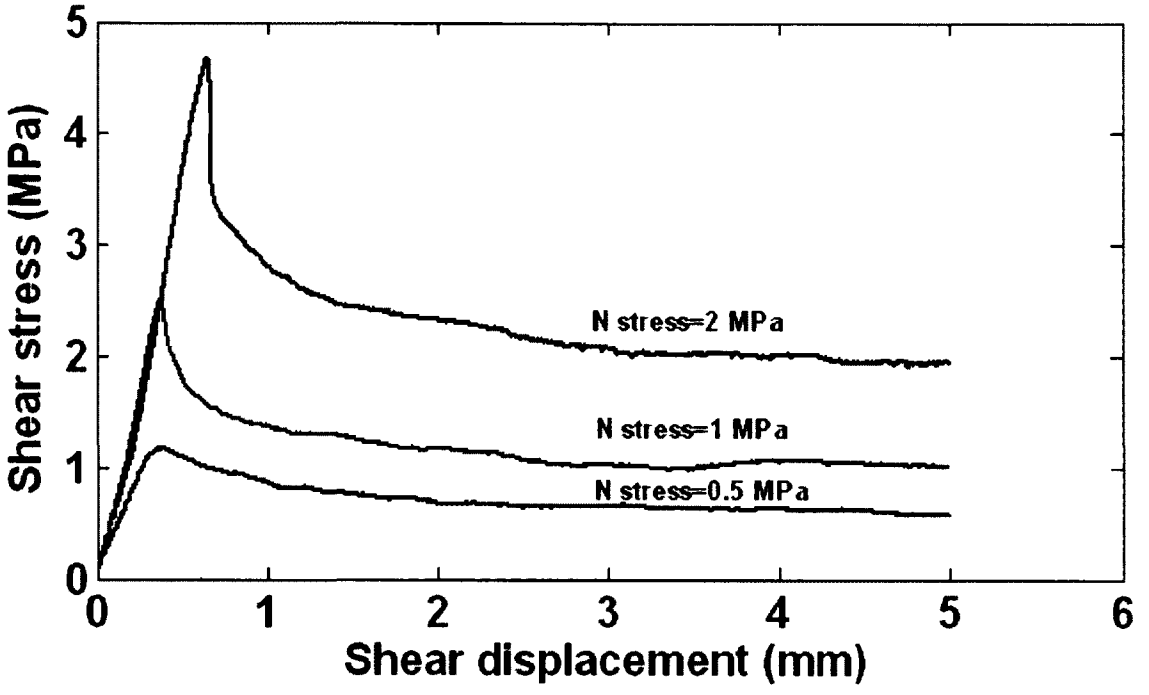

Figure 2-6: shear stress vs. shear displacement

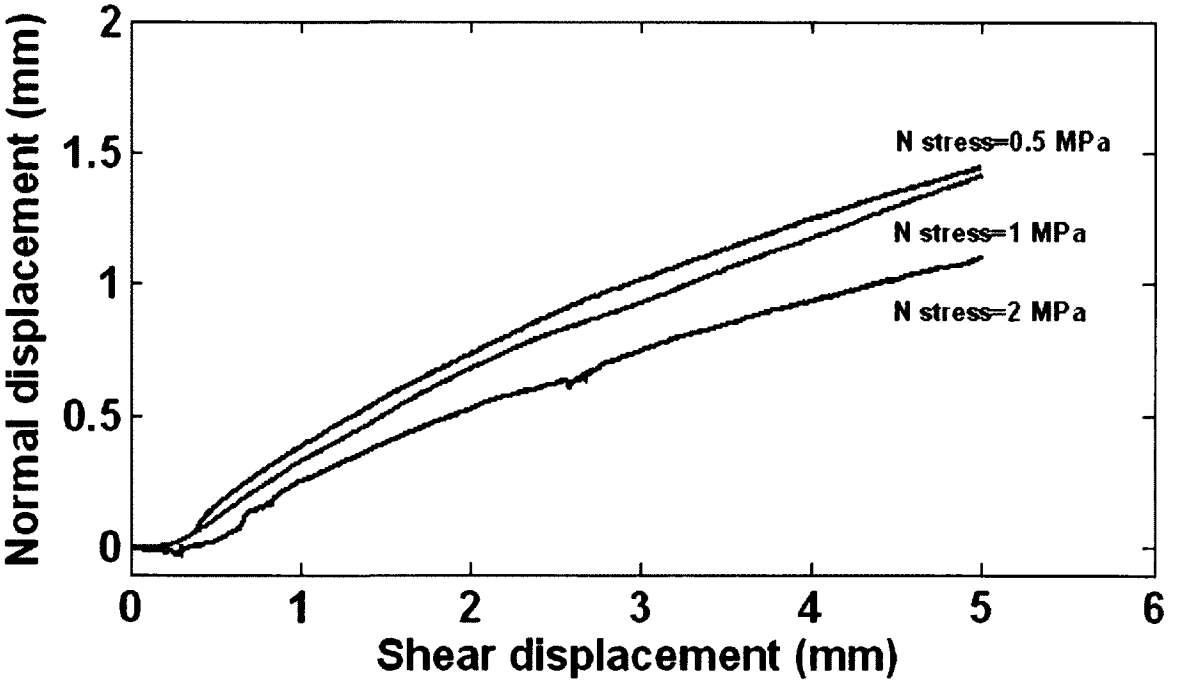

Figure 2-7: Normal displacement vs. shear displacement

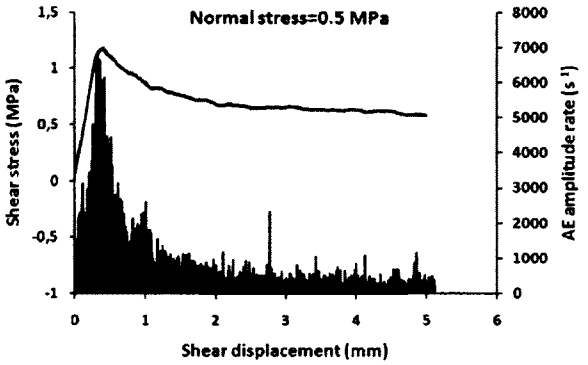
Normal stress=0.5 MPa
Shear stress (MPa)
AE amplitude rate (s⁻¹)
Shear displacement (mm)

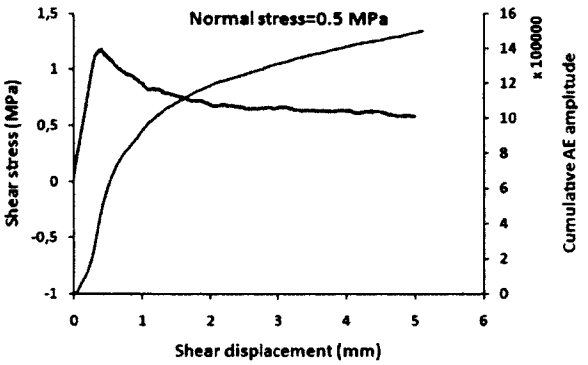
Normal stress=0.5 MPa
Shear stress (MPa)
x 100000
Cumulative AE amplitude
Shear displacement (mm)

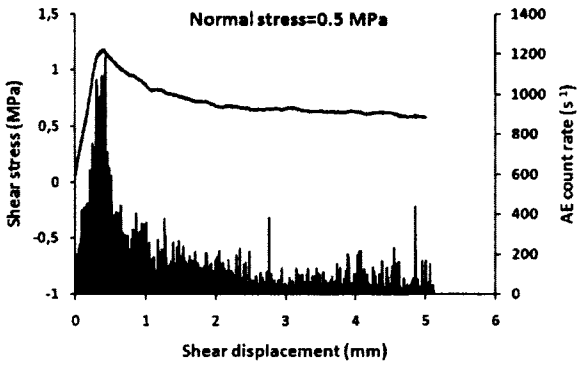
Normal stress=0.5 MPa
Shear stress (MPa)
AE count rate (s⁻¹)
Shear displacement (mm)

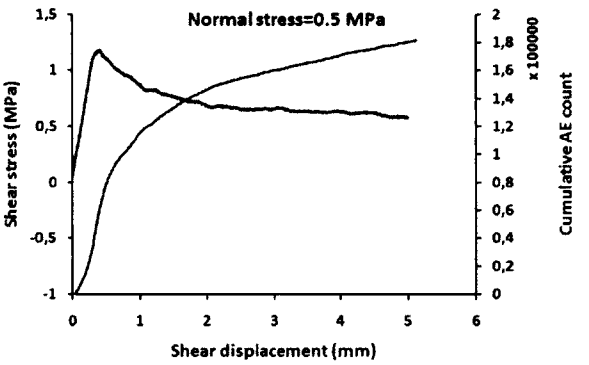
Normal stress=0.5 MPa
Shear stress (MPa)
x 100000
Cumulative AE count
Shear displacement (mm)

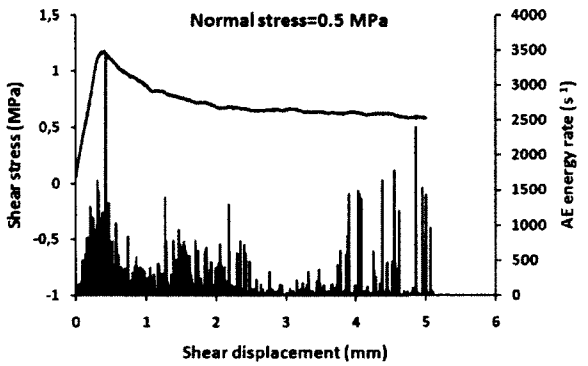
Normal stress=0.5 MPa
Shear stress (MPa)
AE energy rate (s⁻¹)
Shear displacement (mm)

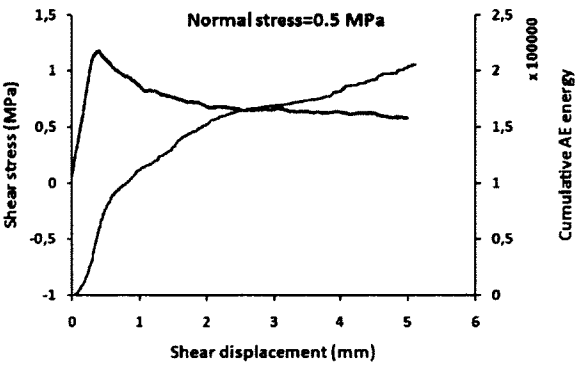
Normal stress=0.5 MPa
Shear stress (MPa)
x 100000
Cumulative AE energy
Shear displacement (mm)

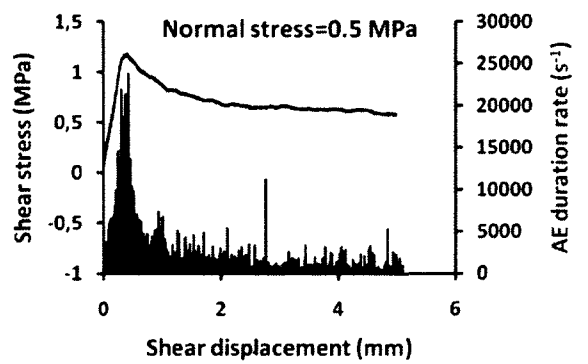
Normal stress=0.5 MPa
Shear stress (MPa)
AE duration rate (s⁻¹)
Shear displacement (mm)

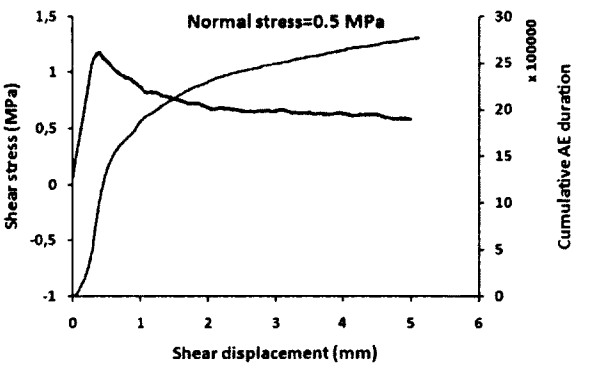
Normal stress=0.5 MPa
Shear stress (MPa)
x 100000
Cumulative AE duration
Shear displacement (mm)

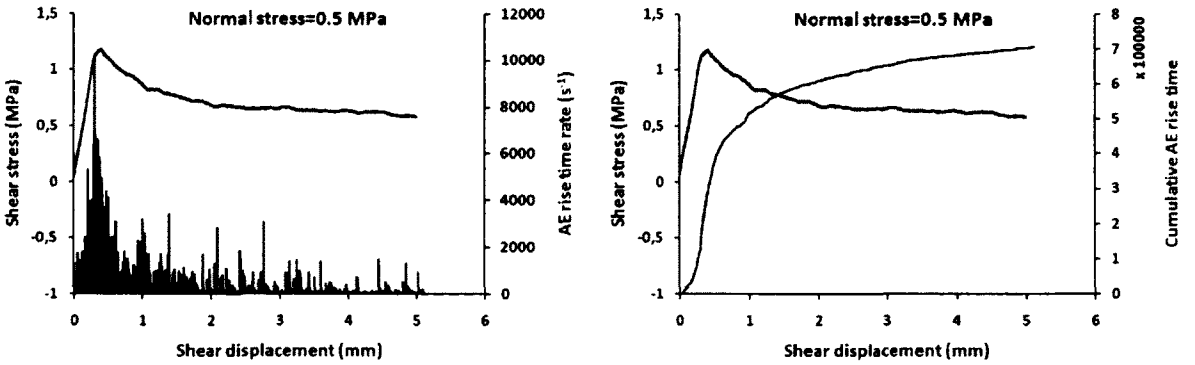

Figure 2-8: On the left, shear stress and rate of AE parameters vs. shear displacement and on the right shear stress and cumulative AE parameters vs. shear displacement for sample number 44 under normal stress=0.5 MPa.

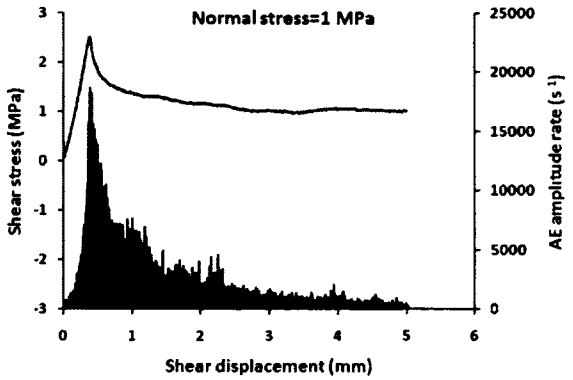
Normal stress=1 MPa
Shear stress (MPa)
AE amplitude rate (s⁻¹)
Shear displacement (mm)

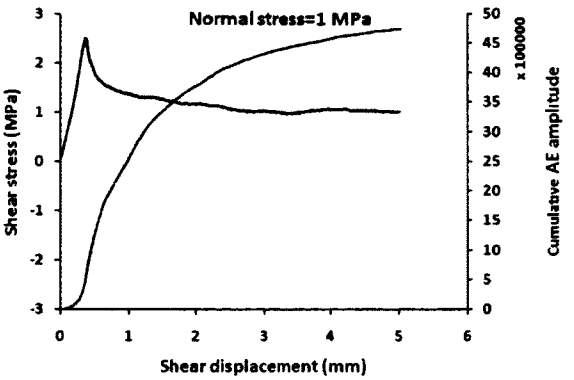
Normal stress=1 MPa
Shear stress (MPa)
x 100000
Cumulative AE amplitude
Shear displacement (mm)

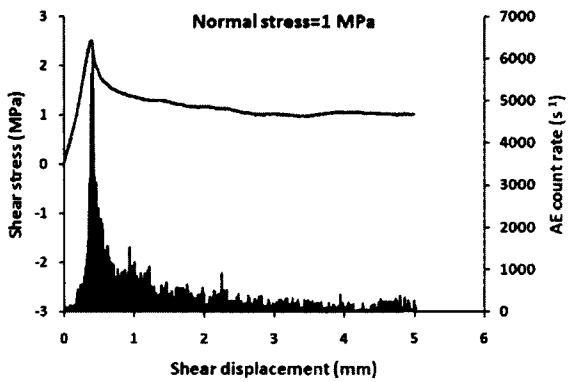
Normal stress=1 MPa
Shear stress (MPa)
AE count rate (s⁻¹)
Shear displacement (mm)

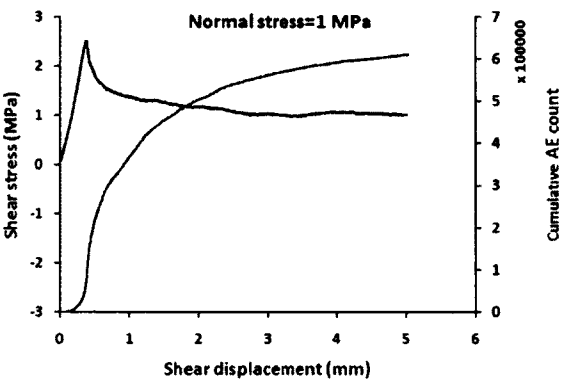
Normal stress=1 MPa
Shear stress (MPa)
x 100000
Cumulative AE count
Shear displacement (mm)

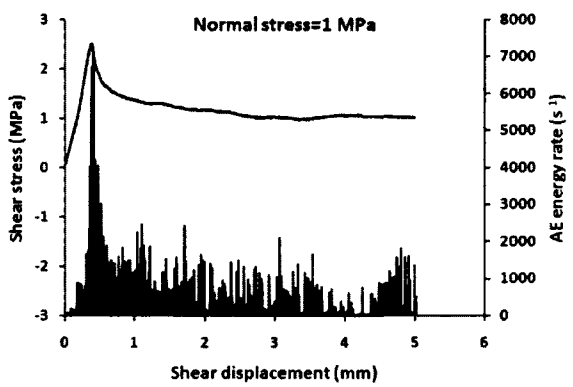
Normal stress=1 MPa
Shear stress (MPa)
AE energy rate (s⁻¹)
Shear displacement (mm)

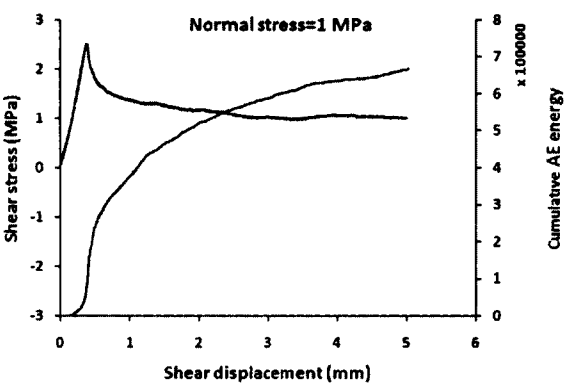
Normal stress=1 MPa
Shear stress (MPa)
x 100000
Cumulative AE energy
Shear displacement (mm)

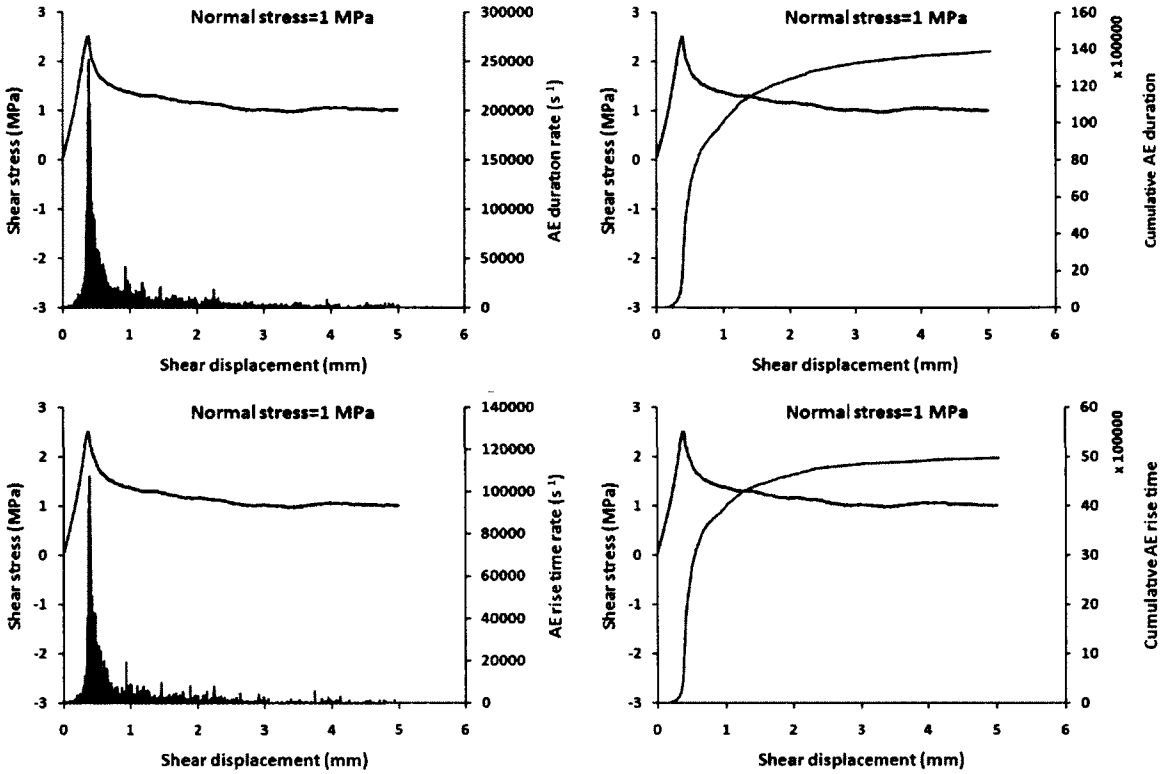

Figure 2-9: On the left, shear stress and rate of AE parameters vs. shear displacement and on the right, shear stress and cumulative AE parameters vs. shear displacement for sample number 25 under normal stress=1 MPa.

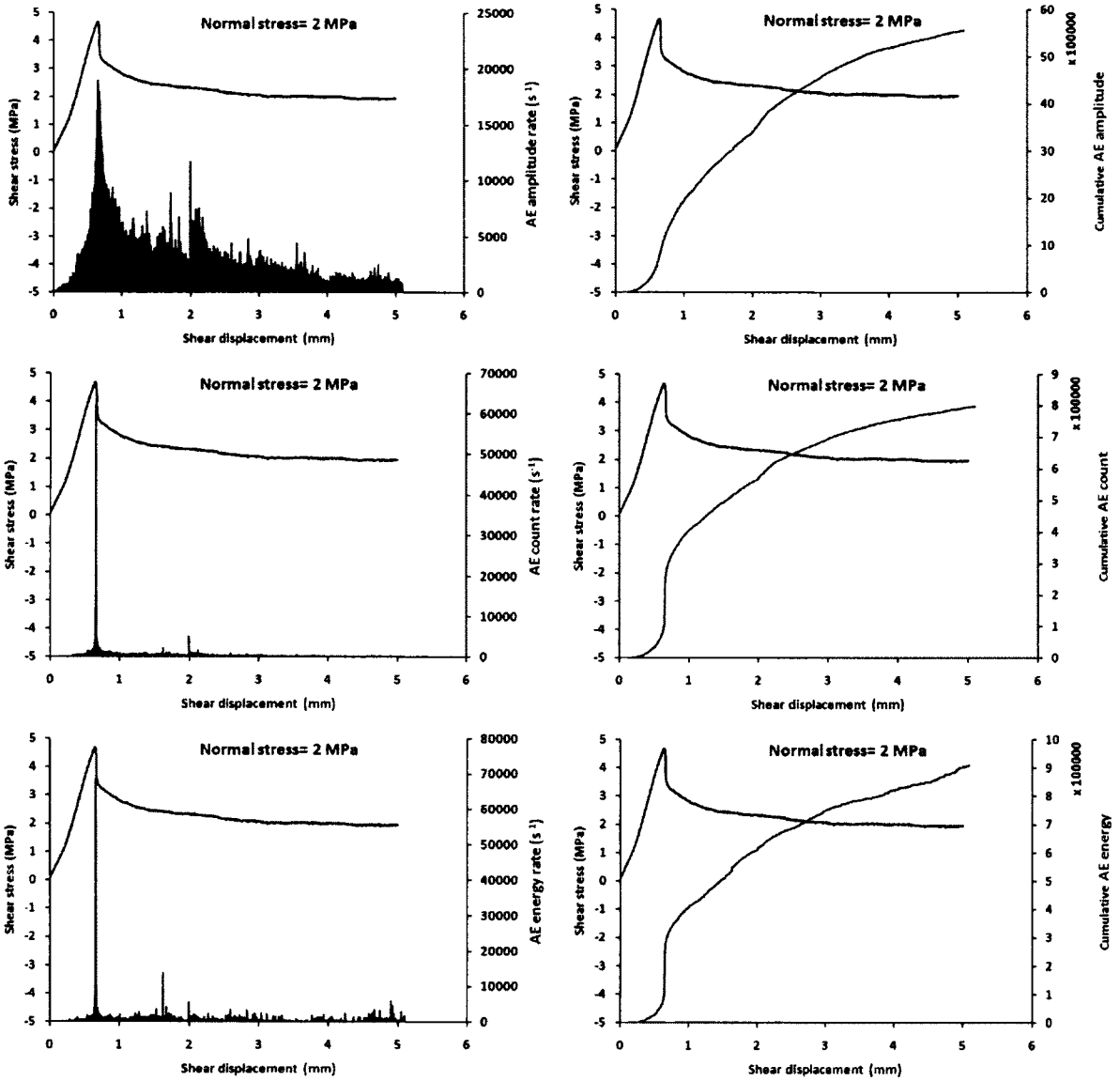
Normal stress= 2 MPa
Shear stress (MPa)
AE amplitude rate (s⁻¹)
Shear displacement (mm)
Normal stress= 2 MPa
Shear stress (MPa)
Cumulative AE amplitude
x 100000
Shear displacement (mm)
Normal stress= 2 MPa
Shear stress (MPa)
AE count rate (s⁻¹)
Shear displacement (mm)
Normal stress= 2 MPa
Shear stress (MPa)
Cumulative AE count
x 100000
Shear displacement (mm)
Normal stress= 2 MPa
Shear stress (MPa)
AE energy rate (s⁻¹)
Shear displacement (mm)
Normal stress= 2 MPa
Shear stress (MPa)
Cumulative AE energy
x 100000
Shear displacement (mm)

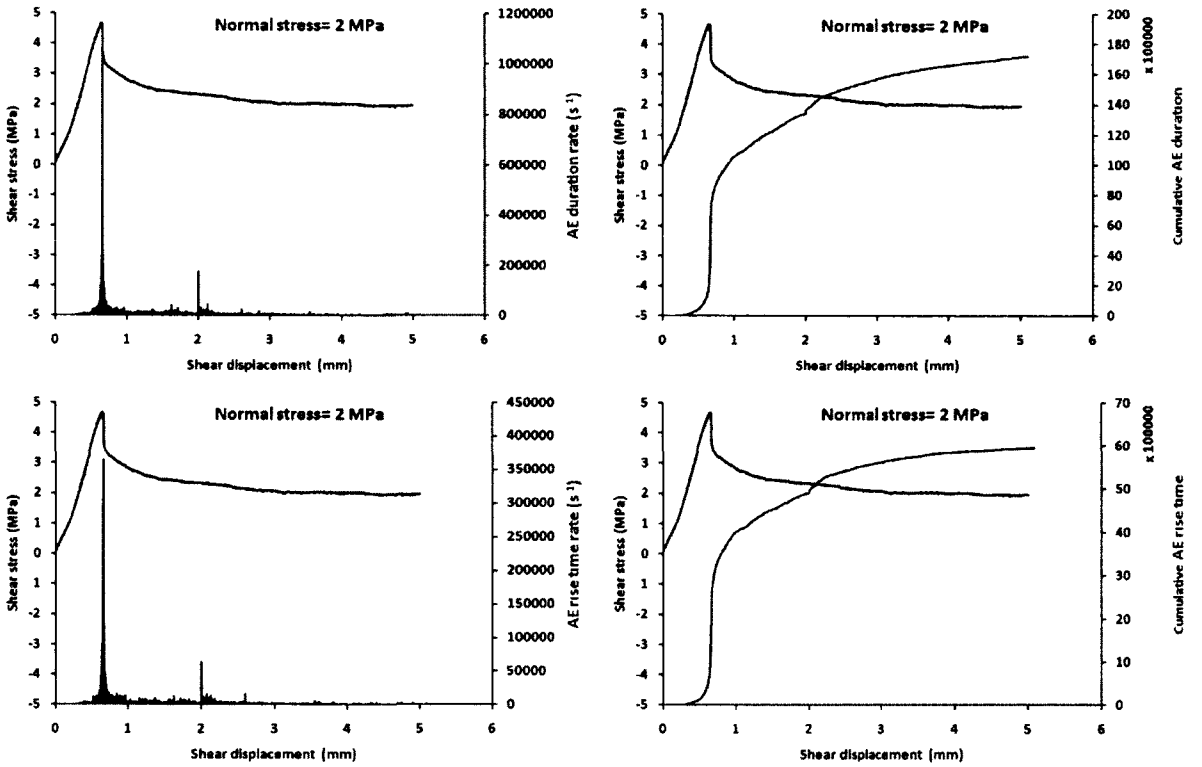

Figure 2-10: On the left Shear stress and rate of AE parameters vs. shear displacement and on the right shear stress and cumulative AE parameters vs. shear displacement for sample number 15 under normal stress =2 MPa

Table 2-5: Characteristics of AE parameters under different values of normal load

Parameters	Normal load 0.5 MPa	Normal load 1 MPa	Normal load 2 MPa
Amplitude	Increasing gradually with an approximately linear rate in (cumulative amplitude graph) until maximum shear strength point. Arriving to 31% of total cumulative amplitude in maximum shear strength point. Decreasing gradually in residual region.	Increasing with a low rate at first and then increasing linearly to 9% of total cumulative amplitude in maximum shear strength point. Showing its maximum peak after maximum shear strength and then decreasing gradually in residual region.	Same as normal load 1 MPa, arriving to 10% of total cumulative amplitude in maximum shear strength point
Count	Same as amplitude but just arriving to 34% of total cumulative count in maximum shear strength point.	Increasing with a low rate at first and then increasing with a high rate to 9% of total cumulative count in maximum shear strength point. Showing its maximum peak after maximum shear strength and then decreasing gradually in residual region.	Same as normal load 1 MPa, arriving to 9% of total cumulative count in maximum shear strength point. Showing a more significant peak after maximum shear strength and then decreasing dramatically in residual region.
Energy	This parameter is more sensitive to instant breaking of the asperities rather than sliding of the joint surface. Increasing gradually with an approximately linear rate in (cumulative energy graph) until maximum shear strength point. Arriving to 29% of total cumulative energy in maximum shear strength point. Decreasing randomly in residual region with some instant peaks with considerable intensities.	Increasing with a low rate at first and then increasing with a high rate to 8% of total cumulative energy in maximum shear strength point. Showing its maximum peak after maximum shear strength and then decreasing randomly with some instant peaks in residual region.	Same as normal load 1 MPa, arriving to 7% of total cumulative energy in maximum shear strength point. Showing a more significant peak after maximum shear strength and then decreasing dramatically in residual region.
Duration	Same as amplitude but just arriving to 37% of total cumulative duration in maximum shear strength point.	Increasing with a low rate at first and then increasing with a high rate to 8% of total cumulative duration in maximum shear strength point. Showing its maximum peak after maximum shear strength and then decreasing dramatically in residual region.	Same as normal load 1 MPa, arriving to 8% of total cumulative duration in maximum shear strength point. Showing a more significant peak after maximum shear strength.
Rise time	Same as amplitude but just arriving to 41% of total cumulative rise time in maximum shear strength point.	Increasing with a low rate at first and then increasing with a high rate to 8% of total cumulative rise time in maximum shear strength point. Showing its maximum peak after maximum shear strength and then decreasing dramatically in residual region.	Same as normal load 1 MPa, arriving to 7% of total cumulative rise time in maximum shear strength point. Showing a more significant peak after maximum shear strength.

2.5. Studying AE parameters by applying constant normal load in the beginning and changing it in residual section of the same sample

Previous section showed that normal stress has a significant effect on AE events radiated from rock joints during direct shear test. Although it was tried to select samples with similar physical and mechanical characteristics however, difference in AE response of rock joints might be due to difference in distribution of asperities and apertures of joint surfaces or coupling conditions of AE sensors.

To eliminate the negative effect of coupling conditions of AE sensors, AE measurement were done on same sample where coupling conditions of the AE transducer remained unchanged. With this attempt, direct shear test was carried out on a sample by increasing and decreasing of normal stress for several times during the residual section of the shear stress-shear displacement graph.

Figures 2-11 and 2-12 show shear stress and normal displacement vs. shear displacement for samples number 33 and 34. Increasing and decreasing of normal load has been shown in these Figures.

Figures 2-13 and 2-14 show the combination of AE parameters and shear stress as a function of shear displacement.

Increasing normal load in any stage of loading process causes a high amount of AE events but not immediately at the jumping point of shear stress graph. This means that AE signals are generated by shearing and damaging of asperities not jumping of shear stress. In the contrary, decreasing normal load causes a low amount of AE activity except for dropping point of normal load which generates a significant peak in AE signals. It can be suggested that these peaks come from releasing of joints halves from interlocking. The more dropping in normal load the more releasing of joint halves is happened and consequently the more significant AE peaks are generated.

Comparing areas number 2 and 4 in Figures 2-13 shows that although they are under a same amount of normal stress (1 MPa), however it can be said that when the normal stress has been increased from a lower amount (here 0.5 MPa), the sample shows more AE signals than when

the normal stress has been decreased from a higher amount (here 2 MPa). This phenomenon can be shown for areas number 2 and 4 in Figure 2-14 too.

Figures 2-13 and 2-14 demonstrate that energy shows its significant peaks in the period of increasing and sudden decreasing of normal stress. Looking at energy curves in Figures 2-13 and 2-14 it can be said that this parameter is very sensitive to sudden damage rather than gradual failure so that its peaks caused by sudden breaking is many times higher than those which caused by gradual shearing.

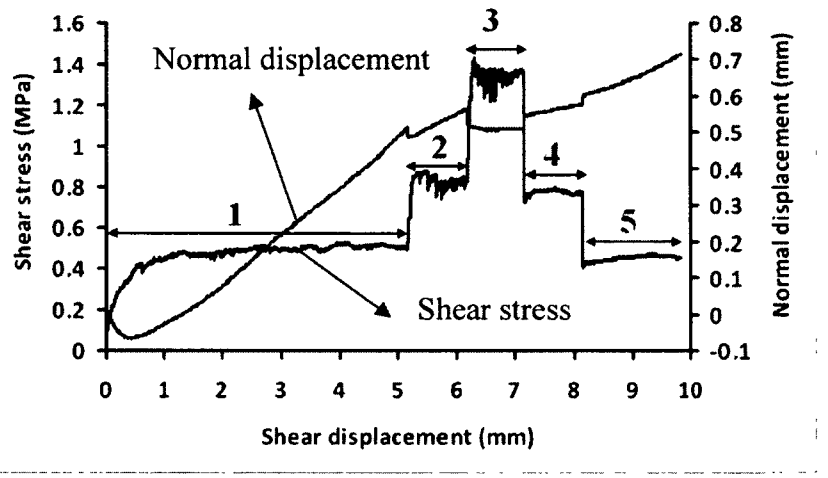

Figure 2-11: Shear stress and normal displacement vs. shear displacement for sample number 33, 1) normal stress=0.5 MPa, 2) normal stress=1 MPa, 3) normal stress=2 MPa, 4) normal stress=1 MPa, 5) normal stress=0.5 MPa.

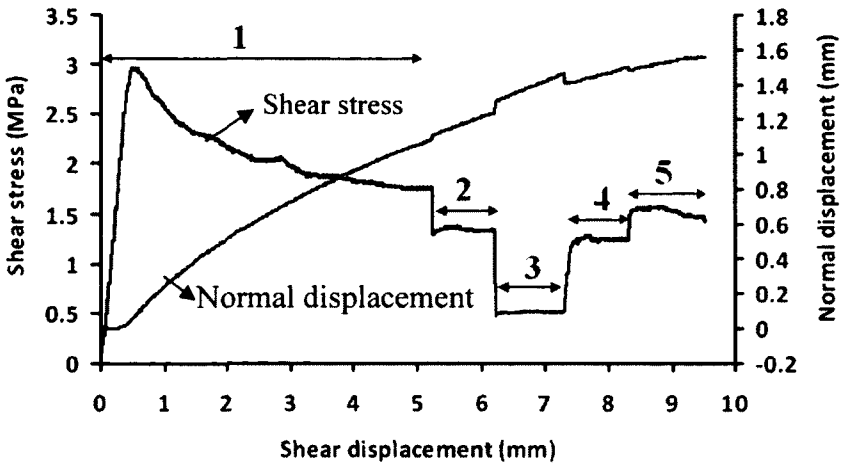

Figure 2-12: Shear stress and normal displacement vs. shear displacement for sample number 34, 1) normal stress=2 MPa, 2) normal stress=1.5 MPa, 3) normal stress=0.5 MPa, 4) normal stress=1.5 MPa, 5) normal stress=2 MPa.

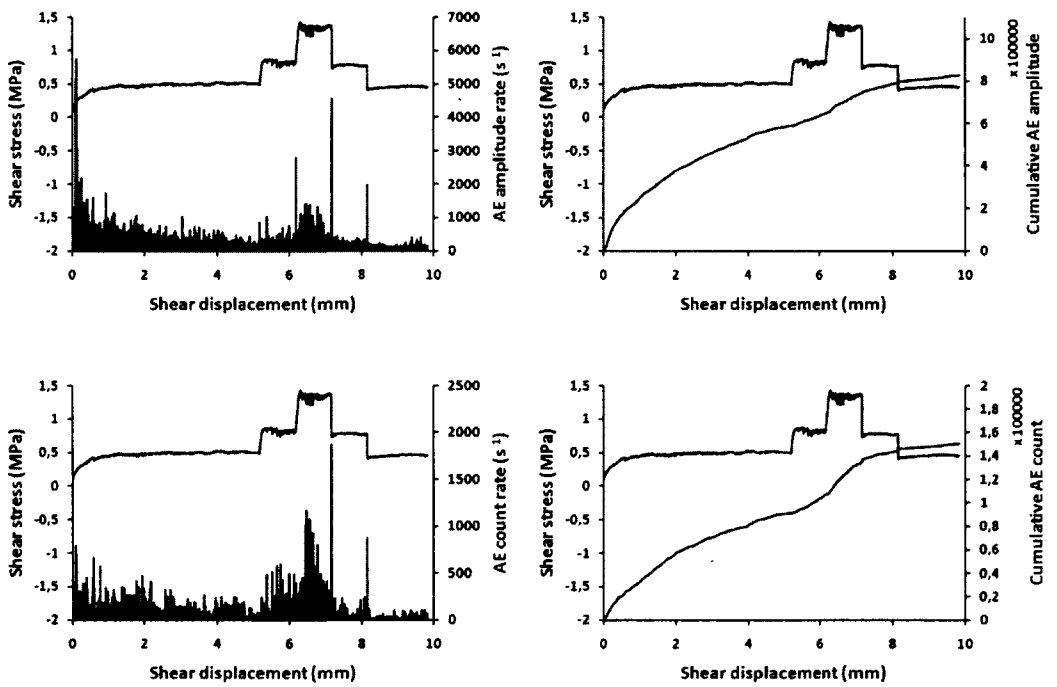

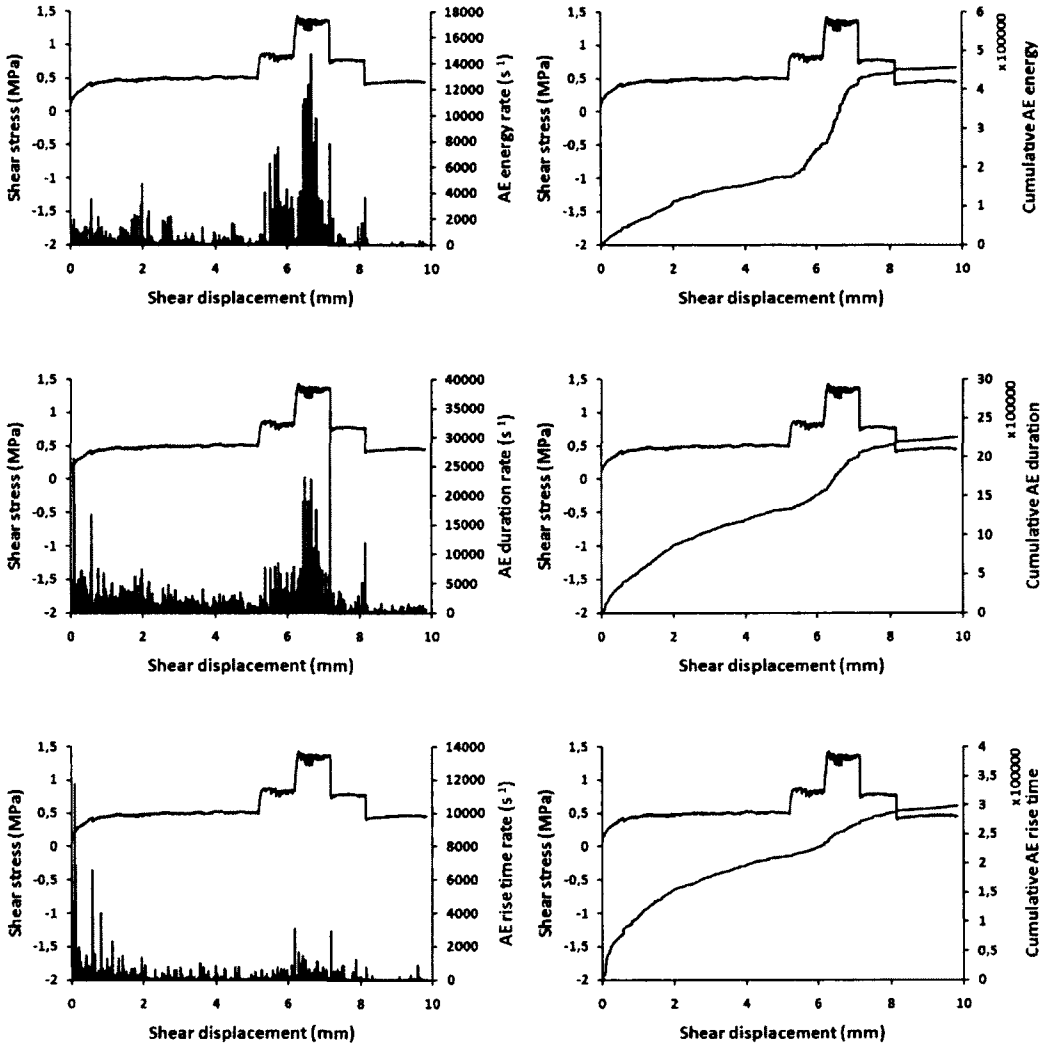

Figure 2-13: On the left, shear stress and rate of AE parameters vs. shear displacement and on the right, shear stress and cumulative AE parameters vs. shear displacement for sample number 33 under normal stresses shown in Figure 2-11.

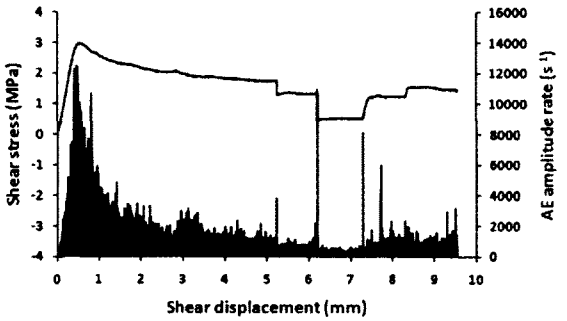
Shear stress (MPa)
AE amplitude rate (s⁻¹)
Shear displacement (mm)

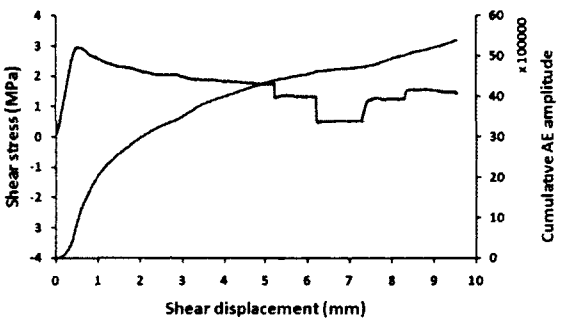
Shear stress (MPa)
x100000
Cumulative AE amplitude
Shear displacement (mm)

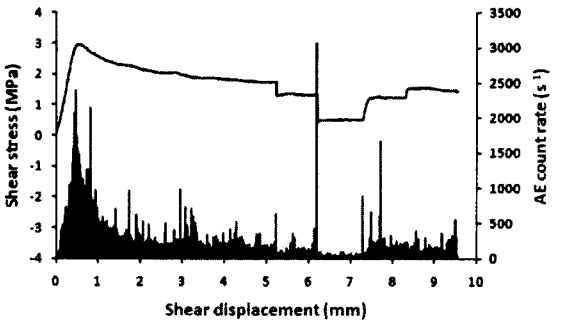
Shear stress (MPa)
AE count rate (s⁻¹)
Shear displacement (mm)

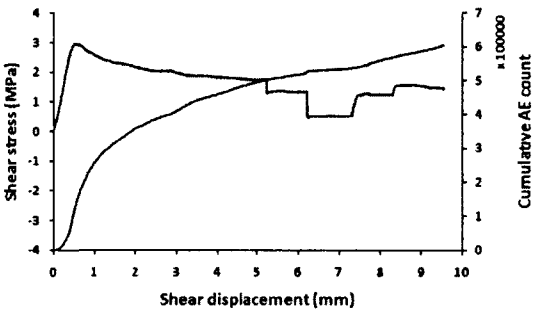
Shear stress (MPa)
x100000
Cumulative AE count
Shear displacement (mm)

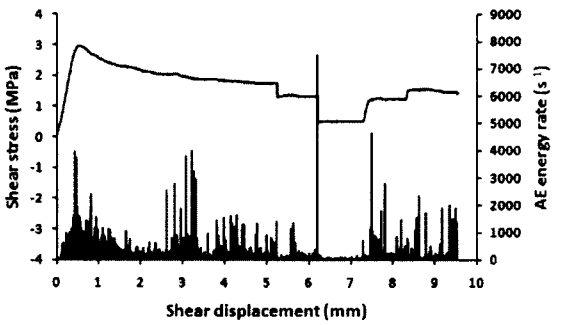
Shear stress (MPa)
AE energy rate (s⁻¹)
Shear displacement (mm)

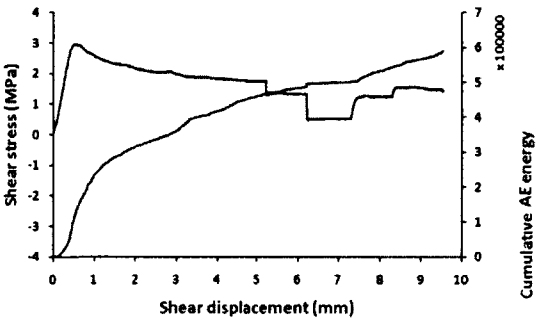
Shear stress (MPa)
x100000
Cumulative AE energy
Shear displacement (mm)

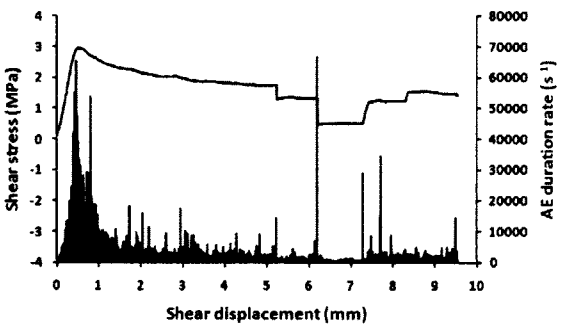
Shear stress (MPa)
AE duration rate (s⁻¹)
Shear displacement (mm)

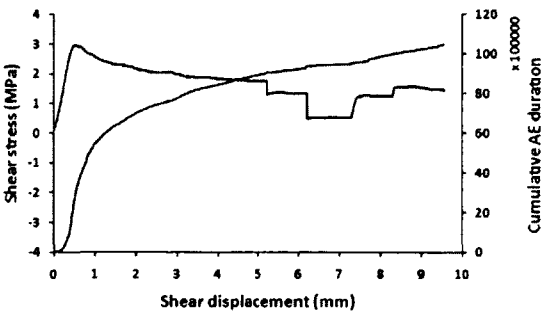
Shear stress (MPa)
x100000
Cumulative AE duration
Shear displacement (mm)

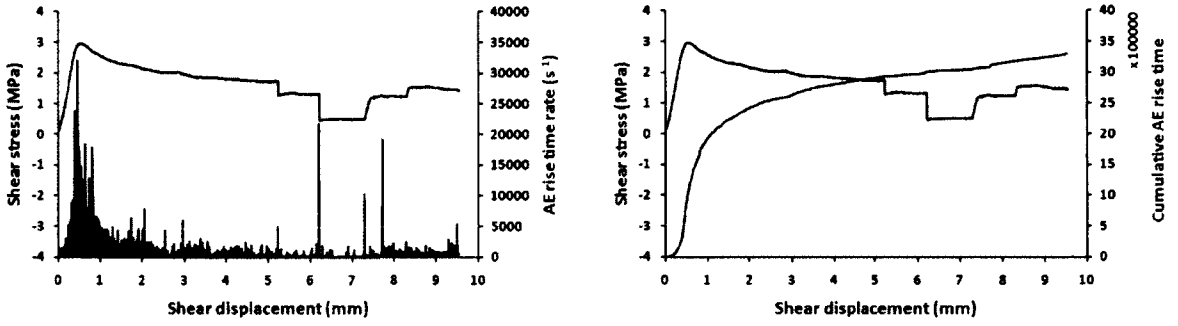

Figure 2-14: On the left, shear stress and rate of AE parameters vs. shear displacement and on the right, shear stress and cumulative AE parameters vs. shear displacement for sample number 34 under normal stresses shown in Figure 2-12.

2.6. Conclusions

Direct shear tests were carried out on rock joints in two ways. At first samples with approximately same physical and mechanical properties were tested under different but constant normal loads. Then different values of normal loads were applied on same sample during its residual behavior of the shear stress graph.

It was found that the combined use of acoustic emission parameters and stress-displacement analysis provide an accurate and reliable method of identifying the shear behavior of structures through weak discontinuities, because each parameter is capable of revealing a number of insights into the progressive failure process of rock joints.

The general behavior of the AE parameters at low values of normal load is that they increase gradually with an approximately linear rate until maximum shear strength point and they show their maximum peaks after this point. Finally they decrease gradually in residual shear strength region. The behavior of the AE energy is a little different because it is more sensitive to instant breaking of the asperities rather than sliding of the joint surface so that it shows some instant peaks in residual region with considerable intensities.

At high values of normal load conditions, the AE parameters increase with a low rate to the maximum shear strength point and then they increase with a very high rate after that. After dropping, they show small peaks in residual region. Amplitude is the only parameter which doesn't show significant change in its behavior. This parameter increases with a low rate at first and then increases linearly after maximum shear strength point. Finally it decreases gradually in residual region.

The experimental results showed that normal load has a very large effect on AE events generated from rock joints under direct shear loading.

In the initial phase of the loading (between start point of the test and ultimate shear stress) samples under lower values of normal load show higher AE parameters than samples under higher values of normal load.

Increasing in normal load always generates more AE events but not immediately at jumping point of normal load. In fact AE events are increased when increasing normal load makes

asperities to be shared. Whereas decreasing normal load produces a significant peak in AE parameters at dropping point. It is believed that this phenomenon is due to releasing of joint halves from interlocking which makes a lot of AE signals. After dropping point, AE parameters are decreased and show small peaks as long as normal load is low. This study is very useful for dam monitoring because in some cases sudden increases of AE activity observed during AE monitoring in dam structures and their rock foundations might be due to normal stress redistribution rather than hydrostatics pressure and shear movements.

Although a comprehensive study contains interpreting of all AE parameters, It is should be noted that energy contains AE amplitude and duration. On the other hand, rise time is related to duration and almost show same behavior as duration. Therefore, AE energy and AE count can be considered as appropriate representatives of AE parameters.

In this paper, it was tried to investigate the characteristic features of acoustic emission parameters during direct shear tests of rock joints under different constant normal loads. It was shown how each parameter changes during shear testing. In the next paper the shear behavior of the joints is studied from shear displacement initiation until residual shear strength of the shear stress-shear displacement graph.

3. EVALUATING DAMAGE DURING SHEAR TESTS OF ROCK JOINTS USING ACOUSTIC EMISSIONS

Autors and affiliation:
Z. Moradian: PhD student, Université de Sherbrooke, Faculté de génie, Département de génie civil.
G. Ballivy: Professeur, Université de Sherbrooke, Faculté de génie, Département de génie civil.
P. Rivard: Professeur, Université de Sherbrooke, Faculté de génie, Département de génie civil.
C. Gravel: Research assistant, Université de Sherbrooke, Faculté de génie, Département de génie civil.
B. Rousseaux: Research assistant, Université de Sherbrooke, Faculté de génie, Département de génie civil.

Date of acceptation: 8 January 2010

Acceptation state: Finale version published

Journal: International Journal of Rock Mechanics and Mining Sciences

Reference: [IJRMMS-D-09-00121, 2010; 47(4):590–598]

Titre français: Evaluation du dommage pendant l'essai de cisaillement des joins rocheux par émission acoustique

Contribution in paper:
The author of the thesis has contributed in this paper as first, principal and corresponding author.

Résumé français:
L'émission acoustique (EA) des signaux générés lors de l'essai de cisaillement direct a été évaluée sur différents types de joints (roche-roche, roche-béton et béton-béton). Plusieurs forages ont été faits à partir d'un barrage; dans la masse rocheuse et à l'interface entre le barrage et la roche. Les échantillons ont été préparés et testés dans des essais de cisaillement direct. Un profilomètre laser a été utilisé pour la numérisation des surfaces des joints afin d'évaluer la rugosité de surface. En corrélant les signaux d'EA avec les graphiques de cisaillement, on peut prédire le début du cisaillement lors de l'essai de cisaillement direct. Les

comptes (counts) et l'énergie ont été analysés à partir de deux méthodes différentes pour surveiller le comportement en cisaillement des joints : un graphique des taux des comptes et de l'énergie, et un graphique des valeurs cumulées des counts et de l'énergie. Quatre périodes séparées ont été observées pour les joints liés et non liés: période linéaire prépic, période non linéaire prépic, période après la rupture et période résiduelle. Cette étude a montré que l'EA est suffisamment quantitative pour surveiller le comportement en cisaillement des joints et qu'elle peut être utilisée de façon fiable.

Abstract

The acoustic emission (AE) signals generated during direct shear test were evaluated on different types of joints (rock–rock, rock–concrete and concrete–concrete). Several boreholes were cored from a dam body; rock mass and interface between dam and rock mass, and the samples were prepared and tested under direct shear test. A laser profilometer scanner was used for scanning the joint surfaces in order to assess surface roughness. By correlating the AE signals with the shear graphs one can predict the starting point of shearing during direct shear test. Count and energy parameters were analyzed in two different methods to monitor the shear behavior of the joints: a graph of the count and energy rates, and a graph of cumulative count and energy. Four separated periods were observed for bonded and non-bonded joints: linear pre-peak period, non-linear pre-peak period, post peak period and residual period. This study showed that AE has enough accuracy to monitor the shear behavior of the joints and it can be used in site confidently.

Keywords: Acoustic emission; Shear behavior; Rock–rock joint; Rock–concrete joint; Concrete–concrete joint

3.1. Introduction

Discontinuities such as joints have an important role in controlling the behavior of a dam under normal and shear loading conditions. They reduce strength and increase deformability in dam structures. Thus, the safe management of dam operation requires a precise evaluation of

the dam stability in terms of the shear strength of the discontinuities (Lo 1990, Seidel and Haberfield 2002, Ballivy et al. 2006, Moradian et al. 2008).

Previous researchers (Barton and Choubey 1977, Grasselli 2006, Hong and Seokwon 2004, Kimura and Esaki 1995, Yang and Chiang 2000, Haberfield and Johnston 1994, Gentier et al. 2000) have tried to show the mechanism of the shear stress–shear displacement graph of joints. As a summary of their works the shear behavior of the joint samples can be divided into four periods:

1. Pre-peak linear period: By applying normal and shear load on joint surface the two halves of the joint are settled and interlocked in this period. The stiffness and contact area are increased.
2. Pre-peak non-linear period: Dilatancy is generated and increased along this period because of the sliding or damaging of the secondary asperities. This period is ended by peak shear stress where steepest primary asperities are broken and dilatancy shows its maximum rate.
3. Post-peak period: All secondary and primary asperities facing the shearing direction are crushed in this period (depending on the amount of normal load) and the shear stress–shear displacement curve shows a progressive softening behavior.
4. Residual strength period: Shear stress is stable in a residual value and asperities degradation is continued in a lower severity than post-peak period.

Dam monitoring has great importance not only for scientific community, but also for engineers and dam managers. Monitoring helps to understand mechanisms of disruptive processes and defining adequate prevention measures for reducing their effects. Besides conventional monitoring techniques such as extensometers, strain gages and joint meters, the AE monitoring has been experimented in several civil engineering structures (Minemura et al. 1998, Sasao et al. 2003, Shiotani et al. 2006 and 2007, Manthei et al. 2007). AE is a transient elastic wave that is generated by the rapid release of energy within a material (Koerner et al. 1981).

In order to apply AE for monitoring the shear behavior of in situ discontinuities, it is necessary to monitor the shear behavior of modeled joint samples in laboratory. To be specific, the system of loading can be controlled, and the reaction (emitted AE signals) of various types of joints to the loading testing conditions can be studied.

Several researches have been conducted related to the application of the AE to monitor the behavior of the geotechnical materials (Falls and Young 1998, Maejima et al. 2001, Butt et al. 2003, Cai et al. 2007, Rudajev et al 1996 and 2007). Among the most important applications of AE is its capability to monitor failure behavior, crack initiation and crack propagation of rocks under loading (Eberhardt et al. 1997, Mlakar et al. 1993, Chang and Lee 2004) as well as possibility to calculate some useful parameters such as in situ stress (Seto et al. 1997).

A few researchers have addressed the application of the AE for monitoring the shear behavior of the joints. Li and Nordlund (1990) characterized AE during shearing of rock joints using artificial and natural joints. Their test results indicated that the AE rate peaks coincide with the stress drops caused by fracturing of asperities during joint shear. Rim et al. (2005) investigated the characteristics of the AE from the artificial saw tooth joints and replicas of the natural rock joints during the CNS shear test. They concluded that the shear behavior of joints can be divided into three periods according to the characteristics of AE count and AE energy. They called these periods as first peak shear stress, linear increasing and second peak shear stress.

Hong et al. (2004) performed a series of direct shear tests to investigate the influence of shear load on AE characteristics of rock–concrete interface under constant normal load. They showed that the location of the AE sources distributed over the entire shear zone, before residual shear stress. They believed that after the residual shear stress attain, the sources are concentrated. Finally they showed that the maximum rates of count and energy were observed when the stress dropped after peak shear stress.

Son et al. (2006) conducted laboratory shear tests under CNS and CNL conditions and studied the influence of the boundary conditions on shear behavior. From the distribution of source locations of AE it was thought that the roughness damage may be strongly correlated with roughness height.

In the present research, laboratory direct shear test in constant normal load condition (CNL) was conducted on various kinds of joints (concrete lift joint, interface joint between concrete and rock or a discontinuity in the rock mass) with different characteristics. In the next step graphs of AE parameters and shear stress-shear displacement graphs were correlated. Two methods are proposed for monitoring the four separated periods in shear stress–shear displacement graphs of joints. The capability of the AE for predicting start point of shear stress–shear displacement graph during direct shear test is evaluated too.

3.2. Sample preparation and testing

Samples have been obtained from drilled cores in Daniel Johnson dam (also known as Manic 5 dam) in Quebec, Canada. The bedrock is of very good quality from gneiss to granitic rock. It is mainly composed of quartz and potassic feldspar and some biotite. The drilling was performed with a special triple tube coring system to recover intact large samples of 150 mm diameters as a good representative of in situ joints. Normally, each core contains all three types of joints. First section of a drilled core contains concrete–concrete joint (construction joint). Around the middle of the core, there is rock–concrete joint (interface between concrete and rock foundation). Final section contains rock–rock joint (rock joints in dam foundation). Photos A2-8 to A2-10 in appendix 2 show cores dried in the site of Manic 5 dam.

The direct shear test was performed on the joint specimens in the constant normal load condition (CNL) using a direct shear apparatus mounted inside a rigid loading frame of a rock and concrete testing machine fabricated by Materials Testing Systems (MTS).

The rate of horizontal displacement in all tests was 0.15 mm/min and the test was finished when horizontal displacement attained 10 mm. The values of shear stress and shear and normal displacements due to applied shear loads have been recorded during each test.

The results of the samples number CC8.35 (non-bonded concrete–concrete joint), BCC3.45 (bonded concrete–concrete joint), RC7.63 (non-bonded rock–concrete joint) and RR10.48 (non-bonded rock–rock joint) from Table 1-6 as the typical shear behavior of each specimen type are analyzed. Figure 3-1 and Figure 3-2 show results of direct shear test on the samples.

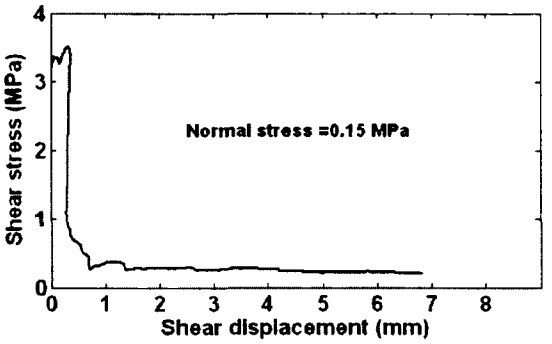

(a) Bonded concrete-concrete joint

(Sample BCC3.45)

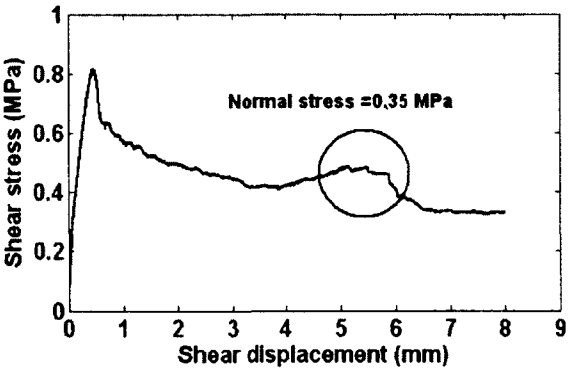

(b) Non-bonded concrete-concrete joint

(Sample CC8.35)

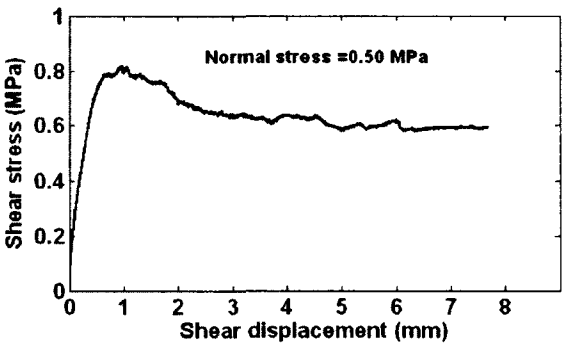

(c) Non-bonded rock-concrete joint

(Sample RC7.63)

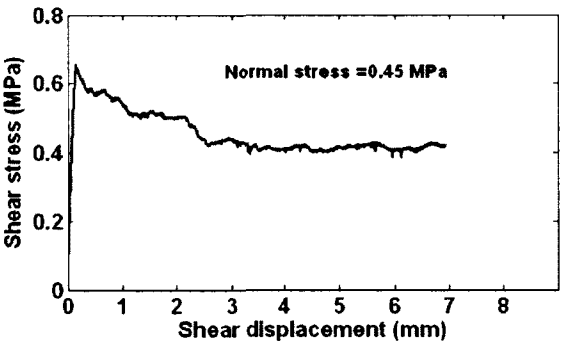

(d) Non-bonded rock-rock joint

(Sample RR10.48)

Figure 3-1: Shear stress vs. shear displacement: (a) bonded concrete–concrete joint (sample BCC3.45), (b) non-bonded concrete–concrete joint (sample CC8.35), (c) non-bonded rock–concrete joint (sample RC7.63) and (d) non-bonded rock–rock joint (sample RR10.48).

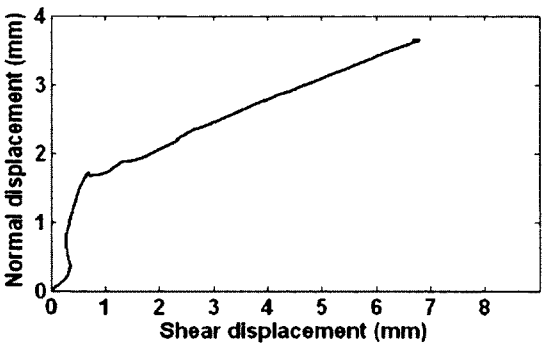

(a) Bonded concrete-concrete joint
(Sample BCC3.45)

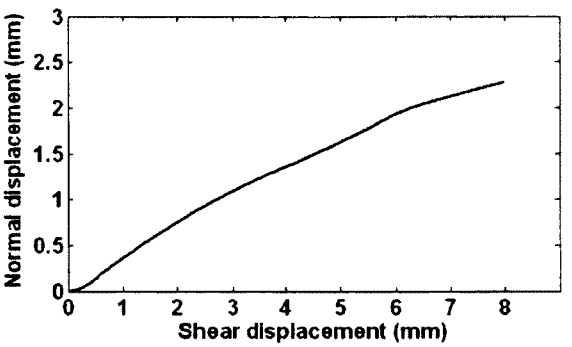

(b) Non-bonded concrete-concrete joint
(Sample CC8.35)

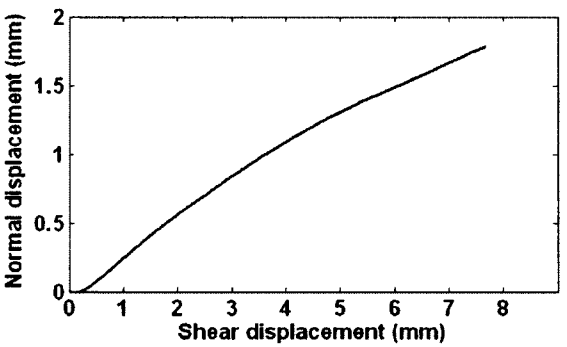

(c) Non-bonded rock-concrete joint
(Sample RC7.63)

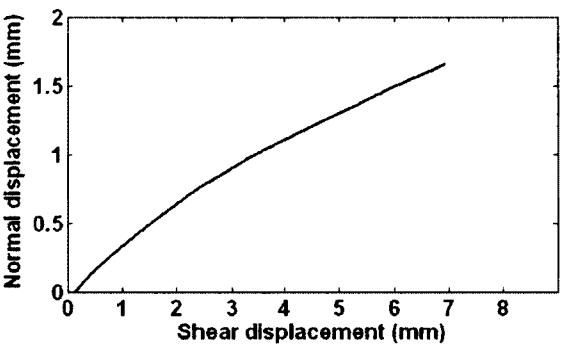

(d) Non-bonded rock-rock joint
(Sample RR10.48)

Figure 3-2: Normal displacement vs. shear displacement: (a) bonded concrete–concrete joint (sample BCC3.45), (b) non-bonded concrete–concrete joint (sample CC8.35), (c) non-bonded rock–concrete joint (sample RC7.63) and (d) non-bonded rock–rock joint (sample RR10.48).

The laser profilometer model Kréon Zephyr 25 was used for scanning the joint surfaces. The laser emits a red luminous light with a wavelength of 670 nm and a maximum output power of 4 mW. The sensor has a number of points/second of 30 000 and depth and width of field 90 and 25 mm. For measuring roughness of the joint surfaces, a 0.5 mm profile interval was chosen. The average Z_2 parameter was calculated for each surface using the following equation (Tse and Cruden 1979):

$$Z_2 = \sqrt{\frac{1}{n}\sum_{i=1}^{n}\left(\frac{z_{i+1} - z_i}{\Delta y}\right)^2} \qquad (3\text{-}1)$$

in which N is the number of points on one profile, and Z and Y are the coordination of the points on profiles parallel to the X direction. Table 3-1 contains the average Z_2 roughness parameter for each sample.

Table 3-1: Z_2 parameter for each sample

No.	**Profile interval (mm)**	**Average Z_2 parameter**
CC8.35	0.5	0.687
RC7.63	0.5	0.487
RR10.48	0.5	0.341

AEs were monitored with PAC μ-SAMOS system. This system consists of two eight-channel AE data acquisition systems (PCI-8). Four AE transducers (PAC, R3α general purpose) were used to detect AE signals. The frequency range of the sensors is 25–530 kHz, the amplification of pre-amplifier was 40 dB, and AE exceeding 50 dB was measured.

3.3. Predicting the start point of the shear movement by means of AE

One of the most important issues in monitoring the behavior of the active joints is detecting the point where shearing starts. When the joint starts moving, one can be aware and implement remedial solutions. By comparing the shear stress–shear displacement graphs and AE parameters graphs the start point of shear movement is shown.

Figure 3-1a shows shear stress vs. shear displacement for bonded concrete–concrete joint (sample BCC3.45). Although shear stress has started to increase, there is no change in shear displacement. When sample passes its elastic behavior, permanent displacements are initiated.

Figures 3-3a and 3-4a show shear stress and count and energy rate vs. time for bonded concrete–concrete joint (sample BCC3.45), respectively. From Figures 3-3a and 3-4a, it can be seen that the AE graphs have no change while there is no shear displacement. As soon as shear displacement begins, the AE parameters increase rapidly so that during failure of the sample the AE parameters attain their maximum values.

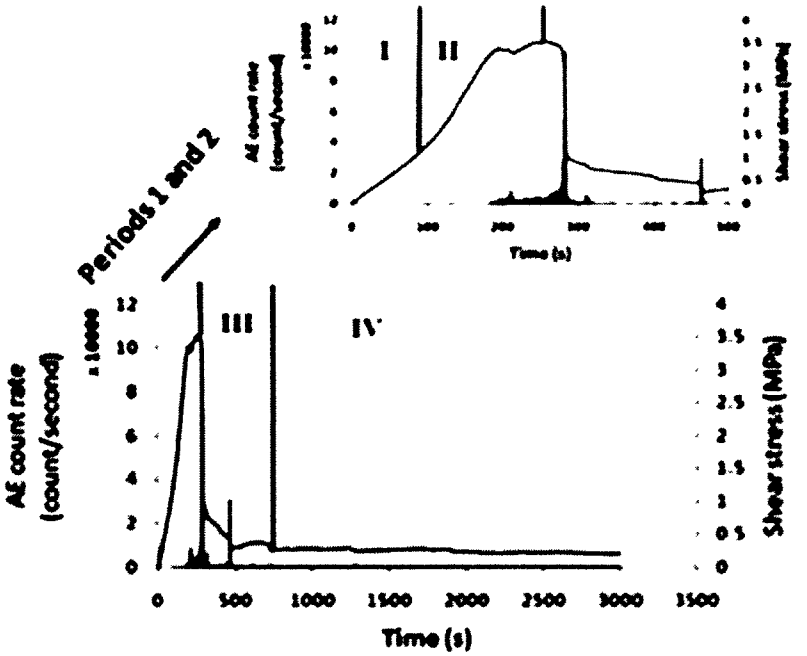

(a) Bonded concrete-concrete joint, (Sample BCC3.45)

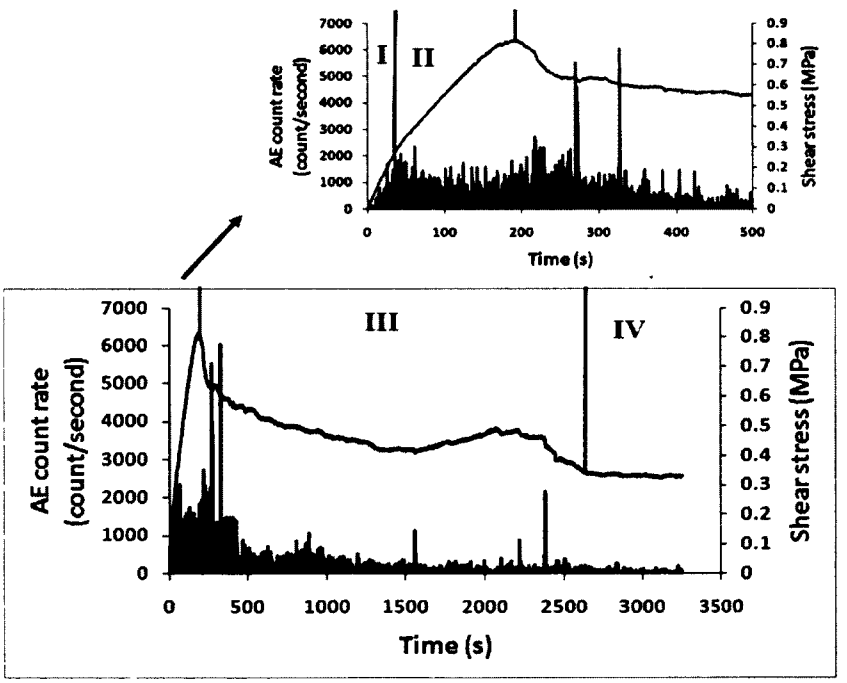

(b) Non-bonded concrete-concrete joint, (Sample CC8.35)

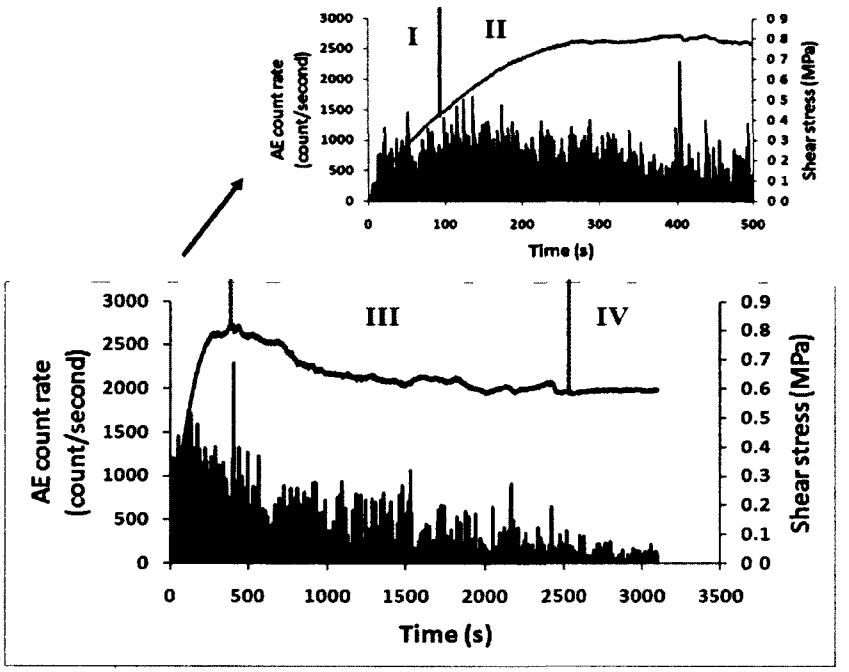

(c) Non-bonded rock-concrete joint, (Sample RC7 63)

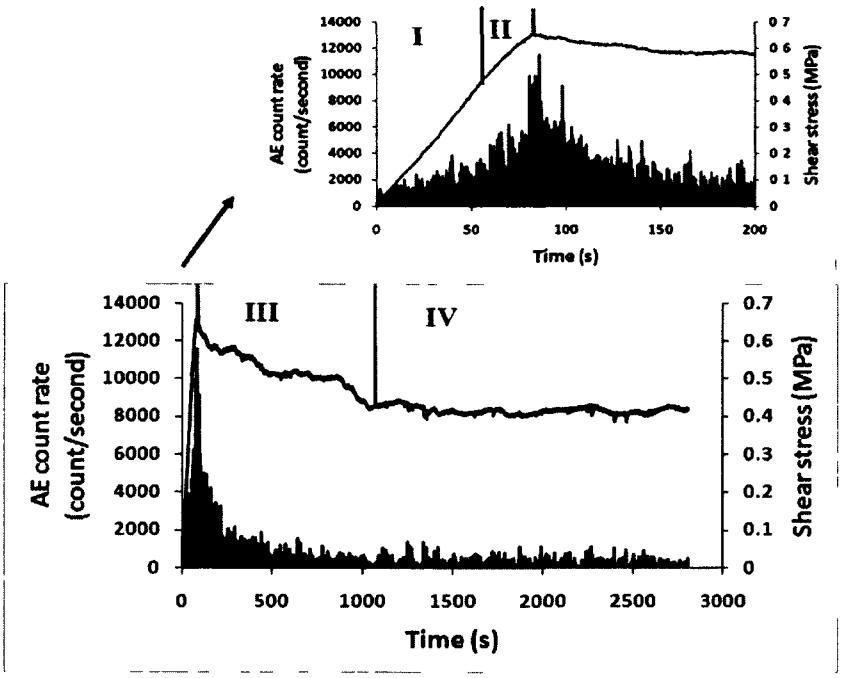

(d) Non-bonded rock-rock joint, (Sample RR10 48)

Figure 3-3: Shear stress and count rate vs. time: (a) bonded concrete–concrete joint (sample BCC3.45), (b) non-bonded concrete–concrete joint (sample CC8.35), (c) non-bonded rock–concrete joint (sample RC7.63) and (d) non-bonded rock–rock joint (sample RR10 48).

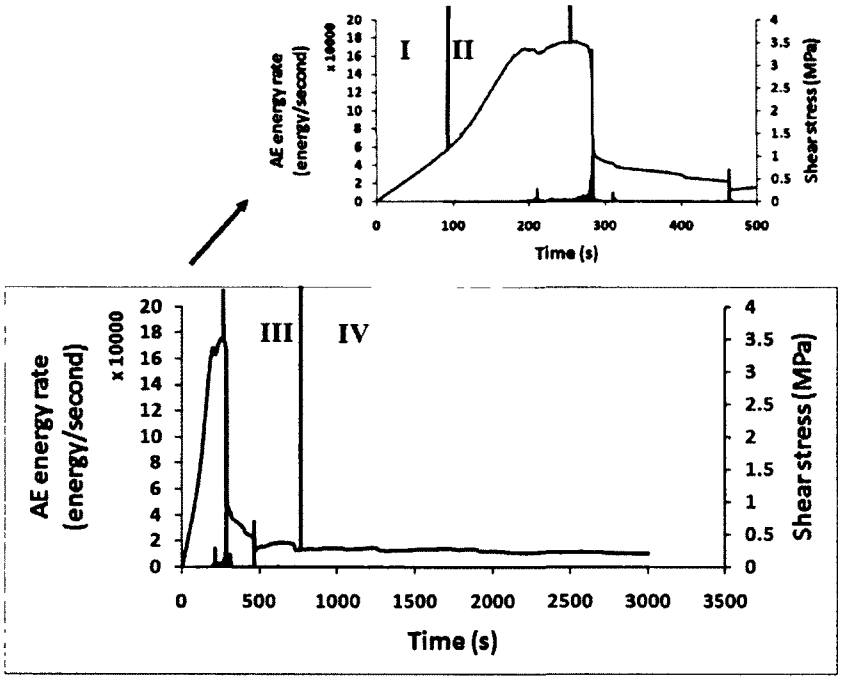

(a) Bonded concrete-concrete joint, (Sample BCC3.45)

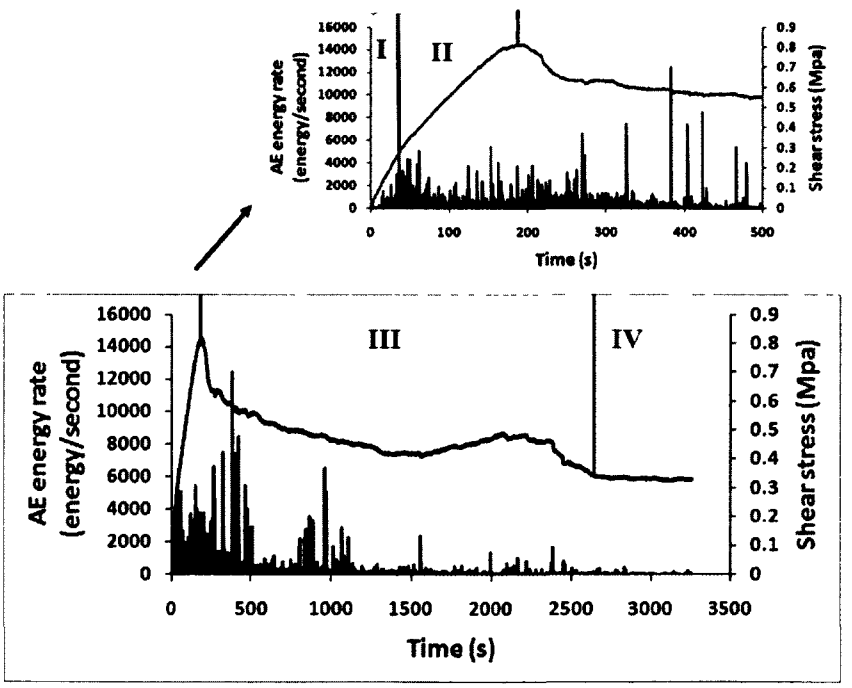

(b) Non-bonded concrete-concrete joint, (Sample CC8.35)

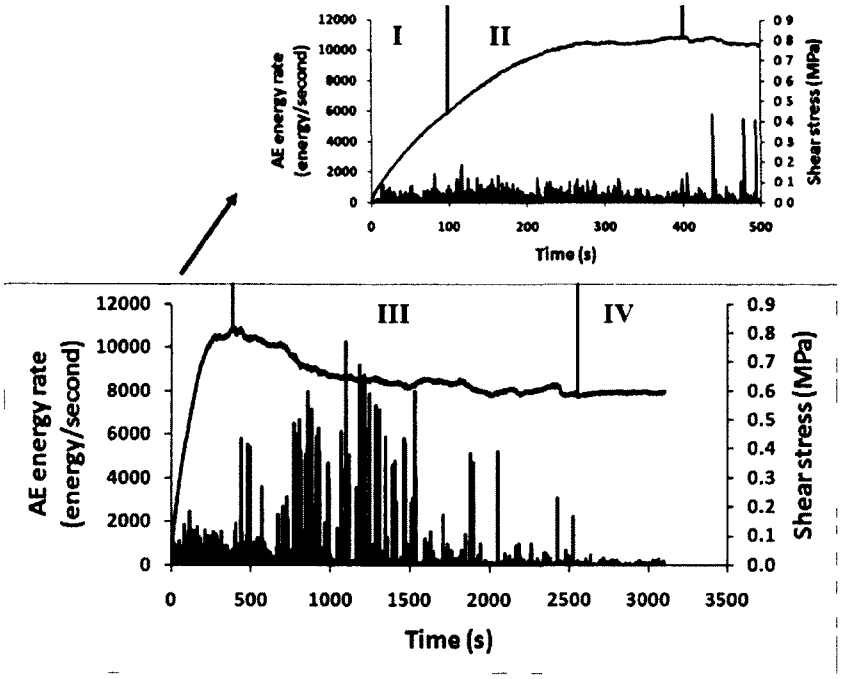

(b) Non-bonded rock-concrete joint, (Sample RC7 63)

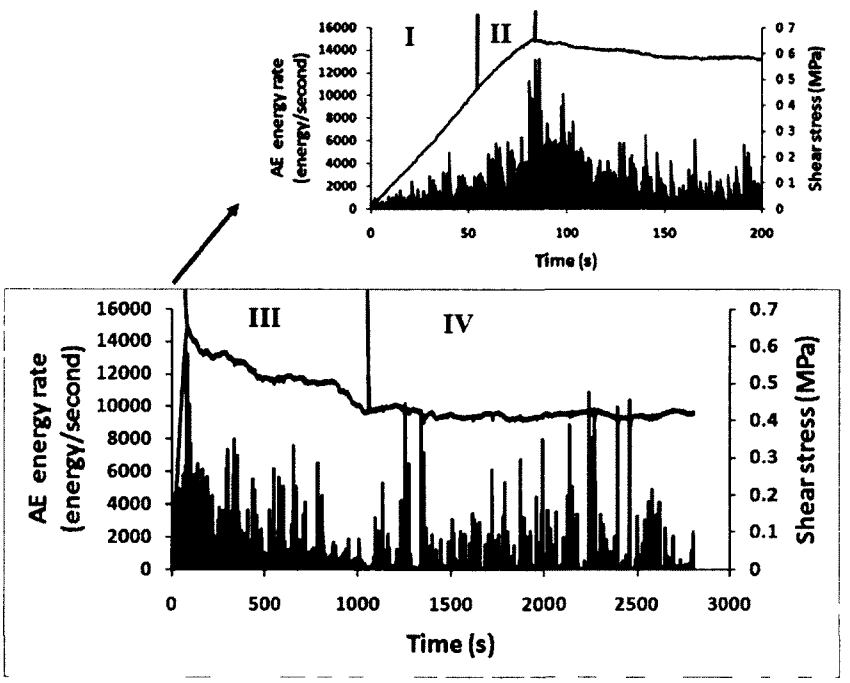

(d) Non-bonded rock-rock joint, (Sample RR10 48)

Figure 3-4: Shear stress and energy rate vs. time: (a) bonded concrete–concrete joint (sample BCC3.45), (b) non-bonded concrete–concrete joint (sample CC8.35), (c) non-bonded rock–concrete joint (sample RC7.63) and (d) non-bonded rock–rock joint (sample RR10.48).

In bonded joint, by applying shear load there is no change in shear displacement and consequently in AE parameters till joint failure (see periods 1 and 2 in Figure 3-4(a)), but it does not mean that the sample is not under loading. Using a load monitoring instrument such as load cell helps us to have a better insight about joint behavior.

The behavior of the bonded joint should be monitored by a combination of instruments because the delay between AE increasing and their maximum value (failure point) is short and it is difficult to predict the starting point of movement just by AE monitoring. Of course in the eventuality that a rupture includes a sequence of events even recording AE signals of the first break is still useful.

Figures 3-1b–d show that for non-bonded joints, shear displacement increases immediately after increasing in shear stress. The displacement generates AE signals right after the beginning of the test (Figs. 3-3b–d for count rate, and Figs. 3-4b–d for energy rate).

3.4. Monitoring pre-peak, peak and post peak of shear strength graph by means of AE

In this section the capability of the AE for monitoring the four periods in shear stress–shear displacement graph is evaluated using the following methods.

3.4.1. Study on the basis of counts and energy rate

A combination of count and energy rate with shear strength vs. time has been used to correlate the shear behavior of the joints with generated AE signals. For bonded joint samples (sample BCC3.45) there are no AEs in pre-peak linear period (period I). In pre-peak non-linear period (period II) some AEs are generated. They come from crack initiation and propagation in the contact surfaces. In post-peak period (period III), because of stress dropping, AEs increase dramatically and show their maximum peak. This process is due to cracking and breaking of the bonded shear surface. Following this large peak, there are some smaller peaks which are

generated from damaging of the secondary and primary asperities. At the residual period of shear stress graph, count and energy rate attain their minimum values. It seems that before this period the entire primary and secondary asperities have been sheared. The only movement in this period is the sliding of the joint surfaces, so since there is no distinct shearing in this period, the count and energy rate showed low values.

It can be seen in Figure 3-3 and Figure 3-4 (samples CC8.35, RC7.63 and RR10.48) that in period I, AEs start from background. It is believed that they come from locking of the joint halves. They show some instant peaks in this period. In period II AEs continue increasing proportionally to loading and almost show peaks in same size before maximum shear stress. These signals are because of breaking of the secondary asperities and sliding of the primary asperities. In period III, whole asperities (secondary and primary) are sheared off. In this period AEs increase suddenly after shear stress peak, so that the maximum value of the count and energy rate is observed in this period, they decrease gradually at the end of this period. Period IV for non-bonded joints is same to bonded joints just there is an exception for energy rate of sample number RR10.48 which shows some peaks in residual periods in Figure 3-4d. Comparing Figs. 3-3d and 3-4d it can be seen that count rate shows minimum values in this period. These peaks are results of instant breaking of the asperities which have low values of count rate but high values of energy rate.

3.4.2. Study on the basis of cumulative count and energy

Figure 3-5 and Figure 3-6 show the combination of the graph of cumulative count and energy with shear stress for joint samples under study. For bonded joint (sample BCC3.45), both cumulative count and energy graphs show nothing in pre-peak linear period. In pre-peak non-linear period they show a few signals near the end of this period. During post-peak period they show a vertical increasing and then a convexity behavior in their values and finally in residual period, they continue increasing with a very low rate.

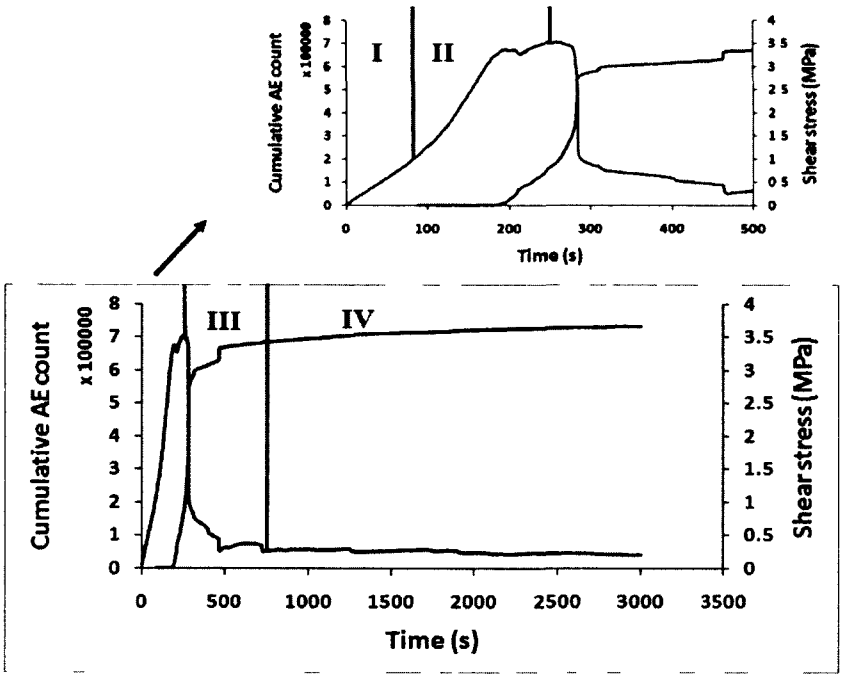

(a) Bonded concrete-concrete joint, (Sample BCC3 45)

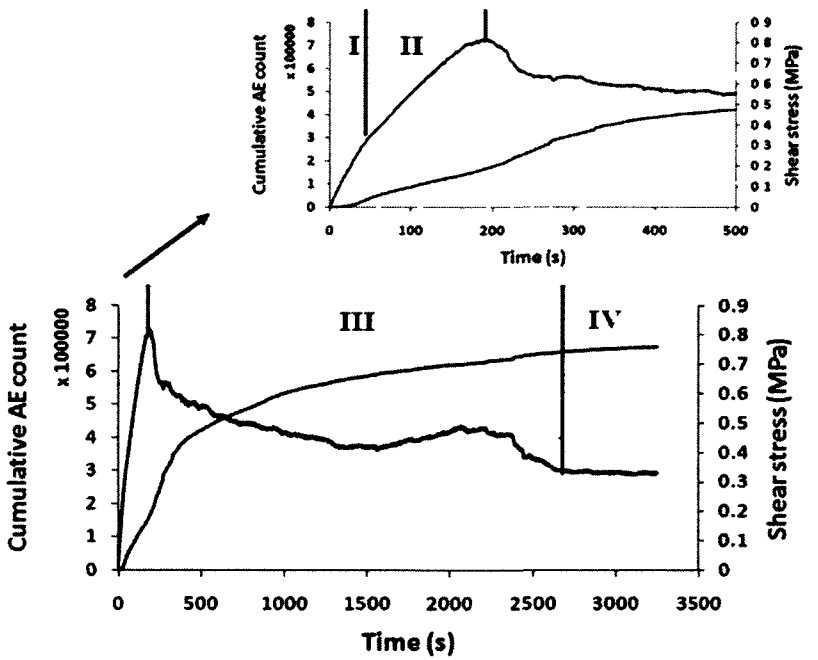

(b) Non-bonded concrete-concrete joint, (Sample CC8 35)

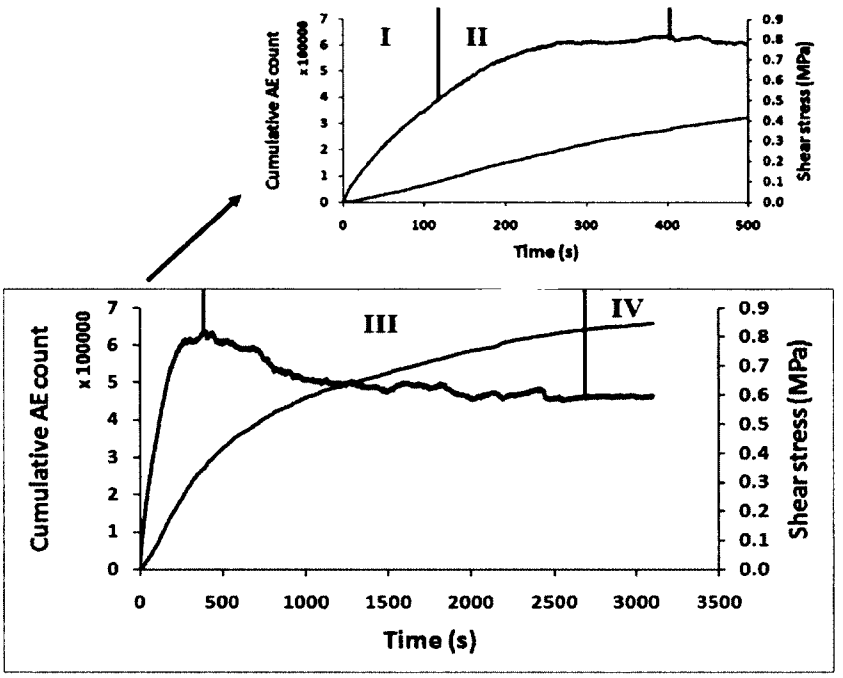

(c) Non-bonded rock-concrete joint, (Sample RC7.63)

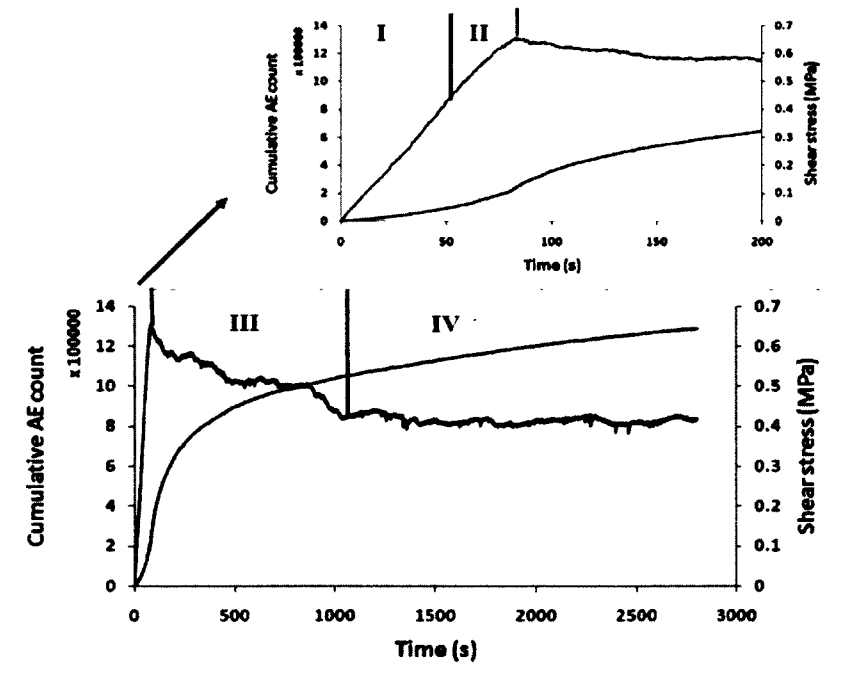

(d) Non-bonded rock-rock joint, (Sample RR10.48)

Figure 3-5: Shear stress and cumulative count vs. time: (a) bonded concrete–concrete joint (sample BCC3.45), (b) non-bonded concrete–concrete joint (sample CC8.35), (c) non-bonded rock–concrete joint (sample RC7.63) and (d) non-bonded rock–rock joint (sample RR10.48).

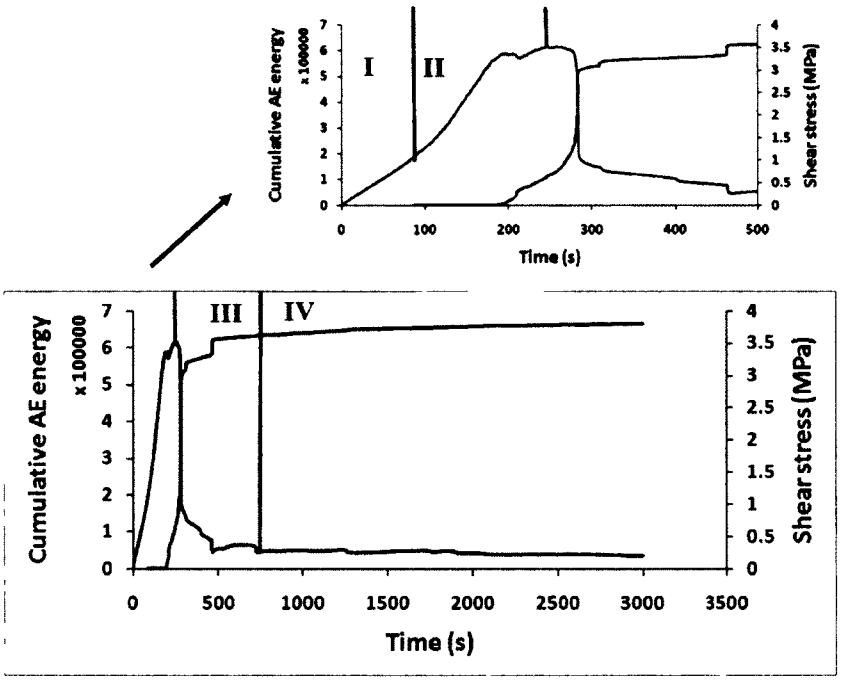

(a) Bonded concrete-concrete joint, (Sample BCC3.45)

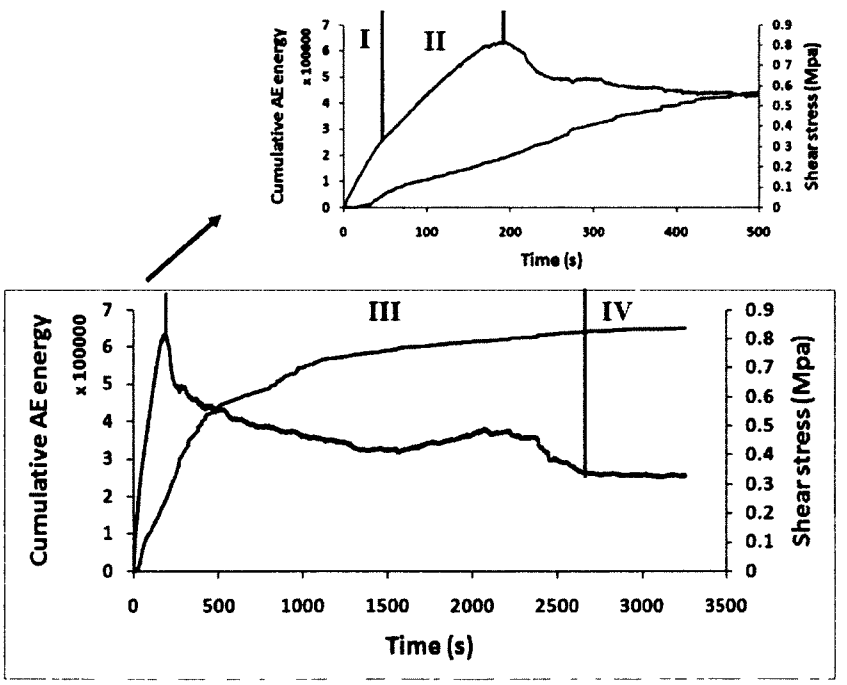

(b) Non-bonded concrete-concrete joint, (Sample CC8.35)

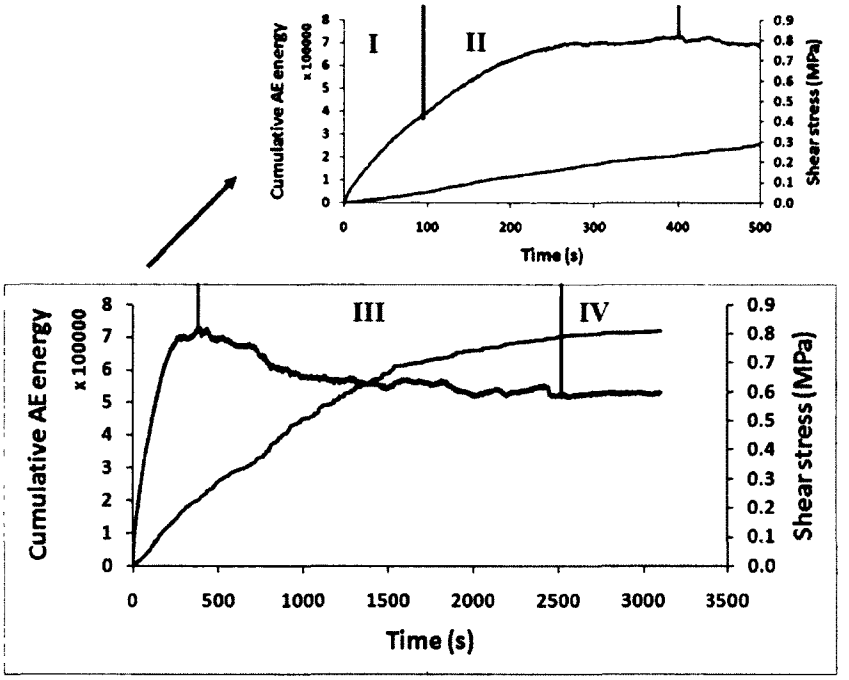

(c) Non-bonded rock-concrete joint, (Sample RC7.63)

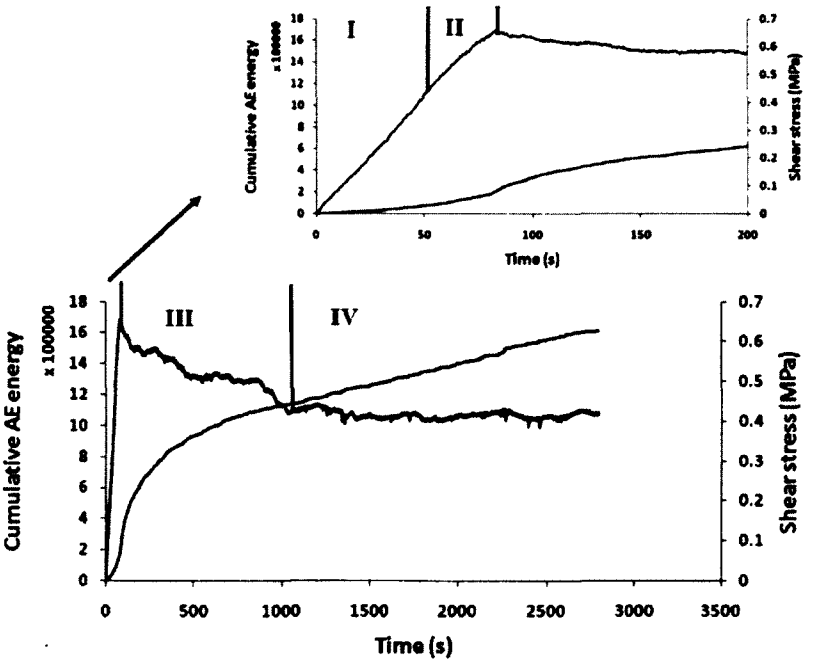

(d) Non-bonded rock-rock joint, (Sample RR10.48)

Figure 3-6: Shear stress and cumulative energy vs. time: (a) bonded concrete–concrete joint (sample BCC3.45), (b) non-bonded concrete–concrete joint (sample CC8.35), (c) non-bonded rock–concrete joint (sample RC7.63) and (d) non-bonded rock–rock joint (sample RR10.48).

For non-bonded joints (samples CC8.35, RC7.63 and RR10.48) cumulative count and energy graphs increase with concavity in pre-peak linear period and they show a linear increasing in pre-peak non-linear period. During post-peak period they show an increasing with convexity behavior. In residual period, like bonded joints, they continue increasing with a very low rate.

3.5. Discussion

For having a better knowledge about shear behavior of joints, 3D view and 2D profiles of the joint surfaces were drawn in Figures 3-7 to 3-12. Sample CC8.35 has rough surfaces with large asperities (see Figure 3-7 and Figure 3-8), corresponding 3D view and 2D profiles for this sample). For sample RC7.63 although the joint surfaces have a major asperity (Figure 3-9) but this is parallel to the shear direction, so that the 2D profile in this direction is almost smooth (Figure 3-10).

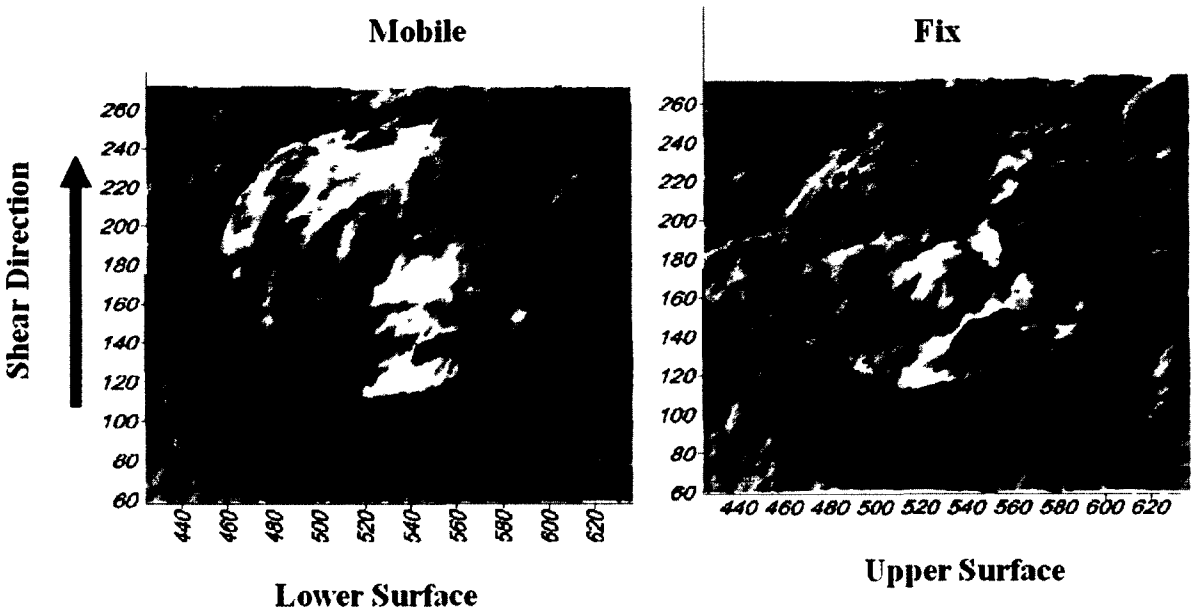

Figure 3-7: A 3D view of lower and upper surfaces of non-bonded concrete–concrete joint (sample CC8.35).

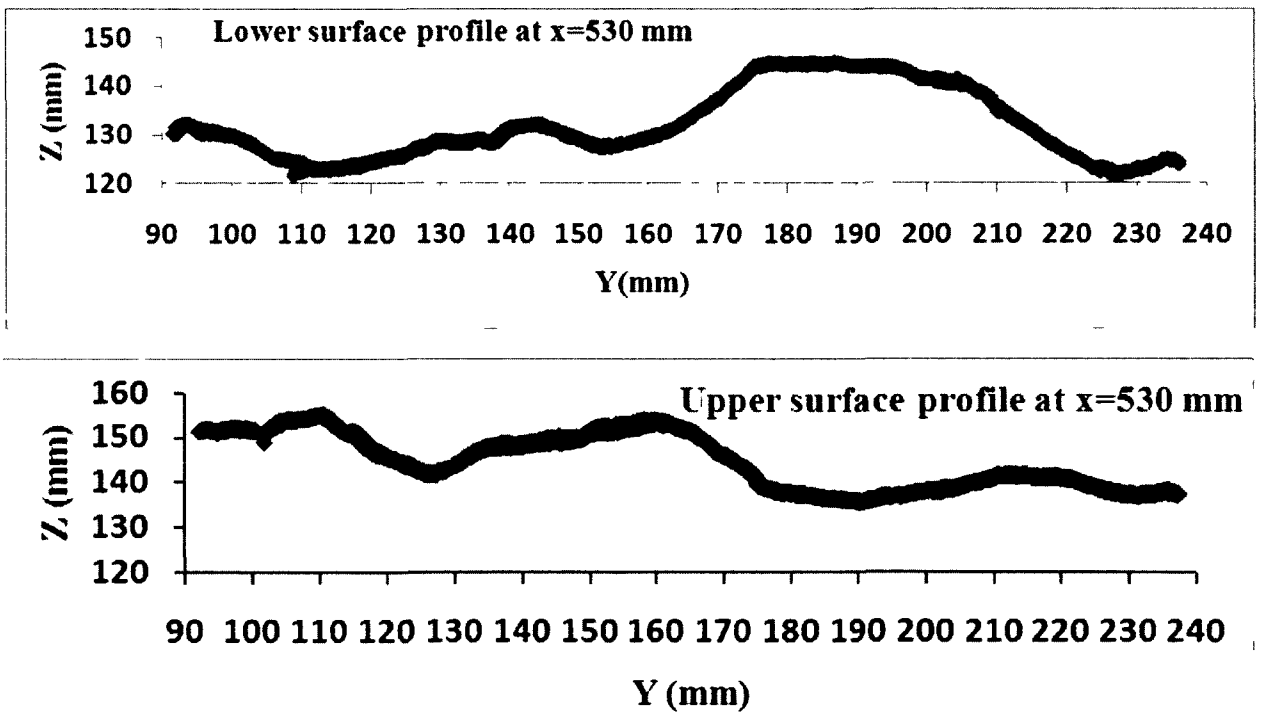

Figure 3-8: A profile drawn at middle of lower and upper surfaces of non-bonded concrete–concrete joint in the direction of shearing (sample CC8.35).

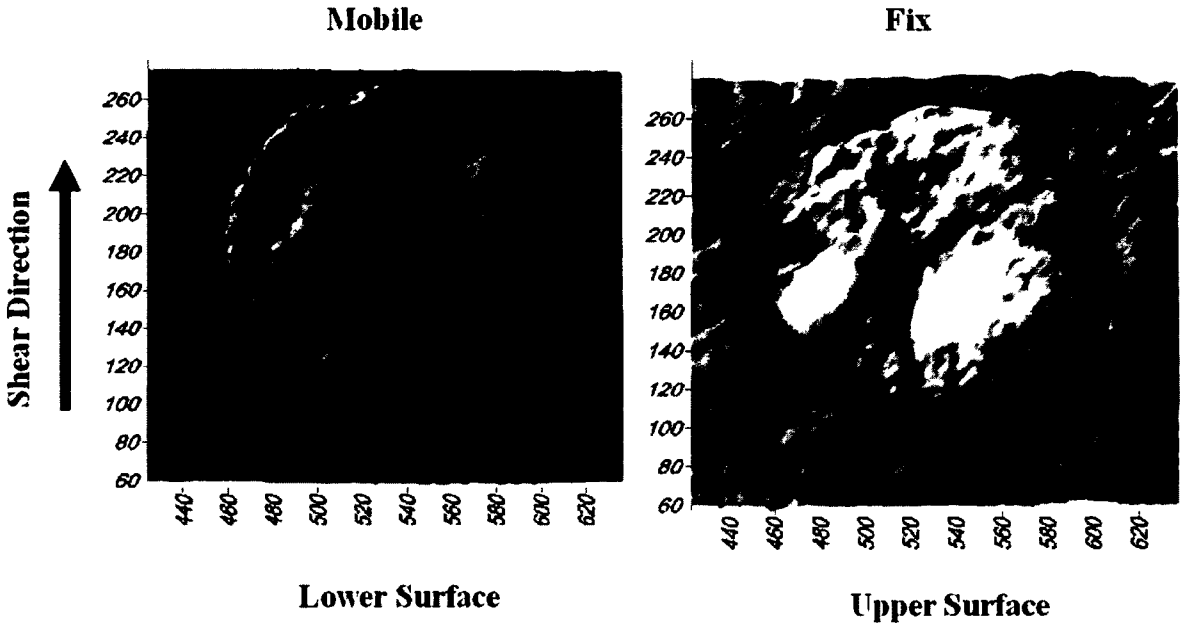

Figure 3-9: A 3D view of lower and upper surfaces of non-bonded rock–concrete joint (sample RC7.63).

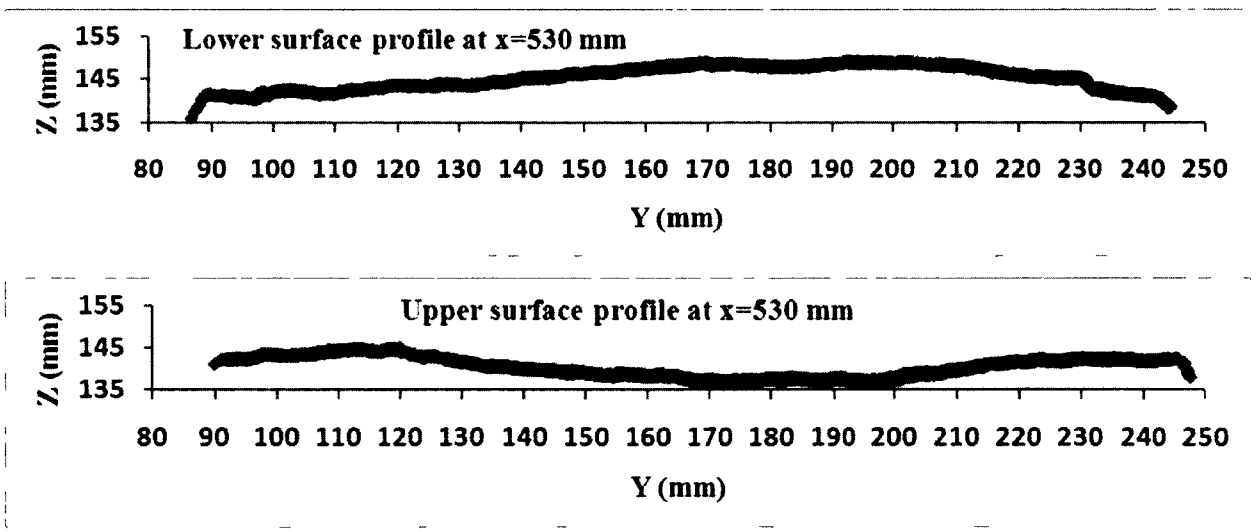

Figure 3-10: A profile drawn at middle of lower and upper surfaces of non-bonded rock–concrete joint in the direction of shearing (sample RC7.63).

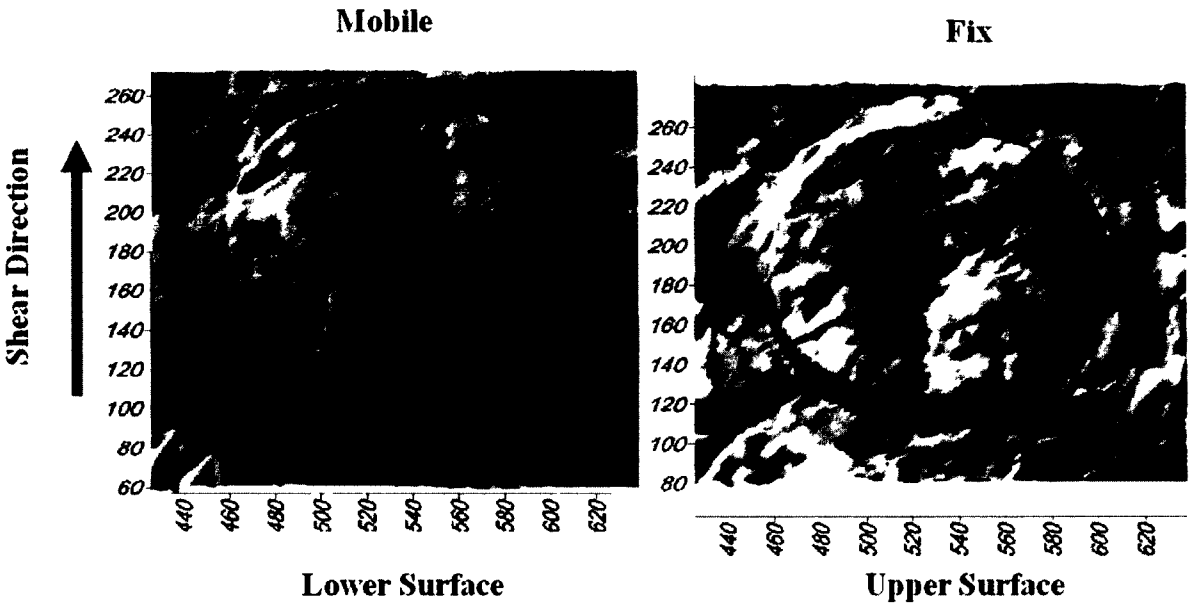

Figure 3-11: A 3D view of lower and upper surfaces of non-bonded rock–rock joint (sample RR10.48).

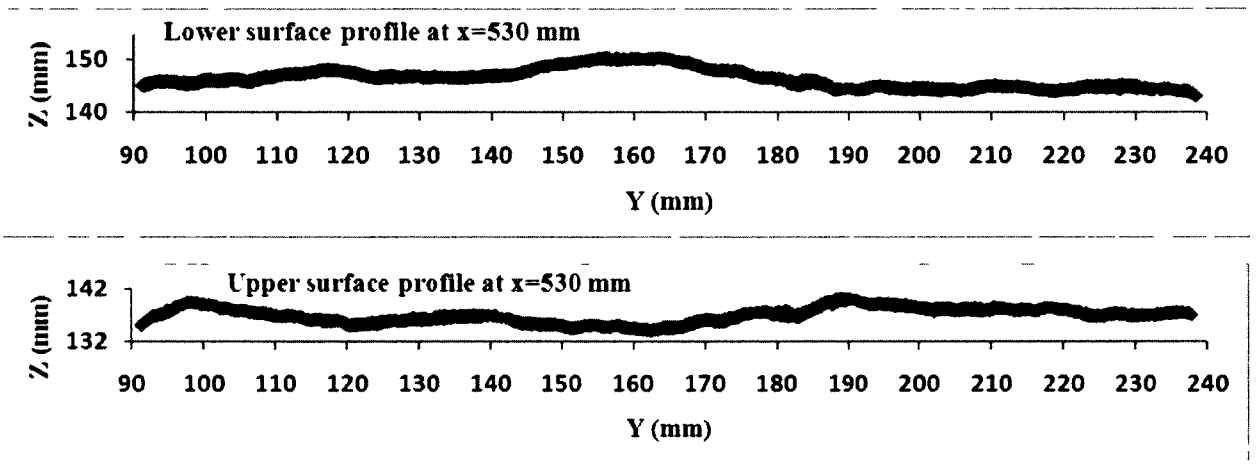

Figure 3-12: A profile drawn at middle of lower and upper surfaces of non-bonded rock–rock joint in the direction of shearing (sample RR10.48).

In Figure 3-1b, the behavior of the sample in section highlighted in circle, is just an overriding trough a major asperity. According to Figs. 3-3b (count rate graph) and 3-4b (energy rate graph) there are no significant changes in this section.

It seems that all of primary and secondary asperities are sheared after maximum shear strength but it strongly depends on the amount of constant normal load and joint roughness. In low values of normal load, large asperities in samples CC8.35 with Z_2=0.687 and RC7.63 with Z_2=0.487 just slide on each other without any significant failure. On the other hand small asperities in sample RR10.48 with Z_2=0.34 (Figure 3-11 and Figure 3-12) are sheared and show significant failure (Figure 3-3d).

Figure 3-3 and Figure 3-4 show that sample RR10.48 with small asperities show larger peaks in the graphs of count and energy rate. The amounts of cumulative count and energy for this sample are much higher than those for samples with larger asperities. This demonstrates that in low values of normal load, joints with smaller asperities generate more AE signals than joint with large asperities. It is due to damaging of the smaller asperities in this loading condition.

Distinguishing shearing or sliding processes of the movements is another purpose that can be achieved by AE signals. By comparing the shear and AE graphs it can be find out when the sample joint has sliding process and when it has shearing process.

Typically non-bonded joints under low value of normal load show sliding behavior. On the other hand non-bonded joints under high values of normal load and bonded joints under any value of normal load show shearing process.

By comparing the shear stress graphs (Figure 3-1) with displacement graphs (Figure 3-2) it can be seen that the shearing process in bonded concrete-concrete joint, sample BCC3.45 (Figure 3-1a) and non bonded concrete-concrete joint, sample CC8.35 (Figure 3-1b) is more dominant. However non-bonded rock-concrete joint, sample RC7.63 (Figure 3-1c) and non bonded rock-rock joint, sample RR10.48 (Figure 3-1d) show sliding process because:

- In shearing process the peak of the maximum shear strength is more significant than in sliding process (comparing Figure 3-1a with Figure 3-1c).
- The difference between maximum shear strength and residual shear strength are more significant in shearing process (comparing Figure 3-1a with Figure 3-1c);

- In shearing process the rate of the normal displacement-shear displacement curve is more than in sliding process (comparing Figure 3-2a with Figure 3-2c).
- In shearing process the maximum normal displacement is higher than in sliding process (comparing Figure 3-2a with Figure 3-2c).

AE counts and AE energy confirm above observations:

- For shearing process the amount of AE parameters is clearly higher than for sliding process (comparing Figure 3-3a with Figure 3-3c).
- The difference between AE peaks after failure and AE peaks during residual section is very significant in shearing process. This represents the failure of asperities before residual section (comparing Figures 3-3a and 3-3c).
- In sliding process since there is not a distinctive shearing or failure for asperities, the AE peaks continue with the same values after failure and during the residual section (Figure 3-3c and 3-3d).

It was found that there are no specific differences between acoustic emission respond of rock-rock, rock-concrete and concrete-concrete joints. Nevertheless, since the majority of natural rock-concrete interfaces had already been altered by physico-chemical changes through agencies such as groundwater and weathering, their surfaces were almost slickensided and during direct shear testing they showed less AE activity than rock-rock and concrete-concrete joints.

3.6. Conclusions

In this paper, acoustic emission was found to be useful and adequate for monitoring the shear behavior of the different joints. Some direct shear tests were performed to investigate the application of the AE for monitoring the shear behavior of rock–rock, rock–concrete and concrete–concrete joints. AE was monitored during shearing of joints under constant normal load (CNL). Count and energy parameters were analyzed to examine the relation between shear behavior and AE.

Two methods were used to monitor pre-peak linear, pre-peak non-linear, post-peak and residual periods in shear stress–shear displacement graphs of joints: using a combination of

count and energy rate with shear graphs, and using a combination of cumulative count and energy with shear graphs. Table 3-2 summaries the behavior of AEs in each period using two different methods.

Table 3-2: Different behaviors in shear stress–shear displacement graphs monitored by AE.

Periods	**Behavior according to count and energy rate**		**Behavior according to cumulative count and energy**	
	Bonded joints	**Non-bonded joints**	**Bonded joints**	**Non-bonded joints**
Pre-peak linear period	No signal	Increasing from background in low values, maybe some instant peaks	No signal	Increasing with concavity
Pre-peak non-linear period	A few signals near the end	Increasing in a constant rate with peaks in same size	Low increasing near the end	Linear increasing
Post peak period	Increasing dramatically till maximum value and decreasing very fast	Increasing dramatically and decreasing gradually	Increasing vertically and continuing with convexity	Increasing with convexity
Residual period	Attaining minimum values with some instant peaks	Attaining minimum values with some instant peaks	Increasing, with a very low rate	Increasing, with a very low rate

The results of this study showed that simulating various kinds of joints and correlating AE and shear graphs in laboratory provides a better interpretation of the shear process of the in situ discontinuities when there are just the results of the AE monitoring.

For non-bonded joint, shear displacement is started and AE is generated by applying shear load. For these joints the distance between AE detection and failure is long enough to implement some remedial solutions.

For bonded joint, shear displacement does not start right after applying shear load, so the start point of movement cannot be detected by AE before failure. The distance between AE initiation and failure is very short; therefore there is not enough time for remedial solution. A combination of other instruments such as loading measuring instruments is needed to be aware of the behavior of the joint before this point. Since this phenomenon can be caused by adhesive bond between rock and concrete replicas, in the next paper the effect of adhesive bond on shear behavior and acoustic emission responds of bonded joints will be evaluated.

4. APPLICATION OF ACOUSTIC EMISSION FOR MONITORING SHEAR BEHAVIOR OF BONDED CONCRETE-ROCK JOINTS UNDER DIRECT SHEAR TEST

Authors and affiliation:
Z. Moradian: PhD student, Université de Sherbrooke, Faculté de génie, Département de génie civil.
G. Ballivy: Professeur, Université de Sherbrooke, Faculté de génie, Département de génie civil.
P. Rivard: Professeur, Université de Sherbrooke, Faculté de génie, Département de génie civil.

Date of submission: 1 November 2010

Acceptation state: Submitted

Journal: Canadian Journal of Civil Engineering

Reference: [10-397]

Titre français: Application de l'émission acoustique pour surveiller le comportement en cisaillement des joints roche-béton liées pendant l'essai de cisaillement direct.

Contribution in paper:
The author of the thesis has contributed in this paper as first, principal and corresponding author.

Résumé français:
La résistance au cisaillement du contact béton-rocher de la fondation des barrages en béton contrôle la stabilité des barrages. Par conséquent, l'étude du comportement en cisaillement et du mécanisme de rupture des interfaces béton-rock entre le corps du barrage en béton et la fondation rocheuse est très intéressante. À cette fin, des essais de cisaillement direct en laboratoire ont été effectués sur plusieurs interfaces liées. En appliquant de faibles valeurs de charge normale, il a été simulé le comportement de charge de terrain le plus près possible de la réalité. L'effet de la contrainte normale, de la vitesse de déplacement et du pourcentage de liaison sur le comportement de cisaillement de joints collés a également été évalué. Les

résultats ont montré que l'adhérence entre le béton et la roche a l'effet le plus important sur le mécanisme de cisaillement des interfaces béton-rock. Lorsque la charge normale est faible, les aspérités ne contribuent pas au processus de cisaillement, de sorte que la résistance au cisaillement des joints est régie par le lien de l'interface. La seule contribution des aspérités, c'est qu'ils montrent un petit pic après le pic de rupture de la liaison. Aucune rupture significative n'a été observée après cette petite pointe. Lorsque la charge normale est élevée, les aspérités rupturent simultanément avec le lien et ils montrent leur contribution dans le processus de cisaillement. En diminuant le pourcentage de liaison, la rupture fragile des interfaces liées est transformée en une rupture avec davantage de déformation en raison de la plus faible contribution de la liaison adhésive et de celle plus forte des aspérités rugueuses en rupture de joint. L'analyse des joints liés par EA a montré que pour tous les échantillons testés dans des conditions de charge différentes, il n'y a pas ou très peu d'activités d'EA avant la rupture du lien. Ceci indique que d'autres paramètres (rugosité, charge normale, vitesse de déplacement) sont des facteurs moins importants que la liaison adhésive du joint. Ainsi donc, la résistance au cisaillement maximale du joint est déterminée principalement par la résistance du lien du joint.

Abstract

Shear resistance of concrete-rock contact in the dam-foundation interfaces influences their stability. Therefore; studying shear behavior and failure mechanism of concrete-rock interfaces between concrete dam and rock foundation is highly important. To this end, laboratory direct shear tests were conducted on several bonded interfaces. By applying low values of normal load, it was tried to simulate the field condition as close as possible. The effect of normal stress, displacement rate and bonding percentage on shear behavior of bonded joints were also evaluated. The results showed that the adhesive bond between concrete and rock has the most important effect on shear mechanism of concrete-rock interfaces. When the normal load is low, the asperities do not contribute in shear process, so the shear strength of the joints is governed by adhesive bond. The only contribution of the asperities is that they show a small peak after bond breaking peak. No significant failure was observed after this small peak. When the normal load is high, the asperities break simultaneously with adhesive bond and they show their contribution in the whole shear process. By decreasing bonding

percentage, the brittle failure of the bonded joints is changed into softening failure because of less contribution of the adhesive bond and more contribution of the rough asperities in joint failure. AE monitoring of bonded joints showed that for all the different tested samples under various loading conditions, there has been no or very few AE activities before adhesive bond breaking point, indicating that other parameters (roughness, normal load, displacement rate) are impressed by adhesive bond and maximum shear strength is just determined by this parameter.

4.1. Introduction

Studying the shear behavior and its governing mechanical properties of concrete - rock joint in interface of dam body and rock foundation provides useful information about shear failure mechanism and interaction circumstances of these interfaces. This information is required in any safety and stability analysis of concrete dams. The main mechanical properties affecting the strength of the concrete-rock joints include roughness, adhesion strength, normal load, displacement (loading) rate and strength difference between rock and concrete.

Although several studies have been done on shear strength of non-bonded concrete-rock joints (Lo et al. 1990, Johnstone & Lam 1984, Kodikara & Johnston 1994, Lam, & Johnston 1989, Seidel & Haberfield 2002, Gu et al. 2003, Haberfield & Seidel 1999), few tests have been conducted on bonded concrete-rock joints (Johnston et al. 1987, Ballivy et al. 2006, Changwoo 2002, Cater & Ooi 1988, Saiang et al. 2005). Cater and Ooi (1998) studied shear hardening and softening behavior of bonded concrete-rock joints. Saiang et al. (2005) conducted laboratory tests on shotcrete-rock joints in direct shear test. They showed that for low values of normal load (less than 1 MPa) the shear strength is determined by the bond strength for genuinely bonded shotcrete-rock interfaces (Saiang et al. 2005).

Acoustic emission (AE) is a useful non-destructive technique for determining on-going damage in materials. AE is defined as an elastic wave which is radiated from rapid release of energy due to damaging of materials. Despite the wide use of AE in rock mechanics fields, a few studies have addressed the application of this technique for monitoring shear mechanism

of rock joints (Hong & Seokwon 2004, Li & Nordlund 1990, Seto et al. 1997, Rim et al. 2005, Son et al. 2006).

Moradian et al. (2010) conducted laboratory tests on natural joints cored from a dam body to study damage during constant normal load direct shear test of concrete-concrete, concrete-rock and rock-rock joints.

Hong & Seokwon (2004) performed a series of direct shear tests to investigate the influence of shear load on AE characteristics of concrete-rock interface under constant normal load. Li and Nordlund (1990) characterized AE during shearing of rock joints using artificial and natural joints. Rim et al. (2005) investigated the characteristics of the AE from the artificial saw tooth joints and replicas of the natural rock joints during the CNS shear test. Son et al. (2006) investigated the characteristics and source locations of acoustic emissions from the joints during the CNS shear test and the CNL shear test. None of the mentioned researches have addressed role of the adhesive bond on shear mechanism of bonded concrete-rock joint. In this study, constant normal load (CNL) direct shear tests were applied on bonded concrete-rock joints and AE signals were detected to study shear mechanism of bonded concrete-rock joint in laboratory as a feasibility study for studying shear behavior of in situ interfaces in concrete dams. By changing bonding percentage, normal load and displacement rate, the shear mechanism of these interfaces under various conditions was evaluated too.

4.2. Methodology

Replica of rock samples with identical distribution of grain size and a constant roughness were cored from a large block of granite (Barre granite from Vermont, USA). The samples were cored using A 6-inch inner diameter diamond bit (Figure A2-1). In the next step, mortar was poured on each rock joint by means of a wrapped steel sheet around the rock replica to fabricate the concrete replica (Figure A2-6). The mixture of mortar used for pouring is shown in Table 4-1.

Table 4-2 contains physical and mechanical properties of the rock and concrete used for direct shear testing of the joints. After curing for 28 days, samples were tested according to ASTM

standard (2002) and using a rigid MTS loading system. Normal load was fixed during direct shear testing of the samples.

A PAC μ-SAMOS AE system with four 3α general purpose sensors was used for detecting AE events. The frequency range of sensors was 25-530 KHz. The sample rate was 1 MSPS, amplification of pre-amplifier was 40 db, and AE exceeding 50 db was measured.

Table 4-1: The mixture recipe for 90 kg mortar

Cement	25.2 (kg)
Sand	56.0 (kg)
Water	8.82 (kg)
Super Plasticizer	387 (gr)

Table 4-2: Physical and mechanical properties of the rock and concrete replicas

	Number of tested samples	**Bulk specific gravity**	**P-wave velocity (m/s)**	**Young modulus (GPa)**	**Poisson ratio**	**Uniaxial compressive strength (MPa)**
Granite	3	2.63	4675	58.1	0.30	179
concrete	3	2.37	4765	40.0	0.23	83

4.3. Shear mechanism of bonded concrete-rock joints

In a previous study (Moradian et al. 2010), the authors divided the shear behavior of joints into four periods: pre-peak linear period, pre-peak non-linear period, post-peak period and residual shear strength period. They concluded that AE can be used as an adequate and confident method for monitoring shear behavior of non-bonded joint. They proposed a combination of AE with other instrumentation measures for monitoring shear behavior of bonded joints because of its lack of ability for monitoring pre-peak behavior of these joints. In order to study the shear behavior of bonded joints comprehensively, several joints samples with different

bonding percentages were tested. The objective was to investigate how bonding percentage changes shear behavior and AE responds of fully and partially bonded joints.

Figure 4-1 shows the four periods in shear behavior of a bonded concrete-rock joint. It can be seen that there are no AEs in pre-peak linear period (period I) for bonded joint samples. In pre-peak non-linear period (period II) some AEs may be generated depending on the bonding percentage and normal load. These signals come from crack initiation and propagation in the adhesive bond. In post-peak period (period III), because of stress dropping, AEs increase dramatically and show their maximum peak. This process is associated with cracking and breaking of the bonded shear surface. At the residual period of shear stress graph, AEs reach their minimum values. The only movement during this period is the sliding of the joint surfaces; since there is no distinct shearing in this period, the AE signals show low values.

As it can be seen in Figure 4-1a and 4-1b, there is a distinct maximum shear stress occurring at a shear displacement of less than 1 mm. This maximum shear stress coincided well with the maximum peak of AE energy. All of the fully bonded concrete-rock joints showed a brittle failure in their maximum shear strength. This brittle failure is due to adhesive bond of the interfaces so that the more adhesive bond the more brittle failure and consequently the more drop in maximum shear strength is occurred. The maximum shear strength is almost an order of magnitude higher than the residual shear strength for these joints, indicating a significant loss of support that occurs when the adhesive bond is broken (Saiang et al. 2005).

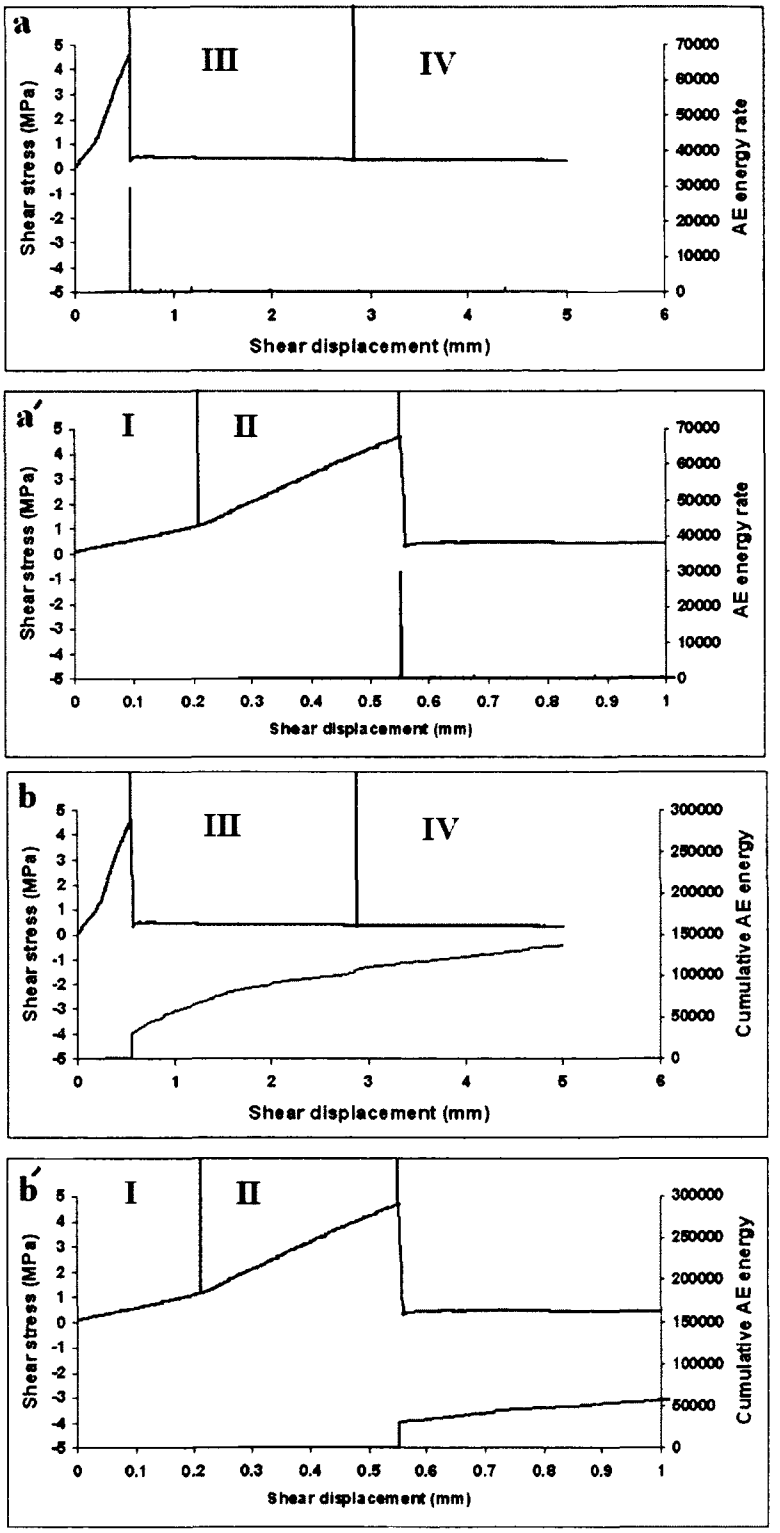

Figure 4-1: Four detected periods in shear behavior of a bonded concrete-rock joint under normal stress of 0.25 MPa a) shear stress and AE energy rate vs. shear displacement, b)shear stress and cumulative AE energy vs. shear displacement, á and b′) are a close-up of the graphs a and b for 1mm of shear displacement

It was observed that for the fully bonded concrete-rock joints under low values of normal load, the adhesive bond breaks separately. Then the asperities show their contribution in shear mechanism by a small peak after adhesive bond breaking peak. Then, the asperities show a little contribution in shear process in residual shear strength period. Figure 4-2 shows the normal displacement vs. shear displacement of the mentioned concrete-rock sample. The upper surface (concrete replica) jumped about 0.3 mm due to adhesive bond breaking and its dilation is continued by shear loading. After this jump, since there is not enough normal stress to override the dilation, the joint surfaces do not perfectly match and this phenomenon cause asperities not to fail completely. It suggests that, at the low values of normal load, the shear behavior of the bonded joints depends mainly on the adhesive bond of the rock and concrete surfaces. At the high values of normal load, the asperities break simultaneously with adhesive bond and have more contribution in shear process.

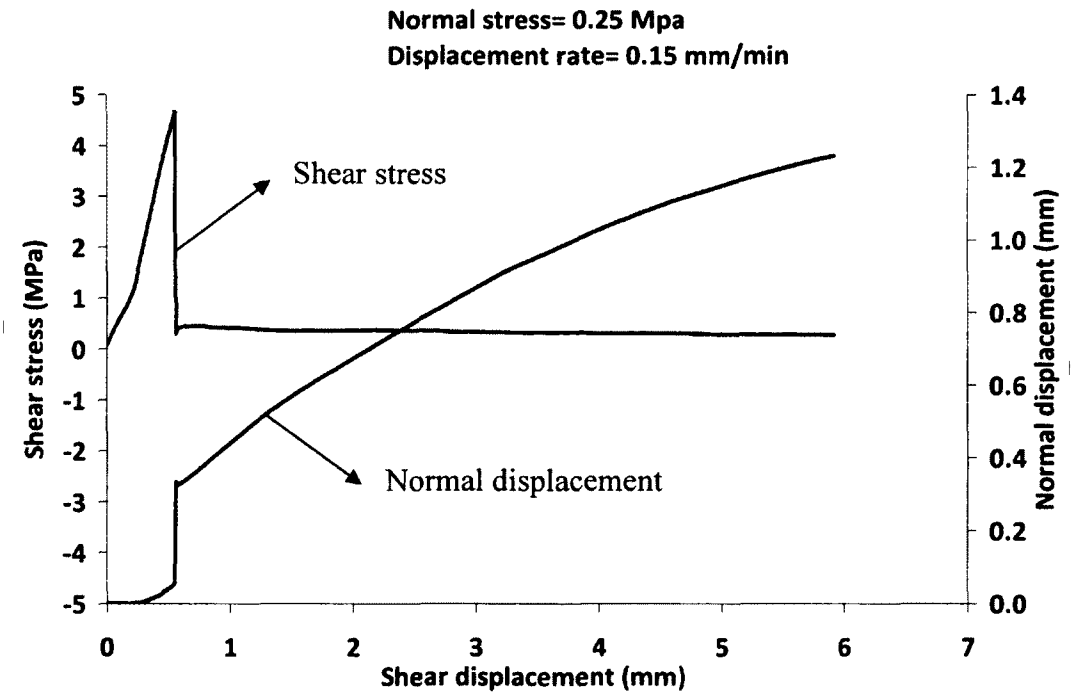

Figure 4-2: Normal displacement vs. shear displacement

4.4. The effect of bonding percentage

The effect of bonding percentage (B.P.) as one of the most important parameters affecting the shear strength of the bonded joints is investigated. For this purpose, concrete-rock joints with same roughness and mechanical properties were tested under different values of bonding percentages. A thin layer of clay was spreaded on the joint surface of rock replica in order to prevent bonding. The rest surface is left to bond with pouring concrete. Figure 4-3 shows a schematic of clayed sections and bonding percentage for every sample.

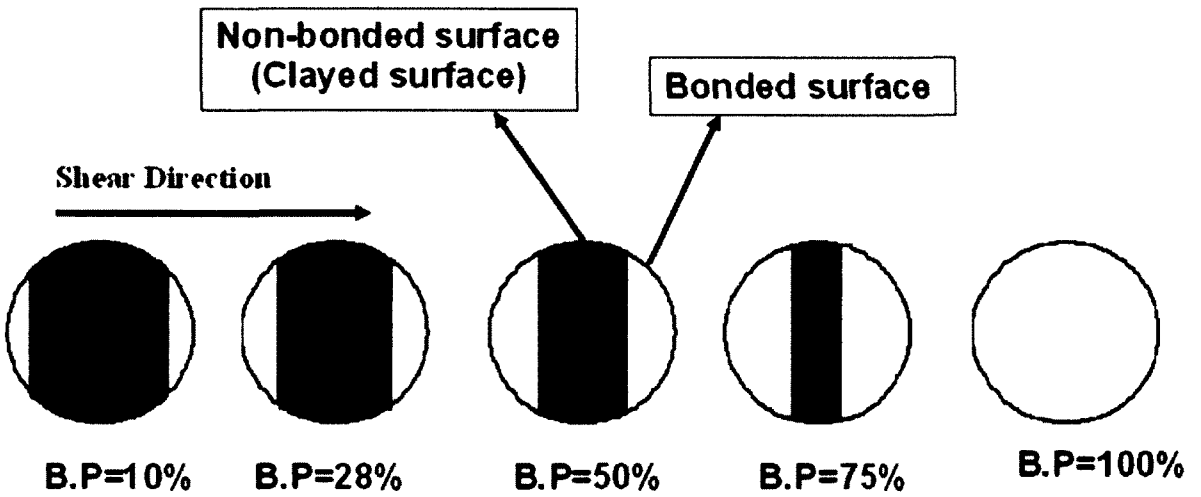

Figure 4-3: Schematic plans showing the bonding percentages of the joint samples

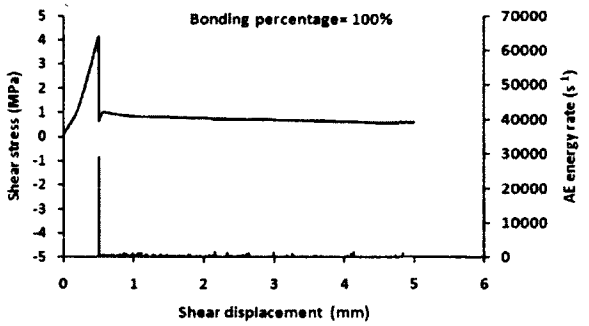
Bonding percentage= 100%
Shear stress (MPa)
AE energy rate (s⁻¹)
Shear displacement (mm)

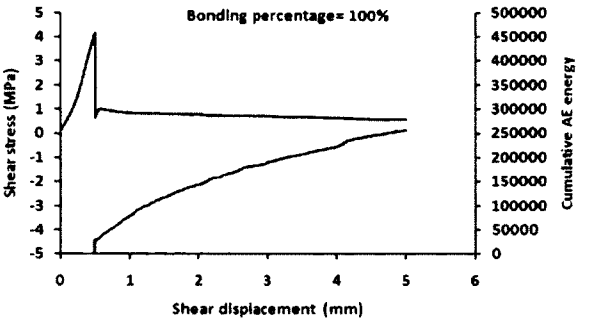
Bonding percentage= 100%
Shear stress (MPa)
Cumulative AE energy
Shear displacement (mm)

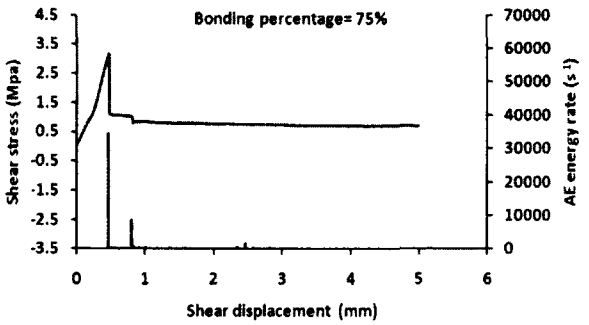
Bonding percentage= 75%
Shear stress (Mpa)
AE energy rate (s⁻¹)
Shear displacement (mm)

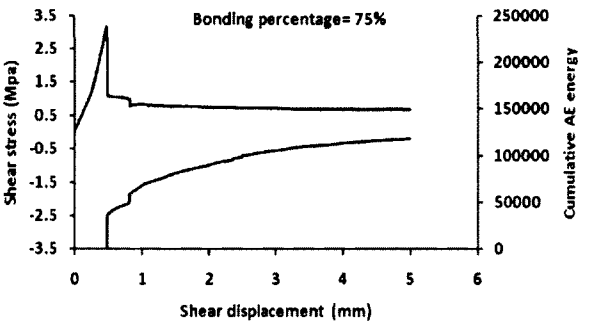
Bonding percentage= 75%
Shear stress (Mpa)
Cumulative AE energy
Shear displacement (mm)

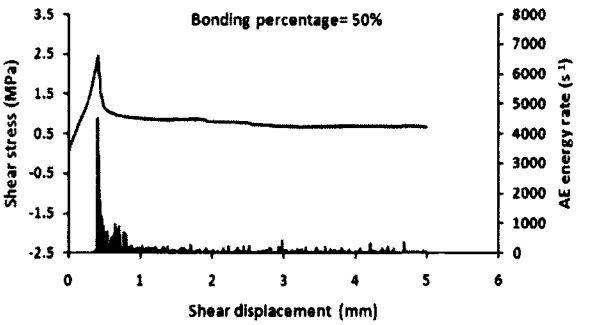
Bonding percentage= 50%
Shear stress (MPa)
AE energy rate (s⁻¹)
Shear displacement (mm)

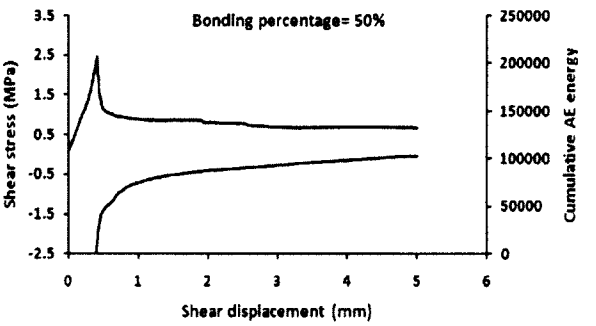
Bonding percentage= 50%
Shear stress (MPa)
Cumulative AE energy
Shear displacement (mm)

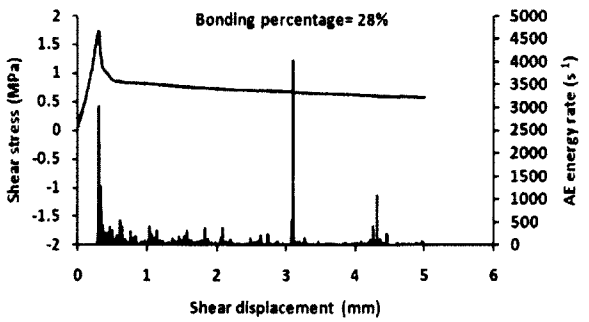
Bonding percentage= 28%
Shear stress (MPa)
AE energy rate (s⁻¹)
Shear displacement (mm)

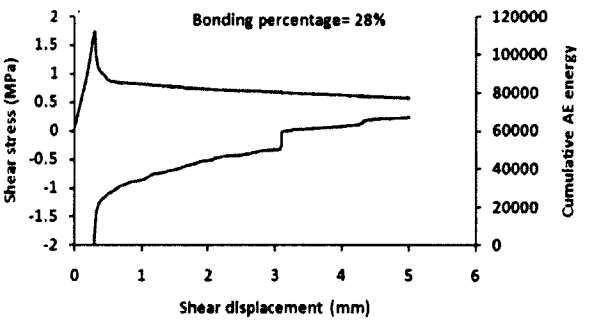
Bonding percentage= 28%
Shear stress (MPa)
Cumulative AE energy
Shear displacement (mm)

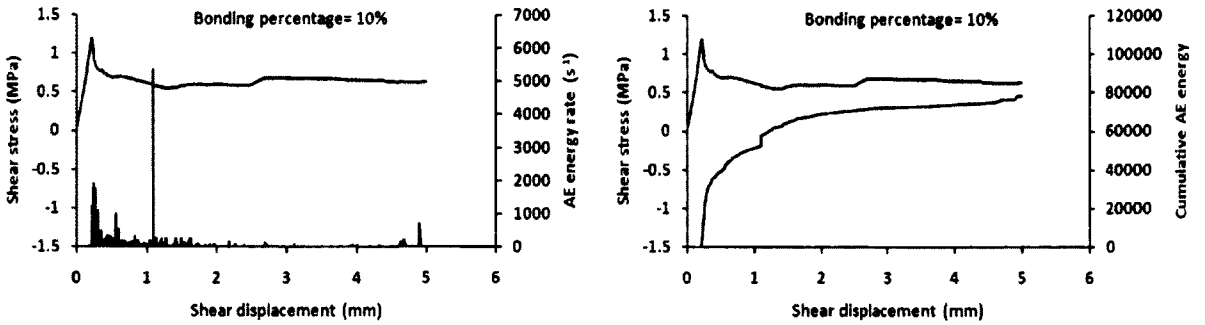

(a) (b)

Figure 4-4: Shear stress and a) AE energy rate b) Cumulative AE energy vs. shear displacement for various bonding percentages.

Table 4-3: Shear strength and AE results of the samples under different values of bonding percentage

Sample	Bonding percentage (%)	Displacement rate (mm/min)	Normal stress (MPa)	Max. shear strength (MPa)	Residual shear strength (MPa)	Shear displacement at the peak (mm)	Max. AE energy rate at the peak	Max. AE energy rate	Cumulative AE energy
1	100%	0.15	0.5	4.13	0.69	0.5	28914	28914	256623
2	75%	0.15	0.5	3.16	0.76	0.47	34406	34406	118840
3	50%	0.15	0.5	2.47	0.79	0.41	4500	4500	102840
4	28%	0.15	0.5	1.74	0.68	0.3	3015	4037	67040
5	10%	0.15	0.5	1.2	0.65	0.2	1911	5355	78240

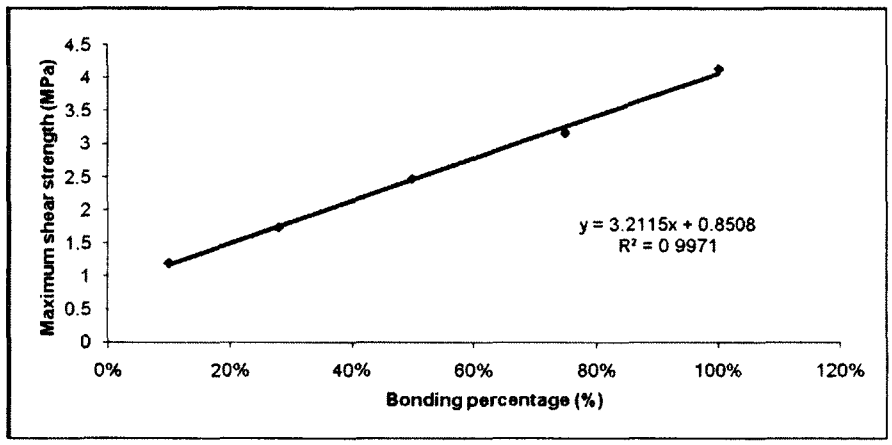

Figure 4-5: Maximum shear strength vs. bonding percentage

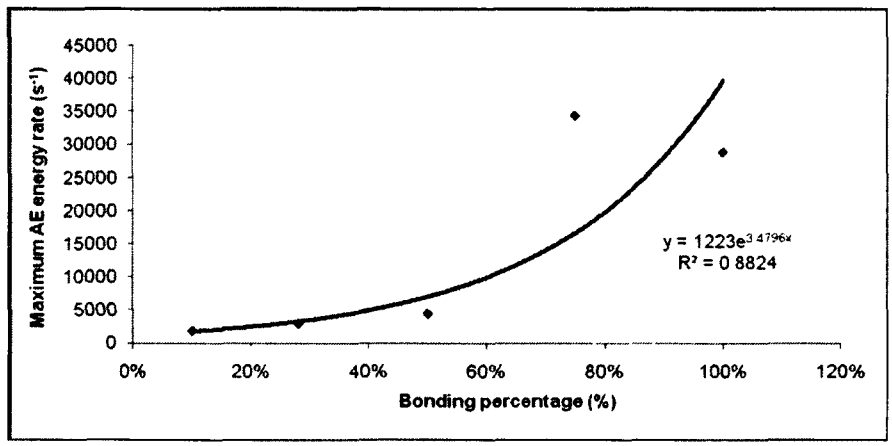

Figure 4-6: Max. AE energy rate at the peak vs. bonding percentage

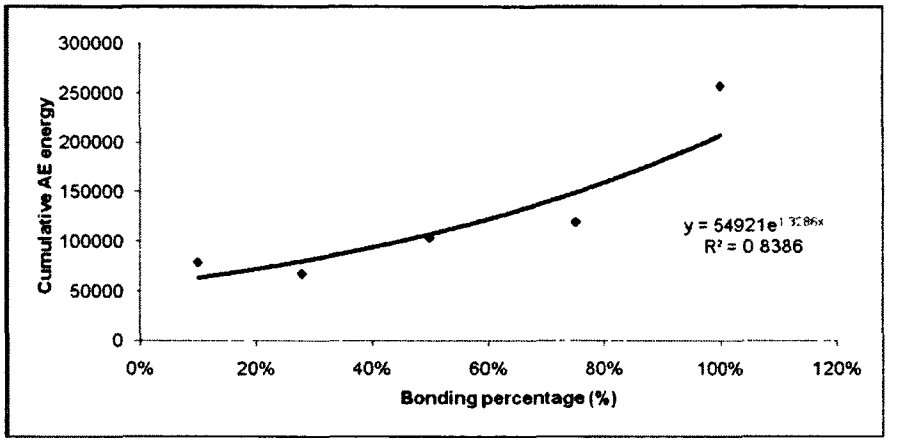

Figure 4-7: Cumulative AE energy vs. bonding percentage

The shear stress and the AE energy rate vs. shear displacement are shown in Figure 4-4 for various bonding percentages. Comparing the graphs in Figure 4-4 reveals that a decrease in the bonding percentage leads to:

1) a gradual drop in shear strength after the peak;

2) a decrease of the maximum shear strength from 4.13 MPa for 100% bonding to 1.2 MPa for 10 % bonding (Figure 4-5).

It must also be pointed out that for bonding percentages lower than 100%, the secondary peak associated with asperities failure did not occur. It suggests that for these samples, the peak shear strength stems from bond strength and friction of joint asperities. Except the sample with 10% bonding percentage (where residual shear strength is governed by spread clay) the residual shear strength of other samples is the almost same, which is related to the similar roughness found on the joint surface.

Figure 4-6 and 4-7 show that the peak of AE energy rate and cumulative AE energy corresponding to maximum shear strength slightly decreased with the reduction of bonding percentage.

Although the decrease of bonding percentage is gradual for cumulative AE energy graphs, there is a significant difference between the amount of AE rates for 100% and 75% bonding percentages with others, so that for 100% and 75% bonding percentages the AE energy rate is between 30000-40000 but for others this value is between 2000-5000 (Table 4-3). Also, in samples with bonding percentage of 20% and 10%, the maximum AE energy rate did not correspond to the maximum shear strength. This phenomenon comes from the nature of the

AE energy. It was observed that in some cases the AE energy of small and rapid break of an asperity is much higher than the AE energy resulting from the break of the adhesive bond of concrete-rock joint. These results are in good agreement with the results from other researchers (14).

It can be inferred that no AE events occurred until the break of the adhesive bond, even for bonding percentage as low as 10%.

At lower values of bonding percentage, the effect of asperities roughness is dominant; after breaking the adhesive bond, the asperities govern the shear mechanism and break during residual period. Due to asperity degradation, the AE activities after maximum shear strength increased with the reduction of the bonding percentage.

4.5. The effect of normal load

The concrete-rock joints were tested under constant normal stresses of 0.15 MPa, 0.65 MPa and 1.25 MPa. The results indicate that the effect of normal load on shear strength of the bonded concrete-rock joints is not significant (Figure 4-8). The peak shear strength value is almost the same for all samples. However, there is no correlation between the normal load and the energy rate or cumulative energy of the acoustic signals. Therefore, when the normal stress is lower than the strength of the adhesive bond, the change of the normal stress does not cause significant changes in shear and AE behavior of the bonded concrete-rock joints. This suggests that the shear and acoustic behavior of the bonded joints in the above case (normal load less than bond strength) are governed by the bonding strength between the joint replicas. Looking at Mohr-Coulomb ($\tau_p = c + \sigma_n \tan\phi$) and Barton ($\tau_p = c + \sigma_n \tan(\phi_b + JRC \log_{10}(\frac{JCS}{\sigma_n})$ failure criterions it can be referred when σ_n is too low $\sigma_n \tan\phi$ and $\sigma_n \tan(\phi_b + JRC \log_{10}(\frac{JCS}{\sigma_n})$ are nearly zero and the shear strength is equal to cohesion between joint halves. Data shown in the 6th column of Table 4-4 demonstrate that on the contrary of the maximum shear strength, the residual shear strength (where is after adhesive bond breaking) increases with increasing normal load.

The comparison of the shear stress curve reveals that the samples tested at normal stresses lower than 1 MPa show the second shear strength peak. In the case of normal stresses higher than 1 MPa, the adhesive bond and the asperities are broken together and samples just show one shear strength peak.

At low normal stress values, the dilation associated with the breaking of the adhesive bond advances the shearing process and because of low amount of normal stress, the asperities do not contribute in shearing process. They just show a small peak after maximum shear strength peak and then no significant asperity degradation occurred.

Samples tested under normal stress lower than 1 MPa show brittle failure. In the case of normal stress above 1 MPa, the samples show a more softening behavior.

Table 4-4: Shear strength and AE results of the samples under different values of normal load

Sample	Bonding percentage (%)	Displacement rate (mm/min)	Normal load (Mpa)	Max. shear strength (Mpa)	Residual shear strength (Mpa)	Shear displacement in max. shear strength (mm)	Max. AE energy rate in max. shear strength	Max. AE energy rate	Cumulative AE energy
1	100%	0.15	0.15	5.1	0.22	0.54	35065	35065	84072
2	100%	0.15	0.65	4.85	1.02	0.65	37500	37500	205889
3	100%	0.15	1.25	5.06	1.48	0.63	21669	21669	73689

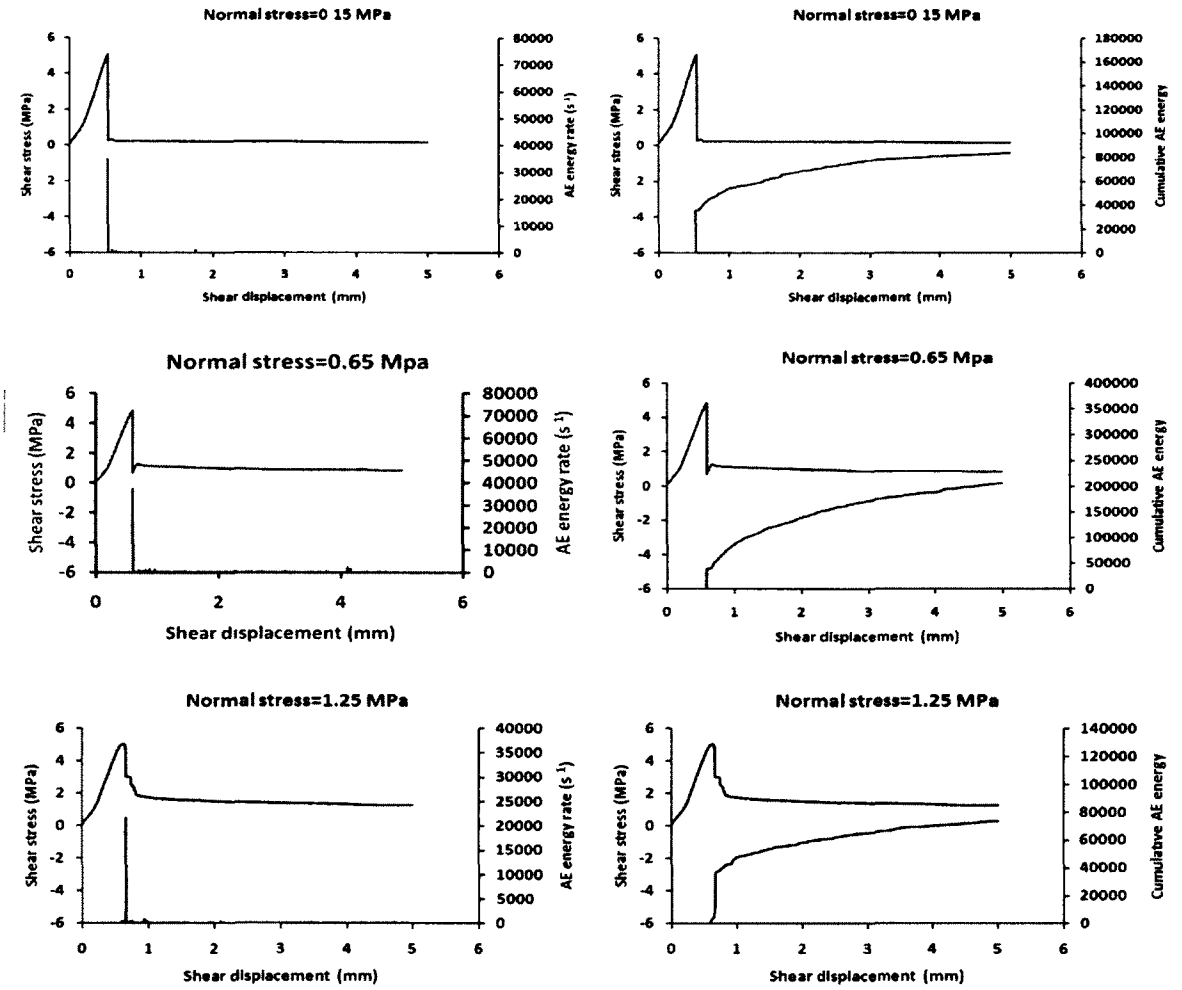

(a) (b)

Figure 4-8: Shear stress and a) AE energy rate b) Cumulative AE energy vs. shear displacement for samples under different values of normal load

4.6. The effect of the displacement rate

The joint samples were tested with displacement rates of 0.05 mm/min, 0.15 mm/min and 0.25 mm/min under the constant normal stress of 0.5 MPa (Table 4-5). The results shown in Figure 4-9 indicate that the displacement rate has no significant effect on shear behavior and AE response of bonded concrete-rock joints for the mentioned loading condition. There is no correlation between displacement rate and shear strength or AE parameters. During the laboratory test conducted on the samples, it was impossible to increase the displacement rate more than 0.25 mm/min. In these conditions, the system has been stopped because of it exceeded the maximum capacity of the shear loading jack (90 KN). These results are in good agreement with the results obtained by Crawford and Curran (1981) by using a vast shear velocity range of 0.10-50 mm/sec. They reported that for granite sample, of intermediate hardness, the frictional resistance was essentially independent of the shear velocity.

Table 4-5: Shear strength and AE results of the samples under different values of displacement rate

Sample	Bonding percentage (%)	Displacement rate (mm/min)	Normal load (Mpa)	Max. shear strength (Mpa)	Residual shear strength (Mpa)	Shear displacement in max. shear strength (mm)	Max. AE energy rate in max. shear strength	Max. AE energy rate	cumulative AE energy
1	100%	0.05	0.5	5.49	0.82	0.6	14499	14499	21384
2	100%	0.15	0.5	4.14	0.72	0.5	28914	28914	256623
3	100%	0.25	0.5	4.73	0.73	0.56	35813	35813	104336

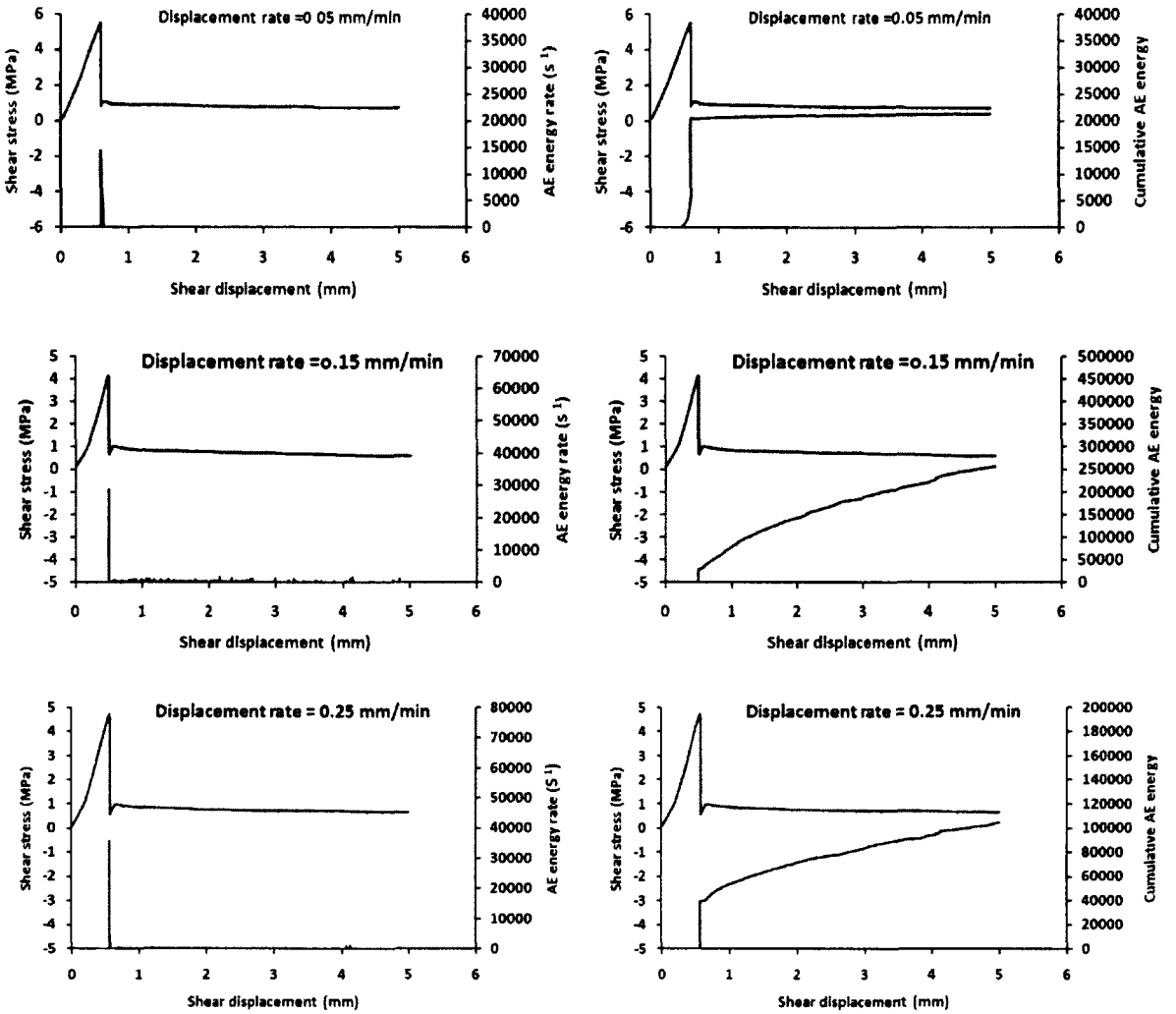

Figure 4-9: Shear stress and a) AE energy rate b) Cumulative AE energy vs. shear displacement for various displacement rates

4.7. Conclusions

Studying shear behavior of the bonded concrete-rock joints is essential for stability analysis of concrete dam foundations, concrete socketed piles, shotcrete, lining, etc. The results of this study indicated that the shear behavior of bonded joints is mainly related to adhesive bond between rock and concrete replicas.

It was observed that when the joint surfaces are bonded (even for bonding percentages as low as of 10 %), AE events show up just a while before break of the adhesive bond; therefore the time between AE detection and joint failure is short for remedial solutions. It is recommended to use a combination of AE with other instrumentation methods for monitoring shear behavior of the bonded joints.

Although several parameters influence the shear behavior of these joints, almost all of them are affected by the adhesive bond between concrete and rock. At low values of normal load, the influence of normal load (increasing or decreasing) does not lead to significant changes on shear behavior of bonded concrete-rock joints. This phenomenon was also observed regarding the effect of the displacement rate on shear behavior.

The shear strength of bonded joints at low values of normal load (until bond strength) can then be considered as equal to the adhesive bond strength between two surfaces.

It can be inferred that changing the normal load in this range (0<normal stress <bond strength) does not make any significant change in shear strength of these joins.

Because of the loading system restrictions, the normal load and displacement rate were not increased up to very high values. In fact, they were too small to affect the shear strength of the bonded concrete-rock joints. Although the normal stress on a dam foundation (except in high water level variation and ice pressure) is normally low, but for other cases (e.g. socked piles) that rock-concrete interfaces are situated, it is recommended to investigate the shear mechanism of bonded concrete-rock joints at high values of normal load and displacement rate.

So far the capability of acoustic emission for monitoring shear behavior of different joints has been evaluated. In the next chapter, it will be indicated how this method can show the position of the AE event sources.

5. CORRELATING ACOUSTIC EMISSION SOURCES WITH DAMAGED ZONES DURING DIRECT SHEAR TEST OF ROCK JOINTS

Autors and affiliation:
Z. Moradian: PhD student, Université de Sherbrooke, Faculté de génie, Département de génie civil.
G. Ballivy: Professeur, Université de Sherbrooke, Faculté de génie, Département de génie civil.
P. Rivard: Professeur, Université de Sherbrooke, Faculté de génie, Département de génie civil.

Date of submission: 24 November 2010

Acceptation state: Submitted

Journal: Canadian Geotechnical Journal

Reference: [10-327]

Titre français: Corrélation entre les sources des émissions acoustiques et les zones endommagées pendant l'essai de cisaillement des joints rocheux

Contribution in paper:
The author of the thesis has contributed in this paper as first, principal and corresponding author.

Résumé français:

Dans cette étude l'applicabilité de l'émission acoustique (EA) pour localiser des zones endommagées et l'intensité de cet endommagement sur les surfaces de joints a été évaluée. Des échantillons de joints rocheux ont été obtenus à partir de la rupture en tension de carottes de forage de roc. Les échantillons ont été testés pendant les essais cisaillement dans des conditions de charge normale constante. Quand une aspérité se brise, il se produit des signaux sonores qui peuvent être détectés par des capteurs d'EA fixés à l'échantillon. L'emplacement des sources d'EA peut être déterminé à partir de la vitesse de propagation des ondes acoustiques et en mesurant le temps de transfert provenant de sources d'événements au capteur. Ces sources correspondent à des zones endommagées des aspérités. L'énergie des

signaux générés doit également être mesurée dans le but d'évaluer l'intensité de la rupture des aspérités. Les signaux d'EA générés par la dégradation des aspérités des surfaces des joints ont été détectés pendant les essais de cisaillement. Les résultats de cette étude indiquent que la méthode d'EA a une très bonne capacité à localiser les zones d'endommagement et l'intensité (énergie) de rupture des aspérités.

Abstract

Applicability of acoustic emission (AE) for localizing asperity damaged zones and damage intensity in the joint surfaces was evaluated in this paper. With this attempt, rock joint samples obtained from tension splitting of the rock cores were tested under constant normal load condition. When an asperity is under failure, it produces some sound signals that can be detected by AE sensors attached to the joint sample. The location of the AE sources can be determined from propagation velocity of acoustic waves and by measuring the transferring time from event source to AE sensor. These sources correspond to asperity damaged zones. The energy of the generated signals should be measured too in order to assess the intensity of the asperity failure. AE signals generated from asperity degradation of joint surfaces were detected during shear testing. The results of this study showed that AE method has a good capability in localizing the asperity failure points and the intensity (energy) of the asperity failure.

5.1. Introduction

The localization of the source of acoustic emission (AE) events is one of the most important advantages of AE monitoring comparing with other geotechnical instrumentation methods. For instance, AE yields instability warning and can be used to determine where it has occurred. This technique has been used in underground mines (Wang and Ge, 2008), rock slope (Shiotani, 2006, Sasao et al. 2003), hydraulic fracturing (Manthei et al. 2001, Ishida, 2001, Ohtsu 1991, Dahm et al. 1999, Moriya et al. 2006), tunnels (Falls and Young, 1998), dams

(Minemura et al. 1998), bridges (Shigeishi et al., 2001) and reinforced concrete beams (Schechinger and Vogel, 2006, Wu et al., 2000).

A few works have been recently published on the application of AE for localizing event sources during direct shear test. Ishida et al. (2010) performed in-situ direct shear tests on a large block to provide some insights as analog models of seismogenic faulting. In their study, AE sources were located with an accuracy expected to fall within 50 mm. Hong et al. (2006) performed a series of direct shear tests to investigate the influence of shear load on AE characteristics of rock-concrete interface under constant normal load. They showed that the location of the AE sources distributed over the entire shear zone before the shear stress reach converged residual value. They believed that after the residual shear stress attain, the sources are localized. Son et al. (2006) conducted laboratory shear tests under CNS and CNL conditions and studied the influence of the boundary conditions on shear behavior. From the distribution of source locations of AE it was thought that the roughness damage may be strongly correlated with roughness height.

In source location techniques, a number of monitoring sensors are placed at various points throughout the body of the specimen or structure under study (Hardy 2003). Their number and location depend on the complexity of the investigated case and on the accuracy that is required. The arrival time difference between each sensor and the others results in a set of arrival time differences which, along with the geometry of the sensor array and propagation velocity of the rock, is used to determine the spatial coordinates of the AE source (Hardy 2003) Figure 5-1 shows the array of the AE sensors around an AE source (Ps).

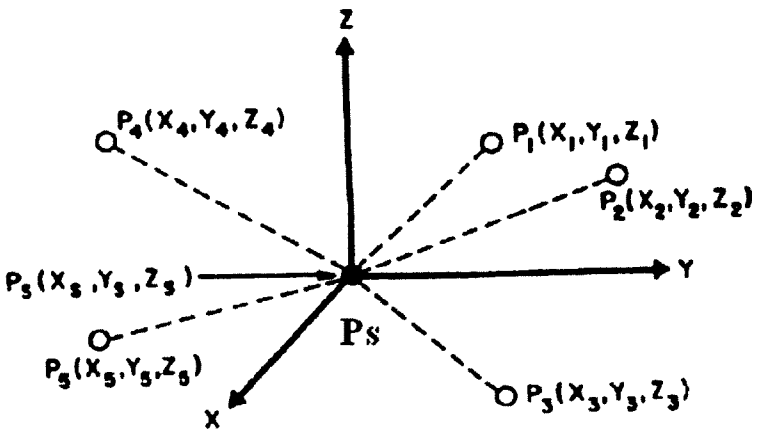

Figure 5-1: An array of the AE transducers around an AE source (after Hardy, 2003)

Least squares interaction technique is typically used for determining source locations. The method involves the solution of the following equation:

$$(X_i - X_s)^2 + (Y_i - Y_s)^2 + (Z_i - Z_s)^2 = V_i^2(t_i - T_s)^2 \qquad (5\text{-}1)$$

where X_i, Y_i and Z_i (i=1,2,3, ...,n) are sensor coordinates, t_i and V_i are the corresponding AE arrival times and velocities. X_s, Y_s and Z_s are the true coordinates of the source and T_s is the true origin time. Since there are four unknown parameters (X_s, Y_s, Z_s and T_s), at least four equations (data from four sensor stations) are necessary to solve the equation exactly (Hardy 2003).

However due to inherent experimental errors related to each equation (i.e., error in sensor locations, determination of arrival time differences and velocities), at least five equations (data from five sensors stations) should be used in order that the set of equations defined by equation 1 are over determined (Hardy, 2003). In the case of 2D localization (where there is no Z_i and Z_s coordinates), at least three sensors should be employed. Additional equations (using more sensor stations) will usually improve the precision of the localization because this allows the computer program to minimize such error terms and gives a best fit for the equation set (Hardy, 2003).

5.2. Scope of work

In this study, it was tried to not only evaluate the source location of each AE event over the joint surface but also show its energy. This provides the contribution percentage of asperities in shearing process and their failure intensity. With this attempt, it was tried to determine what happens with asperities during several stages of shear loading (initial point of shear displacement, yield point, maximum shear strength and residual shear strength). Then, the accuracy of the AE source localization technique was evaluated by comparing with images and scanned surfaces of the joints.

5.3. Experimental works

Joint samples were prepared by tension splitting of the 150mm diameters rock cores drilled on a medium-grained Barre granite from Vermont, USA (Figures A2-1 and A2-2). Table 5-1 shows physical and mechanical properties of the rock cores used for this study.

A dark blue color was sprayed on joint surfaces in order to localize the damaged zones caused by shear loading. After putting the samples in the shear test mold and surrounding them by cement grout, the joint surfaces were scanned using the scanner profilometer. The laser profilometer model Kréon was used in this study. The laser emits a red, luminous plane with a wavelength of 670 nm and a maximum output power of 4 mW. The sensor has wavelength of 670 nm, number of points/second of 30000 and depth and width of field 90 and 25 mm. Profiles parallel and perpendicular to the direction of shear loading were drawn with a 0.5 mm interval over the whole of scanned surfaces. Table 5-2 contains the JRC (joint roughness coefficient) (Barton 1973) of the joint samples calculated from Z2 (root mean square of the first derivative of the profile) (Tse and Cruden, 1979) using this equation:

$$JRC=32.2+32.47\text{Log}(Z2) \qquad (5\text{-}2)$$

The direct shear tests was performed on the joint specimens in the constant normal load condition using a direct shear apparatus mounted inside a rigid loading frame of a rock and concrete testing machine fabricated by Materials Testing Systems (MTS).

The rate of horizontal displacement in all tests was 0.15 mm/min and the test was considered as finished when the horizontal displacement reached 5 mm. The values of shear stress and shear and normal displacements due to applied shear loads have been recorded during each test.

Acoustic emissions were monitored with PAC μ-SAMOS system. This system consists of two 8-channel AE data acquisition systems (PCI-8). Four AE transducers (PAC, R3α general purpose) were used to detect AE signals. The sampling rate was set to 1 MSPS and the frequency range of the sensors is 25-530 KHz. The amplification of pre-amplifier was 40 db, and AE exceeding 50 db was measured.

Pictures of the joint surfaces after the shear test were taken and the joint surfaces were scanned after the test.

Table 5-1: Physical and mechanical properties of the granite rock cores (average value from 3 tests)

Parameter	Bulk specific gravity	P-wave velocity (m/s)	Young modulus (GPa)	Poisson ratio	Uniaxial compressive strength (MPa)
Average value	2.63	4675	58.1	0.30	179

Tableau 5-1: Surface roughness parameters of the joint samples

Parameter	$Z_2 = \sqrt{\frac{1}{n}\sum_{i=1}^{n}\left(\frac{z_{i+1} - z_i}{\Delta y}\right)^2}$	JRC=32.2+32.47Log(Z2)
Sample 15	0.323	16
Sample 25	0.381	19
Sample 44	0.355	18

5.4. Calibrating AE source localization technique

Although the simplest way to attach AE sensor consists to attach them on shear test mold, it was decided to attach them directly to the tested samples in order to increase the precision of the AE localization. So that when AE signals confront with surrounded grout and then steel mold, some of them are reflected. On the other hand, there are three different materials (rock, concrete and steel) with three different velocities, so the only way for calculating velocity is to consider the average velocity which makes error too. So it is suggested to attach AE sensors directly on the test samples.

Before testing of the joint samples, the AE system was calibrated regarding its capability to localize some specific points on the surface of different materials. A mortar slab (Figure 5-2), a granite slab (Figure 5-3), and a concrete slab (Figure 5-4) were used. At first, some points were marked and their position was determined and then with tapping the points it was tried to localize the AE events.

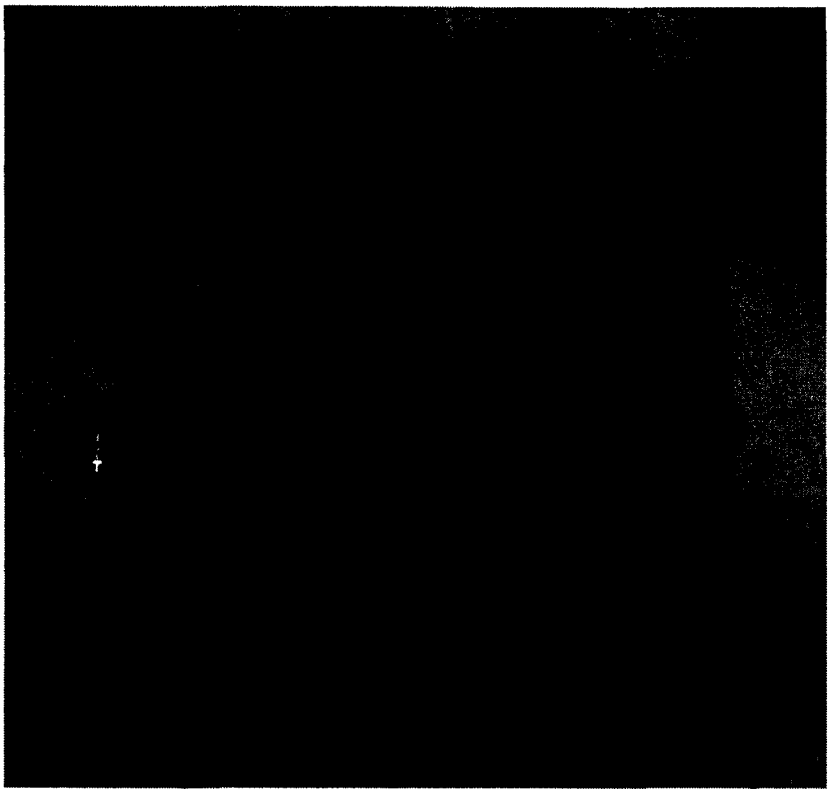

(a)

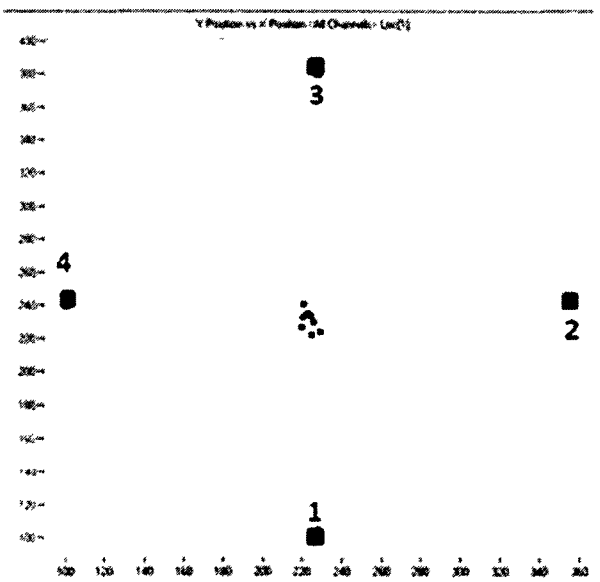

(b)

Figure 5-2: a) A 25.5 ×28 × 8 cm mortar slab and attached sensors, b) localizing AE events by tapping central point of the slab. Points in the sides of 2D location graph show the position of the sensors.

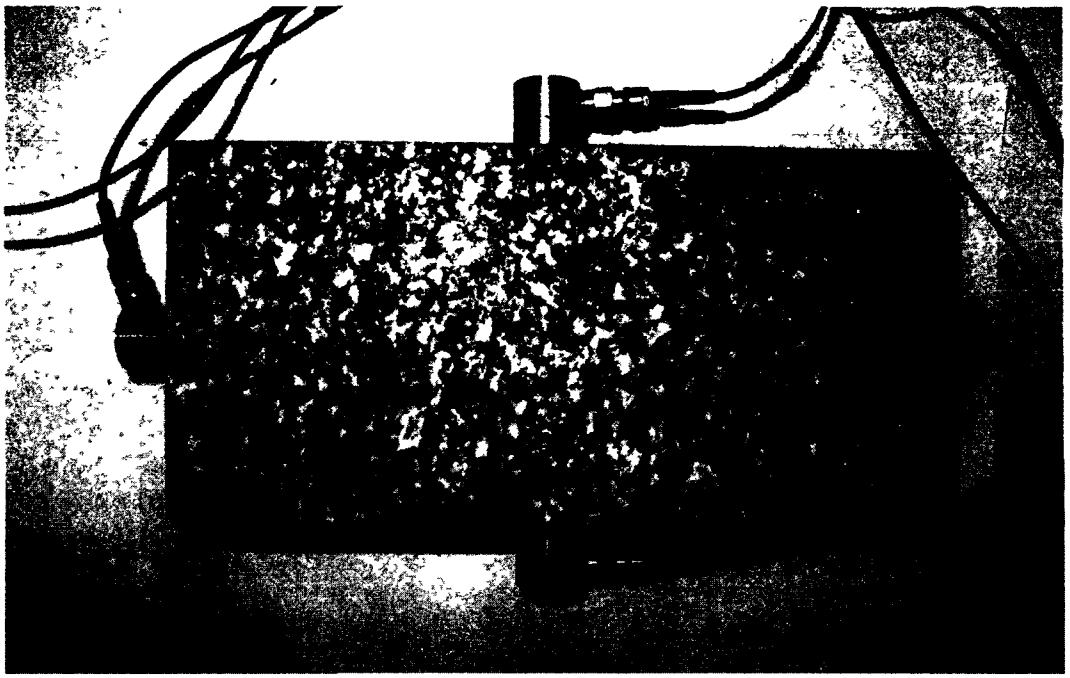

(a)

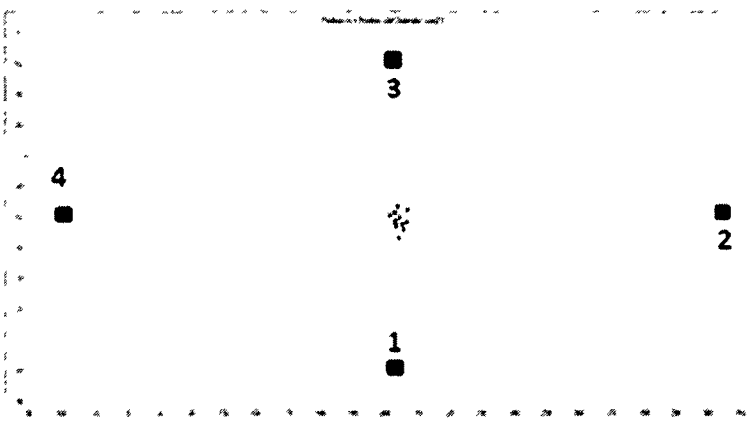

(b)

Figure 5-3: a) A 10 ×20 × 5.5 cm granite slab and attached sensors, b) localizing AE events by tapping central point of the slab. Points in the sides of 2D location graph show the position of the sensors.

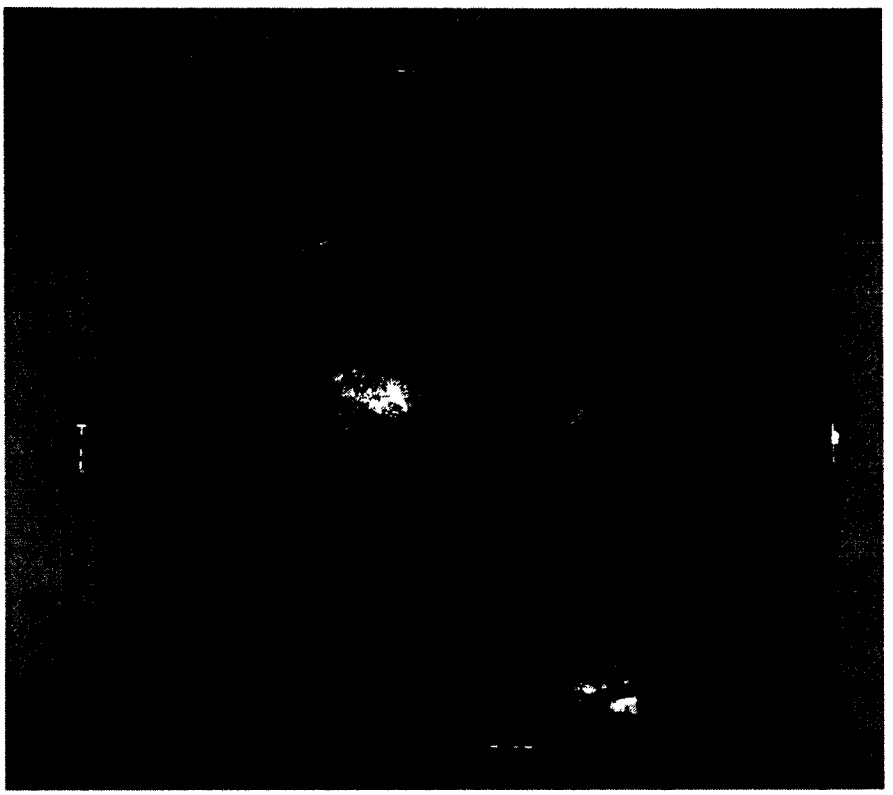

(a)

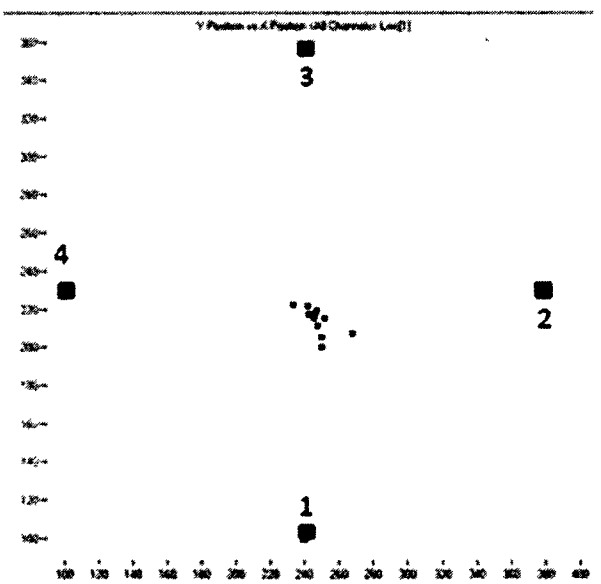

(b)

Figure 5-4: a) A 25.5 ×28 × 6.5 cm concrete slab and attached sensors, b) localizing AE events by tapping central point of the slab. Points in the sides of 2D location graph show the position of the sensors.

One can realize from previous figures that the localization of the AE events for concrete sample has been done with less precision than mortar and granite slab. This difference comes from non homogeneity behavior of the concrete sample. According to the previous tests, it can be concluded that:

- This fact must be accepted that the natural samples are not homogenous, so propagation of the AE signals is changed in each direction.
- Results obtained for concrete sample showed that, although the precision of the AE localization is not the same as for mortar and granite test, one can find that most of the events come from the tapping area.

5.5. Damaged zones and AE source locations

The shear stress-shear displacement of the joint samples was divided into four sections using the results of previous work (Moradian et al., 2010). These sections are pre-peak linear, pre-peak non-linear, post-peak and residual shear strength. Figure 5-5 shows the shear stress versus shear displacement of the samples numbers 44, 25 and 15.

In order to identify AE activity at different sections of shear test, the Y positions of the AE events is drawn versus their X positions. In Figure 5-6, 5-7 and 5-8, the 2D locations of the AE events for four detected sections of samples are shown. Each figure represents the top view of the joint. For each event in the 2D location graphs, its corresponding energy in X and Y directions has been shown in Figures 5-6, 5-7 and 5-8.

As it can be seen, the locations of AE sources were distributed over the entire surface of the joint in pre-peak linear and pre-peak non-linear sections. After the maximum shear stress, the sources became localized. These results could be explained by the concept of first and second order asperities. It seems that secondary asperities, which are distributed in entire surface of joint, are sheared until maximum value of shear strength. In could be concluded that before maximum shear strength, AE sources are distributed as a result of failure of the secondary asperities and they are localized after maximum shear strength as a result of failure of the primary asperities.

Although 2D localization shows damaged zones; this method doesn't provide the intensity of the asperity failure. In other words, this method doesn't distinguish between a strong failure and a weak one. In order to have a better insight about failure intensity of the asperities, the graph of AE energy versus linear location of the AE events was drawn in X and Y directions. For this purpose, the distance between two adjacent sensors is selected and for each event its energy is drawn versus linear distance between event source and the sensor.

The graphs in Figure 5-6, 5-7 and 5-8, show that AE events (red points) and AE energy values (in up and left side of the 2D localization graphs) increased from low values in pre-peak linear section to pre-peak non-linear section. They reached their maximum values in post-peak section and then they decreased in residual section.

In pre-peak linear section, the AE events and AE energy values decreased with increasing in normal load. For samples tested below higher normal load values, the asperities are interlocked tightly and no sliding or movement occurred until the shear load has overridden the normal load, while for samples under lower values of normal load, the shear load overrides the normal load earlier and the sliding or movement of asperities generates AE signals. This indicates that in pre-peak linear section, the density of AE events for samples under lower values of normal load is more than for samples under higher values of normal load.

Although there is a low amount of AE events in residual section, their energy is several times higher than the energy of the AE events in pre-peak linear and pre-peak non-linear sections. This energy is produced by local breaking of the rough asperities that had not been crushed in post-peak section or their failure is still being occurring in residual section.

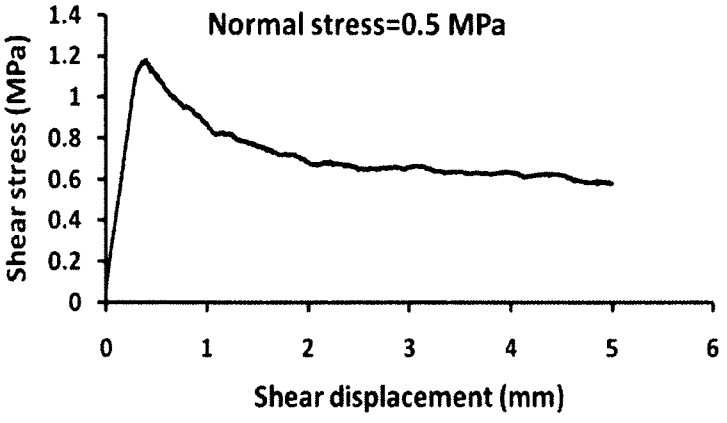

(a)- sample number 44, Normal stress=0.5 MPa

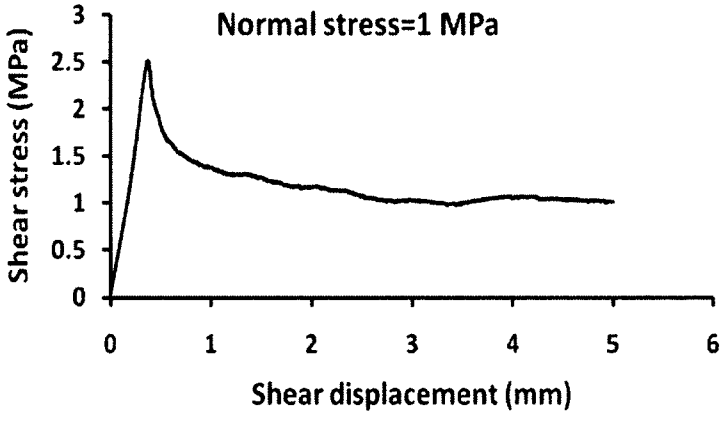

(b)- sample number 25, Normal stress=1 MPa

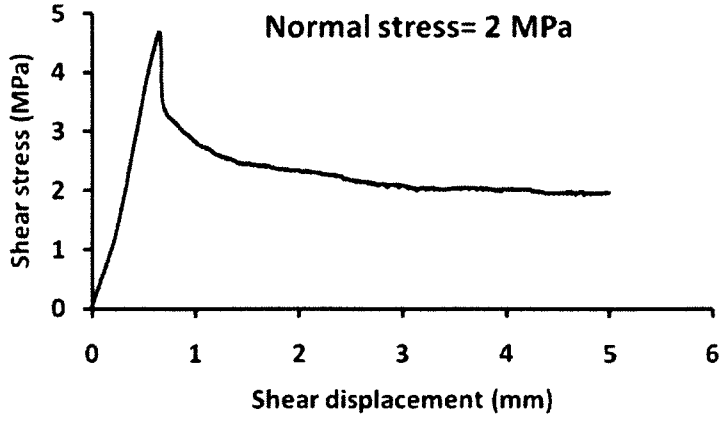

(c)- sample number 15, Normal stress=2 MPa

Figure 5-5: Shear stress vs. shear displacement of the rock joint samples

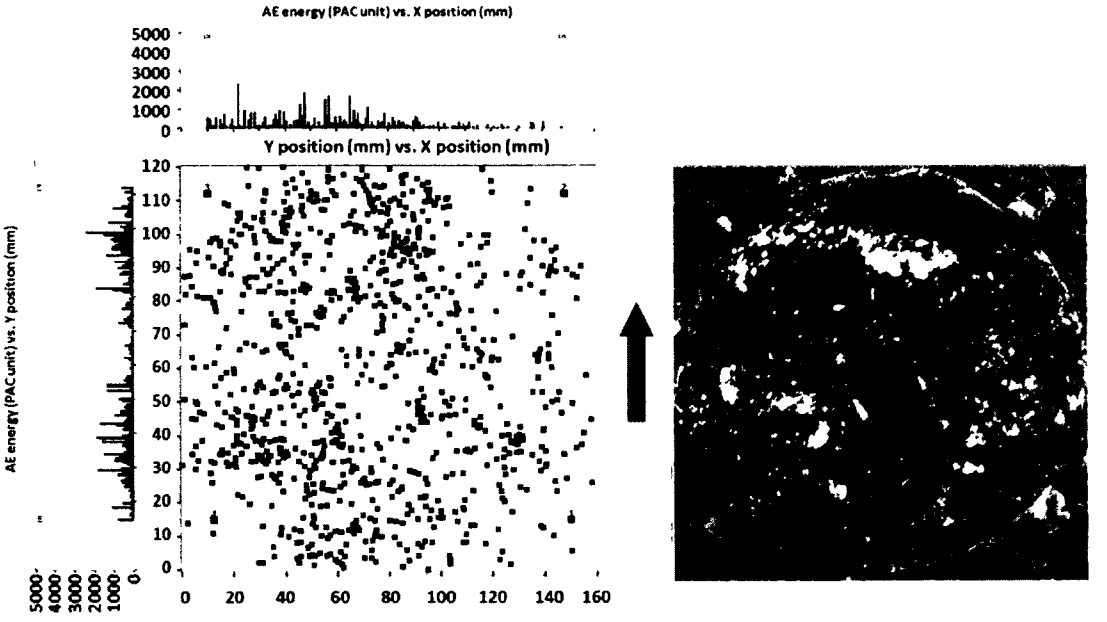

(a) - Pre-peak linear section

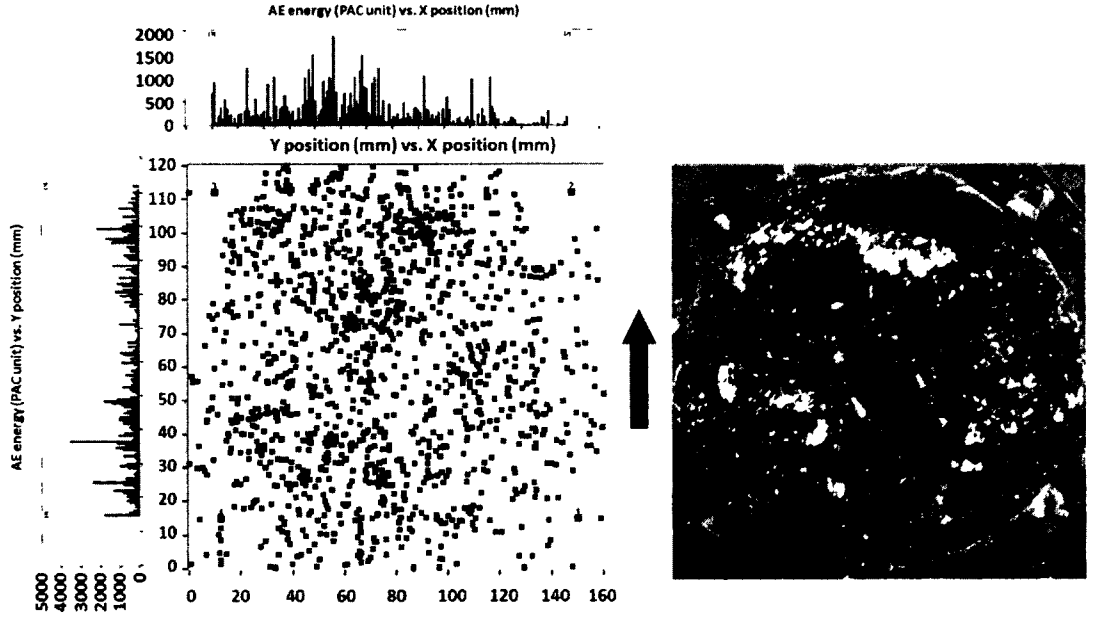

(b) – Pre-peak non-linear section

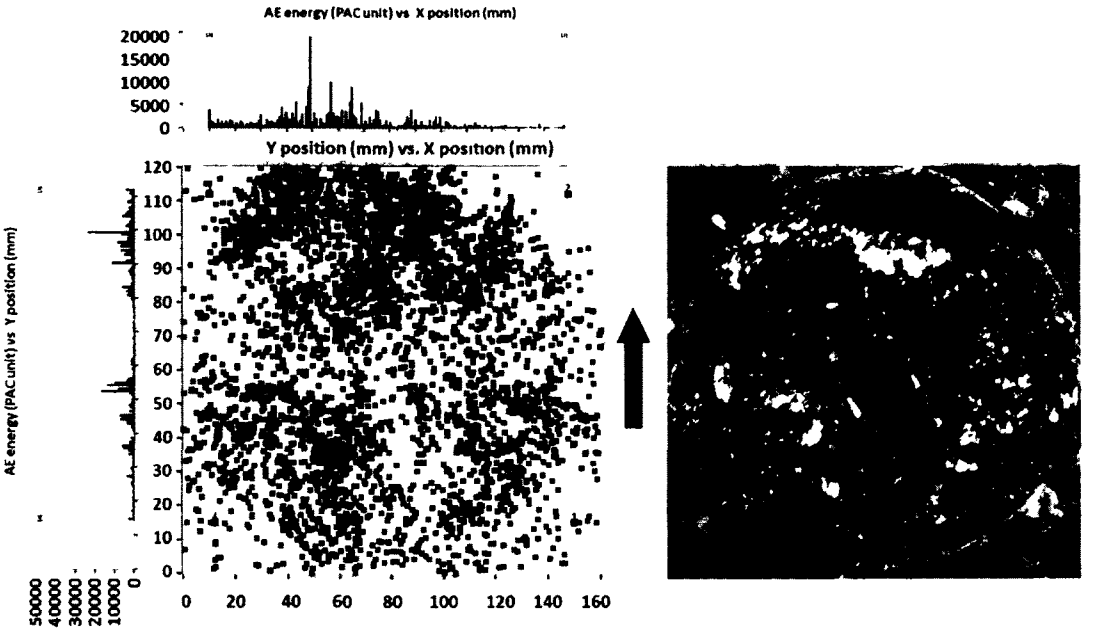

(c) - Post-peak section

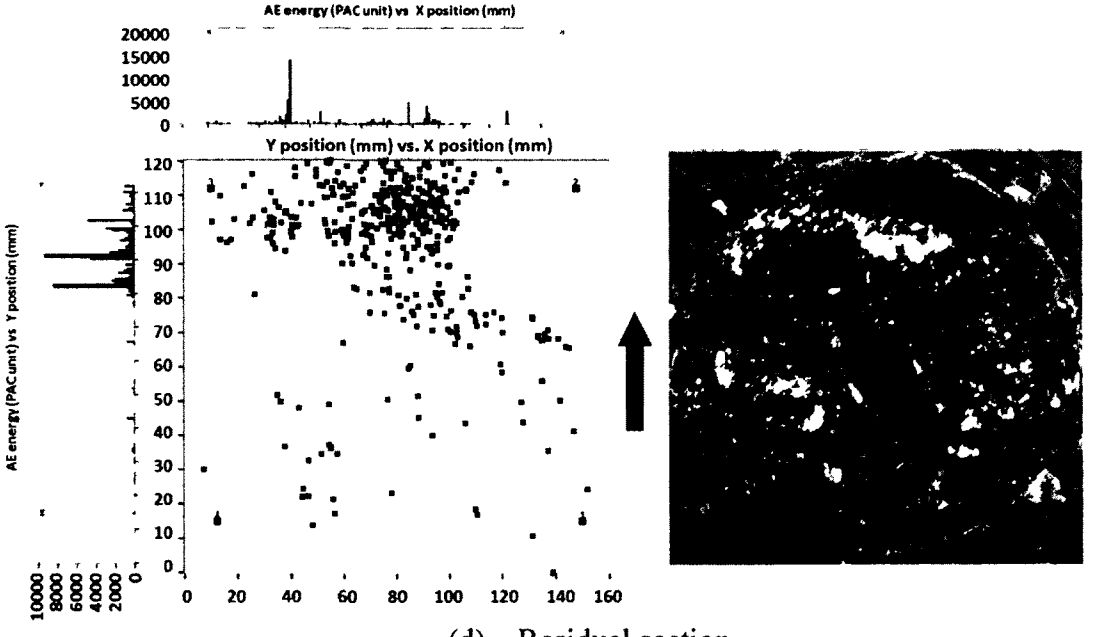

(d) – Residual section

Figure 5-6: 2D source location of the AE events and their corresponding energy in X and Y directions for the mobile surface of the sample number 44 under normal stress of 0.5 MPa. Black points in the 2D location graphs show the position of the sensors. The arrow shows the shear direction and the photo shows the top view picture of the mobile surface after shear test.

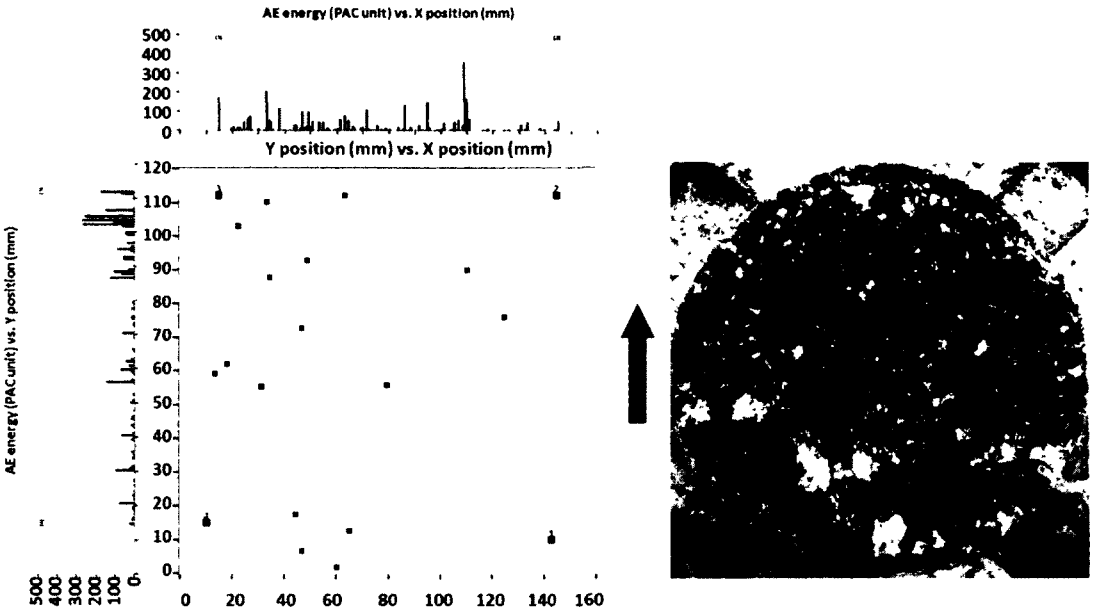

(a) - Pre-peak linear section

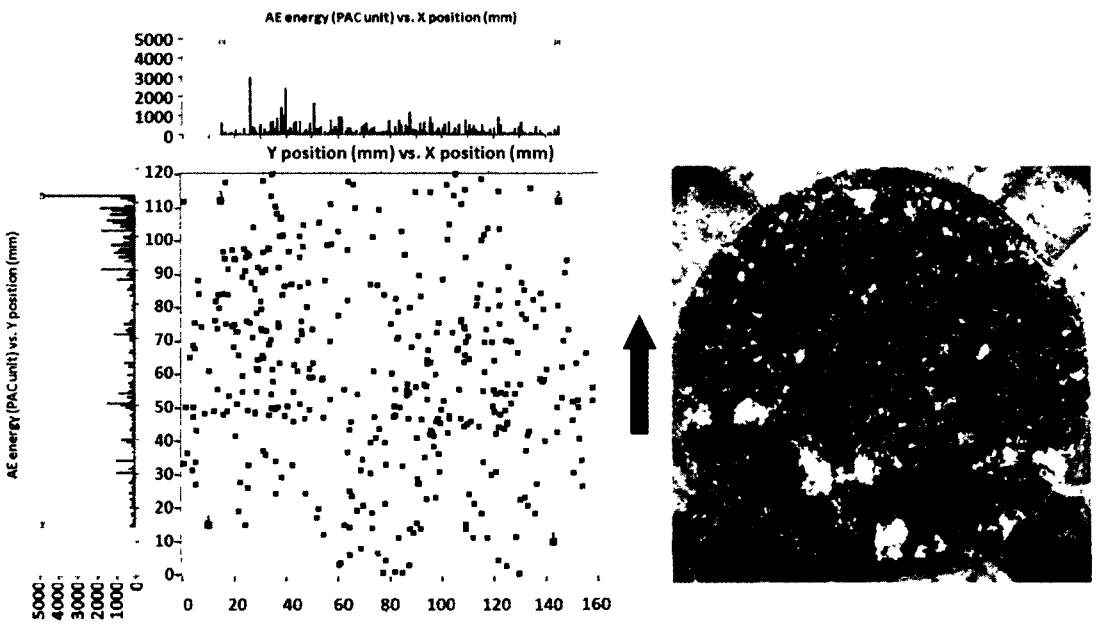

(b) – Pre-peak non-linear section

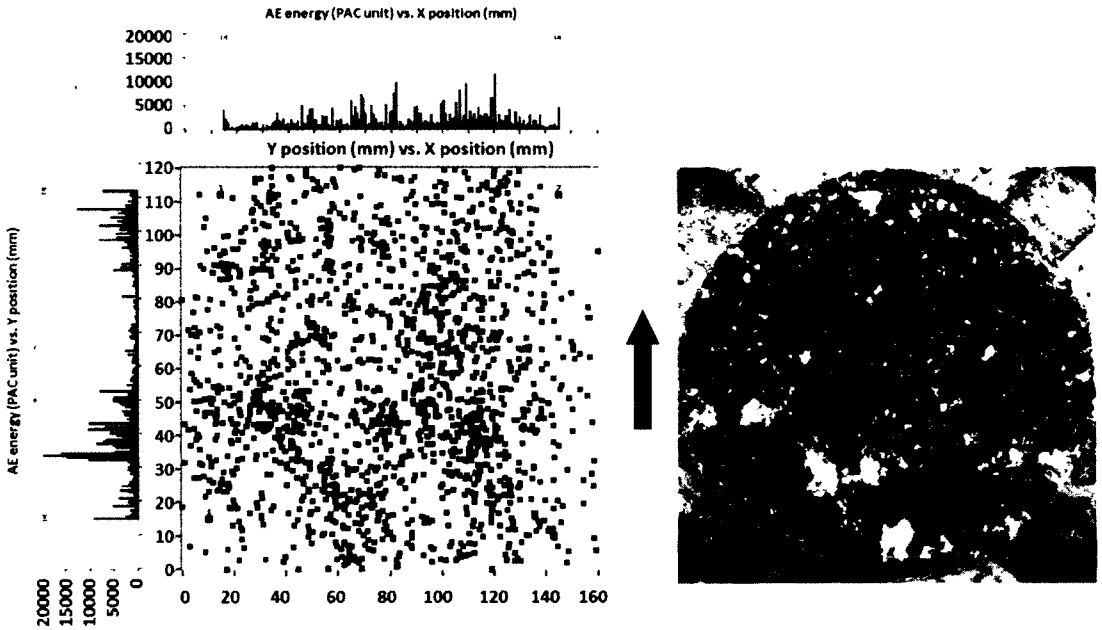

(c) - Post-peak section

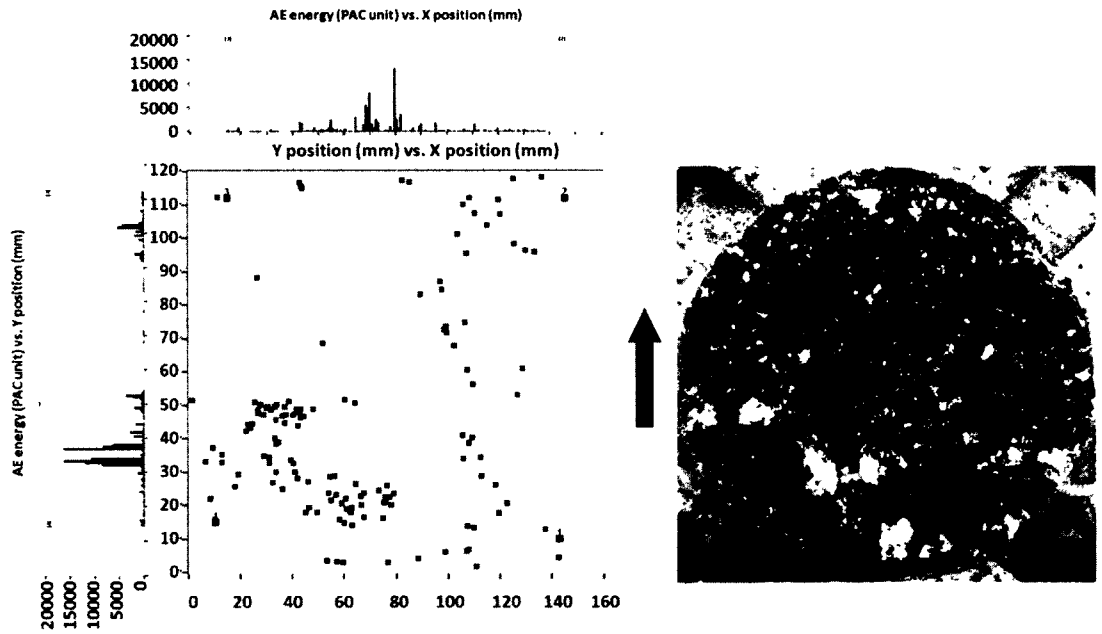

(d) – Residual section

Figure 5-7: 2D source location of the AE events and their corresponding energy in X and Y directions for the mobile surface of the sample number 25 under normal stress 1 MPa. Black points in the 2D location graphs show the position of the sensors. The arrow shows the shear direction and the photo shows the top view picture of the mobile surface after shear test.

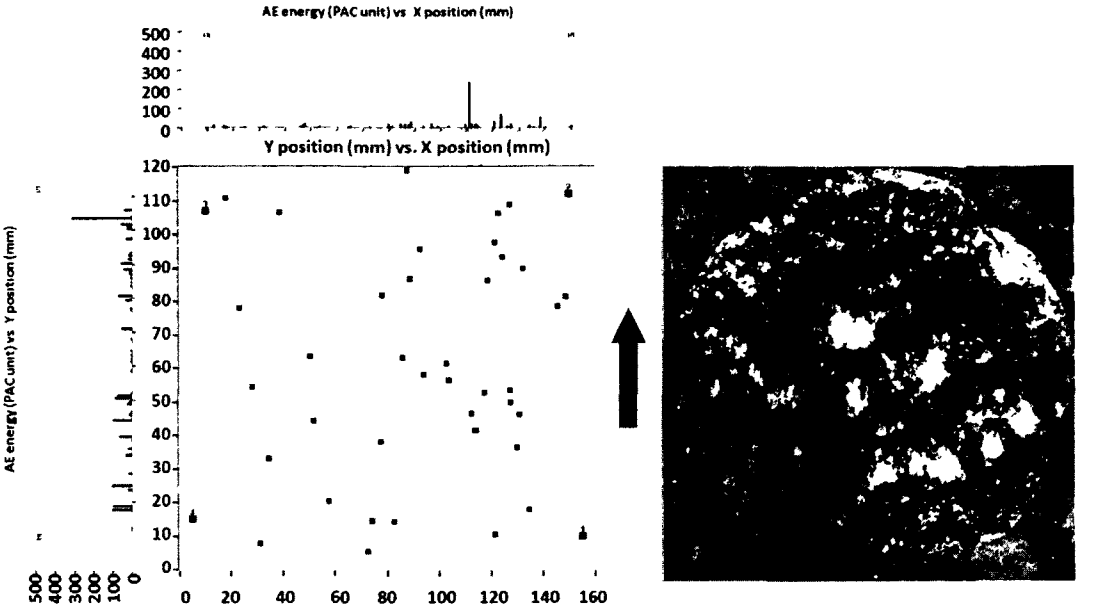

(a) - Pre-peak linear section

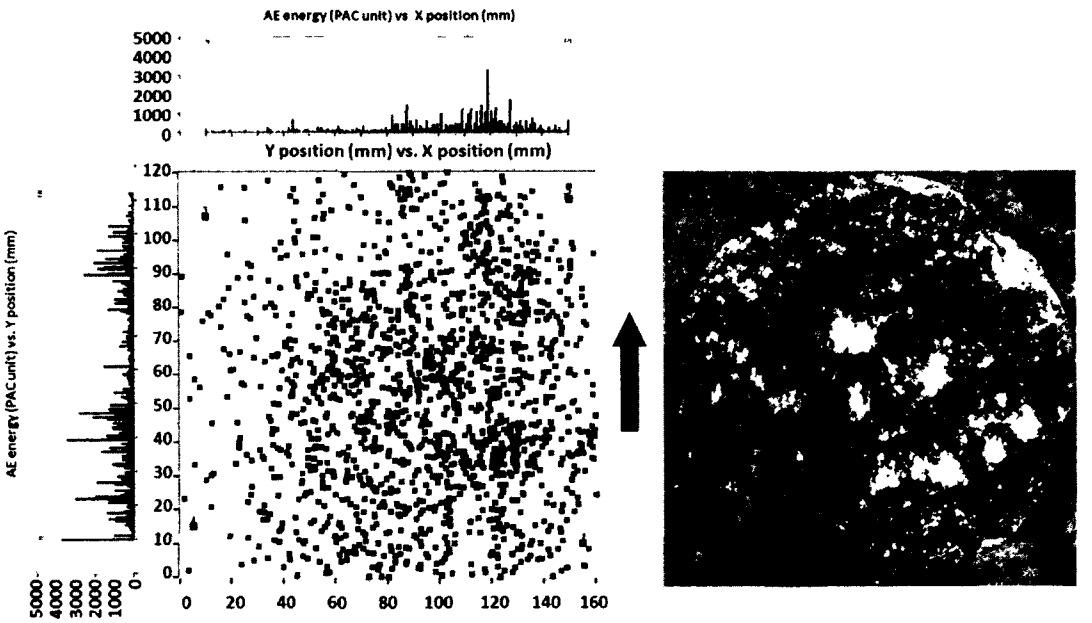

(b) – Pre-peak non-linear section

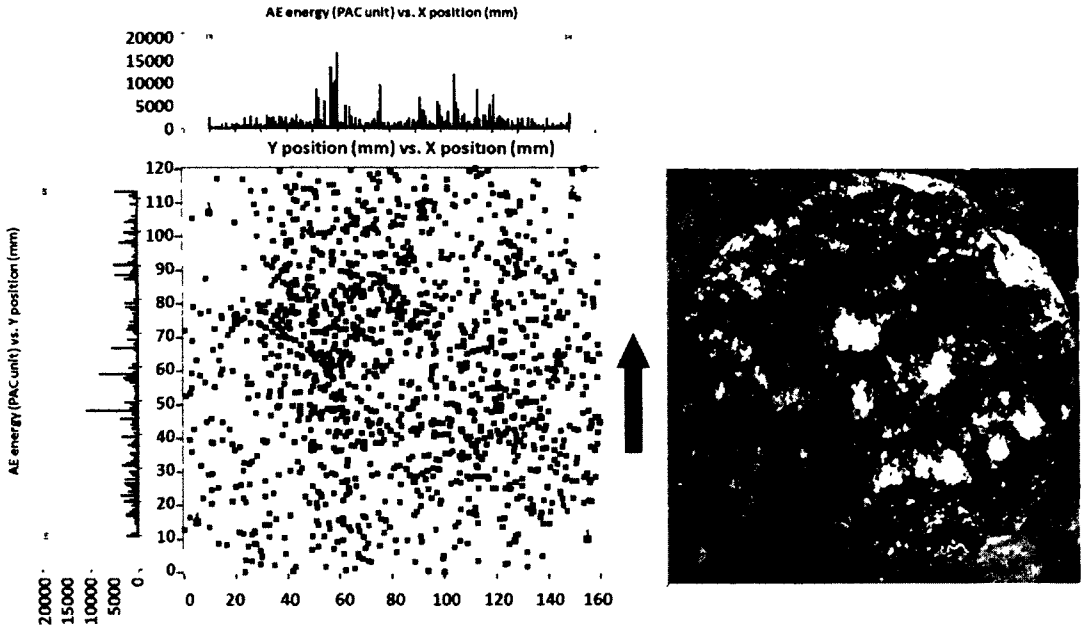

(c) - Post-peak section

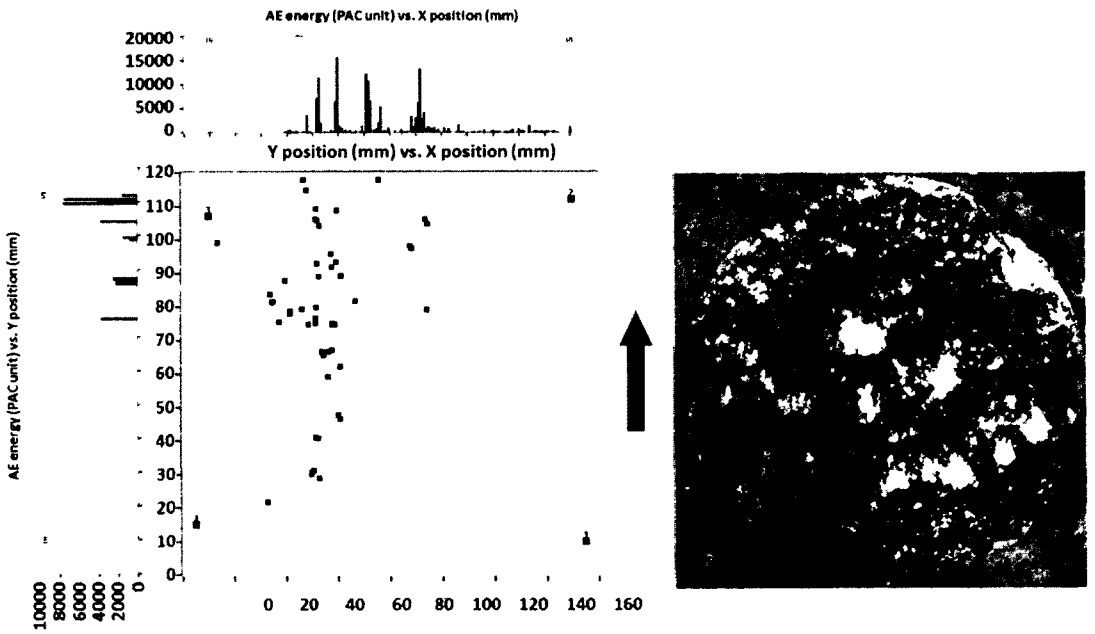

(d) – Residual section

Figure 5-8: 2D source location of the AE events and their corresponding energy in X and Y directions for the mobile surface of the sample number 15 under normal stress 2 MPa. Black points in the 2D location graphs show the position of the sensors. The arrow shows the shear direction and the photo shows the top view picture of the mobile surface after shear test.

In order to compare the AE source locations with asperity damaged zones, the joint surfaces were colored by spraying a dark blue paint before performing direct shear test. This procedure allows pointing out the damaged zones quite easily. If an asperity is crushed, the blue color is removed and the remaining light color exhibits area of damaged zone. Since the AE sensors have been attached to the mobile (upper) replica, the top view photo of the mobile replica of each joint sample is shown in Figures 5-9, 5-10 and 5-11. Comparing Figure 5-6 with 5-9, 5-7 with 5-10 and 5-8 with 5-11, there is a good correlation and similarity between light colored zones and zones with the cluster of the AE events. 2D profile of the mobile surface of each joint sample has been drawn in X and Y direction in Figure 5-9, 5-10 and 5-11. As it can be seen, clustering point of AE events as well as damaged zones (white areas) are related to the rough zones of the joint surfaces.

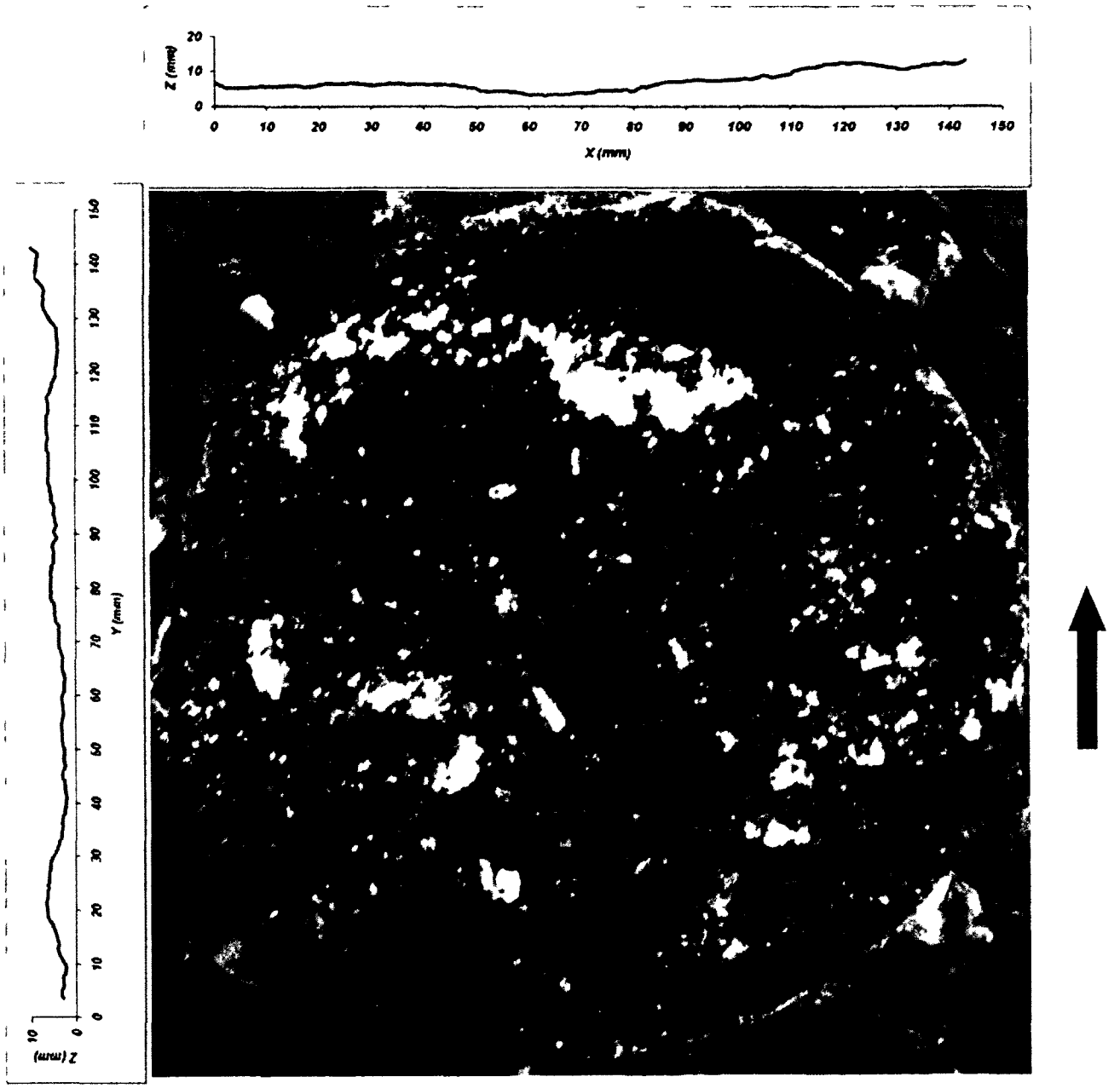

Figure 5-9: Top view picture of the mobile surface after shear test, sample number 44 under Normal stress=0.5 MPa. Picture belongs to mobile replica which the AE sensors were attached to. The arrow shows the shear direction. In the top and left side of the figure, the central 2D profile of the surface roughness drawn in X and Y directions have been shown.

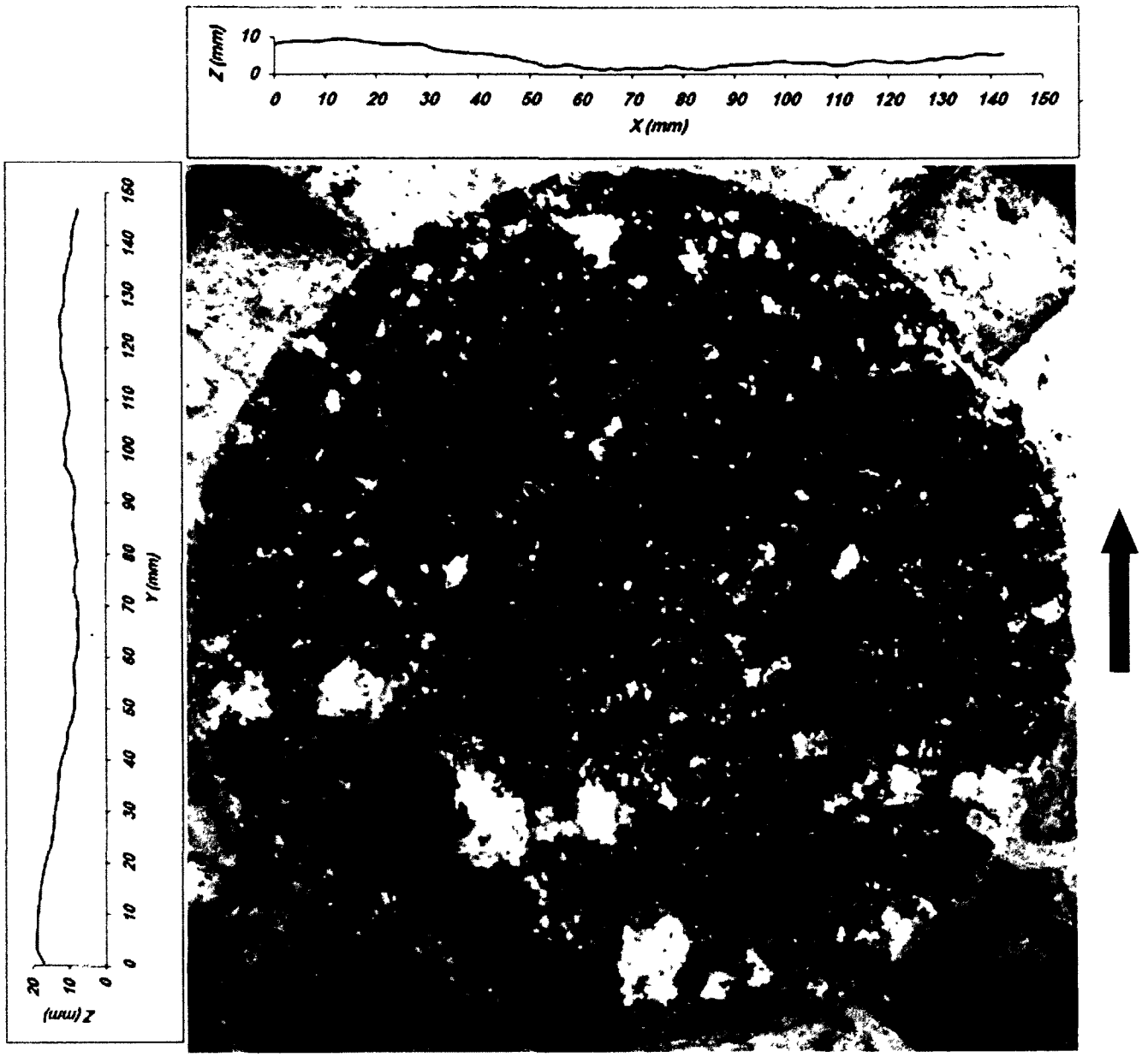

Figure 5-10: Top view picture of the mobile surface after shear test, sample number 25 under Normal stress=1 MPa. Picture belongs to mobile replica which the AE sensors were attached to. The arrow shows the shear direction. In the top and left side of the figure, the central 2D profile of the surface roughness drawn in X and Y directions have been shown.

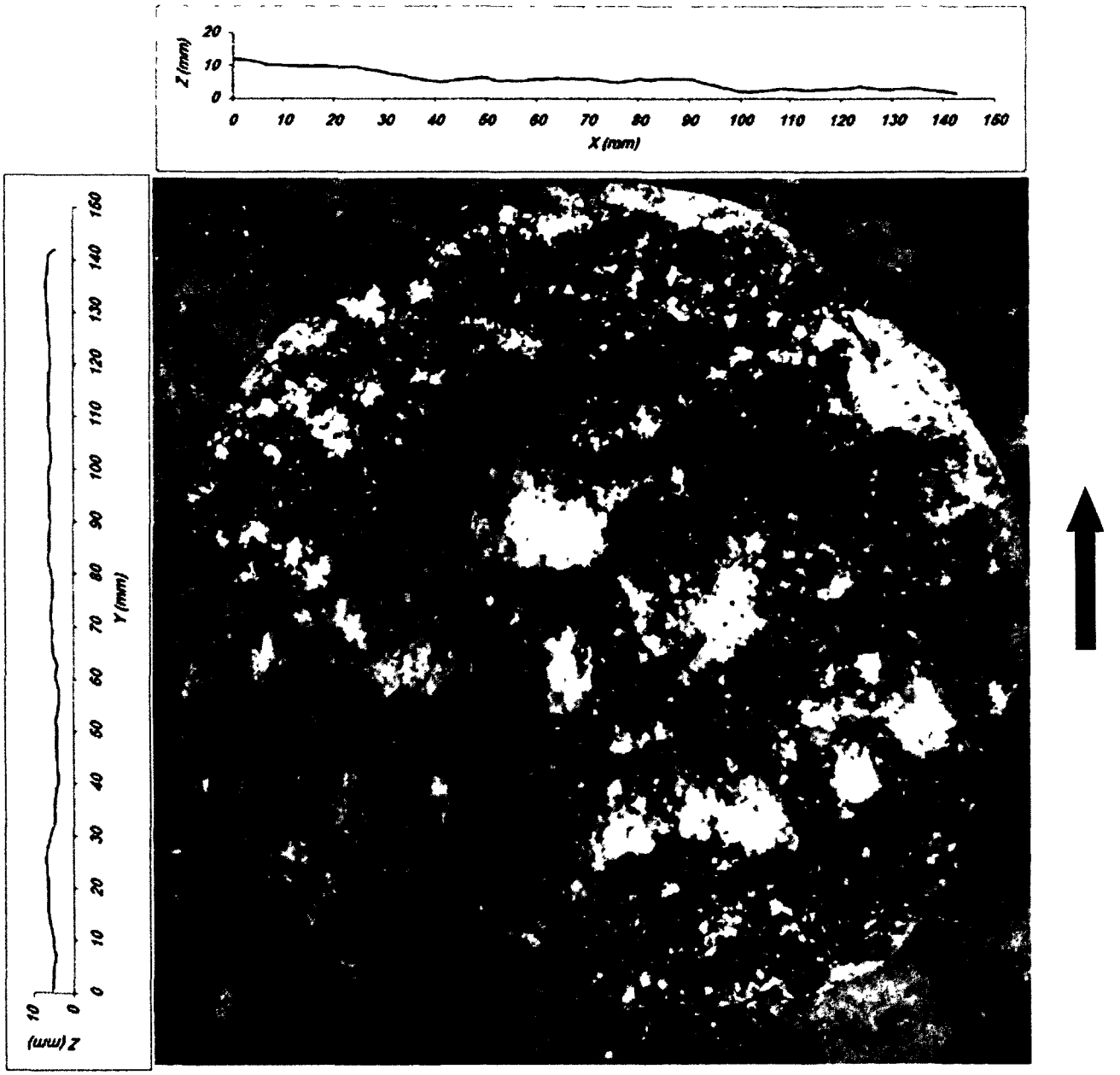

Figure 5-11: Top view picture of the mobile surface after shear test, sample number 15 under Normal stress =2 MPa. Picture belongs to mobile replica which the AE sensors were attached to. The arrow shows the shear direction. In the top and left side of the figure, the central 2D profile of the surface roughness drawn in X and Y directions have been shown.

5.6. Discussion

The contact area of the joint halves determined by geometry of the surfaces has a high important effect on shear behavior of the joints in any stage of shearing process. Shear strength of rock joints, failure mechanism and asperity degradation depend on contact area distribution between joint halves (Grasseli 2006). Damaged zones are strongly related to contact areas, so that wherever both side of a joint perfectly matched, a maximum amount of asperities are crushed increasing the number of damaged zones .

Gentier et al. 2000 stated that size, shape and spatial distribution of the damaged zones depend on shear direction and the amount of the stress (shear and normal) and shear displacement. They found that a little damage has occurred before maximum shear strength point and most of the asperity damages are occurred during post-peak softening and residual section of shear strength (Gentier et al. 2000).

Several researches (Gentier et al. 2000, Grasselli 2006, Kimura & Esaki 1995, Hong & Jeon 2004, Yang & Chiang 2000, Haberfield & Johnston 1994) have indicated that damaged zones tend to occur on steepest zones facing the shear direction but not on those opposite to it.

Kodicara & Johnston (1994) and Yang & Chiang (2000) showed that steeper asperities dominate the shear mechanism in the initial stages of the shearing, while teeth with low steepness values participate in the next stages of the shearing process. This phenomenon is valid not only for first order asperities but also for second order asperities.

Using AE localization, scanned surfaces and image of shear surfaces simultaneously provide the possibility to investigate the degradation mechanism of the asperities well.

Comparing Figures 5-6 and 5-9 for sample number 44 under normal stress of 0.5 MPa shows that after shear strength peak, the failure stemmed from local damaging of the large teeth, while before this peak the shearing process were dominated by shearing of the second order asperities which are distributed in entire shear surface. The normal stress of the 0.5 MPa was not high enough to fully crush the large asperities; therefore, the shearing process has been continued by damaging teeth until the end of the test in residual section.

For sample number 15 under normal stress 2 MPa (Figure 5-11) because of the higher normal stress, almost entire surface of the sample has been affected by shear loading and light colored zones are distributed anywhere in joint surface.

Figure 5-10 shows that for sample number 25 under normal stress 1 MPa, the steep teeth, which were facing the shear direction, were located in upper and lower of the joint surface, while in the center teeth faced the opposite of shear direction. This kind of asperity distribution has caused damaged zones to occur in upper and lower sides of the joint surface, whereas in the center the lack of damaged zones was clear. Figure 5-7 (AE localization of the sample 25) shows that although there are some events in the middle of the joints by looking at their corresponding energy one can find out that these energies are very weak comparing to energy of the events in up and down zones. Another parameter that is important for this phenomenon is the dilation of the joint surface. Dilation is created because of shearing of rough asperities in upper and lower side of this joint surface. This dilation dismatch the two surfaces in the middle zones.

It can be concluded that having clusters of AE events in 2D localization and their corresponding energy, one can localize the steep asperities facing the shear direction. This also gives an insight about contact areas in joint surface.

5.7. Conclusions

AE method showed a good capability for localizing damaged points in discontinuity surfaces as well as the intensity or energy of their failure. This method can recognize the points with rupture potential well. This provides the possibility to reinforce the support systems and be aware about the probable failure of a structure before any unexpected disturbance. The results of this research can be summarized as follows:

- AE source points are increased by increasing the shear load during direct shear testing of rock joints. By approaching the maximum shear strength point they are localized and increased noticeably and then in the residual section they are decreased.
- AE source points are scattered in pre-peak linear and pre-peak non-linear sections because most of the joint activities before maximum shear strength resulted from friction and degradation of the second order asperities that are distributed in entire surface of rock joints.

- In the proximity of the maximum shear strength and after it, the first order asperities are crushed. Since these asperities are located in some specific rough zones of the joint surfaces, the generated AE events are localized in these zones.
- In residual shear strength section, depending on the amount of the normal load, the asperity degradation decreased significantly or continued locally because of failure of the remained rough surfaces. Therefore, in this section the number of AE source points is decreased and localized in some local points.
- AE localization provides an insight about contact area distribution and locations of the asperities facing to shear direction.
- A successful AE monitoring is achieved when one considers not only the source locations of the AE events, but also the amount of the energy that each event generates.

6. CONCLUSIONS AND RECOMMENDATIONS

6.1. Conclusions français

Un des phénomènes les plus importants qui pourrait mener à l'instabilité des barrages en béton est la faible résistance au cisaillement des discontinuités dans ces structures et dans leurs fondations. Ces discontinuités sont les joints béton-béton dans le corps du barrage, les interfaces béton-roc entre le barrage et la masse rocheuse et les joints roche-roche dans la fondation rocheuse. Si le total des contraintes en cisaillement affectant un barrage dépasse la résistance au cisaillement maximal des discontinuités mentionnées, le barrage se brisera en se déplaçant le long de ces discontinuités.

Au cours de ces dernières années, plusieurs méthodes ont été utilisées pour la surveillance des barrages au niveau des discontinuités actives et instables; en effet les ingénieurs et les chercheurs étaient à la recherche d'une méthode précise, intelligente et rapide. Une des méthodes de surveillance qui a été récemment examinée et appliquée est l'émission acoustique (EA).

L'objectif de cette thèse a été d'étudier l'application de l'EA pour la surveillance du comportement en cisaillement des joints béton-béton, béton-roche et des joints roche-roche en laboratoire comme une étude de faisabilité pour la surveillance des joints actifs aux sites de barrage. À cette fin, des échantillons naturels et artificiels ont été testés au Laboratoire de mécanique des roches de l'Université de Sherbrooke : des échantillons artificiels ont été carottés dans un bloc de granite tandis que des échantillons naturels ont été directement obtenus par carottage dans le corps d'un barrage.

Dans cette recherche, divers thèmes ont été abordés de manière intensive:

- Évaluer la possibilité d'application d'EA pour surveiller le comportement au cisaillement des joints lors de chargement en cisaillement direct.
- Étudier l'effet des changements de conditions (par exemple une charge normale, le taux de déplacement) sur la réponse d'EA de joints. Montrer comment les signaux d'EA répondent à la modification de ces paramètres.

- Étudier l'effet des propriétés mécaniques et physiques des échantillons (p.ex. la rugosité, le pourcentage de liaison) sur la réponse d'EA et montrer les caractéristiques des signaux d'EA pour divers types de joints.
- Évaluer la possibilité de localiser les signaux d'EA pour définir les zones endommagées au cours des essais cisaillement direct. Évaluer les pouvoirs de cette méthode pour localiser les zones à fort potentiel de rupture dans un barrage.

  Les signaux d'EA ont été mesurés pendant les essais de cisaillement des joints sous une charge normale constante (CNL). La CNL a été considérée comme la condition de chargement à laquelle les barrages sont soumis à cause de l'état de dilatation libre des discontinuités dans les structures de barrage. Les résultats de cette étude ont montré que l'utilisation de différents types de joints et la corrélation des graphiques d'EA avec ceux de contrainte de cisaillement fournit une meilleure interprétation du processus de cisaillement pour les discontinuité in situ.

  En utilisant l'étude paramétrique et une basée sur l'étude des signaux, les résultats du suivi d'EA peuvent être analysés. Dans cette recherche, la technique d'analyse basée sur les paramètres a été utilisée pour corréler les caractéristiques des évènements d'EA avec le comportement de contrainte-déplacement de joints, en raison du volume élevé de signaux d'EA générés lors des essais et l'impossibilité d'analyser tous ces signaux. Une analyse basée sur l'étude du signal a été utilisée pour localiser la source des événements d'EA et montrer les zones de dégradation.

  Il a été constaté que l'utilisation combinée des paramètres d'EA et l'analyse des contraintes-déplacement est une méthode précise et fiable pour définir le comportement de cisaillement de structures sur des discontinuités de faible résistance. En effet, les paramètres d'EA sont capables de révéler un certain nombre de caractéristiques du processus de rupture progressive des joints rocheux.

  Les résultats de cette thèse ont indiqué que l'EA possède une grande capacité à caractériser le comportement en cisaillement de joints ouverts (non liés), alors que méthode est moins applicable pour surveiller le comportement en cisaillement des joints fermés (liés). Deux méthodes ont été utilisées à partir des graphiques contrainte en cisaillement-déplacement de joints pour définir les périodes pré-pic linéaire, pré-pic non linéaire, post-pic et résiduelle:

1. En utilisant une combinaison de taux des paramètres d'EA avec des graphiques de cisaillement.

2. En utilisant une combinaison de paramètres d'EA cumulatif avec des graphiques de cisaillement.

6.1.1. Les joints liés

Pour les échantillons liés, aucun signal d'EA n'a été mesuré dans la période pré-pic linéaire (période I). En période pré-pic non linéaire (période II), ils montrent certaines activités d'EA. Ces activités viennent de l'initiation et de la propagation des fissures dans les surfaces de contact. En période post-pic (période III), en raison de la rupture du contact, les joints montrent une augmentation spectaculaire d'EA et ils montrent leur pic maximum. Ce processus est dû à la fissuration et à la rupture en cisaillement de la surface lié. Après ce grand pic, il se produit des pics plus petits qui sont générés à partir de l'endommagement des aspérités primaires et secondaires. À la période résiduelle du graphique contrainte cisaillement-déplacement, les joints montrent les valeurs minimums de paramètres d'EA. Le seul mouvement dans cette période est le glissement des surfaces, car il n'y a pas de cisaillement distinct dans cette période, le taux d'EA a ainsi montré des valeurs faibles.

Les graphiques cumulatifs d'EA pour joints liés ne montrent aucune activité pendant la période pré-pic linéaire. En période pré-pic non linéaire, ils montrent quelques signaux vers la fine de cette période. Durant la période post-pic, ils montrent une augmentation abrupte, puis un comportement convexe dans leurs valeurs et enfin à la période résiduelle, ils continuent d'augmenter avec un très faible taux.

Pour les joints liés, les signaux d'EA ne commencent pas tout de suite après l'application de la charge de cisaillement et de l'initiation du déplacement en cisaillement. De cette façon, le point de départ du mouvement ne peut pas être détecté par l'EA avant la rupture. La distance entre la production d'EA (détection) et la rupture est très courte, donc il n'y a pas assez de temps pour empêcher cette rupture. Il convient toutefois de noter que si une rupture comprend une séquence d'événements, même l'enregistrement de signaux d'EA de la première rupture est utile. Une combinaison d'autres instruments tels que les instruments de mesure de la charge nous permettrait d'avoir une meilleure idée sur le comportement de cisaillement des périodes pré-pic du joint lié.

6.1.2. Les joints non liés

Les joints non liés présentent une activité d'EA avec le début du chargement. On croit que ces activités proviennent du blocage du mouvement. Ils montrent des pics très rapides dans cette période. Dans la période II, les joints montrent une augmentation des valeurs des paramètres d'EA proportionnellement à la charge et ils montrent des pics avec la même amplitude avant la contrainte maximum de cisaillement. Ces signaux sont générés par la rupture des aspérités secondaires et le glissement sur les aspérités primaires. Dans la période III, l'ensemble des aspérités (secondaires et primaires) est cisaillé et les joints montrent une augmentation soudaine des paramètres d'EA après le pic de contrainte de cisaillement. De cette façon, la valeur maximale du taux d'EA est observée dans cette période. Ils montrent une diminution progressive à la fin de cette période. Les joints non liés montrent une faible activité d'EA dans la partie résiduelle.

Les graphiques cumulatifs d'EA pour les joints non liés convexes en période linéaire pré-pic montrent une augmentation linéaire pendant le période pré-pic non linéaire. Durant la période post-pic, ils montrent une augmentation des comportements convexes. Dans la période résiduelle, comme pour les joints liés, ils continuent d'augmenter avec un très faible taux.

Pour les joints non liés, les activités d'EA sont générées en appliquant une charge de cisaillement et au début du déplacement en cisaillement. Contrairement aux joint liés, la distance entre la détection d'EA et la rupture est assez longue pour qu'on puisse mettre en œuvre des solutions correctives.

6.1.3. L'effet du pourcentage de liaison

Une étude approfondie a été réalisée pour évaluer l'effet du pourcentage de liaison sur le comportement de cisaillement et de l'activité EA de joints liés. Les résultats indiquent que le comportement en cisaillement des joints liés est principalement relié à l'adhérence entre les deux répliques.

Plusieurs échantillons avec des pourcentages de liaison différents ont été utilisés pour vérifier si les joints avec une liaison faible montraient une activité d'EA dans leur période pré-pic. Il a

été observé que lorsque les surfaces sont liées (même pour les pourcentages de liaison le plus bas de 10%), il n'y a pas d'événement d'EA jusqu'à la rupture de la liaison adhésive.

Bien que plusieurs paramètres influencent le comportement en cisaillement des joints liés, la quasi-totalité d'entre eux est touchée par le l'adhérence entre le béton et le roc. À faibles valeurs de charge normale, la modification de la charge normale (augmentation ou descente) n'entraîne pas de changements significatifs sur le comportement au cisaillement des joints de béton-roc. Ce phénomène a également été observé concernant l'effet de la vitesse de déplacement sur le comportement en cisaillement.

On peut en conclure que tant que la contrainte normale est inférieure à une force de liaison, le mécanisme de cisaillement des joints de béton-roc est régi par cette liaison. L'évolution de la charge normale dans cet intervalle (0 <charge normale < résistance de la liaison) n'apporte pas de changement significatif dans la résistance au cisaillement des joints liés. La résistance au cisaillement de joints liés dans l'intervalle de valeurs faibles de charge normale (jusqu'à la résistance de liaison) peut alors être considérée comme égale à la force de la liaison adhésive entre les deux surfaces.

6.1.4. L'effet de la charge normale

Afin d'étudier les caractéristiques des paramètres d'émission acoustique lors d'essais de cisaillement direct des joints rocheux sous différentes charges normales constantes, les essais de cisaillement direct ont été effectués sur des joints rocheux de deux façons. En premier, les échantillons possédant des propriétés physiques et mécaniques semblables ont été testés avec différentes charges normales constantes. Deuxièmement, différentes valeurs de charges normales ont été appliquées sur le même échantillon lors du déplacement résiduel de la courbe contrainte cisaillement- déplacement.

Le comportement général des paramètres d'EA à de faibles valeurs de la charge normale est tel qu'ils augmentent progressivement avec un taux à peu près linéaire jusqu'au point de résistance au cisaillement maximal et ils montrent leur intensité maximale, après ce point. Après, ils diminuent progressivement dans la région de résistance au cisaillement résiduelle. Le comportement de l'énergie d'EA est un peu différent parce qu'il est plus sensible à la rupture

instantanée des aspérités, plutôt que du glissement des surfaces, de sorte qu'il montre des pics dans la région immédiate résiduelle avec des intensités considérables.

A des valeurs élevées de la charge normale, les paramètres d'EA montrent un pic significatif après la résistance au cisaillement maximale. Les activités d'EA sont convexes à proximité de la résistance pic et ils diminuent avant et après cela. L'amplitude est le seul paramètre qui ne montre pas de changement significatif dans son comportement. Ce paramètre augmente avec un taux faible au début, puis il augmente de façon linéaire après le point de résistance au cisaillement maximal. Après, il diminue progressivement dans la région résiduelle.

Les résultats expérimentaux montrent que la charge normale a un effet très important sur les événements générés par l'EA. Les augmentations et diminutions de la charge normale changent toujours de façon marquée l'activité d'EA. Lorsque la charge normale est augmentée, il est généré plus d'événements d'EA, mais pas immédiatement au point de dépassement de la charge normale. En fait, les événements d'EA augmentent après que l'augmentation de la charge normale suffise à cisailler des aspérités. Considérant que la baisse de charge normale produit un pic dans les paramètres d'EA au point de chute, on croit que ce phénomène est dû à la libération des surfaces conjointes et verrouillées qui produit beaucoup de signaux d'EA. Après, les paramètres d'EA diminuent et des petits pics sont observés aussi longtemps que la charge normale est faible.

6.1.5. Localisation des sources d'EA

Les surfaces de joints rocheux ont été recouvertes par une teinture de couleur bleu. Pendant le chargement de cisaillement des échantillons, la couleur bleue est supprimée des aspérités arrachées. Le processus de cisaillement résulte en la rupture des aspérités qui font face à la direction de cisaillement dans les zones de contact. La localisation d'EA donne un aperçu sur la distribution de la zone de contact et les emplacements des aspérités face à la direction de cisaillement. Pour localiser les sources d'événements d'EA, il a été constaté que les zones de regroupement des sources d'EA correspondent à des zones de différentes couleurs sur les surfaces traitées.

Les résultats de cette recherche montrent que la méthode d'EA possède une bonne capacité de localisation des zones endommagées dans les surfaces de discontinuité ainsi que l'intensité ou l'énergie de leur rpture. Cette méthode peut reconnaître les zones à fort potentiel de rupture. Ceci permet de renforcer les systèmes de soutien mécaniques et d'être conscient de la rupture probable d'une structure avant toute perturbation inattendue. En augmentant la charge de cisaillement, les sources d'EA sont localisées au cours des essais de cisaillement direct des joints rocheux. Les zones ont sensiblement augmenté après le point maximum de résistance au cisaillement, puis dans la section résiduelle, ils ont diminué. Dans les sections pré-pic linéaire et pré-pic non linéaires, les sources d'EA sont dispersées. Ces sources sont produites par le frottement et la dégradation des aspérités du second ordre qui sont répartis sur toute la surface des joints rocheux. Les aspérités du premier ordre se retrouvent dans certaines zones rugueuses et sont arrachées après la résistance de cisaillement maximale. Les événements générés d'EA qui sont dus à la rupture de ces aspérités après la résistance au cisaillement maximale sont localisés dans ces zones.

En général, la dégradation des aspérités dans la région de résistance au cisaillement résiduelle est réduite. Dans certains échantillons, selon le niveau de la charge normale, l'activité d'EA se poursuit localement en raison de la rupture d'aspérités des surfaces rugueuses. En conclusion, dans la période résiduelle, le nombre de sources d'EA est diminué et localisé dans certaines régions locales.

Puisque la localisation des zones endommagées et l'amplitude de cet endommagement sont importantes pour la surveillance du barrage, un programme par EA doit considérer non seulement les emplacements de la source des événements d'EA, mais aussi la quantité d'énergie que chaque événement génère.

Au cours des dernières années, les techniques d'EA se sont considérablement développées pour la surveillance de la stabilité des structures souterraines et de surface. Bien qu'il existe des différences entre les études d'EA sur terrain et les études de laboratoire, les résultats des esais de laboratoire pourraient être utilisées comme une ligne directrice pour l'interprétation des résultats sur le terrain. Une méthodologie établie, la qualification du personnel, du matériel de pointe, les techniques d'installation et la géométrie des capteurs, des capteurs appropriés avec une gamme de fréquences acceptable, l'étalonnage du système, les mesures de réexamen et de vérification du bruit de fond sont nécessaires pour une surveillance globale d'EA. Ces

améliorations représentent une étape majeure dans la création et la maturité de la technologie d'EA pour surveiller le comportement de cisaillement de discontinuités réelles.

6.2. Conclusions

One of the most important phenomena that could cause instability of concrete dams is low shear resistance of the discontinuities in these structures and their foundations. These discontinuities are concrete-concrete joints in dam body, concrete-rock interfaces between dam and rock bed and rock-rock joints in rock foundation. If total shear stresses affecting on a dam structure exceed maximum shear resistance of the mentioned discontinuities, the dam will break by moving along these discontinuities.

During past years several methods have been used for dam monitoring along active and instable discontinuities, nevertheless engineers and researchers were looking for a precise, intelligent and fast method. One of the monitoring methods which recently has been under consideration and has been applied is acoustic emission (AE).

The objective of this thesis was to investigate the application of the AE for monitoring the shear behavior of concrete-concrete, rock-concrete and rock-rock joint samples in laboratory as a feasibility study for monitoring active joints in dam sites. To this end, natural and artificial joint samples were tested in Laboratory of Rock Mechanics in Université de Sherbrooke. Artificial samples were cored from a large granite block whereas natural samples were directly cored from dam body, interface joint between concrete and rock and rock joints in the rock foundation.

In the current research these topics were considered intensively:

- The possibility of AE application for monitoring shear behavior of joints during direct shear loading.
- Investigating the effect of loading conditions (e.g. normal load, displacement rate) on the AE response of joints and demonstrating how AE signals change by changing these parameters.

- Investigating the effect of mechanical and physical properties of samples (e.g. roughness, bonding percentage) on the AE response of joints and showing the characteristics of AE signals for various kinds of joints.
- The possibility of AE application for localizing damaged zones during direct shear loading and evaluating the capability of this method for localizing zones with rupture potential in dam structures.

AE was monitored during shearing of joints under constant normal load (CNL). CNL has been considered as the loading condition that dams are suffering because of free dilation condition of discontinuities in dam structures. The results of this study showed that simulating various kinds of joints and correlating AE and shear graphs in laboratory provides a better interpretation of the shear process of the in situ discontinuities.

Using parameter-based technique and signal-based technique, the results of AE monitoring could be analyzed. In this research parameter-based technique was used to correlate the characteristics of AE parameters with shear stress-shear displacement behavior of joints because of huge volume of generated AE signals during sample tests and impossibility of analysis of all signals. Signal-based analysis was applied to localize the source of AE events and showing the degradation zones.

It was found that the combined use of acoustic emission parameters and stress-displacement analysis provided the most accurate and reliable method of identifying the shear behavior of structures through weak discontinuities, because each parameter is capable of revealing a number of insights into the progressive failure process of rock joints.

The results of this thesis indicated that AE has a high capability in showing shear behavior of opened (non-bonded) joints while it has some restriction for monitoring shear behavior of closed (bonded) joints.

Two methods were used to monitor pre-peak linear, pre-peak non-linear, post-peak and residual periods in shear stress-shear displacement graphs of joints:

1) Using combination of AE parameter rate with shear graphs.

2) Using combination of cumulative AE parameter with shear graphs.

6.2.1. Bonded joint samples

For bonded joint samples no AE signal was seen in pre-peak linear period (period I). In pre-peak non-linear period (period II) they show some AE activities. These activities come from crack initiation and propagation in the contact surfaces. In post-peak period (period III), because of stress dropping, joints show a dramatic increase in AE and show their maximum peak. This process is due to cracking and breaking of the bonded shear surface. Following this large peak, there are some smaller peaks which are generated from damaging of the secondary and primary asperities. At the residual period of shear stress graph, joints show minimum values of AE parameters. The only movement in this period is the sliding of the joint surfaces, so since there is no distinct shearing in this period, the AE rate showed low values.

Cumulative AE graphs for bonded joints show no AE activity in pre-peak linear period. In pre-peak non-linear period they show a few signals near the end of this period. During post-peak period they show a vertically increasing and then a convexity behavior in their values and finally in residual period, they continue increasing with a very low rate.

For bonded joint, AE signals does not start right after applying shear load and initiation of shear displacement; so the start point of movement cannot be detected by AE before failure. The distance between AE generation (detection) and failure is very short; therefore there is not enough time for remedial solution. It should be noted that if a rupture includes a sequence of events even recording AE signals of the first break is still useful. A combination of other instruments such as loading measuring instruments helps us to have a better insight about pre-peak shear behavior of bonded joint.

6.2.2. Non-bonded joint samples

Non-bonded joints show AE activity with start of loading. It is believed that these activities come from locking of the joint halves. They show some instant peaks in this period. In period II, joints show an increase in values of AE parameters proportionally to loading and they show peaks in approximately same magnitude before maximum shear stress. These signals are generated from breaking of the secondary asperities and sliding of primary asperities. In

period III, whole asperities (secondary and primary) are sheared off and joints show a suddenly increase of AE parameters after shear stress peak, so that the maximum value of the AE rates are observed in this period, they show a gradual decrease at the end of this period. Non-bonded joints show low AE activity in residual section.

Cumulative AE graphs for non-bonded joints increase with concavity in pre-peak linear period and they show a linear increasing in pre-peak non-linear period. During post-peak period they show an increasing with convexity behavior. In residual period, like bonded joints, they continue increasing with a very low rate.

For non-bonded joint, AE activities are generated by applying shear load and initiation of the shear displacement. Opposite to bonded joint, for these ones the distance between AE detection and failure is enough long to implement some remedial solutions.

6.2.3. The effect of bonding percentage

In this study a comprehensive study has been done to evaluate the effect of bonding percentage on shear behavior and AE activity of bonded joints. The results indicated that the shear behavior of the bonded joints is mainly related to adhesive bond between rock and concrete replicas.

Several samples with different bonding percentages were used to verify whether joints with weak bonding show AE activity in their pre-failure section. It was observed that when the joint surfaces are bonded (even for bonding percentages as low as of 10 %), there are no AE events until the break of the adhesive bond.

Although several parameters influence the shear behavior of the bonded joints, almost all of them are affected by the adhesive bond between concrete and rock. At low values of normal load, the influence of normal load (increasing or decreasing) does not lead to significant changes on shear behavior of bonded concrete-rock joints. This phenomenon was also observed regarding the effect of the displacement rate on shear behavior.

It can be concluded that as long as normal stress is lower than bond strength, the shear mechanism of bonded concrete-rock joints is governed by adhesive bond. On the other words changing normal load in this range (0<normal stress <bond strength) does not make any

significant change in shear strength of bonded joins. The shear strength of bonded joints in low values of normal load (until bond strength) can then be considered as equal to the strength of the adhesive bond between two surfaces.

6.2.4. The effect of normal load

In order to investigate the characteristic features of acoustic emission parameters during direct shear tests of rock joints under different constant normal loads, direct shear tests were carried out on rock joints in two ways. At first samples with approximately same physical and mechanical properties were tested under different but constant normal loads. Secondly different values of normal loads were applied on the same sample during its residual behavior of the shear stress graph.

The general behavior of the AE parameters at low values of normal load is that they increase gradually with an approximately linear rate until maximum shear strength point and they show their maximum peaks after this point. Finally they decrease gradually in residual shear strength region. The behavior of the AE energy is a little different because it is more sensitive to instant breaking of the asperities rather than sliding of the joint surfaces so that it shows some instant peaks in residual region with considerable intensities.

At high values of normal load conditions, the AE parameters show a significant peak after maximum shear strength. The AE activities are converged near to shear strength peak and they are decreased before and after that. Amplitude is the only parameter which doesn't show significant change in its behavior. This parameter increases with a low rate at first and then increases linearly after maximum shear strength point. Finally it decreases gradually in residual region.

Experimental results showed that normal load has a very large effect on AE events generated from non-bonded joints under direct shear loading.

Increasing and decreasing normal load always change the AE activity markedly. When normal load is increased it generates more AE events but not immediately at jumping point of normal load. In fact AE events increase after a while that increasing normal load makes asperities to be sheared. Whereas decreasing normal load produces a significant peak in AE parameters at

dropping point. It is believed that this phenomenon is due to releasing of joint halves from interlocking which makes a lot of AE signals. After dropping point, AE parameters are decreased and small peaks are observed as long as normal load is low.

6.2.5. AE source locations

Rock joint surfaces were sprayed by a blue color. During shear loading of the samples, the blue color is removed and light colored zones are remained as joint asperities are sheared off. Shearing process is resulted from breaking of the asperities which are facing to shear direction in contact areas, so AE localization provides an insight about contact area distribution and locations of the asperities facing to shear direction.

For localizing sources of AE events, it was found that the clustering zones of AE sources are corresponding to light colored areas of the sprayed surfaces.

The results of this research show that AE method has a good capability for localizing damaged points in discontinuity surfaces as well as the intensity or energy of their failure. This method can recognize the points with rupture potential well. This provides the possibility to reinforce the support systems and to be aware about the probable failure of a structure before any unexpected disturbance.

As shear load is increased, AE source points are grown during direct shear testing of rock joints. They are localized and increased noticeably after maximum shear strength point and then in the residual section they are decreased.

In pre-peak linear and pre-peak non-linear sections, AE source points are scattered. These points are resulted from friction and degradation of the second order asperities which are distributed on entire surface of rock joints.

First order asperities are located in some specific rough zones of the joint surfaces and are sheared off after maximum shear strength. The generated AE events which are due to breaking of these asperities after maximum shear strength are localized in these zones.

Generally the asperity degradation in residual shear strength section is decreased. In some samples, depending on the amount of the normal load, the AE activity is continued locally

because of failure of the remained rough surfaces. As a conclusion, in residual shear strength section, the number of AE source points is decreased and localized in some local points.

Since damaged zones and their failure intensity are both important for dam monitoring, a successful AE monitoring is achieved when one considers not only the source locations of the AE events, but also the amount of the energy that each event generates.

During the last years AE technique has developed considerably for monitoring stability of underground and surface structures. Although there are differences between AE field and laboratory studies, the results of laboratory tests could be used as a guideline for interpretation of the field results. A written test procedure, personnel qualification, advanced equipment, good installation techniques and array geometry, suitable sensors with acceptable frequency range, system calibration, pre-examination measurements and background noise check is needed for a comprehensive AE monitoring. These improvements represent a major step in the establishment and maturity of AE technology for monitoring shear behavior of in situ discontinuities

6.3. Recommendations

It this study it was tried to simulate the in situ discontinuities by several laboratory sample tests. Although these samples are good representatives of natural in situ discontinuities in dam structures, due to scale effect, they cannot show the whole behavior of in situ discontinuities. More samples with various mechanical characteristics are needed to verify the results of this study. Larger samples are more representative of the natural in situ discontinuities although in some cases the size of the samples is related to the periodicity of the discontinuities.

Acoustic emission is a sensitive method to material that waves are transiting, so depending on how many environments are between sensors and AE event source the AE response of joints is different, therefore it is suggested to attach the sensors directly on the medium containing the joint.

The following research subjects are recommended for future study in this field:

6.3.1. Using signal-based analysis of AE results for monitoring shear behavior of joints

In this study parameter-based analysis was used to correlate the AE activity of joints with their shear behavior because of the large amount of AE signals generated during direct shear test. However reducing a complicated signal to only a few parameters may result in a significant limitation. Nevertheless, the signal-based method is a relatively young field of research and pertinent algorithms and softwares are needed where very large number of AE signals must be processed automatically. Knowing the rate of technology progress, it is recommended to use signal-based analysis in new studies.

6.3.2. Detailed analysis of combination of image processing, acoustic emission and scanned surfaces using suitable softwares and instruments

In this study images of fracture surfaces and fracture topography from surface profiles were used to evaluate the applicability of acoustic emission localization method for localizing asperity damaged in joint surfaces. This provides a powerful tool for linking fracture geometry to the mechanical behavior of fractures under shear stress. Studies such as this one that utilize data obtained from a variety of techniques should be conducted with more samples and more details in order to formulate a constitutive law of shear behavior that incorporates fracture geometry. It is suggested to fabricate identical joint samples and stop shear test at the end of each shear stress-displacement section (pre-peak linear, pre-peak non-linear, post-peak and residual). By scanning and taking photo of the joint surfaces in each stage it can be possible to predict the asperity degradation and the location of the damaged zones by AE localization.

6.3.3. 3D localization of the AE source locations

Quantitative methods in acoustic emission analysis require localization techniques to extract the source coordinates of the acoustic emission events as accurately as possible. There are many different ways to localize AEs in practice that can be used to obtain the required resolution in one, two, or three dimensions. The most appropriate technique depends on the objective of the experiment, on the required solution and on the geometric shape. In this study 2D localization method was used to localize damaged zone in shear surface. In order to have a better insight on asperity damaged zones and having a better correlation between these zones and AE sources, 3D localization method is recommended for next studies.

6.3.4. AE monitoring of in situ discontinuities by applying in situ direct shear test

The in-situ direct shear test would provide not only better understanding of the shear mechanism of large discontinuities but also invaluable knowledge for AE monitoring applications in rock engineering, such as the prediction of instable active joints in dam structures, slope stability and other geotechnical structures which are suffering from movement through discontinuities. Therefore AE monitoring of in situ discontinuities by applying in situ direct shear test would be alternative for research in this field.

6.3.5. Borehole geophysical methods for knowing the real circumstances of the discontinuities

Knowing the real circumstances of the discontinuities such as their opening, their bonding percentages, infilling material etc, helps us to have a better interpretation of the direct shear test results and to choose better shear strength parameters in stability analysis. This also helps us to interpret the results of AE monitoring accurately.

Borehole geophysical methods, also called well logging, are continuous monitoring techniques in the borehole aiming at recording rock mass parameters according to depth. Two specific types of well logging are optical imaging and acoustic logging, which will be used in our further studies for monitoring in situ situation of discontinuities.

APPENDIX 1: A FLOWCHART SHOWING METHODOLOGY STEPS

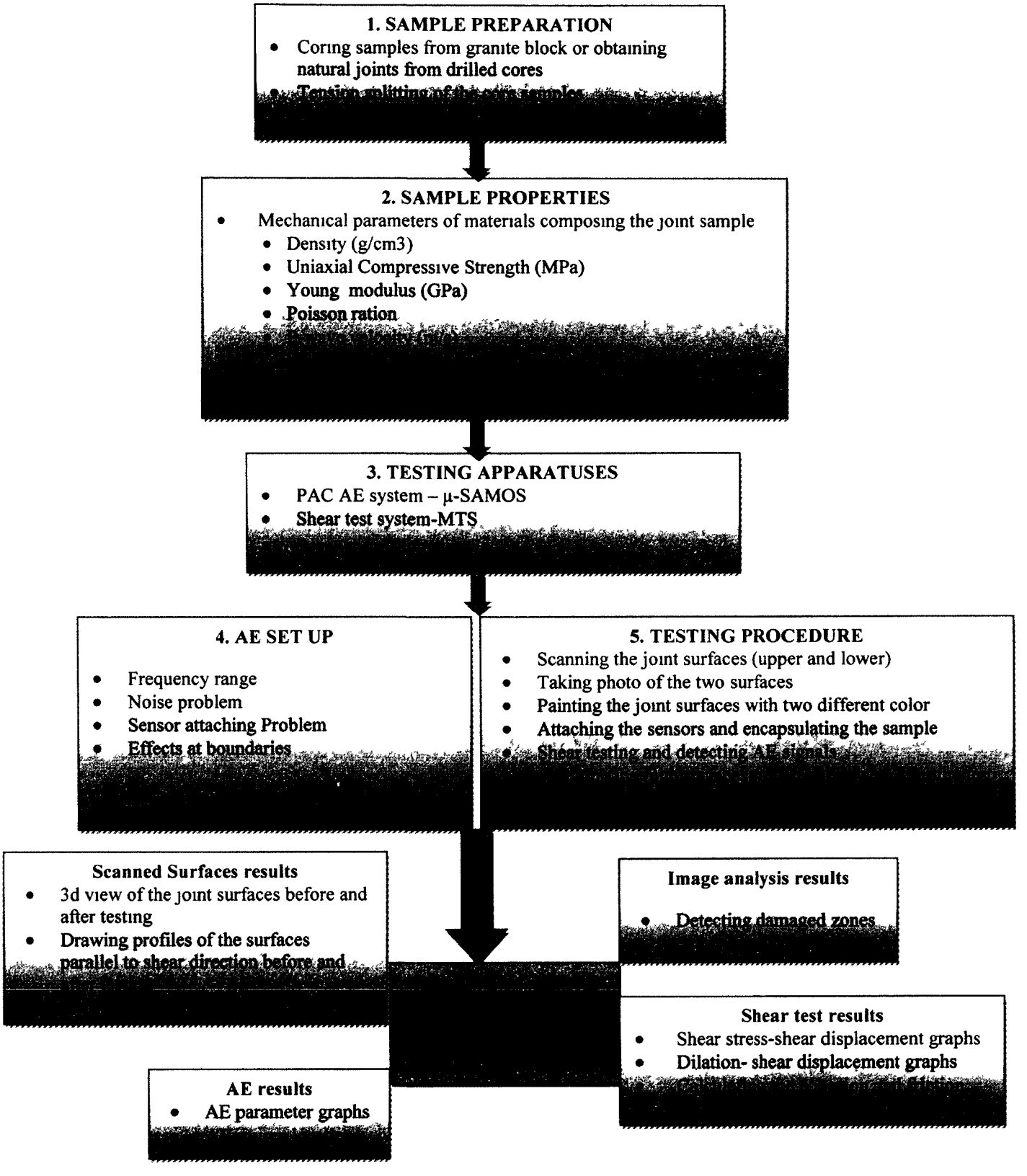

Figure A1- 1: Program of laboratory tests

APPENDIX 2: PHOTOS SHOWING METHODOLOGY STEPS

Figure A2- 1: Coring rock samples from a granite block

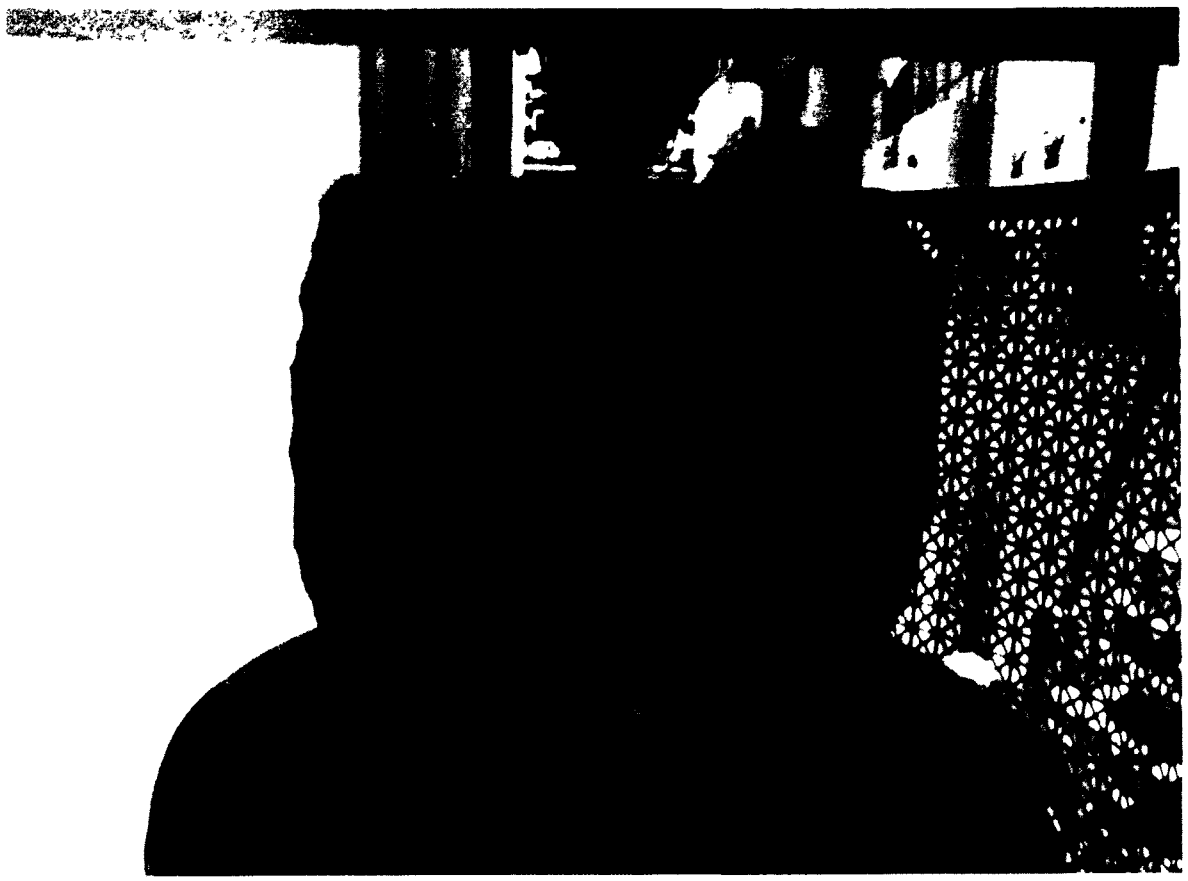

Figure A2- 2: Tension splitting of the rock cores to create a jointed sample

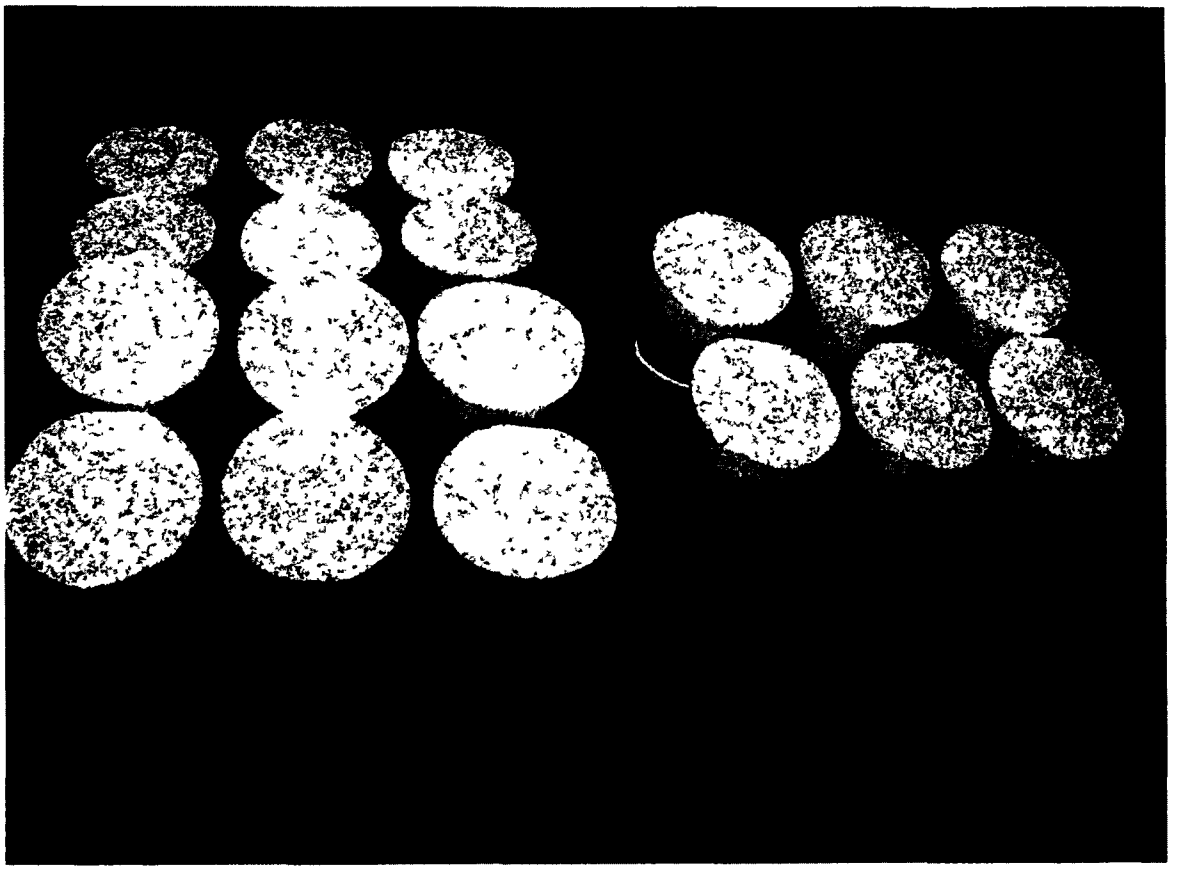

Figure A2- 3· Rock replicas ready for pouring mortar in order to create bonded rock-concrete joints

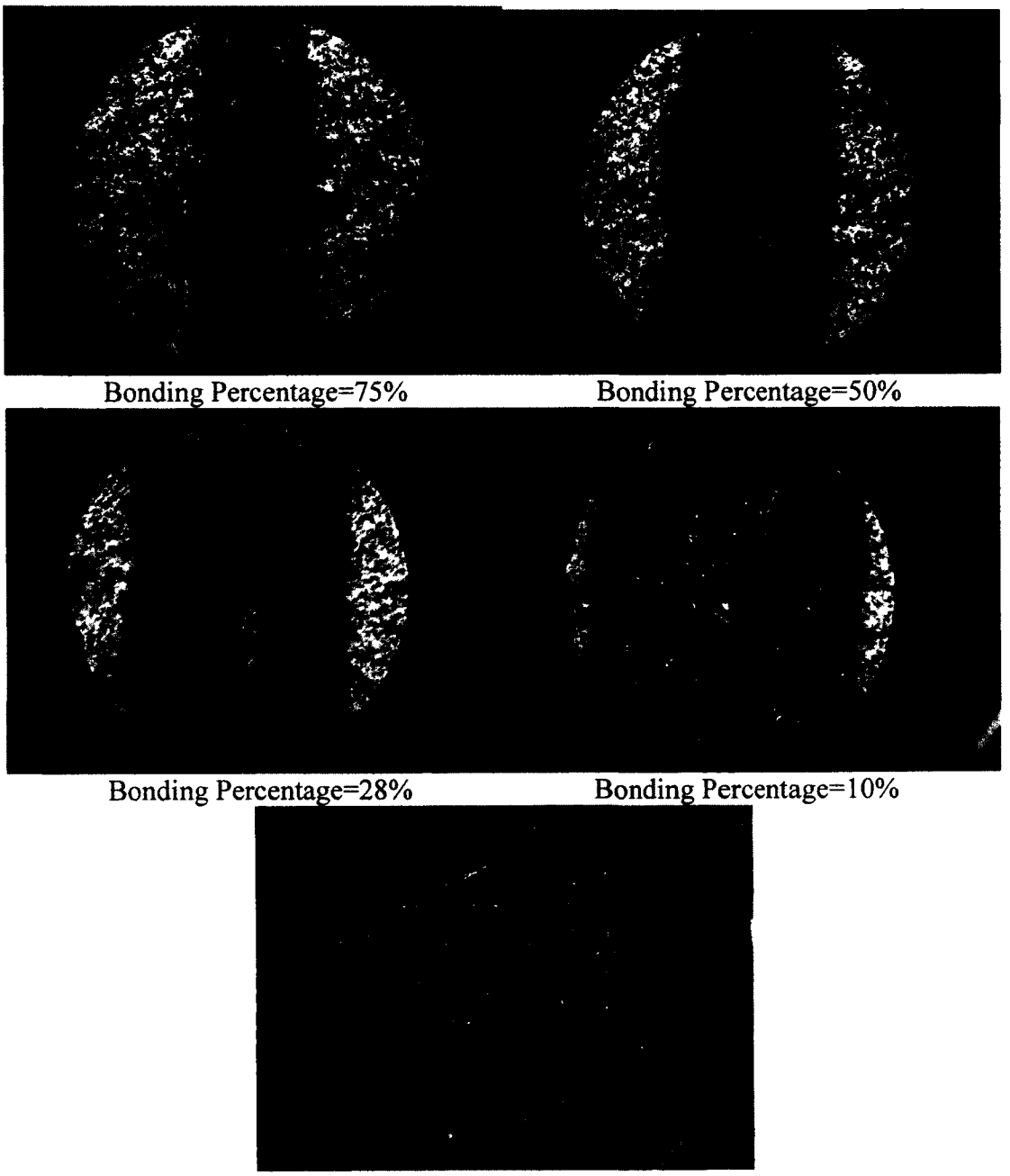

Figure A2- 4: Spreading clay to create bonded rock-concrete joints with different amounts of bonding percentage

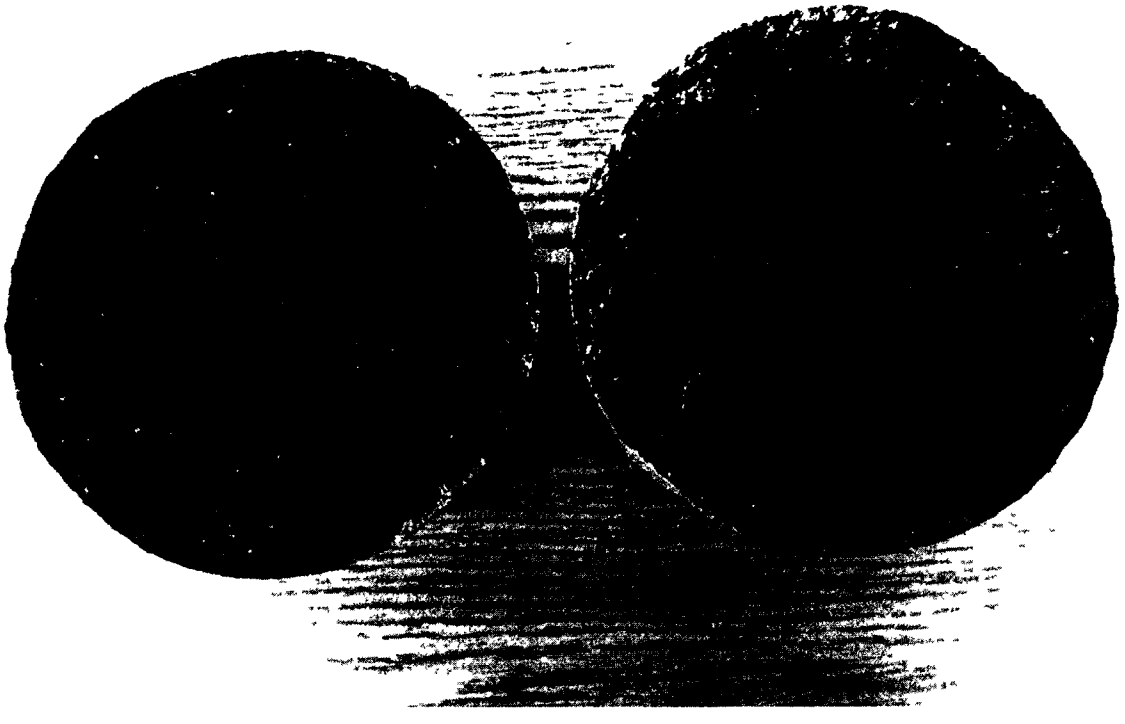

Figure A2- 5: A rock-rock joint sprayed by a blue color ready for shear testing and localization of the AE sources

Figure A2- 6: A prepared bonded rock-concrete joint

Figure A2- 7: Subbing sensor positions by a rotary sander

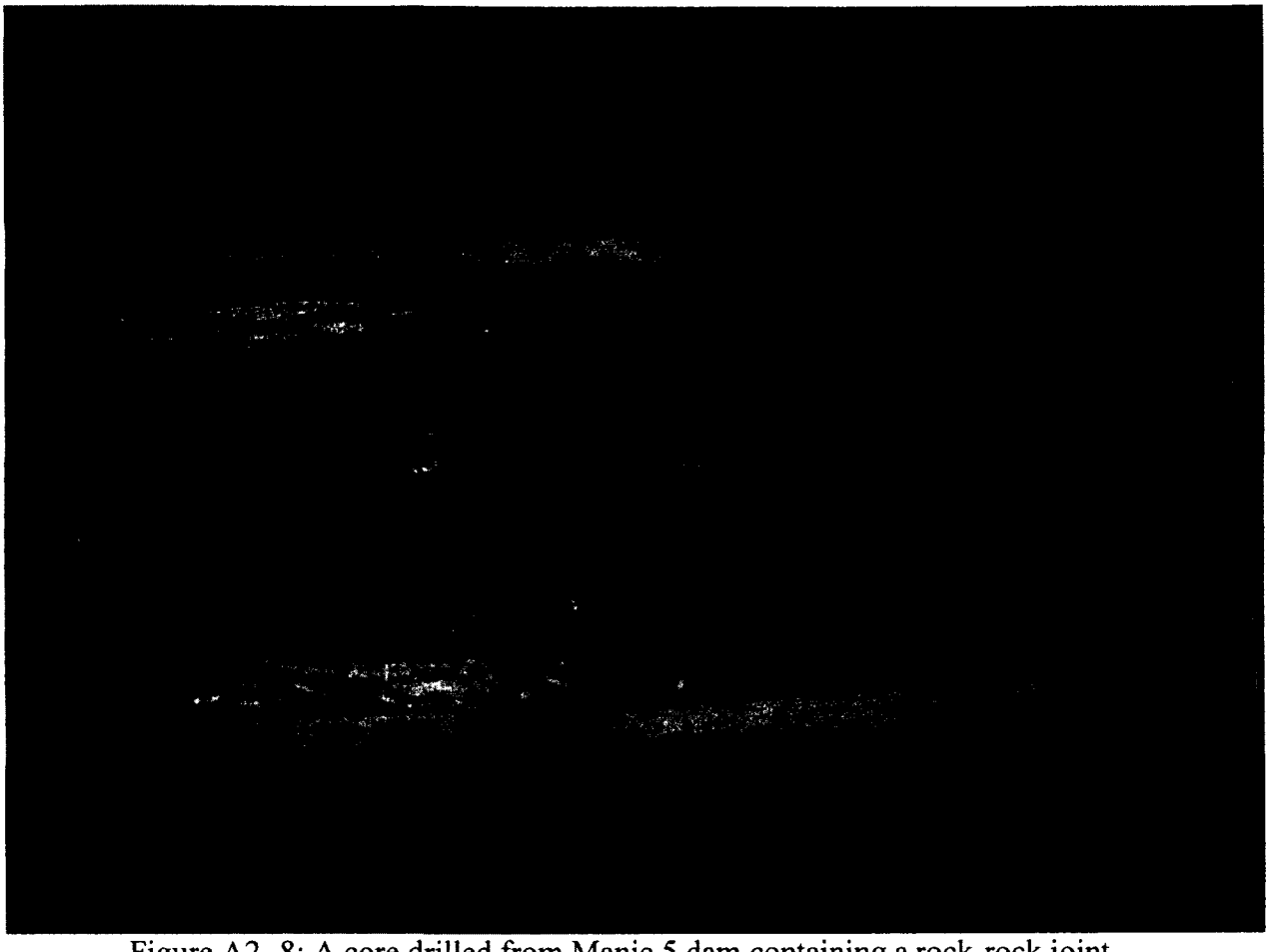

Figure A2- 8: A core drilled from Manic 5 dam containing a rock-rock joint

Figure A2- 9: A core drilled from Manic 5 dam containing a concrete-rock joint

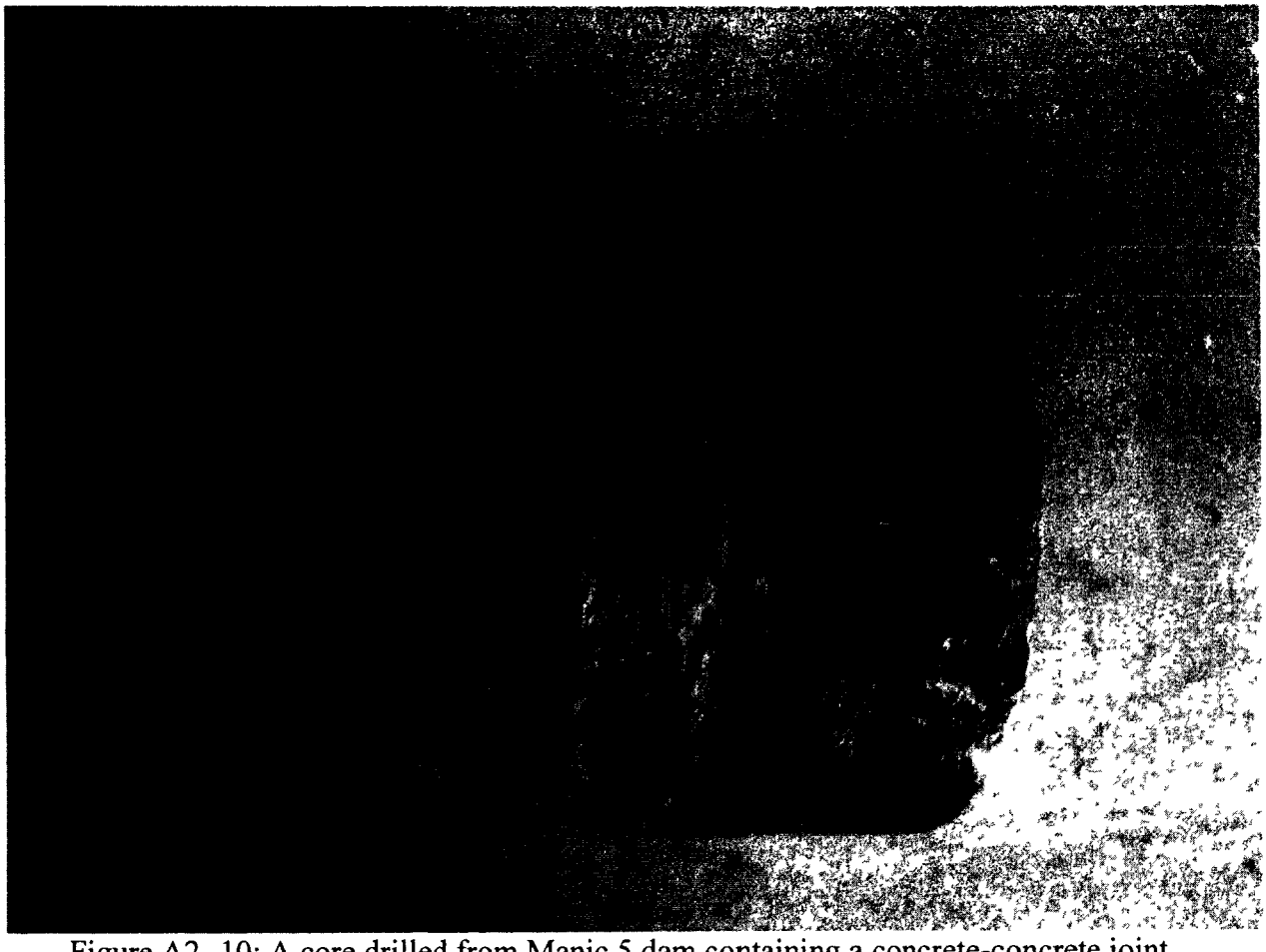

Figure A2- 10: A core drilled from Manic 5 dam containing a concrete-concrete joint

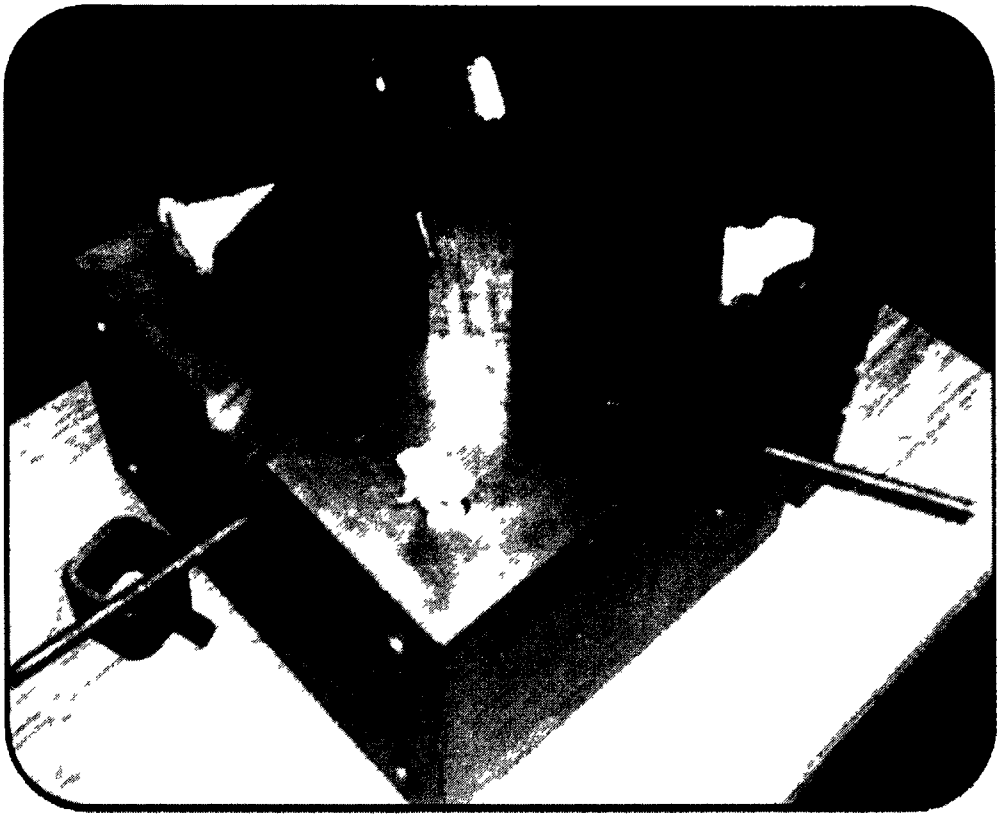

Figure A2- 11: Mobile part of shear test mold ready for encapsulating a sample

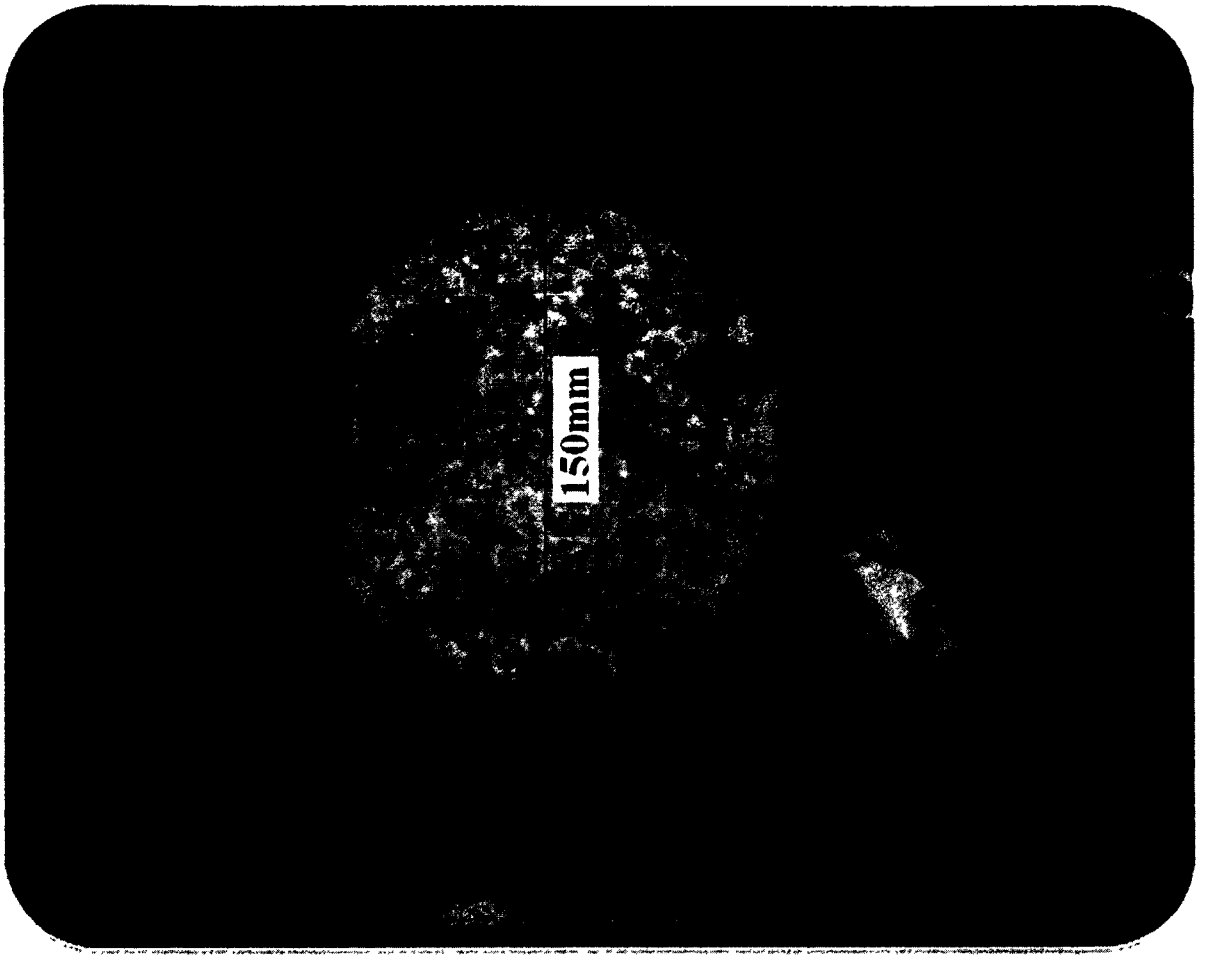

Figure A2- 12: Joint sample positioned in the mold considering the shear direction and horizontal level of the joint surface

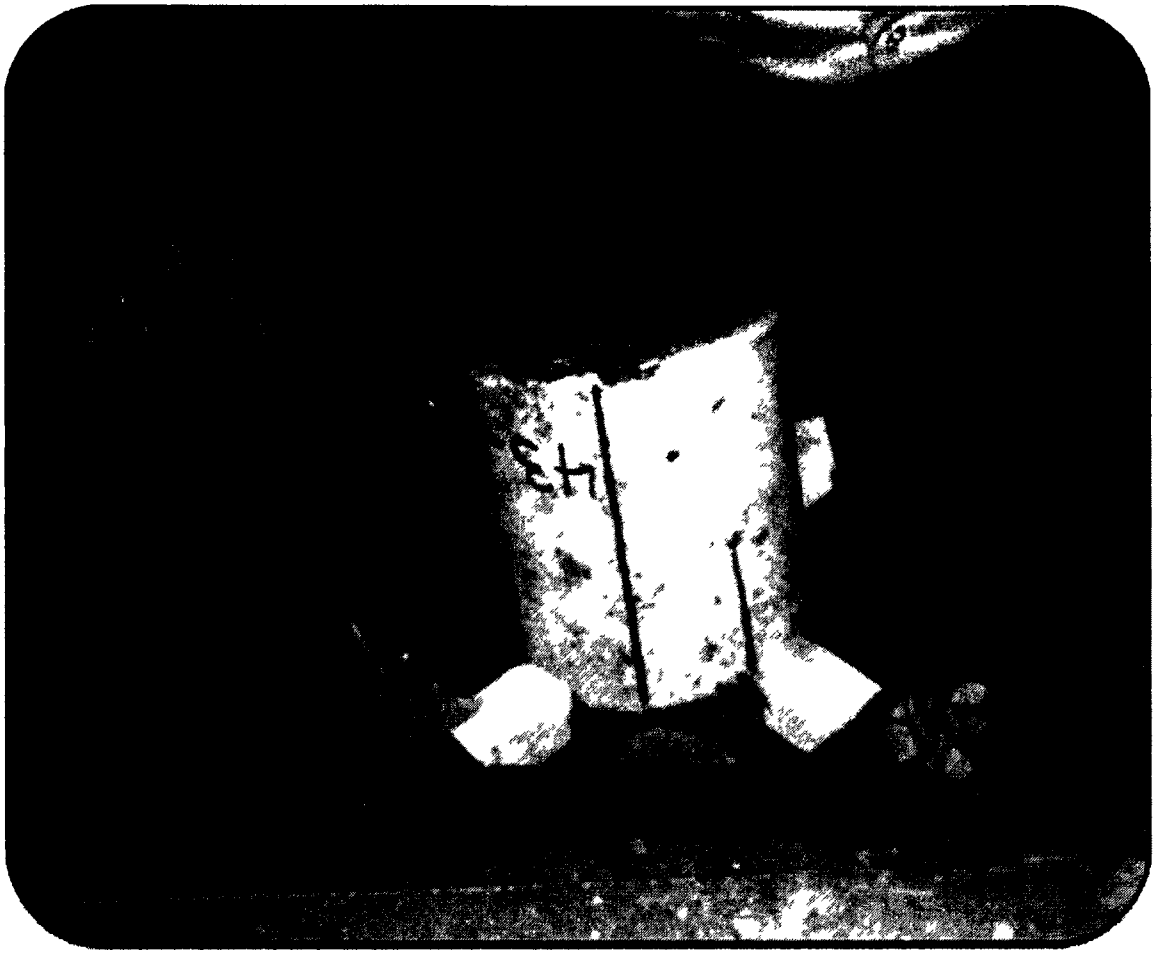

Figure A2- 13: Pouring Ciment Sika Grout 212 with E/C=0.18, before pouring the sensor positions were kept by fixing a fiber piece between each sensor position and the wall of the mould

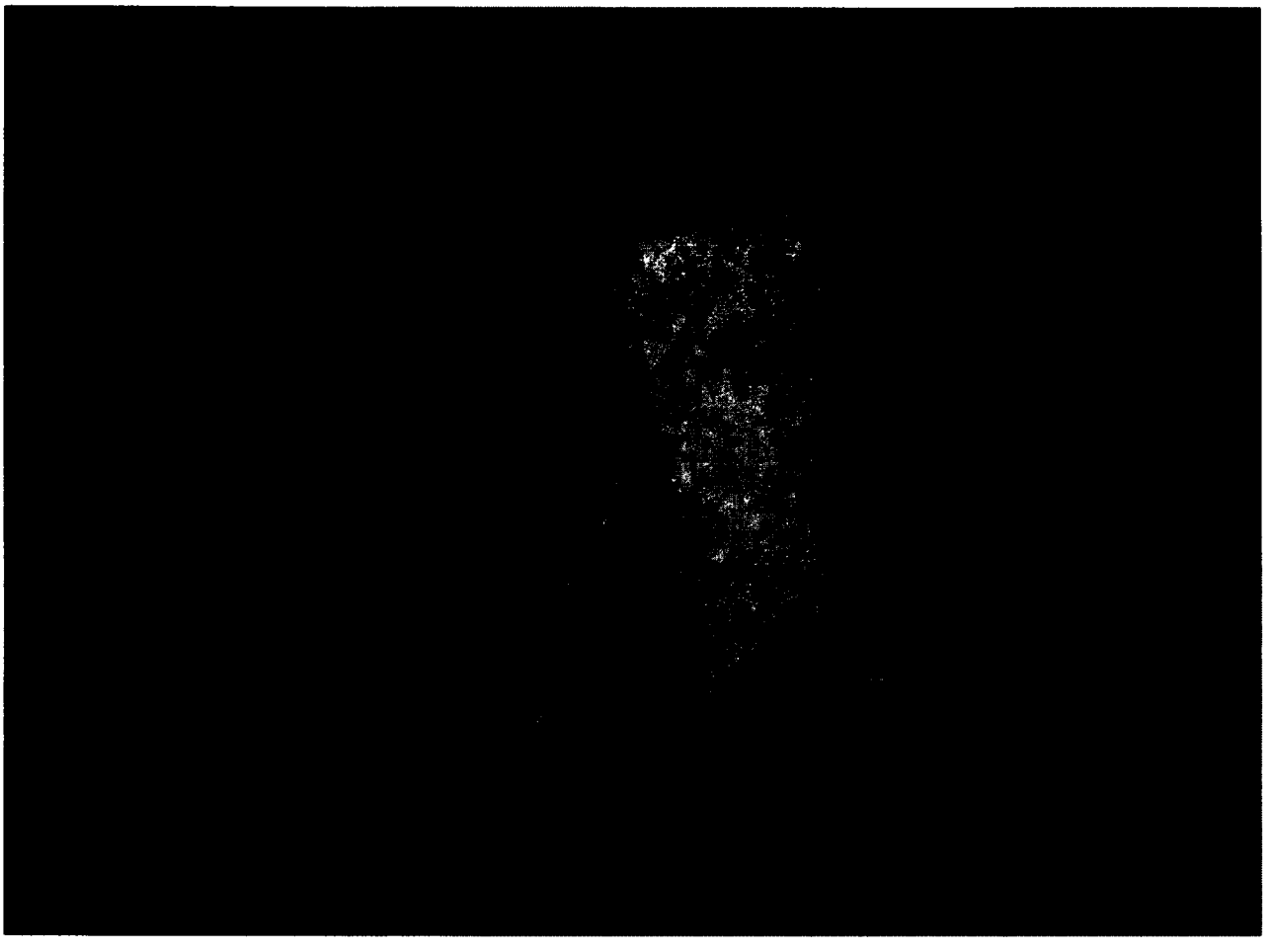

Figure A2- 14: Pouring Ciment Set 45 with E/C=0.08 which is cured very fast and fixes the sample perfectly in the mold

Figure A2- 15: Putting sensors in the considered holes and attaching them to the sample using Loctite Metal/Concrete Epoxy (01-81508) glue

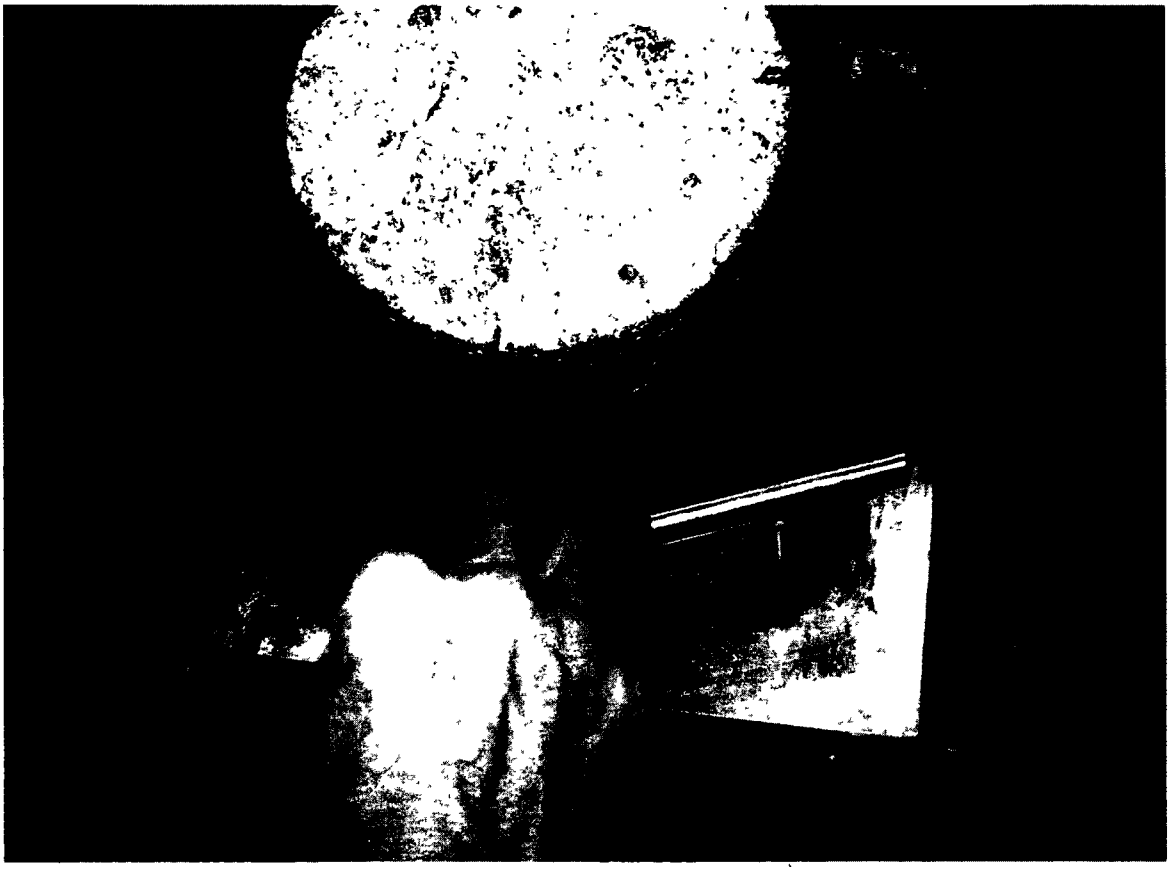

Figure A2- 16: Smooth clay is used to separate the two halves of mold and prevents grout to inter into area between joint surfaces during grouting second mold. The clay covers the sensors and makes a good ambient for shearing of the surfaces

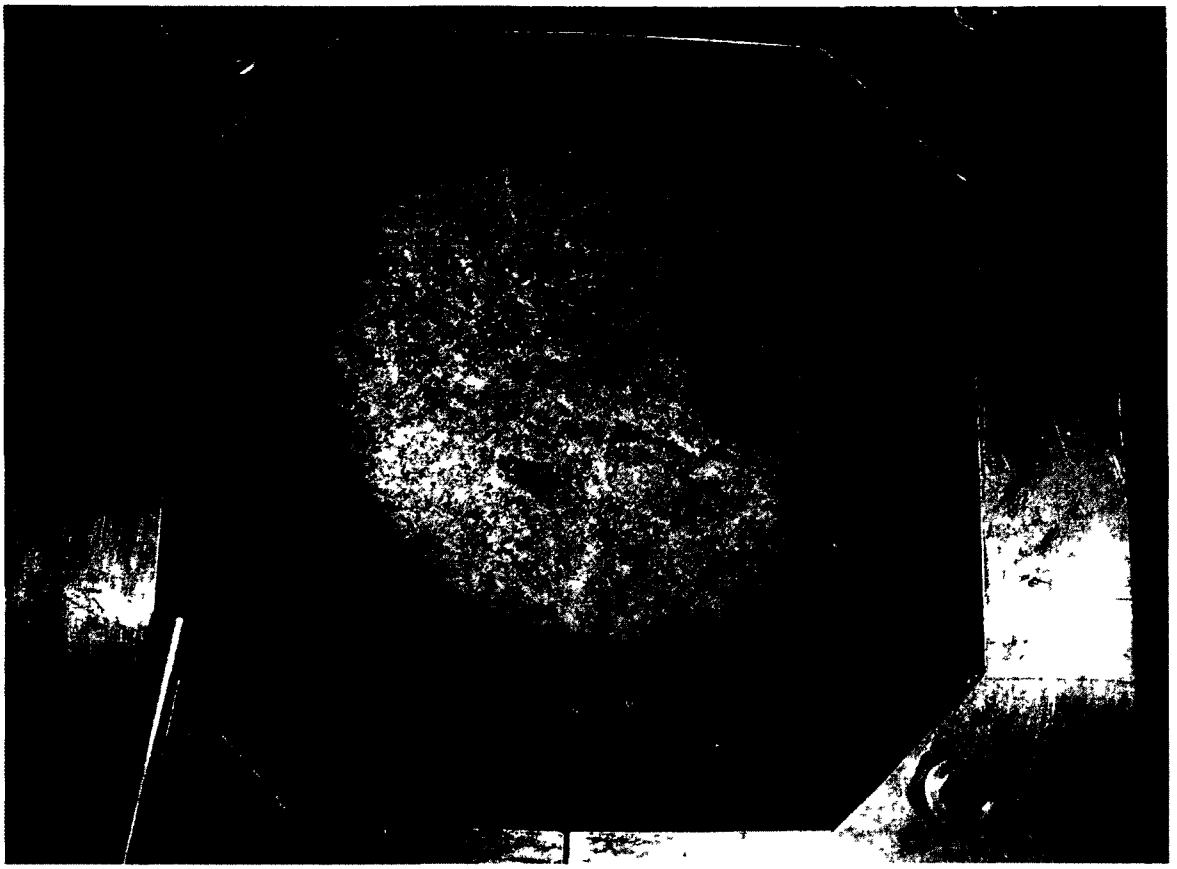

Figure A2- 17: Putting the Fix half of the mould on the mobile half

Figure A2- 18: Encapsulating the whole mold

Figure A2- 19: Mounting mold in the MTS loading system and connecting sensors to the amplifiers and AE PAC system

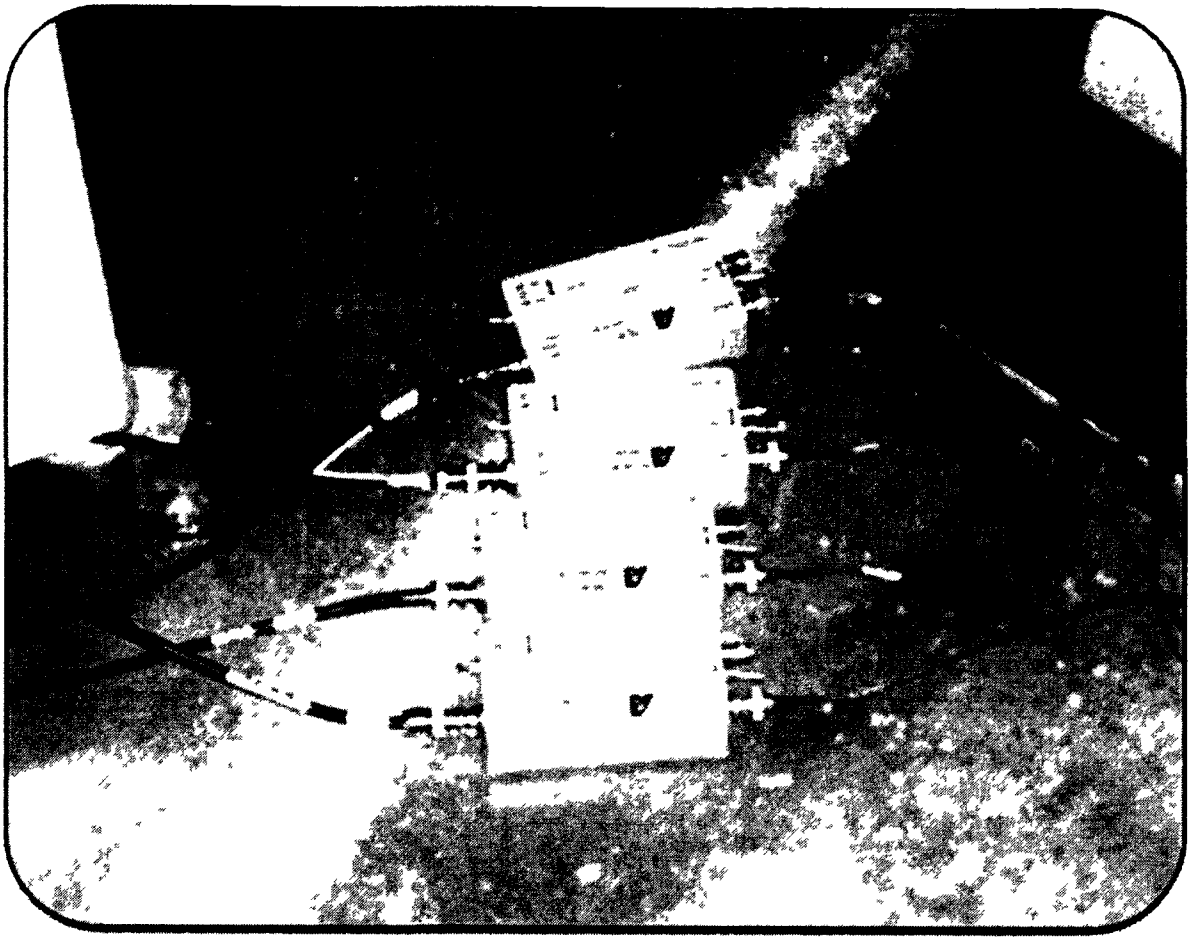

Figure A2- 20: Amplifiers used in this study (preamplifier model 2/4/6 with 10 KHz - 1200 KHz bandpass filter)

Figure A2- 21: Fixed half of the joint sample after shear test

Figure A2- 22: Mobile half of a rock-rock joint with light colored zones which are showing the asperity damaged zones

Figure A2- 23: Fixed half of previous rock-rock joint with light colored zones which are showing the asperity damaged zones

Figure A2- 24: A rock-concrete joint sample after direct shear test, the asperity damaged zones are seen on the concrete replica surface

APPENDIX 3: FIGURES SHOWING SHEAR AND AE BEHAVIORS OF MANIC 5 SAMPLES

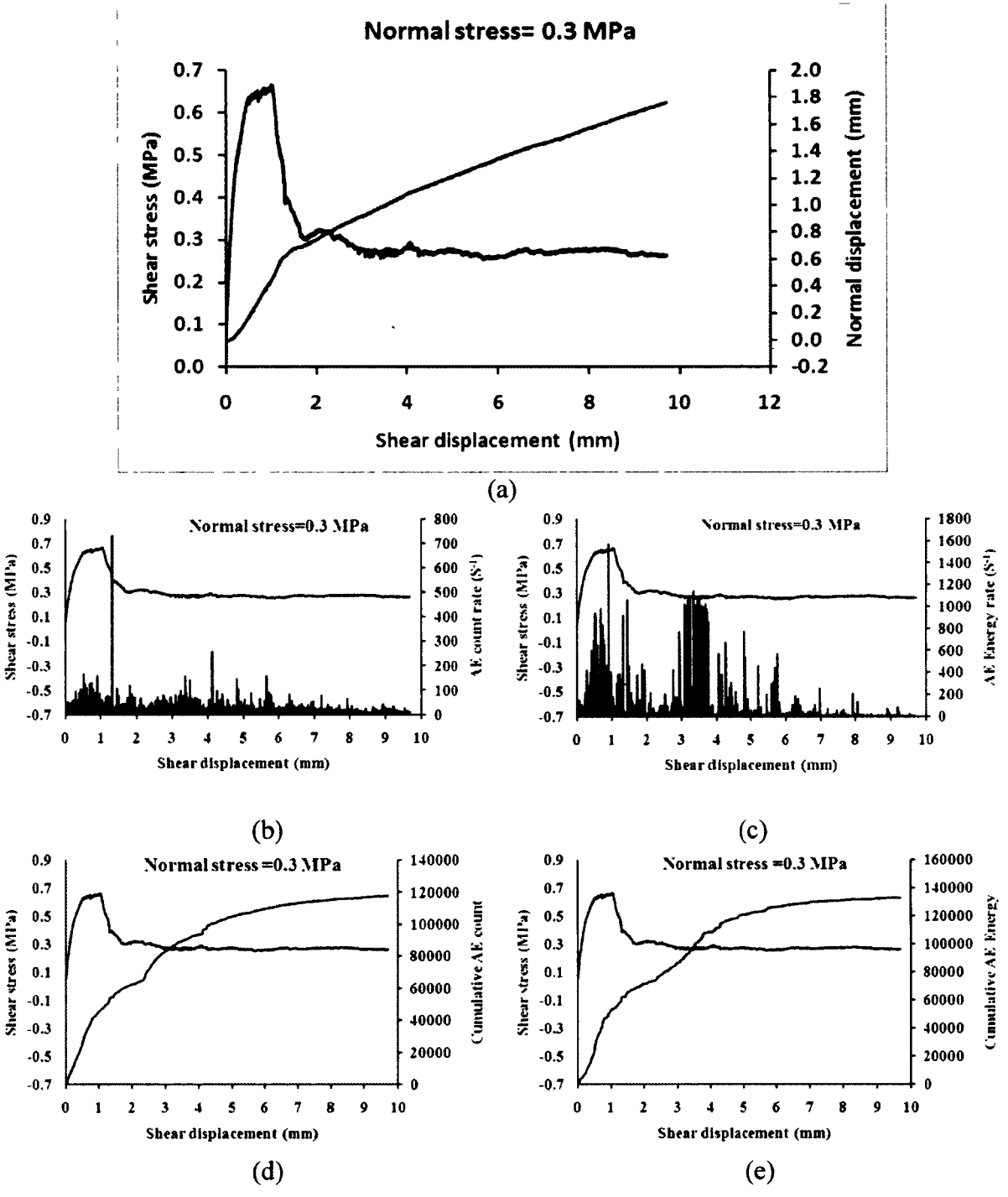

Figure A3- 1: a) Shear stress and normal displacement vs. shear displacement, b) shear stress and AE count rate vs. shear displacement, c) shear stress and AE energy rate vs. shear displacement, d) shear stress and cumulative AE count rate vs. shear displacement and e) shear stress and cumulative AE energy rate vs. shear displacement for non-bonded rock-rock joint (Sample MC6-RR10)

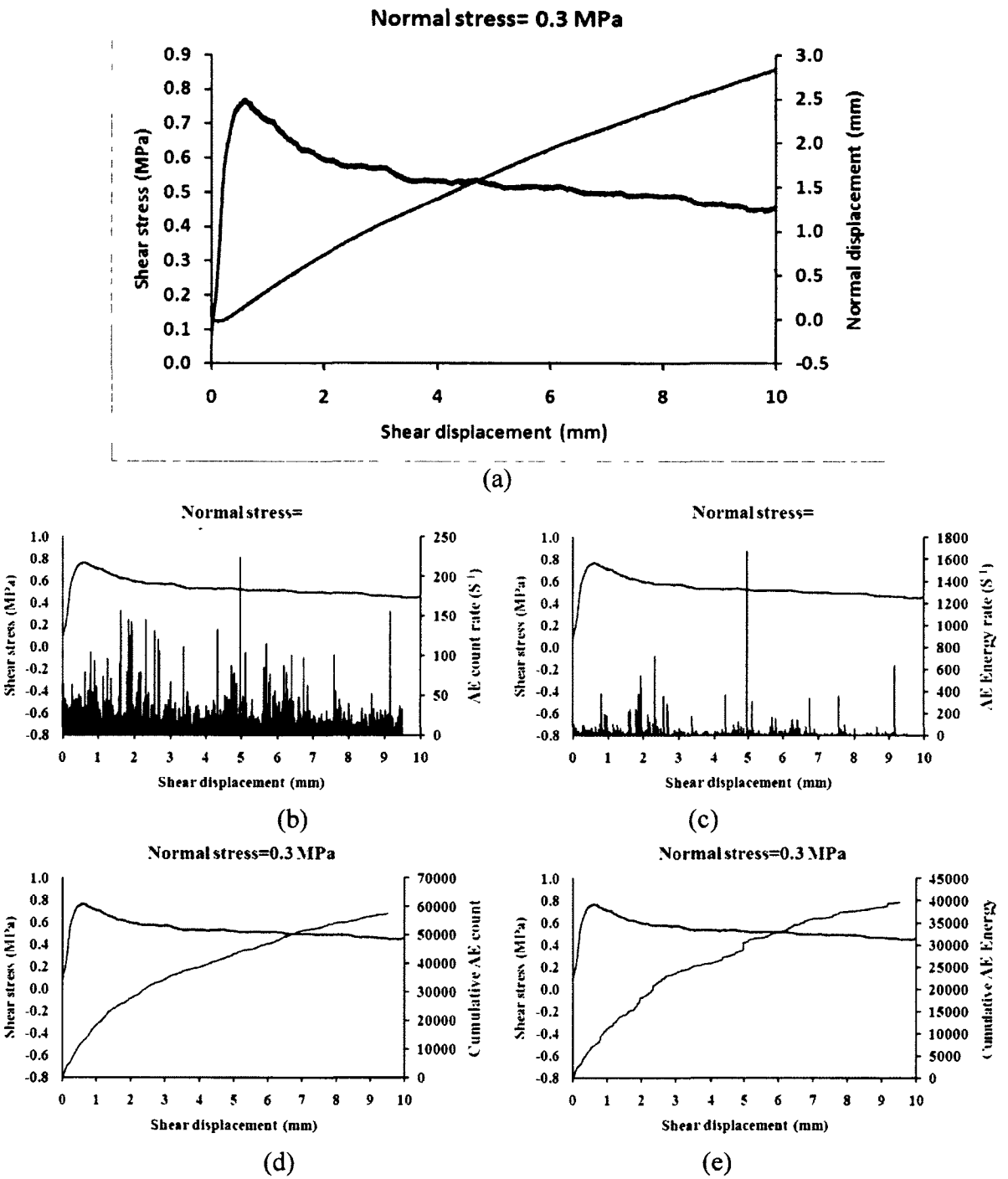

Figure A3- 2: a) Shear stress and normal displacement vs. shear displacement, b) shear stress and AE count rate vs. shear displacement, c) shear stress and AE energy rate vs. shear displacement, d) shear stress and cumulative AE count rate vs. shear displacement and e) shear stress and cumulative AE energy rate vs. shear displacement for non-bonded rock-concrete joint (Sample MC6-RC5.36)

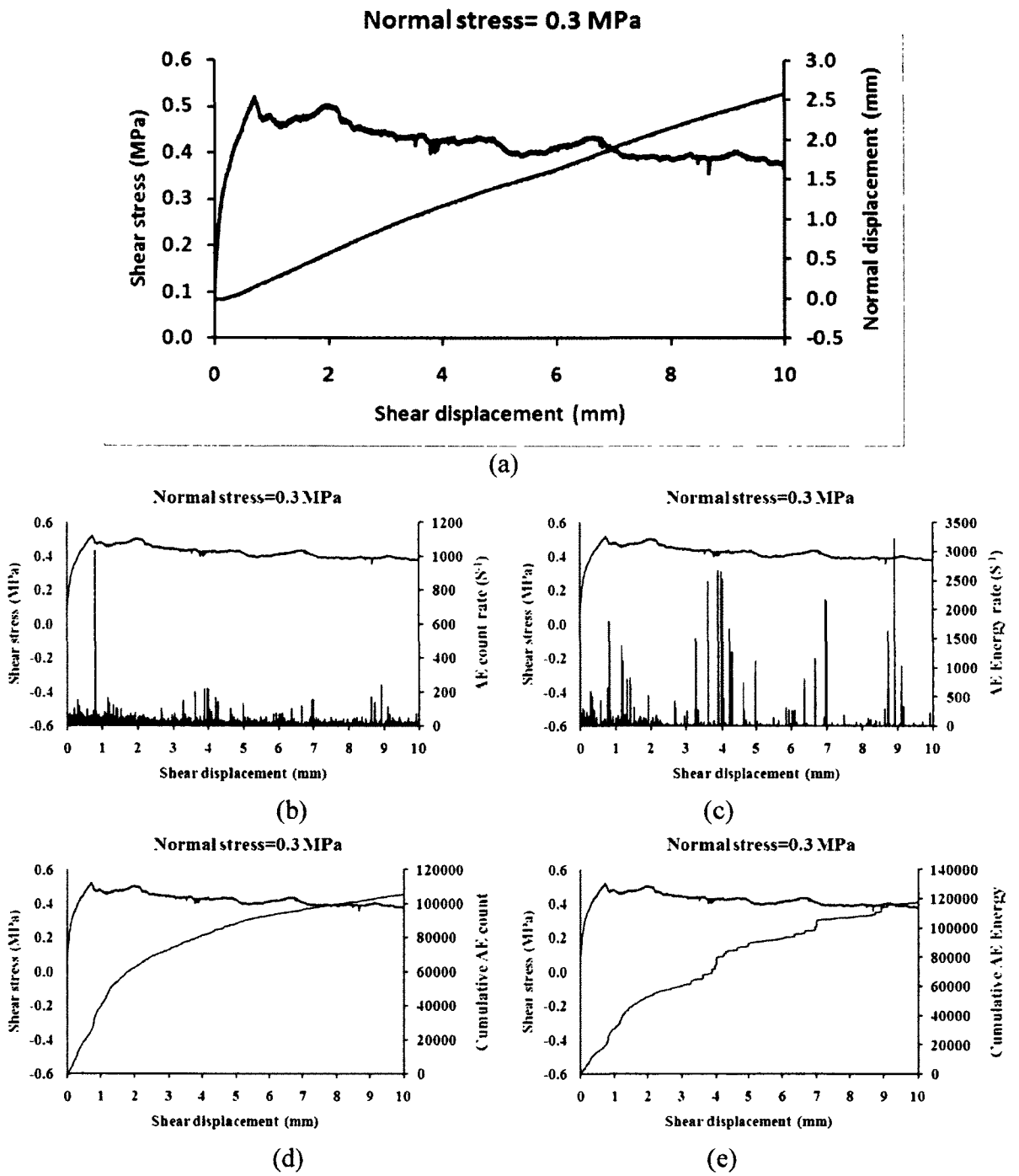

Figure A3- 3: a) Shear stress and normal displacement vs. shear displacement, b) shear stress and AE count rate vs. shear displacement, c) shear stress and AE energy rate vs. shear displacement, d) shear stress and cumulative AE count rate vs. shear displacement and e) shear stress and cumulative AE energy rate vs. shear displacement for non-bonded concrete-concrete joint (Sample MC6-CC2.18)

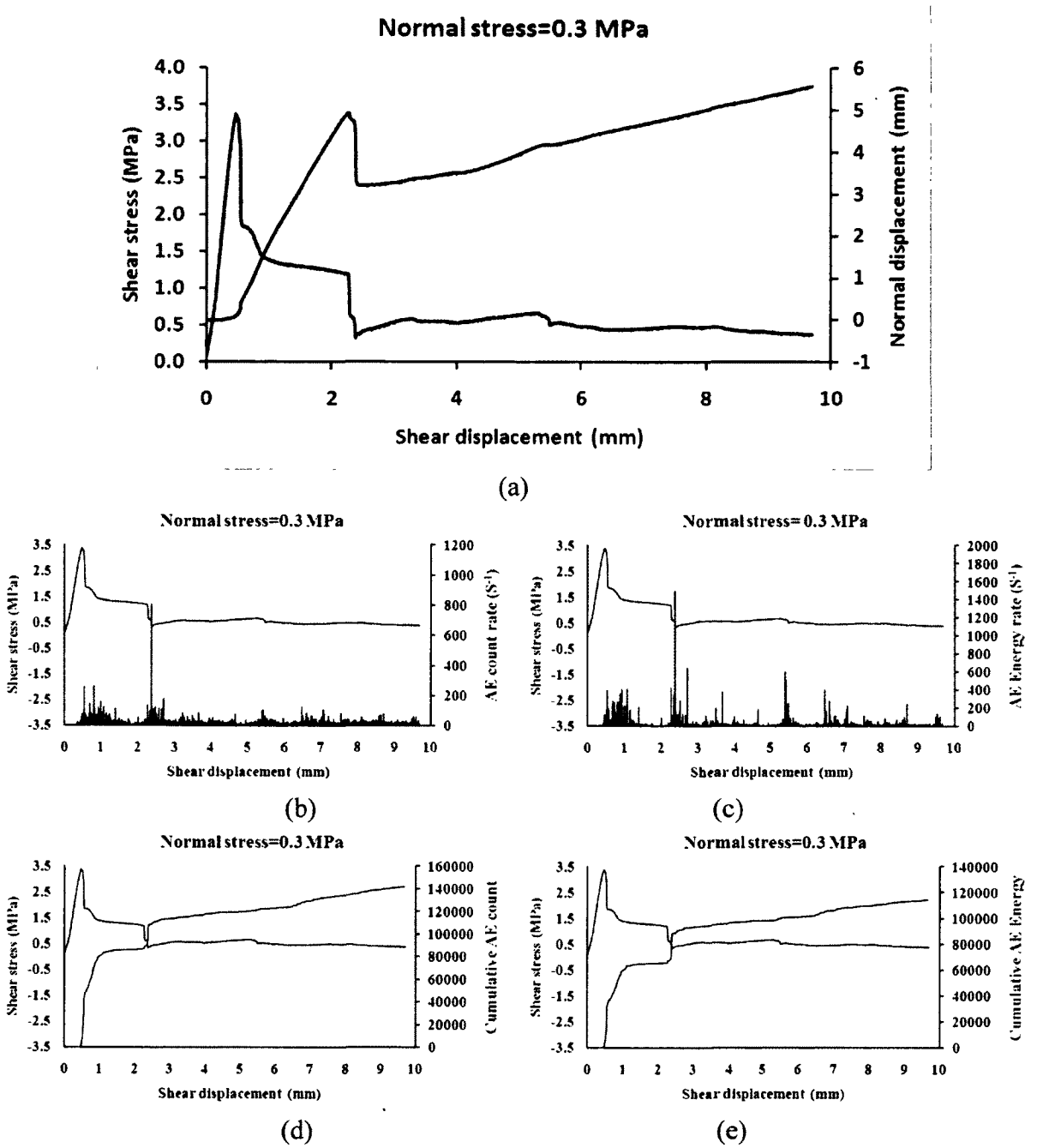

Figure A3- 4: a) Shear stress and normal displacement vs. shear displacement, b) shear stress and AE count rate vs. shear displacement, c) shear stress and AE energy rate vs. shear displacement, d) shear stress and cumulative AE count rate vs. shear displacement and e) shear stress and cumulative AE energy rate vs. shear displacement for bounded concrete-concrete joint (Sample MC6-CC6.60)

REFERENCES

ASTM. (2002), Standard test method for performing laboratory direct shear strength test of rock specimens under constant normal force. Designation D5607-02, Annual book of ASTM standards 2002, p.1358-1369.

Ballivy. G, Gravel. C & El Malki. T, (2006), Development of a new experimental protocol to estimate the shear strength of concrete-rock joints" EUROCK 2006 – multiphysics coupling and long term behavior in rock mechanics – Van Cotthem, Charlier, Thimus & Tshibangu (eds), Taylor & Francis Group, London, p. 563-569.

Barton, N. (1973) Review of a new shear strength criterion for rock joints, Quarterly Journal of Engineering Geology, 7, p. 287–332.

Barton, N., Choubey, V. (1977), The shear strength of rock joints in theory and practice. Rock Mechanics, 10, p. 1–54.

Barton, N.R. and Bandis, S.C. (1982), Effects of block size on the shear behavior of jointed rock. 23rd U.S. symp. on rock mechanics, Berkeley, p. 739-760.

Bouja, A. (1994) Contribution à l'étude de l'injection d'un coulis de ciment en milieu fissuré, Thèse de doctorat, Université de Sherbrooke, Département de génie civil, Sherbrooke, Canada, 194 p.

Brady B. H. G. and Brown E. T. (2005) Rock Mechanics for underground mining Third edition, Springer Science, 628 p.

Brown E. T. (1981), Rock Characterization Testing & Monitoring-ISRM Suggested Methods, p. 211. Pergamon Press, Oxford, 1981, 211 p.

Butt SD, Muckherjee C, Lebans G. (2003), Evaluation of acoustic attenuation as an indicator of roof stability in advancing headings. Int J Rock Mech Min Sci; 37, p.1123–31.

Cai, M.P.K. Kaiser, H. Morioka, M. Minami, T. Maejima and Y. Tasaka, (2007), FLAC/PFC coupled numerical simulation of AE in large-scale underground excavations, Int J Rock Mech Min Sci 44, p. 550–564.

Cai M., H. Morioka, P.K. Kaiser, Y. Tasak, H. Kurose, M. Minami, T. Maejim, (2007), Back-analysis of rock mass strength parameters using AE monitoring data, International Journal of Rock Mechanics & Mining Sciences 44, p. 538–549

Cater, J. P., Ooi, L. H. (1988), Application of joint model to concrete-sandstone interfaces. In: Swoboda, G. (ed.), Numerical methods in geomechanics, Balkema, Rotterdam, p. 889–893.

Chang S.H., C.I. Lee, (2004), Estimation of cracking and damage mechanisms in rock under triaxial compression by moment tensor analysis of acoustic emission, International Journal of Rock Mechanics & Mining Sciences 41, p. 1069–1086

Changwoo, H., Seokwon, J., Sanghyuck, B., Jungseok, Y. (2002), Shear deformation and failure characteristics of rock-concrete interfaces. In: Hammah, R. et al (eds), Proc. 5th NARMS and 17th TAC, p. 721–725.

Crawford A.M. and Curran J.H. (1981), the influence of shear velocity on the frictional resistance of rock discontinuities. Int.J.Rock Mech.Min.Sci. & Geomech.Abstr., 18, p. 505-515.

Dahm T, Mantehi G, Eisenblatter J. (1999), Automated moment tensor inversion to estimate source mechanisms of hydraulically induced micro-seismicity in salt rock. Tectonophysics;306, p. 1–17.

Doyce B. Nunis, Jr. (Ed.) (2002), The Saint Francis Dam Disaster Revisited, Historical Society of Southern California, 182 p.

Eberhardt, E. Stead, D. Stimpson, B. Read, R.S. (1997), Changes in acoustic event properties with progressive fracture damage, Int. J. Rock Mech. & Min. Sci. 34:3–4, Paper No. 071B

El Malki, T. (2006) Développement d'un protocole expérimental pour l'estimation de la résistance au cisaillement d'un contact roc-béton, mémoire de maitrise, Université de Sherbrooke, Département de génie civil, Sherbrooke, Canada, 98 p.

Falls S.D, Young R.P. (1998), Acoustic Emission and ultrasonic-velocity methods used to characterise the excavation disturbance associated with deep tunnels in hard rock. Tectonophysics, 289(1–3), p. 1–15.

Feknous, N. (1991) Etude à l'aide de la technique d'émission acoustique, des mécanismes de détérioration des contacts roche-coulis de ciment, Thèse de doctorat, Université de Sherbrooke, Département de génie civil, Sherbrooke, Canada, 129 p.

Filimonov, Y. Lavrov, A. and Shkuratnik, V. (2005), Effect of confining stress on acoustic emission in ductile rock, Strain, 41, p. 33–35.

Gentier, S.S. Hopkins, D.L. (1997) Mapping fracture aperture as a function of normal stress using a combination of casting, image analysis and modelling techniques, Int J Rock Mech Min Sci Geomech Abstr;34: 3-4, paper No. 132.

Gentier, S., Riss, J., Archambault, G., Flamand, R., Hopkins,D. (2000), Influence of fracture geometry on shear behavior. Int. J. Rock. Mech. Min. Sci. & Geomech. Abstr. 37(1–2) , p. 161–174.

Grasselli G. 2001, Shear strength of rock joints based on quantified surface description, PhD thesis, ecole polytechnique federale de lausanne, Lausanne, Switzerland, 126 p.

Grasselli, G. Wirth, J. Egger, P. (2002) Quantitative three-dimensional description of a rough surface and parameter evolution with shearing, International Journal of Rock Mechanics & Mining Sciences; 39, p.789–800

Grasselli G. 2006. Shear Strength of Rock Joints Based on Quantified Surface Description. Rock Mech. Rock Engng. 39 (4), p. 295–314

Grosse CU. Advances in construction materials 2007. Heidelberg: Springer; 2007, ISBN 978-3-540-72447-6.

Goutal N, (1999), The Malpasset Dam Failure: An Overview and Test Case Definition, National Hydraulic and Environement Laboratory, 8 p.

Gu, X. F., Seidel, J. P., Haberfield, C. M. 2003. Direct shear test of sandstone-concrete joints. International Journal of Geomechanics. September, p. 21–33.

Haberfield, C.M. and Seidel, J.P. (1999) Some recent advances in the modeling of soft rock joints in direct shear, Geotechnical and Geological Engineering, 17(4), p. 177–195.

Haberfield, C. M., Johnston, I. W. (1994) A mechanistically-based model for rough rock joint. Int. J. Rock Mech. Min. Sci. Geomech. Abstr. 31(4) , p. 279–292.

Hardy H.R. Jr. (2003) Acoustic emission/microseismic activity. Balkema publishers, 287 p.

Hoek E and Bray J.W. (1981), Rock slope engineering. (third edition): London, The Institution of Mining and Metallurgy, 358 p.

Hong C, Seokwon Jeon, (2006), influence of shear load on the characteristics of acoustic emission of rock-concrete interface, Key Engineering Materials Vols. 270-273, p.1598-1603.

Huang M, L. Jiang, P. K. Liaw, C. R. Brooks, R. Seeley, and D. L. Klarstrom, (1998), Using Acoustic Emission in Fatigue and Fracture Materials Research, Jom, vol. 50, no. 11

Hydro-Québec (April 2010). Shaping the Future: Annual Report 2009. Montreal: Hydro-Québec. ISBN 978-2-550-58101-7, 114 p.

ICOLD (1973) World Register of Dams. International Commission on Large Dams, Paris.

ICOLD (1976) World Register of Dams 1st Updating. International Commission on Large Dams, Paris.

ICOLD (1979) World Register of Dams 2nd Updating. International Commission on Large Dams, Paris.

ICOLD (1995) Bulletin 99 - Dam Failures Statistical Analysis. International Commission on Large Dams, Paris.

Ishida T. (2001), Acoustic emission monitoring of hydraulic fracturing in laboratory and field, Construction and Building Materials 15, p.283-295.

Ishida T, Tadashi Kanagawa, Yuji Kanaori . (2010), Source distribution of acoustic emissions during an in-situ direct shear test: Implications for an analog model of seismogenic faulting in an inhomogeneous rock mass. Engineering Geology,;110(3-4), p. 66-76.

Johnston, I. W. Lam, T. S. & Williams, A. F. (1987), Constant normal stiffness direct shear testing for socketed pile design in weak rock. Geotechnique 37, p. 83-89.

Johnstone, I. W., Lam, T. S. K. (1984): Frictional characteristics of planar concrete-rock interfaces under constant normal stiffness condition. Proc. 4th Australia-New Zealand Conf. on Geomechanics, Perth: 2, p. 397-401.

Kimura, T., Esaki, T. (1995), A new model for the shear strength of rock joints with irregular surfaces. In: Rossmanith H.-P. (ed.), Mechanics of jointed and faulted rock. Balkema, Rotterdam, p.133–138.

Kodikara, J. K., Johnston, I. W. (1994), Shear behaviour of irregular triangular rock-concrete joints. Int. J. Rock. Mech. Min. Sci. & Geomech. Abstr. 31(4), p. 313–322.

Koerner, R.M.W.M. McCabe and A.E. Lord, (1981), Overview of acoustic emission monitoring of rock structures, Rock Mech 14, p. 27–35.

Kulatilake PHSW, Shou G, Huang TH, Morgan RM., (1995), New peak shear strength criteria for anisotropic rock joints. Int J Rock Mech Min Sci Geomech Abstr;32, p. 673–97.

Kurz JH, Grosse CU, Reinhardt H-W. (2005), Strategies for reliable automatic onset time picking of acoustic emissions and of ultrasound signals in concrete. Ultrasonics 43, p.546–58.

Ladanyi, B., Archambault, G. (1970), Simulation of shear behavior of a jointed rock mass. 11th Symposium on Rock Mechanics, Berkeley, p. 105–125.

Lam, T. S. K., Johnston, I.W. (1989), Shear behaviour of regular triangular concrete-rock joints evaluation. J. Geotech. Eng. Div. ASCE 115, p. 711–727.

Lanaro, F. Jing, L. Stephansson, O. (1998) 3-D-laser measurements and representation of roughness of rock fractures, Mech Jointed Faulted Rock. Rossmanith: Vienna, 1998. p. 185–189.

Lee, Y.-H., J.R. Cart', D.J. Barr, and C.J. Haas. (1990), The fractal dimension as a measure of the roughness of rock discontinuity profiles. International Journal of Rock Mechanics and Mining Sciences & GeomechanicsAbstracts 27, p. 453-464.

Li C, Nordlund E. (1990), Characteristics of acoustic emissions during shearing of rock joints. In: Barton N, Stephansson O, editors. Proceedings of first international symposium on rock joints. Rotterdam: Balkema; p. 251–258.

Lo, K. Y., Ogawa, T., Lukajic, B., Dupak, D. D. (1991), Measurements of strength parameters of concrete-rock contact at the dam foundation interface. Geotechnical Testing Journal., 14(4), p. 383–394.

Lo KY, Lukajic B, Wang S, Ogawa T, Tsui KK. (1990), Evaluation of strength parameters of concrete–rock interface for dam safety assessment. In: Proceedings of Canadian dam safety conference. Toronto; September, p. 71–93.

Maejima T, Morioka H, Mori T, Aoki K. (2001), Estimation of rock mass behavior for AE monitoring in excavation of Kannagawa underground powerplant cavern. In: Proceedings of the 31th symposium on rock mechanics, p. 256–60.

Mlakar, V. F.P. Hassani and M. Momayez, (1993), Crack development and acoustic emission in potash rock, Int J Rock Mech Min Sci 30 (3), p. 305–319.

Mandelbrot BB. The fractal of nature. (1983), New York: W.H. Freeman, 468 p.

Manthei G, Jurgen Eisenblatter and Thomas Spies, (2007), Source mechanisms of acoustic emission events between large underground cavities in a salt mine, ICAE-6 / AEWG-50: Lake Tahoe, NV, USA, Oct 29-Nov 2, 2007

Manthei G, Jurgen Eisenblatter, Torsten Dahm. (2001), Moment tensor evaluation of acoustic emission sources in salt rock. Construction and Building Materials.15, p.: 297-309

Martin, F. A. (2011) Stabilité des barrages: influence de la température et étude de sensibilité sur la résistance au cisaillement des joints de coulée, mémoire de maitrise, Université de Sherbrooke, Département de génie civil, Sherbrooke, Canada, 103 p.

Minemura O, Noboru Sakata, Shigenori Yuyama,U, Takahisa Okamoto, Kyuichi Maruyama, (1998), Acoustic emission evaluation of an arch dam during construction cooling and grouting, Construction and Building Materials 12, p. 385-392.

Moradian ZA, Ballivy G, Gravel C, Saleh K. (2008), Analysis the shear strength of the active joints using results of the constant normal load shear test. In: Proceedings of fourth Asian rock mechanics conference. Tehran.

Moradian, Z. A, G. Ballivy, P. Rivard, C. Gravel and B. Rousseau. (2010), Evaluating damage during shear tests of rock joints using acoustic emission. International Journal of Rock Mechanics and Mining Sciences, 47(4), p. 590–598.

Moradian, Z. A, G. Ballivy, P. Rivard and C. André. (2010), Effect of normal load on shear behavior and acoustic emissions of rock joints under direct shear loading. European Rock Mechanics Symposium (Eurock 2010), 15 to 17 June 2010, Lausanne, Switzerland

Moriya H, T. Fujita, H. Niitsuma, J. Eisenblatter, G. Manthei. (2006), Analysis of fracture propagation behavior using hydraulically induced acoustic emissions in the Bernburg salt mine, Germany. International Journal of Rock Mechanics & Mining Sciences.43, p. 49–57

Nicholson, G. A. (1983). Design of Gravity Dams and Rock Foundations: Sliding Stability Assessment by Limit Equilibrium and Selection of Shear Strength Parameters, Technical Report GL-83-13, U.S. Army Engineer Waterways Experiment Station, Vicksburg, MS 39180.

Ohtsu M. (1991), Simplified moment tensor analysis and unified decomposition of acoustic emission source: application in situ hydrofracturing test. J. Geophys. Res.96, p. 6211–21.

Patton, F.D. (1966) Multiple modes of shear failure in rocks, Proceedings of First Congress of International Society of Rock Mechanics, Portugal, Vol.1, p. 509–513.

Pollock A. (2003), Acoustic emission inspection. Technical report: TR-103-96-12/89, Physical acoustic corporation.p. 261-276.

Rim H, Hae-jun Choi, Bong-Ki Son, Chung-In Lee & Jae-Joon Song. (2005), Experimental study for shear behavior of pseudo rock joint under constant normal stiffness condition, Underground Space Use: Analysis of the Past and Lessons for the Future – Erdem & Solak (eds), 2005 Taylor & Francis Group, London,

Rousseau, B. (2010) Comportement des interfaces fragiles des ouvrages hydroélectriques, Thèse de doctorat, Université de Sherbrooke, Département de génie civil, Sherbrooke, Canada, 296 p.

Rudajev V., J. Vilhelmt, J. Kozakt, T. Lokajiceks, (1996), statistical precursors of instability of loaded rock samples based on acoustic emission, Int. J. Rock Mech. Mm. Sri. & Geomech. Abstr. Vol. 33, No. 7, p. 743-748

Rudajev, V. Vilhelma, J. Lokajõacĭek, T. (2007), Laboratory studies of acoustic emission prior to uniaxial compressive rock failure, International Journal of Rock Mechanics and Mining Sciences 37, p. 699-704

Saiang D, Malmgren L, and Nordlund E. (2005), Laboratory tests on shotcrete-rock joints in direct shear, tension and compression. Rock Mech. Rock Engng. 38 (4), p. 275–297

Sasao, H., Hirata, A., Obara, Y. (2003), Measurement of acoustic emission and interpretation of its results during excavation of a rock cliff with opening joints, ISRM 2003–Technology roadmap for rock mechanics, South African Institute of Mining and Metallurgy, p. 1031-1034.

Schechinger B, Vogel T . (2006), Acoustic emission for monitoring a reinforced concrete beam subject to four-point-bending. Construction and Building Materials.; 21(3), p. 483-490.

Seidel, J. P., Haberfield, C. M. (2002): Laboratory testing of concrete-rock joints in constant normal stiffness direct shear. Geotech. Test. J. 25(4), p. 391–404.

Seto, M. Utagawa, M. Katsuyama, K. Nag, D.K. Vutukuri, V.S. (1997), In situ stress determination by acoustic emission technique, Int. J. Rock Mech. &Min. Sci. 34:3-4, Paper No. 281

Shigeishi M., S. Colombo, K.J. Broughton,, H. Rutledge, A.J. Batchelor, M.C. Forde. (2001), Acoustic emission to assess and monitor the integrity of bridges. Construction and Building Materials.15, p. 35-49

Shiotani T, D.G. Aggelis, O. Makishima, (2007), Global Monitoring of Concrete Bridge Using Acoustic Emission. Journal of Acoustic Emission; 25: 308-315.

Shiotani T., Evaluation of long-term stability for rock slope by means of acoustic emission technique. NDT & E International.2006;39(3): 217-228.

Shiotani T. (2008), Parameter analysis. In: Acoustic emission testing, CU Grosse and M Ohtsu, Eds. :Springer, p. 41-51

Son B.K., C.I. Lee, Y.J. Park, Y.K. Lee.z. (2006), Effect of boundary conditions on shear behaviour of rock joints around tunnel. Tunneling and Underground Space Technology. 21, p. 347–348.

Tse R, Cruden DM. (1979), Estimating joint roughness coefficients. Int J Rock Mech Min Sci Geomech Abstr, 16, p. 303–7.

U.S. Army Corps of Engineers. (1994). Engineering and Design, Rock Foundations. Engineer Manual EM 1110-1-2908, 120 p.

U.S. Army Corps of Engineers. (1995). Engineering and Design, Gravity Dam Design. Engineer Manual EM 1110-2-2200, 88 p.

USCOLD (1975), Lessons from Dam Incidents USA. ASCE, New York.
USCOLD (1988), Lessons from Dam Incidents. USA-II. ASCE, New York.
USCOLD Committee on Dam Safety (1996), Anthology of Dam Modification Case Histories. USCOLD, Denver, 138 p.
Wang H. and Maochen Ge. (2008), Acoustic emission/micro seismic source location analysis for a limestone mine exhibiting high horizontal stresses. International Journal of Rock Mechanics and Mining Sciences.45(5), p. 720-728
Wakabayashi, N., and I. Fukuahige. (1992). Experimental study on the relation between fractal dimension and shear strength .Coherence of Fractured and Joined Rock Masses. Preprints.June3-5, 1992. Lake Tahoe, CA, p. 687-695.
Wu K., B. Chen and W. Yao. (2000), Study on the AE characteristics of fracture process of mortar, concrete and steel-fiber-reinforced concrete beams, Cement and Concrete Research.30, p. 1495-1500
Yang, Z. Y., Chiang, D. Y. (2000), An experimental study on the progressive shear behavior of rock joints with tooth-shaped asperities. Int. J. Rock Mech. Min. Sci. Geomech. Abstr.37(8), p. 1247–1259.